

DESIGN, DEVELOPMENT AND ANALYSIS OF SMALL ANTENNAS

Thesis submitted by

DEEPAK U

*in partial fulfilment of the requirements for
the degree of*

DOCTOR OF PHILOSOPHY

Under the guidance of

Prof. P. MOHANAN



Department of Electronics

Faculty of Technology

Cochin University of Science and Technology

Cochin - 682 022, Kerala, India

May 2018

Design, Development and Analysis of Small Antennas

Ph.D. Thesis under the Faculty of Technology

Author

Deepak U
Centre for Research in Electromagnetics and Antennas (CREMA)
Department of Electronics
Cochin University of Science and Technology
Cochin - 682 022, Kerala, India.
Email: Deepak.palath@gmail.com

Supervisor

Dr. P. Mohanan
Professor (UGC BSR)
Centre for Research in Electromagnetics and Antennas (CREMA)
Department of Electronics
Cochin University of Science and Technology
Cochin - 682 022, Kerala, India.
Email: drmohan@gmail.com

Department of Electronics
Cochin University of Science and Technology
Cochin - 682 022, Kerala, India.
www.doe.cusat.edu

May 2018



Dedicated to the Almighty... Teachers...
Parents... & Dear Ones...



DEPARTMENT OF ELECTRONICS
COCHIN UNIVERSITY OF SCIENCE AND TECHNOLOGY
COCHIN-682 022, INDIA.

Dr. P. Mohanan
(Supervising Guide)
Professor (UGC BSR)
Department of Electronics
Cochin University of Science and Technology.

Certificate

This is to certify that this thesis entitled “**Design, Development and Analysis of Small Antennas**” is a bonafide record of the research work carried out by **Mr. DEEPAK U** under my supervision and guidance in the Centre for Research in Electromagnetics and Antennas (CREMA), Department of Electronics, Cochin University of Science and Technology in partial fulfilment of the requirements for the Ph.D. degree under the Faculty of Technology. The results embodied in this thesis or parts of it have not been presented for the award of any other degree. All the relevant corrections and modifications suggested by the audience and recommended by the doctoral committee of the candidate during the pre-synopsis seminar have been incorporated in the thesis.

Cochin – 22
May 2018

Prof. P. Mohanan

Declaration

I hereby declare that the work presented in this thesis entitled “**Design, Development and Analysis of Small Antennas**” is based on the original research work carried out by me under the supervision and guidance of Dr. P. Mohanan in the Centre for Research in Electromagnetics and Antennas (CREMA), Department of Electronics, Cochin University of Science and Technology in partial fulfilment of the requirements for the Ph.D. degree under the Faculty of Technology and that no part of this thesis has been submitted before for the award of any other degree.

Cochin – 22

May 2018

Deepak U
Research Scholar
Department of Electronics
CUSAT

Acknowledgements

The work presented in this thesis would not have been completed without the immense support from quite a lot of people and organizations. I take this opportunity to acknowledge each one of them from the bottom of my heart. I express my sincere thanks to my supervisor Prof. P. Mohanan, first of all for giving me a chance to work under his guidance. I thank him for his insightful and timely advices with passionate encouragements and understandings throughout the journey of my doctoral research. My heartfelt thanks are also due to Prof. K. Vasudevan, Prof. C. K. Aanandan and Dr. Supriya M H for their moral support and timely advices which paved a smooth path for my research at Department of Electronics, CUSAT.

All those people who were a part in the success of my doctoral journey must be credited for the successful completion of this work. Special thanks to Mr. Nijas C M, Mr. Sujith Raman, Mr. Sarin V P, for their timely support and advices. I extend my thank to Ms. Sajitha R, Ms. Sumitha Mathew, Mr. Prakash K C, Mr. Dinesh R, Mr. Lindo A O, Mr. Vivek R for the corporation and coordination they had with me. My sincere thanks to all staffs of the Department of Electronics for the support they extended for the success of my research. The University Grants Commission (UGC) is duly acknowledged for the financial support they provided during my research period.

Last, but most importantly, I thank my parents and family for all the support and trust during the entire course. I thank my wife Roshna T K for giving me immense support, advices and holding high trust in me which was my pillar support in all difficult situations. And, my son Vedik Dev for all his patience and love.

Abstract

The thirst of human kind for compact and handy gadget are soaring up day by day. To fulfil his needs, to bring many sophisticated communication gadgets in to smaller space, all the departments should come to miniaturisation. One of the biggest challenge in this process is to make the wireless communication antennas very smaller to comply miniaturisation. In this scenario, novel design for smaller antennas are a big challenge. Three such small antenna are developed and analysed in this thesis. Out of the three, two such antennas are electrically small and the third one is a physically small antenna. Stepped Impedance Resonators (SIR) are used in two antennas to achieve compactness. The biggest challenge was to find a mechanism for exciting the SIR to radiate electromagnetic energy. Two different designs with different excitation technique for SIR are presented here. The thesis proposes design equations for designing with different substrate material and frequency. The third antenna is based on chip inductor loading technique for achieving compactness.

Contents

Contents	xi
List of Figures	xvii
1 Introduction	1
1.1 Introduction	1
1.2 The Journey Begins....	2
1.2.1 Definition	6
1.2.2 Applications	6
1.3 Present Antenna Types and Design Techniques	8
1.3.1 Microstrip Antenna	8
1.3.2 PILA-PIFA Based Antenna	11
1.3.3 Meatmaterial Based Antenna	12
1.3.4 Photonic Band Gap Based Antenna	13
1.3.5 LTCC Based Antenna	14
1.3.6 Small Antennas	14
1.3.6.1 Why Small Antennas?	15
1.3.6.2 Electrically Small Antenna (ESA)	15
1.3.6.3 Physically Constrained Small Antenna (PCSA)	16
1.3.6.4 Functionally Small Antenna (FSA)	16
1.3.6.5 Physically Small Antenna (PSA)	17
1.3.7 Motivation of Current Research	17
2 Literature Review & Methodology	21
2.1 Instant peep - Small Antennas	21

2.2	Dual Band Antennas	31
2.3	Methodology	33
2.3.1	Right substrate	33
2.3.2	Photo lithography	34
2.3.3	Amenities for antenna measurement	35
2.3.3.1	Network Analyzer	35
2.3.3.2	PNA E8362B Network Analyzer	37
2.3.3.3	Anechoic Chamber	37
2.3.3.4	Measurement of Return loss	38
2.3.3.5	Measurement of radiation pattern	39
2.3.3.6	EMSCAN RFxpert	40
2.3.3.7	Gain Measurement	41
2.3.3.8	Efficiency	41
2.3.4	High Frequency Simulation Softwares	42
2.3.4.1	Steps in HFSS simulation	45
2.3.5	Finite Difference Time Domain (FDTD)	46
2.3.5.1	Numerical investigations: Finite Difference Time Domain	47
2.3.5.2	Fundamental concepts of FDTD	48
2.4	Conclusion	49
3	Lumped Inductor Loaded CPW Based Electrically Small Antenna (ESA)	51
3.1	Introduction	51
3.2	Evolution	51
3.3	Geometry	56
3.4	Simulated and measured results	59
3.4.1	Scattering Parameters	59
3.4.2	The effective inductance	61
3.4.3	Design	62
3.4.4	Surface Current Distribution	64
3.5	Parametric Analysis	65
3.5.1	Effect of transmission line length L	66

3.5.2	Effect of CPW ground width G_w	67
3.5.3	Effect of metal strip geometry	68
3.5.3.1	Effect of length P_h	68
3.5.3.2	Effect of changing P_w symmetrically	68
3.5.3.3	Asymmetric variation of P_w	70
3.5.4	Effect of substrate thickness	71
3.5.5	Effect of substrate relative permittivity	72
3.6	Result and Discussion	74
3.6.1	Radiation Pattern	74
3.6.2	Gain and Efficiency	75
3.6.3	Design for Different Frequency Bands	76
3.6.4	Electrical Size	79
3.7	Conclusions	80
4	An Electrically Small Frequency Reconfigurable Antenna	81
4.1	Introduction	81
4.1.1	Evolution	81
4.2	Design	87
4.2.1	SIR Design	87
4.2.2	New mode of operation	94
4.2.3	Fabry-Perot mode	98
4.2.4	Design for different bands in Fabry-Perot mode	100
4.3	Reconfigurability of the antenna	103
4.4	Optimised Geometry	104
4.5	Field Analysis in the SIR Mode	107
4.6	Parametric Analysis	108
4.6.1	Ground Width Variation	108
4.6.2	High Impedance Microstripline Width Variation	115
4.6.3	Stacking height variation	116
4.6.4	Feeding Position Variation	117
4.6.5	Effect of k on fabry-perot mode	120
4.6.6	Effect of Width Variation	120
4.6.7	Parametric analysis of substrate permittivity	123

4.7	Radiation Pattern	123
4.8	Gain And Efficiency	125
4.9	Electrical Size	126
4.10	Conclusions	126
5	SIR Loaded Modified Dipole Antenna	129
5.1	Introduction	129
5.2	Evolution of the Antenna	130
5.3	Geometry	134
5.4	Analysis of the effect of the radiation characteristics on top loading	135
5.5	Optimised Geometry	141
5.6	Analysis of the parasitic element	143
5.6.1	Resonant Condition	145
5.6.2	Design Equation for Parasitic Element	151
5.6.3	Design Equation for Bent Dipole	153
5.7	Analysis of Electric Field, Surface Current and Polarization of the Antenna	155
5.8	Parametric Analysis	157
5.8.1	Parametric Analysis of the dipole width	157
5.8.2	Parametric Analysis of coupling gap C_g	158
5.8.3	Parametric Analysis of impedance ratio k	160
5.8.4	Parametric Analysis of the α ratio	160
5.8.5	Parametric Analysis of folded SIR	162
5.8.6	Parametric Analysis of the aspect ratio	163
5.8.7	Parametric Analysis of the substrate thickness	164
5.8.8	Parametric Analysis of the substrate permittivity	165
5.9	Result and Discussion	166
5.9.1	Radiation Pattern	167
5.9.2	Gain of the antenna	168
5.9.3	Efficiency of the antenna	169
5.9.4	Bandwidth measurement	170
5.10	Electrical Size	171
5.11	Conclusions	171

6	Conclusions ...	173
6.1	Summary	173
6.1.1	Lumped Inductor Loaded CPW Based ESA	173
6.1.2	An Electrically Small Frequency Reconfigurable Antenna	174
6.1.3	SIR Loaded Modified Dipole Antenna	175
6.2	Future possibilities	176
A	A Compact ACS Fed ESA	179
A.1	Introduction	179
A.2	Evolution of the Antenna	180
A.3	Antenna Design and Geometry	180
A.4	Reflection characteristics	181
A.5	Parametric Analysis	183
A.5.1	Meander line width variation	183
A.5.2	Meander line to feed line coupling gap variation	184
A.5.3	Meander line length L1 variation	185
A.5.4	Substrate thickness variation	185
A.6	Radiation Pattern	187
A.7	Gain	188
A.8	Electrical size	188
A.9	Conclusion	190
	References	191
	Resume of Author	207

CONTENTS

List of Figures

1.1	Patch Antenna	9
1.2	PIFA	11
2.1	Photo lithographic process	34
2.2	Basic block diagram of Network Analyser	36
2.3	Photograph of Anechoic Chamber at Dept. of Electronics, CUSAT	38
2.4	Flow diagram of HFSS solution process	44
2.5	Flow diagram of HFSS process steps	46
2.6	Yee Cell illustration	49
3.1	Coplanar Waveguide	52
3.2	CPW fed Monopole Antenna, [$L_{ant} = 31$ mm, $W_g, W = 3$ mm, $G = 0.4$ mm, $h = 1.6$ mm, $\epsilon_r = 4.4$]	53
3.3	CPW Fed planar Monopole antenna Designed for 2.4 GHz. [L_{ant} $= 31$ mm, $W = 3$ mm, $G = 0.4$ mm, $h = 1.6$ mm, $\epsilon_r = 4.4$] . . .	54
3.4	CPW Fed planar Monopole antenna Designed for 2.4 GHz and the input reflection characteristics. [$L_{ant} = 28.9$ mm, $W = 1$ mm, G $= 0.4$ mm, $h = 1.6$ mm, $\epsilon_r = 4.4$]	55
3.5	Geometry of the antenna with length and width reduction, $L=1.6$ mm, $W = 1$ mm	56
3.6	Return loss of the CPW Fed planar Monopole with highly trun- cated length.[$L_{ant} = 1.6$ mm, $W = 1$ mm, $h = 1.6$ mm, $\epsilon_r = 4.4$]	56
3.7	Geometry of the proposed antenna	57
3.8	Geometry of the Coilcraft 0603CS chip inductor [1]	58

LIST OF FIGURES

3.9	Prototype of the proposed antenna. [$\epsilon_r = 4.4$, Ph = 0.8 mm, Pw = 1 mm, Gw = 3 mm, Coilcraft 0603CS 23 nH Chip Inductor, Sh = 1.6 mm]	58
3.10	(a) Return loss and Transmission characteristics of Inductor Loaded ESA. [L = 0.8 mm, W = 1 mm, Coilcraft 0603CS 23 nH Chip Inductor, Sh = 1.6 mm, $\epsilon_r = 4.4$], (b) Impedance Characteristics in Smith chart	59
3.11	Return loss of the antenna with and without inductor. [$\epsilon_r = 4.4$, Ph = 0.8 mm, Pg = 0.8 mm, Pw = 1 mm, Gw = 3 mm, Inductor 37.5 nH, Sh = 1.6 mm]	60
3.12	Interpolated and curve fitted values of inductance for the data from coilcraft 0603CS chip inductor data sheet	62
3.13	Impedance plot of the proposed antenna [L = 0.8 mm, W = 1 mm, Coilcraft 0603CS 23 nH Chip Inductor, Sh = 1.6 mm, $\epsilon_r = 4.4$]	63
3.14	Surface current distribution along the small metal strip and the chip inductor, for two different scenarios. [$\epsilon_r = 4.4$, Ph = 0.8 mm and 5.8 mm, Pw = 1 mm, Gw = 3 mm, Inductance = 37 nH] . .	64
3.15	Resonance frequency shift for inductor loading at different locations on the small metal strip. [$\epsilon_r = 4.4$, Ph = 5.8 mm, Pw = 1 mm, Gw = 3 mm, Inductance = 37.5 nH]	65
3.16	Simulated return loss of the antenna w.r.t feed line length. [$\epsilon_r = 4.4$, Pw = 1 mm, Gw = 3 mm, Inductance = 37.5 nH]	66
3.17	Measured return loss of the antenna w.r.t feed line length. [$\epsilon_r = 4.4$, Pw = 1 mm, Gw = 3 mm, Coilcraft 0603CS 23 nH Chip Inductor]	67
3.18	a) Simulated return loss of the antenna w.r.t ground width variation. b) Impedance variation [$\epsilon_r = 4.4$, Pw = 1 mm, Inductance = 37.5 nH]	68
3.19	Change in the resonance characteristics of the antenna w.r.t change in the small metal strip length. [$\epsilon_r = 4.4$, Pw = 1 mm, Gw = 3 mm, Inductance = 37.5 nH]	69

LIST OF FIGURES

3.20 Change in the resonance characteristics of the antenna w.r.t change in the small metal strip width $P_w = 2$ mm to 5 mm. [$\epsilon_r = 4.4$, $Ph = 0.8$ mm, $G_w = 3$ mm, Inductance = 37.5 nH]	69
3.21 Change in the resonance characteristics of the antenna w.r.t asymmetric change in the small metal strip width P_w . [$\epsilon_r = 4.4$, $P_w = 1$ mm - 4 mm, $ph = 0.8$ mm, $G_w = 3$ mm, Inductance = 37.5 nH]	70
3.22 Change in the radiation pattern as the width P_w is varied asymmetrically. [$\epsilon_r = 4.4$, $P_w = 2$ mm - 5 mm, $ph = 0.8$ mm, $G_w = 3$ mm, Inductance = 37.5 nH]	70
3.23 Change in the resonance characteristics of the antenna w.r.t change in the substrate thickness Sh . [$\epsilon_r = 4.4$, $Ph = 0.8$ mm, $P_w = 1$ mm - 4 mm, $ph = 0.8$ mm, $G_w = 3$ mm, Chip Inductor = CoilCraft 0603CS 23 nH]	71
3.24 Change in the resonance as the relative permittivity is varied. [$Ph = 0.8$ mm, $P_w = 1$ mm, $G_w = 3$ mm, Inductance = 37.5 nH]	72
3.25 Measured radiation pattern of the coplanar antenna at 2.395 GHz. [$Ph, P_g = 0.8$ mm, $P_w = 1$ mm, $G_w, C_w = 3$ mm, $G = 0.327$ mm, $L = 4$ mm, Coilcraft 0603CS 23 nH Chip Inductor, $\epsilon_r = 4.4$] . . .	74
3.26 Measured 3D radiation pattern of the coplanar antenna at 2.395 GHz using RFXpert. [$Ph, P_g = 0.8$ mm, $P_w = 1$ mm, $G_w, C_w = 3$ mm, $G = 0.327$ mm, $L = 4$ mm, Coilcraft 0603CS 23 nH Chip Inductor, $\epsilon_r = 4.4$]	75
3.27 Measured gain of the prototype antenna fabricated w.r.t Table 3.1, $\epsilon_r = 4.4$	76
3.28 Return loss of the antenna designed using equation (3.1) and (3.5) at different frequency bands	77
3.29 Measured and simulated reflection characteristics of the antenna designed at 2.7 GHz [$Ph, P_g = 0.8$ mm, $P_w = 1$ mm, $G_w, C_w = 3$ mm, $G = 0.327$ mm, $L = 4$ mm, Inductance = 30.75 nH, $\epsilon_r = 4.4$]	78
3.30 Measured radiation pattern of the coplanar antenna designed for 2.7 GHz. [$Ph, P_g = 0.8$ mm, $P_w = 1$ mm, $G_w, C_w = 3$ mm, $G = 0.327$ mm, $L = 4$ mm, Inductance = 30.75 nH, $\epsilon_r = 4.4$]	78

LIST OF FIGURES

3.31	Measured radiation pattern of the antenna designed at 2.7 GHz using RFXpert [Ph,Pg = 0.8 mm, Pw = 1 mm, Gw,Cw = 3 mm, G = 0.327 mm, L = 4 mm, Inductance = 30.75 nH, $\epsilon_r = 4.4$] . . .	79
4.1	Conventional SIRs	82
4.2	a) Coaxial excitation of a $\lambda/4$ SIR, b) simulated return loss of the antenna ($\epsilon_r = 4.4$, h = 1.6 mm, $l_1 = 9$ mm, $l_2 = 3.5$ mm, k = 0.7, $\alpha = 0.285$)	83
4.3	Evolution of the excitation of the proposed antenna	83
4.4	Simulated resonant properties of the antenna w.r.t Figure 4.3 (a) ($\epsilon_r = 4.4$, h = 1.6 mm, $l_1 = 9$ mm, $l_2 = 3.5$ mm, feed line width = 3 mm, k = 0.7, $\alpha = 0.285$)	84
4.5	Simulated resonant properties of the antenna w.r.t Figure 4.3 (b)($\epsilon_r = 4.4$, h = 1.6 mm, $l_1 = 9$ mm, $l_2 = 3.5$ mm, feed line width = 3 mm, k = 0.7, $\alpha = 0.285$)	84
4.6	Simulated resonant properties of the antenna w.r.t Figure 4.3 (c)($\epsilon_r = 4.4$, h = 1.6 mm, $l_1 = 9$ mm, $l_2 = 3.5$ mm, feed line width = 3 mm, k = 0.7, $\alpha = 0.285$)	85
4.7	Simulated resonant properties of the antenna w.r.t Figure 4.3 (d)($\epsilon_r = 4.4$, h = 1.6 mm, $l_1 = 9$ mm, $l_2 = 3.5$ mm, feed line width = 3 mm, k = 0.7, $\alpha = 0.285$)	85
4.8	Simulated resonant properties of the antenna w.r.t Figure 4.3 (e) ($\epsilon_r = 4.4$, h = 3.2 mm, $l_1 = 9$ mm, $l_2 = 3.5$ mm, feed line width = 3 mm, k = 0.7, $\alpha = 0.285$)	86
4.9	Geometry of Quarter wave SIR used in the design (Top View) . . .	87
4.10	Geometry of the proximity coupled antenna	88
4.11	Measured and simulated return loss of the antenna at 2.4 GHz. [L = 15 mm, S1 = 9 mm, S2 = 3.5 mm,W = 10 mm, W1 = 1.6 mm, W2 = 3.6 mm, Wm = 3 mm, Cg = 0.6 mm, H = 1.6 mm, $\epsilon_r = 4.4$]	89
4.12	Simulated return loss of the antenna designed using (4.4) for different frequencies. [W1 = 1.6 mm, W2 = 3.6 mm, Wm = 3 mm, Cg = 0.6 mm, H = 1.6 mm, $\epsilon_r = 4.4$]	90

LIST OF FIGURES

4.13	Spurious frequency variation and the simulated spurious frequency for the proposed SIR with $k = 0.71$	91
4.14	Simulated return loss of the antenna designed at 2.4 GHz for different α values [$H = 1.6$ mm, $\epsilon_r = 4.4$]	92
4.15	Simulated and measured return loss of the antenna designed at 2.4 GHz for $\alpha = 0.6$ and $k = 0.65$ [$H = 1.6$ mm, $\epsilon_r = 4.4$, $l_1 = 4.45$ mm, $l_2 = 6.6$, $W1 = 1.2$ mm, $W2 = 3.6$ mm]	93
4.16	Simulated fundamental and first spurious frequency for different α , [$H = 1.6$ mm, $\epsilon_r = 4.4$, $W1 = 1.6$ mm, $W2 = 3.6$ mm, $k = 0.7$]	93
4.17	Measured and simulated return loss of the antenna at the higher 5.45 GHz. [$L = 15$ mm, $S1 = 9$ mm, $S2 = 3.5$ mm, $W = 10$ mm, $W1 = 1.6$ mm, $W2 = 3.6$ mm, $Wm = 3$ mm, $Cg = 0.6$ mm, $H = 1.6$ mm, $\epsilon_r = 4.4$]	94
4.18	Simulated Electric and Magnetic Field in the structure for the open circuited mode [Spatially Orthogonal]. [$L = 15$ mm, $S1 = 9$ mm, $S2 = 3.5$ mm, $W = 10$ mm, $W1 = 1.6$ mm, $W2 = 3.6$ mm, $Wm = 3$ mm, $Cg = 0.6$ mm, $H = 1.6$ mm, $\epsilon_r = 4.4$]	95
4.20	The surface current distribution in the open circuited fabry-perot mode of the antenna at 5.4 GHz. [$L = 15$ mm, $S1 = 9$ mm, $S2 = 3.5$ mm, $W = 10$ mm, $W1 = 1.6$ mm, $W2 = 3.6$ mm, $Wm = 3$ mm, $Cg = 0.6$ mm, $H = 1.6$ mm, $\epsilon_r = 4.4$]	96
4.19	Normalised Magnitude of Simulated Electric and Magnetic Field in the structure. [$L = 15$ mm, $S1 = 9$ mm, $S2 = 3.5$ mm, $W = 10$ mm, $W1 = 1.6$ mm, $W2 = 3.6$ mm, $Wm = 3$ mm, $Cg = 0.6$ mm, $H = 1.6$ mm, $\epsilon_r = 4.4$]	96
4.21	Simulated field plot of temporal orthogonality of electric and magnetic fields. [$L = 15$ mm, $S1 = 9$ mm, $S2 = 3.5$ mm, $W = 10$ mm, $W1 = 1.6$ mm, $W2 = 3.6$ mm, $Wm = 3$ mm, $Cg = 0.6$ mm, $H = 1.6$ mm, $\epsilon_r = 4.4$]	97
4.22	Electric and Magnetic field distribution in different fabry-perot resonators. Courtesy: [3]	98
4.23	Return loss of Antenna designed using equation (4.8) for different frequency bands, w.r.t Table 4.3[$\epsilon_r = 4.4$, $h = 3.2$ mm]	100

LIST OF FIGURES

4.24	Impedance variation of Antenna designed using equation (4.8) for different frequency bands, [$\epsilon_r = 4.4$, $h = 3.2$ mm]	101
4.25	LC matching network and return loss characteristics of the antenna at 1 GHz. [$\epsilon_r = 4.4$, $h = 3.2$ mm, $S1 = 76.65$ mm, $S2 = 3.5$ mm, $W1 = 2.6$ mm, $W2 = 3.6$ mm]	102
4.26	Effect of capacitive matching network on return loss characteristics of the antenna at 6 GHz. [$\epsilon_r = 4.4$, $h = 3.2$ mm, $S1 = 7.55$ mm, $S2 = 3.5$ mm, $W1 = 2.6$ mm, $W2 = 3.6$ mm]	103
4.27	Geometry of the proposed antenna, $\epsilon_r = 4.4$	105
4.28	Implementation of frequency reconfigurability in the antenna using PIN diode [$L = 15$ mm, $S1 = 9$ mm, $S2 = 3.5$ mm, $W = 10$ mm, $W1 = 1.6$ mm, $W2 = 3.6$ mm, $Wm = 3$ mm, $Cg = 0.6$ mm, $H = 1.6$ mm, $\epsilon_r = 4.4$]	106
4.29	Prototype of open and short circuited SIR antenna [$L = 15$ mm, $S1 = 9$ mm, $S2 = 3.5$ mm, $W = 10$ mm, $W1 = 1.6$ mm, $W2 = 3.6$ mm, $Wm = 3$ mm, $Cg = 0.6$ mm, $H = 1.6$ mm, $\epsilon_r = 4.4$, $k = 0.7$, $\alpha = 0.285$]	106
4.30	Simulated Electric and Magnetic Field in the structure for the short circuited mode. [$L = 15$ mm, $S1 = 9$ mm, $S2 = 3.5$ mm, $W = 10$ mm, $W1 = 1.6$ mm, $W2 = 3.6$ mm, $Wm = 3$ mm, $Cg = 0.6$ mm, $H = 1.6$ mm, $\epsilon_r = 4.4$, $k = 0.7$, $\alpha = 0.285$]	107
4.31	The surface current distribution in the short circuited SIR mode of the antenna at 2.4 GHz. [$L = 15$ mm, $S1 = 9$ mm, $S2 = 3.5$ mm, $W = 10$ mm, $W1 = 1.6$ mm, $W2 = 3.6$ mm, $Wm = 3$ mm, $Cg = 0.6$ mm, $H = 1.6$ mm, $\epsilon_r = 4.4$, $k = 0.7$, $\alpha = 0.285$]	107
4.32	Extension of ground plane length for both the SIR mode and fabry-perot mode resonance. The length L is varied from 15 mm to 20 mm. [$S1 = 9$ mm, $S2 = 3.5$ mm, $W = 10$ mm, $W1 = 1.6$ mm, $W2 = 3.6$ mm, $Wm = 3$ mm, $Cg = 0.6$ mm, $H = 1.6$ mm, $\epsilon_r = 4.4$]	109
4.33	Simulated radiation pattern of the antenna in the lower 2.4 GHz. [$L = 15 - 20$ mm, $S1 = 9$ mm, $S2 = 3.5$ mm, $W = 10$ mm, $W1 = 1.6$ mm, $W2 = 3.6$ mm, $Wm = 3$ mm, $Cg = 0.6$ mm, $H = 1.6$ mm, $\epsilon_r = 4.4$]	110

LIST OF FIGURES

4.34 Fringing electric field variation with respect to change in ground plane width. [S1 = 9 mm, S2 = 3.5 mm, W = 10 mm, W1 = 1.6 mm, W2 = 3.6 mm, Wm = 3 mm, Cg = 0.6 mm, H = 1.6 mm, $\epsilon_r = 4.4$]	111
4.35 Simulated radiation pattern of the antenna in the higher 5.4 GHz. [L = 15 - 20 mm, S1 = 9 mm, S2 = 3.5 mm, W = 10 mm, W1 = 1.6 mm, W2 = 3.6 mm, Wm = 3 mm, Cg = 0.6 mm, H = 1.6 mm, $\epsilon_r = 4.4$]	112
4.36 Fringing electric field variation with respect to change in ground plane width. [S1 = 9 mm, S2 = 3.5 mm, W = 10 mm, W1 = 1.6 mm, W2 = 3.6 mm, Wm = 3 mm, Cg = 0.6 mm, H = 1.6 mm, $\epsilon_r = 4.4$]	113
4.37 Radiation pattern at 2.4 GHz for infinite ground plane. [S1 = 9 mm, S2 = 3.5 mm, W = 10 mm, W1 = 1.6 mm, W2 = 3.6 mm, Wm = 3 mm, Cg = 0.6 mm, H = 1.6 mm, $\epsilon_r = 4.4$]	113
4.38 Radiation pattern at 5.4 GHz for infinite ground plane. [S1 = 9 mm, S2 = 3.5 mm, W = 10 mm, W1 = 1.6 mm, W2 = 3.6 mm, Wm = 3 mm, Cg = 0.6 mm, H = 1.6 mm, $\epsilon_r = 4.4$]	114
4.39 Reflection characteristics of the antenna with symmetric large ground plane [S1 = 8 mm, S2 = 6 mm, W = 12 mm, W1 = 2 mm, W2 = 4 mm, Wm = 3 mm, Cg = 0.6 mm, H = 1.6 mm, $\epsilon_r = 4.4$]	114
4.40 Radiation pattern at 4.84 GHz for infinite ground plane. [S1 = 8 mm, S2 = 6 mm, W = 12 mm, W1 = 2 mm, W2 = 4 mm, Wm = 3 mm, Cg = 0.6 mm, H = 1.6 mm, $\epsilon_r = 4.4$]	115
4.41 The variation of the electric and magnetic field of the fabry-perot mode when the width W1 of the small microstrip line S1 is varied from 0.4 mm to 1.6 mm [L = 15 mm, S1 = 9 mm, S2 = 3.5 mm, W = 10 mm, W2 = 3.6 mm, Wm = 3 mm, Cg = 0.6 mm, H = 1.6 mm, $\epsilon_r = 4.4$]	116
4.42 Variation in the SIR and Fabry-Perot resonance w.r.t. change in stacking height from 0.4 mm to 1.6 mm. [L = 15 mm, S1 = 9 mm, S2 = 3.5 mm, W = 10 mm, W1 = 1.6 mm, W2 = 3.6 mm, Wm = 3 mm, Cg = 0.6 mm, $\epsilon_r = 4.4$]	117

LIST OF FIGURES

4.43	Variation in the Fabry-Perot resonance w.r.t. change in the feeding position, $\epsilon_r = 4.4$, $L = 12$ mm, $H = 1.6$ mm, $W = 3$ mm	118
4.44	Simulated variation in the Fabry-Perot resonance w.r.t. change in the feeding position using SIR, $\epsilon_r = 4.4$, $S1 = 9$ mm, $S2 = 3.5$ mm, $H = 1.6$ mm, $W1 = 1.6$ mm, $W2 = 3.6$ mm	119
4.45	Measured variation in the Fabry-Perot resonance w.r.t. change in the feeding position, $\epsilon_r = 4.4$, $L = 12$ mm, $H = 1.6$ mm, $W = 3$ mm, $f = 5.795$ GHz, 5.795 GHz, 5.83 GHz, 5.86 GHz, 5.86 GHz . .	119
4.46	Variation in the Fabry-Perot resonance w.r.t. change in impedance ratio k. [$L = 15$ mm, $S1 = 9$ mm, $S2 = 3.5$ mm, $W = 10$ mm, $Wm = 3$ mm, $Cg = 0.6$ mm, $H = 1.6$ mm, $\epsilon_r = 4.4$]	120
4.47	The effect of width W on the resonance of the antenna, $L = 12$ mm, $\epsilon_r = 4.4$, $H = 1.6$ mm	121
4.48	The measured effect of width (W) change on the resonance of the antenna, [$L = 12$ mm, $\epsilon_r = 4.4$, $H = 1.6$ mm]	122
4.49	Antenna designed to work at 2.4 and 5.4 GHz on two different material with relative permittivity 2.2 and 6	123
4.50	Normalized Radiation pattern at 2.4 GHz. [$L = 15$ mm, $S1 = 9$ mm, $S2 = 3.5$ mm, $W = 10$ mm, $W1 = 1.6$ mm, $W2 = 3.6$ mm, $Wm = 3$ mm, $Cg = 0.6$ mm, $H = 1.6$ mm, $\epsilon_r = 4.4$]	124
4.51	Normalized Radiation pattern at 5.4 GHz. [$L = 15$ mm, $S1 = 9$ mm, $S2 = 3.5$ mm, $W = 10$ mm, $W1 = 1.6$ mm, $W2 = 3.6$ mm, $Wm = 3$ mm, $Cg = 0.6$ mm, $H = 1.6$ mm, $\epsilon_r = 4.4$]	124
4.52	Measured gain of the antenna using gain comparison method for both the bands. [$L = 15$ mm, $S1 = 9$ mm, $S2 = 3.5$ mm, $W = 10$ mm, $W1 = 1.6$ mm, $W2 = 3.6$ mm, $Wm = 3$ mm, $Cg = 0.6$ mm, $H = 1.6$ mm, $\epsilon_r = 4.4$]	125
5.1	Reflection behaviour of the dipole antenna resonating at 5 GHz band. [Width = 2 mm, Length = 10 mm, Substrate thickness = 1.6 mm, $\epsilon_r = 4.4$]	130

LIST OF FIGURES

5.2	Return loss variation of dipole antenna top loaded with UIR resonating at 5-6 GHz band. [Dipole width = 2 mm, Dipole length = 10 mm, Parasitics element width = 2 mm, Parasitics element length = 37.6 mm, Substrate thickness = 1.6 mm, $\epsilon_r = 4.4$] . . .	131
5.3	Return loss of the bent dipole antenna top loaded with UIR resonating at 5-6 GHz band. [Width = 2 mm, Length = 10 mm, Parasitics element width = 2 mm, Parasitics element length = 37.6 mm, Substrate thickness = 1.6 mm, $\epsilon_r = 4.4$]	131
5.4	Return loss of the bent dipole antenna top loaded with folded UIR resonating at 5-6 GHz and 2.54 GHz band. [Width = 2 mm, Length = 10 mm, $\epsilon_r = 4.4$]	132
5.5	Return loss of the bent dipole antenna top loaded with UIR resonating at 5-6 GHz band. [Width = 2 mm, Length = 10 mm, $\epsilon_r = 4.4$]	133
5.6	Basic geometry of the antenna	134
5.7	Simulated Radiation Pattern for different antenna configurations	135
5.8	Surface current distribution at 4.2 GHz in the antenna with bent dipole and UIR top loading [UIR length = 37.6 mm, UIR width = 2 mm, dipole width = 2 mm, $\epsilon = 4.4$, substrate thickness = 1.6 mm]	136
5.9	Simulated reflection characteristics of the structure with and without SIR [k = 0.45, $\alpha = 0.73$, $\epsilon_r = 4.4$, h = 1.6 mm]	137
5.10	Simulated Reflection Coefficient for UIR and SIR top loading [UIR length = 37.6 mm, UIR width = 2 mm, k = 0.45, $\alpha = 0.73$, $\epsilon_r = 4.4$, h = 1.6 mm]	138
5.11	Fabricated prototype of planar antenna as per Table 5.1, $\epsilon_r = 4.4$, substrate thickness = 1.6 mm	139
5.12	Measured and Simulated Reflection Coefficient of the coplanar antenna fabricated according to the dimensions given in Table 5.1, $\epsilon_r = 4.4$, substrate thickness = 1.6 mm	140
5.13	Measured radiation pattern of the coplanar antenna fabricated according to the dimensions given in Table 5.1, $\epsilon_r = 4.4$, substrate thickness = 1.6 mm	140

LIST OF FIGURES

5.14	Modified antenna and return loss characteristics [L1 = 9.62 mm, L2 = 6.7 mm, L3 = 7.7, L4 = 4 mm, L5 = 7 mm, W1 = 2 mm, W2 = 0.2 mm, W3 = 3 mm, R1 = 7 mm, R2 = 9 mm, C = 0.4 mm, H = 4.1 mm, $\epsilon_r = 4.4$, Substrate thickness = 1.6 mm, k = 0.45, $\alpha = 0.73$]	142
5.15	Fabricated prototype of the modified antenna [L1 = 9.62 mm, L2 = 6.7 mm, L3 = 7.7, L4 = 4 mm, L5 = 7 mm, W1 = 2 mm, W2 = 0.2 mm, W3 = 3 mm, R1 = 7 mm, R2 = 9 mm, C = 0.4 mm, H = 4.1 mm, $\epsilon_r = 4.4$, Substrate thickness = 1.6 mm, k = 0.45, $\alpha = 0.73$]	142
5.16	The evolution SIR from UIR	144
5.17	Conventional SIRs	145
5.18	$\lambda/2$ SIR	145
5.19	Different types of SIR based on Impedance Ratio	146
5.20	Electric field distribution in the SIR at fundamental mode	147
5.21	Evolution of coplanar SIR	147
5.22	CPS and ACPS line Design	148
5.23	The Electric field at different frequencies with plane wave excitation of different coplanar SIR configurations as mentioned in Table 5.3	151
5.24	Simulated Return loss for the lower band of antenna designed with the derived design equation for SIR corresponding to the dimension mentioned in Table 5.4 $\epsilon_r = 4.4$, h = 1.6	152
5.25	Transformation from straight dipole to a bent dipole	153
5.26	Field Distribution on the antenna at 2.4 GHz [L1 = 9.62 mm, L2 = 6.7 mm, L3 = 7.7, L4 = 4 mm, L5 = 7 mm, W1 = 2 mm, W2 = 0.2 mm, W3 = 3 mm, R1 = 7 mm, R2 = 9 mm, C = 0.4 mm, H = 4.1 mm, $\epsilon_r = 4.4$, Substrate thickness = 1.6 mm, k = 0.45, $\alpha = 0.73$]	155

LIST OF FIGURES

5.27 Surface Current Distribution at 2.4 GHz and 5.3 GHz [L1 = 9.62 mm, L2 = 6.7 mm, L3 = 7.7, L4 = 4 mm, L5 = 7 mm, W1 = 2 mm, W2 = 0.2 mm, W3 = 3 mm, R1 = 7 mm, R2 = 9 mm, C = 0.4 mm, H = 4.1 mm, $\epsilon_r = 4.4$, Substrate thickness = 1.6 mm, k = 0.45, $\alpha = 0.73$]	156
5.28 Effect of dipole width on return loss of the antenna [L1 = 9.62 mm, L2 = 6.7 mm, L3 = 7.7, L4 = 4 mm, L5 = 7 mm, W1 = 2 mm, W2 = 0.2 mm, W3 = 3 mm, C = 0.4 mm, H = 4.1 mm, $\epsilon_r = 4.4$, Substrate thickness = 1.6 mm, k = 0.45, $\alpha = 0.73$]	157
5.29 Effect of coupling gap on return loss of the antenna (Cg) [L1 = 9.62 mm, L2 = 6.7 mm, L3 = 7.7, L4 = 4 mm, L5 = 7 mm, W1 = 2 mm, W2 = 0.2 mm, W3 = 3 mm, R1 = 7 mm, R2 = 9 mm, H = 4.1 mm, $\epsilon_r = 4.4$, Substrate thickness = 1.6 mm, k = 0.45, $\alpha = 0.73$]	159
5.30 Return loss of the antenna with different impedance ratio k with constant α [L4 = 4 mm, L5 = 7 mm, W3 = 3 mm, R1 = 7 mm, R2 = 9 mm, C = 0.4 mm, H = 4.1 mm, $\epsilon_r = 4.4$, Substrate thickness = 1.6 mm, $\alpha = 0.73$]	159
5.31 Return loss of the antenna designed for different values of α with constant k [L3 = 7.7, L4 = 4 mm, L5 = 7 mm, W3 = 3 mm, R1 = 7 mm, R2 = 9 mm, C = 0.4 mm, H = 4.1 mm, $\epsilon_r = 4.4$, Substrate thickness = 1.6 mm, k = 0.45]	161
5.32 Effect of L ₃ on return loss of the antenna [L1 = 9.62 mm, L2 = 6.7 mm, L4 = 4 mm, L5 = 7 mm, W1 = 2 mm, W2 = 0.2 mm, W3 = 3 mm, R1 = 7 mm, R2 = 9 mm, C = 0.4 mm, H = 4.1 mm, $\epsilon_r = 4.4$, Substrate thickness = 1.6 mm, k = 0.45]	162
5.33 Reflection characteristics of the antenna with change in the aspect ratio [L4 = 4 mm, L5 = 7 mm, W1 = 2 mm, W2 = 0.2 mm, W3 = 3 mm, R1 = 7 mm, R2 = 9 mm, C = 0.4 mm, H = 4.1 mm, $\epsilon_r = 4.4$, Substrate thickness = 1.6 mm, k = 0.45]	163

LIST OF FIGURES

5.34	Variation of return loss of the antenna with substrate thickness of the antenna [L1 = 9.62 mm, L2 = 6.7 mm, L3 = 7.7, L4 = 4 mm, L5 = 7 mm, W1 = 2 mm, W2 = 0.2 mm, W3 = 3 mm, R1 = 7 mm, R2 = 9 mm, C = 0.4 mm, H = 4.1 mm, $\epsilon_r = 4.4$, $k = 0.45$, $\alpha = 0.73$]	164
5.35	Reflection characteristics of the antenna with change in relative permittivity	165
5.36	Simulated radiation pattern of the antenna [L1 = 9.62 mm, L2 = 6.7 mm, L3 = 7.7, L4 = 4 mm, L5 = 7 mm, W1 = 2 mm, W2 = 0.2 mm, W3 = 3 mm, R1 = 7 mm, R2 = 9 mm, C = 0.4 mm, H = 4.1 mm, $\epsilon_r = 4.4$, Substrate thickness = 1.6 mm, $k = 0.45$, $\alpha = 0.73$]	166
5.37	Measured radiation pattern at 2.48 GHz	167
5.38	Measured radiation pattern at 5.32 GHz	168
5.39	Measured Gain of the antenna [L1 = 9.62 mm, L2 = 6.7 mm, L3 = 7.7, L4 = 4 mm, L5 = 7 mm, W1 = 2 mm, W2 = 0.2 mm, W3 = 3 mm, R1 = 7 mm, R2 = 9 mm, C = 0.4 mm, H = 4.1 mm, $\epsilon_r = 4.4$, Substrate thickness = 1.6 mm, $k = 0.45$, $\alpha = 0.73$]	168
5.40	Measured radiation efficiency of the antenna	170
A.1	Geometry of the proposed antenna. $\epsilon_r = 4.4$, $h = 1.6$ mm	181
A.2	Simulated and measured reflection characteristics of the antenna fabricated according to Table A.1. [$\epsilon_r = 4.4$, $h = 1.6$ mm]	182
A.3	Simulated electric field for the antenna at 2.48 GHz designed according to Table A.1. [$\epsilon_r = 4.4$, $h = 1.6$ mm]	182
A.4	Effect of variation in the width of the meander line [L = 16.1 mm, Lg = 7.4 mm, L1 = 7.6 mm, L2 = 4.5 mm, L3 = 6.25 mm, W = 10.5 mm, Wg = 7.7 mm, W1 = 1.6 mm, W2 = 3.6 mm, Sw = 2.6 mm, Sg = 0.2 mm, Cg = 0.4 mm, $\epsilon_r = 4.4$, $h = 1.6$ mm]	183

LIST OF FIGURES

A.5	Effect of variation in the gap between the meander line and the feed line [L = 16.1 mm, Lg = 7.4 mm, L1 = 7.6 mm, L2 = 4.5 mm, L3 = 6.25 mm, W = 10.5 mm, Wg = 7.7 mm, W1 = 1.6 mm, W2 = 3.6 mm, Mw = 0.5 mm, Sw = 2.6 mm, Sg = 0.2 mm, $\epsilon_r = 4.4$, h = 1.6 mm]	185
A.6	Effect of variation in the length L1 of the meander line [L = 16.1 mm, Lg = 7.4 mm, L2 = 4.5 mm, L3 = 6.25 mm, W = 10.5 mm, Wg = 7.7 mm, W1 = 1.6 mm, W2 = 3.6 mm, Mw = 0.5 mm, Sw = 2.6 mm, Sg = 0.2 mm, Cg = 0.4 mm, $\epsilon_r = 4.4$, h = 1.6 mm] . .	186
A.7	Effect of variation in the substrate thickness h of the antenna [L = 16.1 mm, Lg = 7.4 mm, L1 = 7.6 mm, L2 = 4.5 mm, L3 = 6.25 mm, W = 10.5 mm, Wg = 7.7 mm, W1 = 1.6 mm, W2 = 3.6 mm, Mw = 0.5 mm, Sw = 2.6 mm, Sg = 0.2 mm, Cg = 0.4 mm, $\epsilon_r = 4.4$]	186
A.8	Radiation pattern of the prototype antenna [L = 16.1 mm, Lg = 7.4 mm, L1 = 7.6 mm, L2 = 4.5 mm, L3 = 6.25 mm, W = 10.5 mm, Wg = 7.7 mm, W1 = 1.6 mm, W2 = 3.6 mm, Mw = 0.5 mm, Sw = 2.6 mm, Sg = 0.2 mm, Cg = 0.4 mm, $\epsilon_r = 4.4$, h = 1.6 mm]	187
A.9	Measured gain of the prototype antenna [L = 16.1 mm, Lg = 7.4 mm, L1 = 7.6 mm, L2 = 4.5 mm, L3 = 6.25 mm, W = 10.5 mm, Wg = 7.7 mm, W1 = 1.6 mm, W2 = 3.6 mm, Mw = 0.5 mm, Sw = 2.6 mm, Sg = 0.2 mm, Cg = 0.4 mm, $\epsilon_r = 4.4$, h = 1.6 mm] . .	188

LIST OF FIGURES

Chapter 1

Introduction

This chapter voyages through brief historical developments in the field of electromagnetic waves and antennas, witnessing different chronological stages of developments in antennas. Various types of antennas are covered with its relevance in the timeline.

1.1 Introduction

Science is always a wonder kid for human being. Mankind has started habituating this planet for millions of years. The five sensors have given abundant information for these long years quite enough to fascinate him. With the information that he got through those sensors, he started relating things, understating the world, finding reasoning. He came out with many theories and philosophies about the world that he has sensed. As time went on, many theories had been put forward to define the world through his understanding and still continuing. But most of the theories had many limitations. Some of the Theories failed in the microscopic level where as some in the macroscopic level. Out of the many theories proposed, electromagnetism stands out as something which has been defined properly and can work both in macroscopic and microscopic level. Electromagnetism is beyond the reach of the direct sense of our five sensors. We can only feel the effect of electric and magnetic fields. In order to look into the vast and

wide information about the universe contained in the form of these two fields, we need a second eye which opens to the universe.

The antenna is the electronic eye to this vast information field of the universe, which are beyond the direct sense of our sensors. The invention of the antenna made possible all the advancement that we see today in our space research and electronic communication industry. We see the universe, dig millions and millions of years in to our past and communicate in light speed. All these are happening with the help of this wonderful eye called Antenna.

1.2 The Journey Begins....

The journey of antenna started with the beginning of electricity back in 600 AD. When amber was rubbed against a piece of silk, sparks were found. This started the beginning of a wonderful era of electromagnetism. Later in AD 1600 William Gilbert conducted systematic experiments of electric and magnetic phenomena. He was first to recognize that earth itself is a huge magnet.

Benjamin Franklin in 1750 introduced the conservation of charges and the concept of positive and negative charges. Charles Augustine de Coulomb measured electric and magnetic forces. Contemporarily Karl Friedrich Gauss formulated divergence theorem. In 1819 Christian Oersted established the relation between electric and magnetic forces. In the mean time the world saw the rising of a laymen turned scientist, Michael Faraday. A true enthusiast who worked as a book binder at a younger age, who happened to read many scientific books that he was binding, which provoked his scientific thoughts. Faraday was hired by Humphry Davy as his laboratory assistant at the Royal Institution in 1813. Later in 1831 Michael Faraday discovered that magnetic field creates EMF. He went further and discovered, that a magnetic field influenced polarised light, in the year 1845. A phenomenon which is called magneto-optic effect or Faraday effect which led the first indication that electromagnetism and light were related.

James Clerk Maxwell, in 1864 kindled the world through his "treaties" about the dynamic nature of light [83]. He summarised the works of Hans C Oersted, Karl F. Gauss, Andre M. Ampere, Michael Faraday and others into a total of 20 equations and added his own concept of displacement current to unify the the-

ories of electric and magnetic fields. Though the work was a real breakthrough in the field of electromagnetics, the 20 Lagrange scalar equations were discouragingly complicated conceptual approach. It was the powerful insight of the London based mathematical physicists Oliver Heaviside which formulated those equations in the form of those beautiful and simple four equations that we see today. In 1884 drawing interest from Maxwell's work Heaviside unified those 20 equations into differential equations in the form of the Maxwell's equation prevalent today. Around 1888 Heinrich Rudolph Hertz discovered electromagnetic waves experimentally and verified Maxwells equations [50]. This gained him the name father of radio [67]. Hertz used an end loaded half wave dipole as a transmitting antenna and a resonant square loop as a receiver [67]. Jagdish Chander Boss in 1899 devised a detector for radio waves using a semiconductor diode [18]. Guglielmo Marconi, inspired from the works of Hertz and Boss, in 1986 demonstrated increased signalling range by Hertzian dipole (1.75 miles) using elevated areal and earth connection. Following this in 1901 Marconi performed the ever famous Trans Atlantic Experiment [45, 67]. This initiated the commercial enterprise for radio communication. This has been done with transmitting the letter S in Morse code over a distance of 700 nautical miles, making a milestone in the communication industry. The wave length used was around 600 m shorter, wave lengths which were relegated to amateurs initially, were experimented in 1921 for long distance communication by American Radio League. The wavelength used was around 200 m. Around 30 plus amateur radio stations operating in US were received at Europe. In 1930 Karl Jansky of Bell Telephone Laboratory, serendipitously discovered the presence of cosmic static while studying the atmospheric disturbance [67]. This opened the wide window of radio astronomy and Jansky has been named as the father of radio astronomy. Grote Reber, following Jansky, in 1937 made the first ever parabolic reflector antenna to be used in radio astronomy and to map the sky [57, 58, 59, 60, 67].

Following the First World War, vacuum tubes became available for transmission; continuous waves replaced spark and radio broadcasting began in the 200 to 600 meter range. During World War II, battles were supposed to be won by the side that was first to spot enemy aeroplanes, ships or submarines. The British and American scientists developed radar technology to see targets from

hundreds of miles away, even at night. This research resulted in the development of high-frequency radar antennas such as wire type antennas and aperture type (Reflector and Horn) antennas, since antenna became an essential device in the radio broadcasting, communication and radar system. Broadband antennas, circularly polarized antennas, planar antennas and active antennas etc. were subsequently developed for emerging applications and, opened new era in the development of antennas.

The three dimensional huge antennas were replaced by planar antennas with the invention of microstrip antennas by [31]. However, it took nearly 20 years to fabricate such an antenna. Their invention went in full swing with the support of the booming material science industry, producing good substrates with low loss tangent and interesting thermal and mechanical properties, improved photolithographic techniques, and better theoretical models. The development in wireless communication is rapid and highly progressive. The 1G analog systems of 1980s evolved into 2G digital technology in the 90s and to third generation of mobile communication which includes wireless multimedia services. The 3G mobile system evolved in 2002 eliminating previous incompatibilities and became a truly global system. The forthcoming 4G mobile communication systems are projected to solve the still remaining problems of 3G systems and to provide a wide diversity of new services, from high quality voice to high definition video to high data rate wireless channels. The proposed G communication system is intended to improve the throughput of the communication system. A chronological overview of the development in wireless communication are summarized in Table 1.1

Table 1.1: Chronological Overview

1837	Morse demonstration of telegraph
1865	Prediction of Electromagnetic wave propagation by Maxwell
1876	Alexander Graham Bell invented the telephone
1887	The existence of EM waves verified by Hertz
1894	Wireless Telephony by Marconi
1895	J C Boss gave his first public demonstration of EM waves
1901	Marconi's famous Trans-Atlantic Experiment
1906	Lee de Forests Radio Telephone company sold the first radio
1915	Direct telephone communications opened for service
1921	Radio dispatch service initiated for police cars in Detroit, Michigan
1924	Directive Yagi-Uda antenna developed by Prof.Hidetsugu Yagi
1927	First television transmission
1929	Microwave communication established by Andre G . Clavier
1933	Demonstration of Frequency Modulation by Armstrong
1934	AM(Amplitude Modulation)mobile communications systems used by state and municipal forces in the U.S
1935	RADAR by Watson Watt, Radio astronomy by Jansky
1943	The first telephone line from Calcutta, India to Kunming, China
1944	Telephone cable laid across the English channel
1946	Radiotelephone connections made to PSTN (Public-switched telephone network),3.7-4.2 LOS link by AT&T
1947	First Mobile phone demonstration
1953	Deep space communication proposed by John Pierce
1957	Soviet Union launches Sputnik, humanitys first artificial satellite
1958	Invention of Integrated Circuit
1968	Development of the cellular telephony concept at Bell Laboratories.
1979	A 62,000 mile telecommunications system is implemented in Saudi Arabia
1980	1G first generation - only mobile voice service
1981	Beginning of first commercial cellular mobile communication
1982	Two way video teleconferencing service started
1986	Integrated Service Digital Network deployed
1990	2G-Second generation digital cellular deployed throughout the world

1995	CDMA is introduced
2000	3G Standard is proposed
2008	ITU-R organization specified the IMT-Advanced (International Mobile Telecommunications Advanced) requirements for 4G standards
2008	4G is launched in March
2008	The South Korean IT R&D program of "5G mobile communication systems based on beam-division multiple access and relays with group cooperation" was formed
2015	The European 5G research project Flex5Gware was launched

1.2.1 Definition

The IEEE Standard Definition of Terms for Antennas (IEEE Std. 145-1983) defines the Antenna or areal as, a means for radiating and receiving radio waves. From the circuit point of view, antenna is a load impedance connected to a transmission line, with the fictitious resistance R_r called the radiation resistance. In general an antenna is a transition device or transducer, between a guided wave and a free space wave. The radiation resistance may be thought of as a virtual resistance that does not exist physically, but a quantity coupling the antenna to distant regions of space via a virtual transmission line.

1.2.2 Applications

Antennas fit into a wide range of applications, from the classical telegraphy to the more established broadcasting to the fascinating radio astronomy. 1990s were the era which enthralled the mankind with the magic wand of data and personal communication creating a boom in the market, which is now literally flooded with mobile and fixed wireless devices of various types. Other potential applications include air, maritime and space navigation, search for extra terrestrial intelligence (SETt), military, medical, disaster warning and management. The more recent commercial applications include wireless gadgets ranging from simple pagers, cell phones, RF enabled toys, car locks, PC locks, GPS, Radio frequency identification (RFID) to bio chips. Active antennas, smart (intelligent or adaptive) antennas and reconfigurable antennas are just around the corner. The boom of revisit

1. Introduction

to the metamaterial based antennas using the engineered materials opened a wide window for smaller and smarter antennas, making the gadgets smaller and smaller. With the 4G and 5G standards, MIMO antenna came in place to increase the data rate of mobile communication. The IEEE standard frequency allocation for various applications in the 0.3GHz-30GHz band is illustrated in Table 1.2

The wide range application of the antennas throughout the electromagnetic spectrum may give rise to congestion. To mitigate this, specific frequency bands are allocated to different applications. There are different governing bodies like Federal Communications Commission (FCC) to look in to the frequency band allocation and licensing issues in the modern wireless communication service. The different frequency band allocated by the governing council for smooth running of communication process is given in the Table 1.3 with corresponding category of antennas

Table 1.2: Frequency band allocation for various applications

Band	Frquency	Usage
VLF	3-30 KHz	Long distance telegraphy and navigation
LF	30-300 KHz	Aeronautical navigation service, long distance communications radio broadcasting
MF	300-3000 KHz	Regional broadcasting, AM Radio
HF	3-30 MHz	Communications, broadcasting, surveillance CB radio
VHF	30-300 MHz	Surveillance TV Broadcasting, FM radio
UHF	30-1000 MHz	Cellular communication
L	1-2 GHz	Long range surveillance, remote sensing
S	2-4 GHz	Weather, traffic control, tracking, hyperthermia Microwave Oven, WLAN
C	4-8 GHz	Weather detection, long range tracking
X	8-12 GHz	Satellite communication, missile guiding, mapping
Ku	12-18 GHz	Satellite communication, altimetry, high resolution mapping
K	18-27 GHz	Very high resolution mapping
Ka	27-40 GHz	Air port surveillance

Table 1.3: Modern Wireless Communication System

Name of the service	Allocated Frequency band	Commonly Used Antennas
Digital Video Broadcasting (DVB-H)	470 MHz-702 MHz	Compact printed antennas
Radio Frequency Identification (RFID)	865-868 MHz, 2.446-2.454 GHz	Loop, Folded-F, Patch and Monopole
Global System for Mobile GSM 900	890-960 MHz	Dipole, patch arrays and monopoles
Global Positioning System GPS1400, GPS1575	1.227-1.575 GHz, 1.565-1.585 GHz	Patch or bifilar helix
Digital Communication System DCS 1800	1.71-1.88 GHz	Dipole or stack arrays in base station, Monopoles, sleeve dipoles and patch in mobile handset
Personal Communication System PCS 1900	1.85-1.99 GHz	
International Mobile Telecommunication 2000 3G IMT 2000	1.885-2.2 GHz	
Universal Mobile Telecommunication System UMTS 2000	1.92-2.17 GHz	
Industrial, Scientific, Medical ISM 2.4 ISM 5.2 ISM 5.8	2.4-2.484 GHz 5.15-5.35 GHz 5.725-5.825 GHz	
Ultra Wide Band (UWB) Communication	3.1-10.6 GHz	Planar printed antennas, Horn antenna

1.3 Present Antenna Types and Design Techniques

1.3.1 Microstrip Antenna

The basic printed antenna, Microstrip antenna concept was first proposed in 1953 by [31] of USA. Then Byron in 1970 proposed a strip radiator separated from a ground plane by a substrate for phased array application. He used a half wavelength wide strip, fed coaxially at the radiating edges, as the basic array element [21]. The microstrip element was patented by [103] and design data about basic rectangular and circular patch antennas were published by [53]. The simple fundamental configuration of microstrip antenna with radiating metallic patch on

one side and a ground plane on other side of a substrate having uniform dielectric constant and thickness is shown in Figure 1.1. The patch conductors are normally of copper or gold and can assume any shape and its length is typically about one half of the dielectric wavelength corresponding to the resonant frequency.

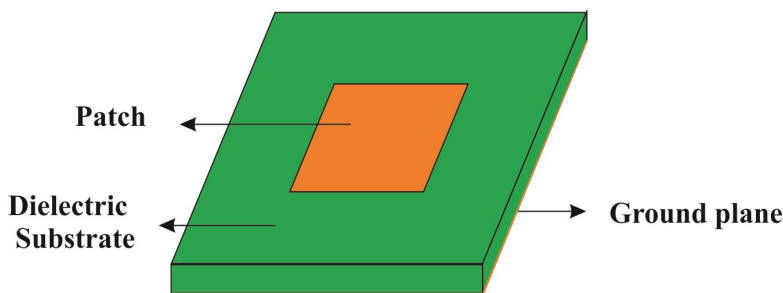


Figure 1.1: Patch Antenna

The dielectric substrate material used will determine the size and radiation characteristics of the antenna. Increasing the dielectric constant can assure compactness but lowers the bandwidth and efficiency of the antenna and vice versa. The thickness of microstrip antenna is also important in determining the resonant characteristics. As the thickness increases the bandwidth increases at the risk of exciting surface waves and vice versa. There are different schemes employed for feeding the microstrip antenna.

- Coaxial Feed or Probe feed: Usually a microstrip antenna is fed by a coaxial probe. The inner conductor of the Sub Miniature Amphenol (SMA) connector is soldered to the patch metallization through a via hole and outer conductor is attached to the back side ground.
- Microstrip Line Feed: A Microstrip line on the same substrate appears to be a natural choice to feed a patch as the patch can be considered an extension of the Microstrip line, and both can be fabricated simultaneously.
- Proximity Coupled Microstrip Feed: Proximity feed uses two substrate layers with a Microstrip line on the lower substrate, terminating in an opening below the patch which is printed on the upper substrate.

- Aperture Coupled Microstrip Feed: It consists of a Microstrip feed line on the bottom substrate coupled through a small aperture in the ground plane, to a Microstrip patch on the top substrate.

Microstrip antennas have several advantages compared to conventional microwave antennas, and therefore used for many applications covering the broad frequency range from 100MHz to 100GHz. Few advantages of microstrip antennas compared to conventional microwave antennas are[2,4,12]:

- Light weight, low volume and thin profile configuration suitable for modern wireless gadgets.
- Low fabrication cost
- Easy large scale fabrication.
- Suitable for integration with Monolithic Microwave Integrated Circuits (MMICs).
- Compatible for producing linear and circular polarization with broadside radiation with simple feed.
- Feed lines and matching circuits can be simultaneously fabricated with antenna structure.
- Dual frequency or multi frequency operation can be possible with geometry modifications.
- Dual polarization antennas can be easily made.
- No cavity backing is required.

However, microstrip antennas have some inherent disadvantages which limit the use in many wireless applications. These major demerits include

- Narrow band width and associated tolerance problems.
- Uniplanar radiation; Microstrip antennas radiate into half space.
- Lower power handling capacity and poor end fire radiation.

- Excitation of surface waves when thick substrates.
- Low gain (6dBi).
- Large ohmic loss in the feed structure of arrays.

Even though microstrip antennas have some demerits, they are widely used for lot of applications. Several other types of antennas have emerged to cater to the new varieties of application and are discussed in detail in the forthcoming sections.

1.3.2 PILA-PIFA Based Antenna

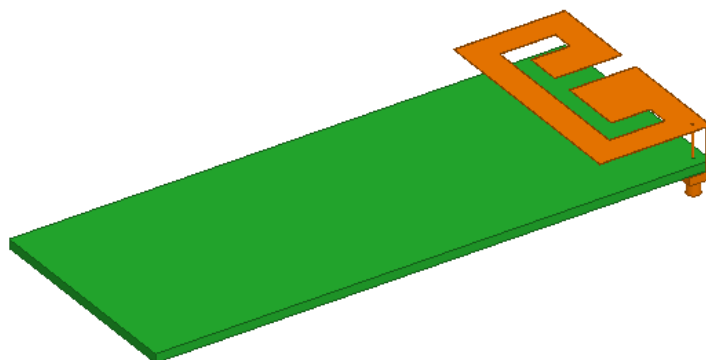


Figure 1.2: PIFA

Planar Inverted L-Antenna (PILA) and Planar Inverted F-Antenna(PIFA) are the promising alternatives for external monopoles. Small size and low profile nature of the PIFA make it an excellent choice on portable equipment. Typical geometry of a PIFA is shown in figure 1.2. The PILA/PIFA can be considered as a combination of the inverted-L/F (ILA/IFA) antenna and the short circuited rectangular microstrip antennas (SCMSA). The Inverted F Antenna and Microstrip Antenna have narrow bandwidth but their combinations resulting in PIFA have higher bandwidth to cover the popular communication bands. The basic PIFA consists of a ground plane, a top plate element, a feed wire feeding the resonating top plate, a shorting plate that is connecting the ground and the top plate at one

end of the resonating patch. Stacking and insertion of slits are included in PIFAs to create multiband operation [14, 29].

1.3.3 Metamaterial Based Antenna

Metamaterials (MTM) are artificially created materials which possess unusual electromagnetic properties. As with any other naturally occurring material, the behavioural properties of any metamaterial is defined by its basic constituent building block called the unit cell. A single unit cell defines all the properties of the new engineered material, where the size of the unit cell is very small compared to the wavelength of interest. This will keep the material within the effective homogeneity limit. Many limitations of the naturally available materials are overcome by MTM by engineering the desired property like the permittivity and permeability. It took a long time for the boom of MTM after its theoretical inception by Victor Veselago in 1968. Veselago theoretically proposed the existence of negative wave propagation and published the seminal work *The Electrodynamics of Substances with Simultaneously Negative Values of ϵ and μ* [124]. This will keep the material within the effective homogeneity limit. Many limitations of the naturally available materials are overcome by MTM by engineering the desired property like the permittivity and permeability. It took a long time for the boom of MTM after its theoretical inception by Victor Veselago in 1968. After three long decades, in 2000, D. R. Smith, experimentally demonstrated the Double Negative material (DNG) [28].

MTMs find application in many areas like cloaking, invisible metamaterials and super lens. The engineerable dispersion relation of MTM made them suitable for various guiding and radiating structures [22, 27, 34, 35, 81]. MTM based antennas are a class of antennas inspired by MTM to enhance their capabilities or to achieve novel functions. They are broadly divided into two categories,

- Leaky Wave Antennas (LWA)
- Resonator type antennas.

In LWA the guided waves leak away in the form of radiation and are implemented by Composite Right Left Handed Transmission Lines (CRLH-TL),

enabling the backward to forward beam scanning with the broadside radiation [12, 23, 38, 66]. Antenna size miniaturisation with good radiation characteristics is the main and attractive advantage of MTM based antennas. The efficiency-bandwidth limitation can be overcome by MTM antennas. The MTM antennas are classified as,

- CRLH based or dispersion engineered resonant antennas. This includes the antennas with negative order modes and zeroth order resonators.
- Miniature antennas based on the metamaterial loading, such as epsilon/mu-negative materials, high permittivity shells and the magnetic photonic crystals.
- Metaresonator antennas, particularly for the antennas based on the split ring resonators (SRRs) and complementary split ring resonators (CSRRs).
- Antenna loaded with metasurfaces such as the electromagnetic band gap (EBG) mushroom structures or patch type reactive impedance surface (RIS).

1.3.4 Photonic Band Gap Based Antenna

A Photonic Band Gap (PBG) material is a periodic dielectric, ferromagnetic, ferroelectric or metallic structure which is used to control and manipulate the propagation of electromagnetic waves. Initial PBG researches have been done on optical region but can be extended into a wide range of frequencies. A standard antenna printed on a substrate radiates a fair amount of energy into the substrate. If one uses a substrate of PBG material whose stopband includes the operating frequency of the antenna, most of the energy radiated into the substrate is reflected back to the free space, and thus the radiation efficiency is improved. The PBG structures can be used to modify the radiation pattern and to improve the gain of conventional Microstrip antennas. PBG structures are also known as high impedance surface due to their ability to suppress surface waves at certain operational frequencies. Recently there has been increasing interest in the microwave and millimeter wave application of Photonic Band Gap structures. Literature has various designs of PBG structures for bandwidth enhancement, size reduction, suppression of unwanted harmonics, reduction of cross polarization etc..

1.3.5 LTCC Based Antenna

The Low Temperature Co-fired Ceramic (LTCC) technology can be defined as a way to produce multilayer circuits with the help of single tapes, which are to be used to apply conductive, dielectric and / or resistive pastes on. These different single sheets (50-250 μ m) have to be laminated together and fired in one step. This saves time, money and reduces circuits dimensions. Another great advantage is that every single layer can be inspected (and in the case of inaccuracy or damage) and replaced before firing; this prevents the need of manufacturing a whole new circuit. LTCC makes it possible to pack the filters and other components used in a mobile phone into a package having dimensions of few mm³. These LTCC technologies are viable alternative for miniaturization technique. Lot of ultra compact antennas are available in the literature utilizing this technology [95].

1.3.6 Small Antennas

Small antennas are categories whose overall size is small compared to its operating frequency. The very first antenna used by Marconi for the trans-atlantic ocean communication was an Electrically Small Antenna (ESA). The antenna appeared to be very large, as it was hung by two masts 48 meters high and 60 meters apart so that it could never be considered small [41]; however, since the dimensions were a small fraction of wavelength (about 1/6 of the operating wavelength, 366 meters), it was electrically small. With the advent of technology in almost all areas of science and technology, the frequency used for the telecommunication has been gradually raised from MF and HF band to SHF band. The development, particularly in the semiconductor technology which was mainly concentrated on miniaturization promoted the use of higher frequencies and smaller devices. This trend in technology over years resulted in the development of many handheld mobile communication systems. Sensing and medical equipments demanding for miniaturization of antenna systems with improved functioning and further sophistication. The latest application of small antennas is in the mobile communication industry where the technology has reached from 1st generation to 5th generation over years. In the 5th generation a single handset required more number of antennas in it to improve the data rate of communication, since most

of them use MIMO technology.

1.3.6.1 Why Small Antennas?

The importance of small antenna is evident from its inevitable demand in various wireless systems. For any wireless system, even if all the circuitry can be integrated into a single chip, at the end the component which decides the compactness and efficiency is the antenna, without which no wireless communication is possible. In the earlier days of communication when vacuum tubes were not available, antennas were used for improving the communication range. In those days most of the antennas used were electrically small antennas, because the frequency range used for the communication were MF and HF bands. In the last few decades the advancements in the communication industry has started using frequencies in the higher microwave frequency region. In this microwave frequency range the antennas are normally small in size as the wavelength is very small. The advent of planar antennas furthered the development in small antennas. The recent development in the mobile communication technology with 4G in place the communication industry forces more number antennas to be placed in a small package without having much coupling among them. For this to happen, the antenna should be compact enough to fit into the space perfectly. Downsizing an antenna without degrading its performance is the most challenging concern for an antenna designer. There is always a trade-off between the antenna size and its performance. The biggest concern in the small antenna design is how to minimize this trade off by retaining the antenna performance. These small antennas are mainly classified in to four different types as Electrically Small Antennas (ESA), Physically Constrained Small Antennas (PCSA), Functionally Small Antennas (FSA) and Physically Small Antennas (PSA) [41]

1.3.6.2 Electrically Small Antenna (ESA)

An ESA is an antenna conventionally defined as an electrically small-sized antenna; i.e., one having dimensions much smaller than the wavelength. However, this definition is unclear, since the dimensions are not described precisely.

Wheeler defined the ESA as an antenna having the maximum size that can be circumscribed by a radian sphere, with a radius of one radian in length ($=\lambda/2\pi$) [128]. However, an antenna having the maximum dimension of a radian length may not necessarily be categorized as an ESA, because taking a dipole antenna as an example which has the length of a radian length, $2 * \lambda/2\pi (= 0.32\lambda)$ it can no longer be called electrically small, as the size becomes no longer a small fraction of the wavelength. Hence classifying the radian-length dipole antenna as an ESA is not reasonable. There was another definition for ESA that was an antenna having dimension not greater than one eighth of a wavelength [41]. One more definition was given by King, who used the term very short antenna for ESA, that referred to an antenna having the length in terms of $ka < 0.5$, where a : half-length of a thin linear dipole, $k = 2\pi/\lambda$ [41]. This is the best followed definition for ESA. The major principles for realising an ESA are

- Lowering the resonance frequency for an antenna of given dimensions
- Full use of space or volume circumscribing the maximum dimension of an antenna
- Arranging for uniform current distributions on the antenna element
- Increasing the number of radiation modes in an antenna structure.

1.3.6.3 Physically Constrained Small Antenna (PCSA)

A PCSA is an antenna, not having dimensions of ESA, but a part of which has dimensions corresponding to the ESA [41]. A low-profile antenna, for example, with the height over the ground plane or the thickness of say $\lambda/50$ or so, like an Inverted-L antenna, planar antennas such as a patch antenna, a microstrip antenna (MSA), and so forth, can be classified into Physically Constrained Small Antenna (PCSA) [41].

1.3.6.4 Functionally Small Antenna (FSA)

Another classification of small antennas relates to antenna functions. When an antenna can attain either additional functions or enhanced performances with the

dimensions being kept unchanged, it can be said to have an equivalent reduction in the antenna size, because with normal antennas such enhanced function or improved performance could result only from enlargement of dimensions [41]. An example is an antenna designed to have wide band, multiband performance, radiation pattern shaping, and array thinning without any change in the dimensions. This class of antenna is referred to as Functionally Small Antenna (FSA) [41].

1.3.6.5 Physically Small Antenna (PSA)

A Physically Small Antenna (PSA) is an antenna, which differs from any of the above, but has physically small dimensions as measured. When the volume of an antenna is bounded by 30 cm or less, we may call the antenna a PSA [41]. There is not any strict physical meaning in the definition, but only a sensual measure based on the common understanding of smallness in physical size. An example is a millimeter-wave horn antenna with an aperture size of, say 5 cm approximately. Many of the MSAs may be classified into either PCSA or PSA [41].

1.3.7 Motivation of Current Research

The ultimate aim of an antenna design is to make a structure radiate the energy into the space. Many such attempts have been in place in literature for a long time. Any structure which can create a change in the acceleration of the electrons causes radiation. It can be either acceleration or a deceleration.

Modification of transmission line is an effective method widely used in antenna design. A discontinuity created in a transmission line causes a change in the electron acceleration there by producing an effective electromagnetic radiation. For eg: a dipole antenna is designed by introducing a flaring in a two line transmission line where as a horn antenna is designed by introducing the flaring in a rectangular waveguide.

Microstrip antenna technology is the pioneer in the printed antenna technology. This invention has revolutionised the wireless communication technology and drawn great attention from mobile wireless system designers, which is an

extension of the microstrip transmission line.

Modern communication technology demands for compact equipment which is very handy. ISM bands are widely used in the industry, scientific and medical areas. The 2.4 GHz and 5-6 GHz bands are in greater demand for many of such applications. The 2.4 GHz is widely used in mobile phones, Bluetooth, WiFi networks, car alarms, microwave oven, video devices, ZigBee etc. This band provides 13 overlapping channels in general and a 14th channel used only in Japan. This band has been approved worldwide. 5-6 GHz band provides 23 non overlapping channels. The latest wireless network standard IEEE 802.11n, published in 2009, supports both 2.4 and 5-6 GHz bands. All these advancements in the technology demand for compact size antennas with good performance. Planar antenna technology had provided a seamless transition from the electronics circuit board to the antenna.

Semiconductor technology has travelled miles and miles in terms of miniaturisation. Different technologies emerged in fabrication process has helped in making components which were once very large in size to very compact. This evoked the thought of the possibility of embedding such a device in the antenna design. An attempt is made to make an electrically small antenna with the help of a surface mounted wire wound inductor. One such antenna is proposed and its analysis is given in the thesis.

Planar microwave filter technology is a well grown field. There Stepped Impedance Resonators (SIR) play a major role in the filtering. They are resonators with more number of control parameters for a designer, which occupies a very small metal area as compared to other type of resonators. SIR is also an extended version of transmission line. Moreover in SIR it is possible to maintain a non integer relationship between the fundamental frequency and the harmonics.

Considering all the aforesaid peculiarities, I am interested in modifying a planar dipole antenna along with a SIR to an efficient and effective radiator. The very first modification done on the conventional planar dipole is by bending the dipole which works in the 5 GHz band with a sufficient bandwidth. The second aim was to make the SIR, which is generally considered as a resonator, to a radiating structure. For that the planar dipole is top loaded with a SIR, which is totally a variant of the conventionally employed microstrip based SIR. Another attempt

1. Introduction

is made to excite a conventional SIR to radiate electromagnetic energy. This antenna is proposed as a frequency reconfigurable antenna, where two different modes of operations are considered for two different frequency bands. The lower band is based on SIR whereas the higher band is radiating based on Fabry-Perot mode.

Chapter 2

Literature Review & Methodology

2.1 Instant peep - Small Antennas

The quest for compact antennas is on a greater demand from a very long time. Small antennas are prevalent from the beginning of the invention of antennas, with the first commercial antenna used by Marconi for the Trans-Atlantic experiment. At that time the urge for a small antenna was not that important since the frequency used for communication was in the Medium Frequency (MF) range. When the frequency used for the wireless communication is translated to the higher end of the frequency spectrum, and with the introduction of planar antenna structures, the physical dimension of the antenna gradually reduced. As the physical dimension of the antenna reduced, the metalization area of the antenna reduced causing a diminution in the radiation resistance of the antenna, which makes the antenna less efficient. The quality factor for such antennas are high, resulting in a very narrow operational bandwidth. With this trade off, the realization of electrically small antenna in the high frequency range, on a planar substrate, having a finite $\tan(\delta)$ became a tedious task. Many methods have been proposed for designing small antennas and for the improvement of its performance.

2. Literature Review & Methodology

J T Bolljahn and R F Reese did a brief analysis based upon quasi-static principle on the properties of electrically small antennas in 1953 in connection with the design of low frequency aircraft antennas, [102].

To improve the performance of electrically small antennas, an impedance matching method was proposed by [127], which used conventional methods for getting maximum power transfer. An L matching circuit is used for this purpose, showing one fixed and one variable tuning element is adequate for certain small antennas. V. H. Rumsey and W. L. Weeks of University of Illinois has framed approximate formula for the impedance, efficiency and quality factor (Q) of electrically small, ferrite loaded loop antennas [109].

For the first time, in 1959 McCann used an electrically small antenna for direction finding [84]. This antenna has a size restricted to a cylindrical volume approximately 0.15λ in diameter and 0.35λ in length at the lowest operating frequency. The antenna consists of two metallic cylinders consisting two diametrically opposed slots with a polarization at an angle of 45° from vertical

In the year 1965 R. C. Fenwick introduced a new class of electrically small antennas. They possess the advantage of having resistive input impedance, radiation resistance transformation which may be obtained from the structure itself and a vast variety of shapes the antenna can take [40].

In the year 1970 D. H Shreve and G. A. Thiele of ElectroScience Laboratory at the Ohio State University developed a new electrically small antenna for application as an exciter element in vehicular antenna system [120]. The antenna consists of a long conductor coiled into several turns. Glenn S. Smith calculated the efficiency of the antenna used in the upper atmosphere propagation experiment, which is mounted in the nose cone of a high altitude rocket [115, 116]. Later in 1977 DeVore formulated an analytical model for the multiturn loop antenna and modified this antenna by inserting a magnetic core into the loop [17], achieving a transmitted signal enhancement of 10 dB. The experiment was conducted in the 3-86 MHz range.

2. Literature Review & Methodology

In 1971 D. Otto showed that in the case of a tubular cylindrical antenna with length to radius ratio is $O(1)$ or smaller can be reduced into simple singular equation having the form of elementary functions [97].

An analysis of the design of efficient regenerative broad band electrically small folded dipole antenna is presented by [122].

Le Huy Hoang and Martin Fournier in 1972 studied the performance of electrically small antennas under noisy condition. They formulated the method to derive the Signal to Noise ratio and compared it with the ideal case [74].

Chamler M. Butler, in 1974 formulated the integral equation for an electrically small aperture in a conducting screen. The formulation is based on Rayleigh series expansion and potential theory [20].

Two different approximate methods for analyzing electrically small circular loop antenna in a dissipative medium is introduced and are compared with a twenty term fourier series method and applied necessary corrections by Glenn S. [117]. In the very next year the efficiency of a cassegrain antenna is enhanced, by shaping the reflector with the help of ray optics, by [19]. In the same year Glenn S. Smith determined the efficiency of electrically small antennas combined with matching network with the help of principle of conservation of energy [11]. He analyzed the condition for attaining maximum efficiency and found that for most of the ESA, the maximum efficiency can be met using L-section matching network.

A comprehensive analysis of the electrically-small material-clad monopole is performed by representing the various fields by discrete and continuous eigenvalue spectrum by [55]. The cladding creates a dominant quarter-wavelength resonant-cavity effect whereby the leakage of radiation at the terminal plane is transformed into low impedance at the annular feed. The mode coupling taking place at both feed and terminal plane is solved by variational methods to yield the antenna radiation pattern, bandwidth, efficiency and input impedance as a function of

2. Literature Review & Methodology

electrical size and frequency.

Krall introduced a new electrically small antenna using a shorted microstrip quarter wave resonator. The strip is wrapped around a cylinder, producing an omni directional radiation pattern normal to the axis of the cylinder [85].

David C Chang calculated the input conductance of an ESA based on the effective aperture area by relating the conductance at the feed point to an integral involving the magnitude of the short circuit current at the same point [104].

The electrically small antennas used in the HF, which is operated in association with the frequency hopping technique having a narrow band operation, is made to appear broadband by [94]. A frequency hopping antenna matching technique is used for achieving this broadband operation.

Maeda [77] proposed and experimentally verified a method to calculate the radiation efficiency of an electrically small antenna integrated in a practical circuit, taking consideration of the human body effect coming in contact with the device. The method utilized the indoor Random Field Measurement (RFM), which is an extended version of RFM proposed by [6], and only simulation results were reported till then. He gave a practical verification for RFM [77].

A complete RLC equivalent circuit for an electrically small antenna is presented using a single quasi-static solution by Simpson. This provided a precise definition of circuit parameters limiting the performance of ESA [105].

Khamas showed the significance of matching network in the performance enhancement of ESA when supercooled. He showed when the tuning and matching networks are supercooled, there is only negligible improvement in the antenna performance for an actual radiating dipole element and a modest improvement is obtained in the case of a loop [65].

John P. Casey conducted a theoretical and experimental study on small an-

2. Literature Review & Methodology

tennas. The study was based on a quasi-static numerical study of a conducting body of revolution above a perfectly conducting ground plane [24].

A three loop method for determining the radiation characteristics of an electrically small source is presented by Motohisha Kanda. Three loop antennas are arranged orthogonally terminated with identical loads at diametrically opposite points. The electrically small source is kept at the center of the loops, which is represented by equivalent electric and magnetic dipole moments [51].

Different methods are available in the literature for the input impedance calculation of insulated monopole or dipole, embedded with in an electrically dense medium. These methods differ by the applied degree in the approximation of the current calculation of the insulated conductor which effects the wave number and the characteristics impedance calculation of the antenna. For electrically longer antennas, an additional term in the formula improves the numerically calculated values, making closer to the measured one. But in the case of electrically small antennas, this term introduces significant error in the numerical result. Debicki introduced two different methods to correct this error in the calculation of input impedance of electrically small antennas [30].

Electrically small antennas have an inherent difficulty in achieving good efficiency, because of the high loss resistance in comparison with the radiation resistance of the antenna. A solution to improve the efficiency is by reducing the loss resistance below the radiation resistance of the antenna. For normal materials the reactive current and there by the I^2R loss will be high. The use of High Temperature Superconducting (HTS) materials can significantly reduce the surface resistance below the small radiation resistance, there by increasing the efficiency. Donald R. Bowling fabricated a three element super directive array of electrically small HTS half loops at 500 MHz using YBCO and TlBaCaCuO HTS materials [32]. The performance analysis of an electrically small printed thin film $\text{YBa}_2\text{Cu}_3\text{O}_{7-x}$ antenna is carried out by [90]. Four efficient designs with different feeding techniques are used for the analysis. The numerical estimation of loss mechanism and the assessment of overall efficiency is carried using microwave

2. Literature Review & Methodology

network analysis and method of moments.

A study is conducted on the Radar Cross Section of YBCO HTS based small circular loop as a function of applied magnetic field strength by Cook. It reviews the change in RCS with applied magnetic field and the radiation resistance. Increase in surface resistance with magnetic field and detuning effect caused by a change in the loop input reactance are identified as two factors causing the RCS reduction [114].

McLean analysed electrically small compound antenna with collocated electric and magnetic dipole using method of moments. He considered two configurations with two different orientations, i.e. with aligned and orthogonal dipole moments. The orthogonal configuration is found to be in a category of antennas where handed-down radiation Q limit do not apply [86]. Grimes discussed possible methods to get efficient radiation from an electrically small antenna and the control of higher order modes. The findings disclose the limitation of the use of time domain pointing vector to only fields generated by either TE or TM sources and it fails with sources with both fields. Further, the falsification of the relation that "Q increases with the decrease in size of the antenna" is done and showed that the increase in the Q is not as swift as believed. For sources with both TE and TM fields, the input impedance is purely resistive and independent of electrical size [46]. An exact method for the calculation of the Q of electrically small antennas is proposed by McLean. The derived expression is in good agreement with the then existing approximate equation in the lower end of electrical size, where as for the higher end of the electrical size, the expression given is entirely new one [87].

A meandered line as an electrically small antenna is used to get a better feeding point for impedance matching circuit for the purpose of improving the performance of ESA [126].

Overfelt determined the electric lines of force of an electrically small dipole loop antenna array for both near and far field. He related the field contours

2. Literature Review & Methodology

with a coupling parameter, which is taken as a ratio between loop and dipole size and currents. The coupling parameter has a hand in controlling the point of equilibrium of radiated fields analysed on a real phase plane [98]

Foltz put forward the lower limit on Q of a vertically polarized antenna required to fit in regions bounded by a prolate spheroid. The limits are formulated by determining equivalent circuits for the transverse magnetic spheroidal wave function outside the bounding spheroid [48].

The invention of Microstrip antenna was a break through in the field of communication. This made possible the seamless integration of antennas with the modern communication circuitry, by facilitating the component mounting and the antenna fabrication on the same substrate material. When it comes to the fabrication of low frequency antennas, microstrip patch antenna size becomes huge. Choon Sae Lee introduced an electrically small microstrip antenna and the same technique is extended to cylindrical structure [93].

A printed antenna with multiple resonance is introduced by [64]. When considering the lowest frequency, the antenna is 5 times smaller than a conventional microstrip patch antenna.

Genetic algorithm (GA) has been widely used in the design of small antennas, especially electrically small antennas. Edward E. Altshuler used genetic algorithm in the optimization of small self resonant wire antenna, which otherwise are inefficient and require matching networks to tap the best possible radiation. The use of genetic algorithm searched for resonant wire shape that best utilize the volume in which the antenna is confined [5]. Hosung Choo furthered Altshuler's work by emphasizing on the bandwidth and efficiency of the antenna. Pareto GA is used for optimizing the antenna for bandwidth, efficiency and size [106]. Further study by Choo contributed the implementation of the inductive coupling concept to planar structures viz. meander shaped windings and spiral shaped windings [107, 108].

2. Literature Review & Methodology

It was in 2000 the intellectual foresight of Victor [125], who theoretically put forward the possibility of the existence of metamaterial in 1968, came to exist [2]. It took decades to practically implement the metamaterials. This invention made a boom in different areas of science and technology, and the boom rippled into the microwave antenna research area with its eye catching backward wave propagation property. The negative permittivity, permeability and double negative engineered structures entered the field of electrically small antennas. Richard W. Ziolkowski investigated the possibility of improving the radiation efficiency of an electrically small elementary dipole antenna. The reactance power of an elementary dipole ESA is greater than the power radiated. The application of a Double Negative (DNG) structure, having a negative propagation constant, as a shell to the antenna, added inductive reactance and made the reactive power less than the power radiated making the antenna more efficient [137, 138]. Following this, J. S. Petko used Negative Index Material (NIM) to load a cavity to reduce the size of a circular microstrip patch antenna [101]. David A. Tonn pondered the practical feasibility of the method of improving the radiation efficiency put forward by Ziolkowski on a physically realizable antenna. This has been proved on a short monopole over an infinite ground plane [121]. The DNG shell surrounding a cylindrical dipole antenna is replaced by layers of ENG shells to attain radiated power enhancement. This is achieved by making reactive power very low by nullifying the capacitive reactance of the antenna with the inductance of the ENG shell [37]. A negative permittivity based resonator is used for getting an ESA, and a quasi-static analysis is performed by [52]. An analysis based on Method of Moment is carried out to characterise a metamaterial based ESA, considering magneto-dielectric and negative permittivity materials for constructing the antenna by [42]. A two dimensional lumped capacitor based metamaterial inspired electrically small antenna is introduced by [36]. This antenna can scaled to operate at different frequencies by changing the capacitance value. A negative permeability based ESA is presented by [112], in which a hemispherical negative permeability resonator excited by a slot aperture is characterised by Green's function analysis using Method of Moments (MoM)

A novel miniaturized planar antenna using split ring resonator based cell is presented by Meng Li. The antenna offered good performance instead of its low

2. Literature Review & Methodology

profile [88]

Andrew J. Campston developed a propagation formula, which is applicable in both near and far field. From this formula the fundamental limit of antenna gain is found out, which is limited by the electrical size of the antenna [7].

An electrically small coplanar wave guide fed folded slot antenna, which is loaded with capacitors to reduce the size is presented by [82]. The antenna is fabricated on a Rogers Duroid substrate providing a good return loss and gain.

A novel MEMS antenna for biomedical application is introduced by [70]. The antenna is very small covering an area of 1.5 x 1.5 mm². The antenna uses a carrier in the KHz range to receive the signals.

Hiroyuki Arai presented antenna clearance, which is considered as one of the index factor for electrical size of small antennas. The antenna clearance is defined as the minimum space for an antenna operation without effected by the disturbance [9]. For the definition, variation ratio of input impedance of the antenna is considered. The variation ratio in the input impedance is defined as

$$\delta = \frac{|Z_i - Z_{if}|}{Z_{if}} \quad (2.1)$$

where Z_{if} is the input impedance in free space and Z_i in presence of conducting wire.

A compact multiband folded loop chip antenna for small-size mobile phone is presented by [133]. This antenna is of size 40 x 5 x 5 mm³ on a ground plane of 60 mm. This is highly suited for small sized mobile phone applications. This antenna supports 900 MHz GSM band and 1900 MHz band used for DCS/PCS/UMTS operation with a gain of -1.5 dBi - 0.5 dBi in the GSM band and 0.7 - 2.3 dBi in the DCS/PCS/UMTS band.

An optimal design for broadband matching network for ESA is introduced by [134]. For the optimization purpose, two methods viz, real frequency method and direct numerical optimization are combined and used. A comparative study of the performance of the broadband matching network designed using two methods is also performed.

Andrew J. Compston derived the fundamental limit on antenna gain for electrically small antennas [8]. The derived equation is compared with measurement

2. Literature Review & Methodology

taken on a number of different antennas. The equation applicable on both near and far fields are developed and using these results, it is showed that the gain of the antenna is limited by its electrical size.

In 2008 Bo Zaho presented an ESA using the negative permittivity and permeability simultaneously, i.e., combining negative ϵ and μ with the natural materials. The combined structure forming a transmission line is known as Composite Right Left Handed (CRLH) transmission line. Using this CRLH microstrip transmission line, they presented a Zeroth Order Resonator (ZOR) antenna [16]. The resonance of a ZOR antenna do not depends on the physical dimension. The antenna resonates at 915 MHz and 2.4 GHz

Metamaterial inspired 2D and 3D scalable electrically small antenna is presented by [10]. The antenna achieved natural matching to 50Ω source without the introduction of any matching network.

An electrically small TE mode magnetic dipole antenna with low Q is presented by [15]. The antenna is designed on a hollow copper sphere by introducing slots, which is a complementary to electric dipole folded spherical helix antenna. The radiation pattern achieved is omni directional.

A tuning method for electrically small antenna with low Q, without the introduction of any external matching network is introduced by [54]. The antenna is excited in TM_{10} mode with suppressed higher order modes.

A study on the quality factor Q of a magneto-dielectric radiator is carried out by [96]. They used the current distribution of a practical antenna for TE_{10} magnetic dipole field. The spherical surface enclosing a magneto dielectric material serve to reduce the internal stored energy. A closed form expression is derived for the internal stored energy and quality factor. The effect of sphere radius, permittivity and permeability on Q is determined and verified numerically. An optimum permeability for the lowest Q is found for an antenna of given size and permittivity. It is observed that the smaller the antenna, the Q approaches closer to the Chu's lower bound Q for a permittivity of 1 and optimum permeability.

Negative Impedance Converters (NICs), are proposed by [33] to improve the radiation characteristics of small antennas. The NIC is incorporated to improve the bandwidth and efficiency short falls of metamaterial based antennas.

Milan Polivka conducted a detailed analysis on impedance and radiation effi-

ciency properties of two electrically small antennas, namely a double and triple split ring antennas for UHF RFID applications, respectively [89]. It is concluded that the triple split ring resonator has the advantage of keeping the same impedance properties with enhanced radiation efficiency with a smaller real estate over the double split ring resonator antenna. A comparison on the measured data of both antennas are provided.

A comprehensive investigation of time domain behavior of high Q small size resonant type antennas are conducted by [91]. Equivalent circuits of radial wave impedance for spherical modes are used for establishing the concept of energy storage and its relation with size and Q factor. A planar inverted F antenna is used for the study of impact of antenna structure on field response. An RLC circuit with same value of Q is used for the study of transient response of antenna

2.2 Dual Band Antennas

The fast growing modern wireless communication technology is in greater demand for the use of different application bands comprehended in a single device, since most of the modern devices uses multiple communication technologies in a single hand set. The real estate management of these devices can not handle individual antennas for this purpose, and instead urge for a single antenna which can operate in different application bands by restricting itself into smaller area. Many such devices requires antennas working in 2.4 GHz and 5-6 GHz bands. For complying this requirement, many dual band antennas using different methods can be seen in literature.

A novel dual band circular microstrip antenna is presented by [56]. The antenna operates in 2.4 and 5.2 GHz band, which is achieved by embedding an offset open ring slot in circular patch. Mari Komulainen designed a dual band antenna in the same frequency bands using a rectangular patch antenna by introducing a slot in it [80]. Two different dual band PIFA working in the GSM/DCS bands are introduced by [130]. The first antenna comprises of three different coplanar elements whereas the second antenna is used a driven smaller patch along with a parasitic larger patch for achieving the dual resonance. Another simple dual band

2. Literature Review & Methodology

inverted F antenna operating in the UNNI band is introduced by [63]. A new dual band antenna for WLAN applications, inspired from PIFA and meander line structure is introduced by [49]. Unlike PIFA the structure has no ground plane under the radiating element, and at the same time, the meander line is shorted to the ground. A dual band PIFA for WLAN and Bluetooth on a foam substrate with a U shaped slot on top plate is introduced by [43].

A novel chip type ceramic dielectric antenna is introduced by [44], resonating in the 2.4 and 5.8 GHz bands. The antenna is made from an alumina dielectric on a 1.52 mm thickness substrate located at the corner of the substrate. Another compact dual band PIFA antenna on a FR4 substrate is proposed by [99]. A single layer strip fed printed monopole antenna introduced by [72] is operating in the 2.4 and 5.8 GHz bands. The serial slot and end stepped feed trip structure provides the dual band operation. A high gain dual band antenna in the 2.4/5.8 GHz band is proposed by [71]. The antenna provides a gain of 5.9 dBi in 2.4 GHz and 4 dBi in 5.8 GHz. The antenna consists of two strip dipoles printed on a thin substrate. A planar chip antenna for 2.4/5.2 GHz band is presented by [39], where an insert modeling approach is used to manufacture the antenna. The chip antenna is formed by enclosing the meander strip with liquid crystal polyester. A dual band patch antenna suitable for implementing in laptops working in 2.4/5.2 GHz bands is proposed by [100]. It radiates in an omnidirectional back to back radiation pattern in spite of the large ground provided by the TFT panel of the antenna. The antenna has an independent tunable frequencies with a broad range ratio of 1.2 - 3.5 with no change in the patch external dimensions. A dual band dual polarized antenna operating in the 2.4/5.8 GHz is presented by [136]. Another dual band dual polarized antenna operating in 2.4/5.8 GHz band is proposed for Body Area Network (BAN) by [132]. It is based on a circular patch type antenna with polarization parallel to the body surface. A dual band hybrid dielectric resonating antenna with a CPW fed planar monopole and a circular disk shaped high permittivity dielectric resonator is proposed by [76]. The antenna operates in the ISM and UNNI bands with a peak gain of 5.17 dBi and 7.88 dBi respectively. A CPW fed square loop printed antenna operating in 2.4/3.4 GHz band is proposed by [111]. A dual band diamond shaped antenna is proposed for RFID applications which operates in the 902-920 MHz UHF band and 2.4-2.5

GHz ISM band [92]. The shape and size of the radiating element determines the resonant frequency of the antenna. The antenna has a good radiation properties with 7.8 dBi gain in lower band and 9.4 dBi gain in the higher band. Li-Jie Xu proposed an implantable dual band inverted F antenna with an open end slot on ground [1]. It operates at 402 MHz, 433 MHz and 2.4 GHz bands.

Stepped impedance resonators are widely used in the design of filters. They are employed in Ultra Wide Band antennas for getting band notch. SIRs rarely find application as a main radiator. Though SIR is a very old candidate in the field of Microwave Engineering, literature is scant of antennas with SIR as main radiator.

2.3 Methodology

In the development of a novel antenna, the antenna is first designed with the prior knowledge gained from the existing literature and then the antenna is transformed to a prototype for testing in the real environment.

2.3.1 Right substrate

The design of a planar antenna start with the selection of the right substrate material. The selection is based on certain key parameters of the material which will effect the performance of the antenna at the selected frequency of operation. For efficient radiation, the substrate material should possess low dielectric constant and low dielectric losses which in turn reduces propagation delay and speed up the signal flow. The use of substrate with high dielectric constant will increase the chances for surface wave excitation and in turn low bandwidth performance. With high loss tangent, the efficiency of the antenna goes down. Another important factors which are taken into consideration are the cost of the material and the availability. The material should have good thermal conductivity to dissipate the heat generated and should possess good mechanical stability, as required by specific applications. For the prototyping purpose of the antenna, the substrate material selected is the widely used FR4 material.

2.3.2 Photo lithography

To realize the designed structure, the blueprint is transferred on to the selected substrate. This transfer of blueprint requires a good amount of precision, because the dimensions chosen in the design of the antenna at the selected frequency will be critical. Because of this criticality, photo lithography or optical lithography is selected for this purpose. Light is the key content in the transfer of design on to the substrate. The small wavelength of light gives the required precision, and UV light is used for this purpose. The process involves the transfer of design through a photo mask on to the metal surface.

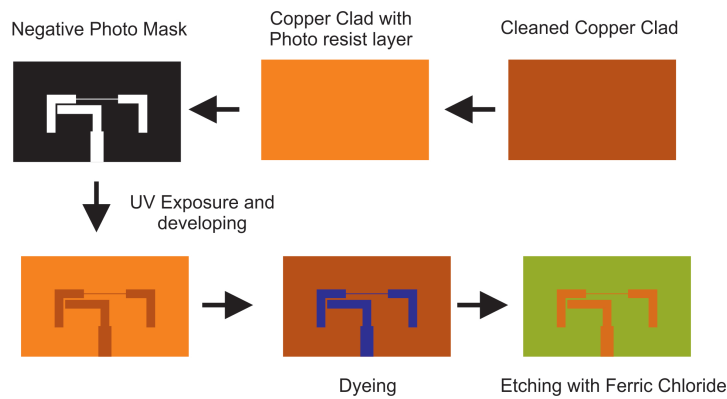


Figure 2.1: Photo lithographic process

To begin the process, the FR4 substrate is first chemically cleaned with acetone or chloroform to get rid of the impurities present on the metal surface. A thin layer of photo resist is applied over the cleaned surface. This process is done with a spinner in order to get an evenly distributed coating on the metal surface. There are two types of photo resists available. The positive photo resist, when exposed to UV light become more soluble in developer solution where as the negative resist gets harden and less soluble in developer on exposure to UV light. While using the positive photo resist to transfer the structure on to the substrate, the photo mask is an exact copy of the design, on contrary, for a negative resist the mask is an inverted version of the design. The Photo resist coated substrate is exposed to UV light through this mask and then the resist is removed from the

substrate using developer solution, leaving back a window at those areas where the metal has to be removed. The substrate is then treated with Ferric Chloride solution, which removes the metal from unwanted areas. The different steps involved are shown in Figure 2.1.

2.3.3 Amenities for antenna measurement

All the measurements of the antenna are carried out using a network analyzer from Agilent. The measurement of gain and radiation pattern of the antenna is conducted inside an anechoic chamber. To ease the measurement procedure, indigenously developed proprietary software is used.

2.3.3.1 Network Analyzer

Network Analyzer plays a crucial role in the analysis of a microwave antenna. To analyse any microwave structure it is necessary to measure the parameters associated with it. Usually for electronics devices the quantifying quantities are the associated voltages and currents. But at high frequency, it will be very difficult to quantify these two parameters accurately as the frequency goes high the lumped parameters will become distributed and as the size of the device become comparable to the wavelength, small variations in the measurement locations will result in considerable changes in the measured voltages and currents. On the other hand, at high frequency, power is more quantifiable than voltage and current. Due to this, for characterising a device at microwave frequency, scattering matrix, also known as s parameters, which are measured based on power and matched loads are employed for measurements. Network analysers are used for measuring s parameters. On broad classification, network analysers are divided into two

- Scalar Network Analyser (SNA)
- Vector Network Analyser (VNA)

A SNA measures the amplitude property only whereas the VNA measures both amplitude and phase properties.

The network analyser mainly consist of

2. Literature Review & Methodology

- Signal generator
- Test set
- Receiver
- Processor and Display

The use of a Network Analyser makes the measurements at different microwave frequencies easier. It enables us to characterise the Device Under Test (DUT) over a wide range of frequencies in a single measurement. The test signals for the analysis is generated using a signal generator. In the older Network Analysers, the signal generators were a separate entity connected through GPIB. But in the modern device, they are integrated together. The test set paves the path between the Network Analyser and the DUT. It takes the signal generator output to the DUT and back to the receiver. The measurements are made using the receivers connected to the test ports. After the measurements are made, it should be displayed in an interpretable format. Processor and display unit does this in a sophisticated way where it displays the reflection and transmission data in different format. Figure 2.2 shows the basic block diagram of a Network Analyser

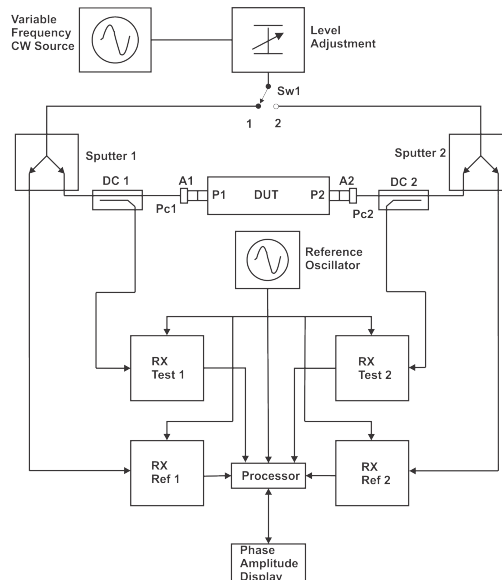


Figure 2.2: Basic block diagram of Network Analyser

2.3.3.2 PNA E8362B Network Analyzer

The heart of any antenna measurement is a Network Analyzer which is used to characterise the antenna behavior. Agilent PNA (Performance Network Analyzer) E8632B is used for the measurement of the antenna. This PNA provides excellent performance, advanced automation features, flexible connectivity and is easy to use. Its key features are

- The operation range is from 10 MHz to 20 GHz
- 123 dB dynamic range and < 0.006 dB trace noise
- 26 μ s/point measurement speed, 32 channels, 16,001 points
- TRL/LRM calibration, on-wafer, in-fixture, waveguide, and antenna measurements
- Mixer conversion loss, return loss, isolation, and absolute group delay
- Amplifier gain compression, harmonic, IMD, and pulsed-RF

The return loss characteristics of the antenna is measured using one of the ports of the network analyzer. Prior to measurement, the port is calibrated using known standard reference. The references used are the open, short and matched load.

2.3.3.3 Anechoic Chamber

The free space environment required for antenna pattern measurement is emulated by anechoic chamber. Anechoic chamber is a big room which provides a quiet zone free from all kind of spurious signals and multi path electromagnetic interferences, which distort the measured radiation pattern of the antenna. The quiet zone is achieved by pasting the walls, roof and floor of the chamber with microwave absorbers. The absorbers are made up of high quality foams in pyramidal shape, impregnated with dielectrically and magnetically lossy medium. A carbon black impregnated polyurethane foam can also be used. The pyramidal structure provides geometrical impedance matching to the waves impinging on

2. Literature Review & Methodology

it, at the same time carbon provides attenuation to the signal, there by providing an echo free zone. The chamber is covered with thin aluminum sheets which shields any spurious signals entering the chamber. The chamber is designed with an average reflectivity of -35 dB in the frequency range from 2 GHz to 18 GHz.

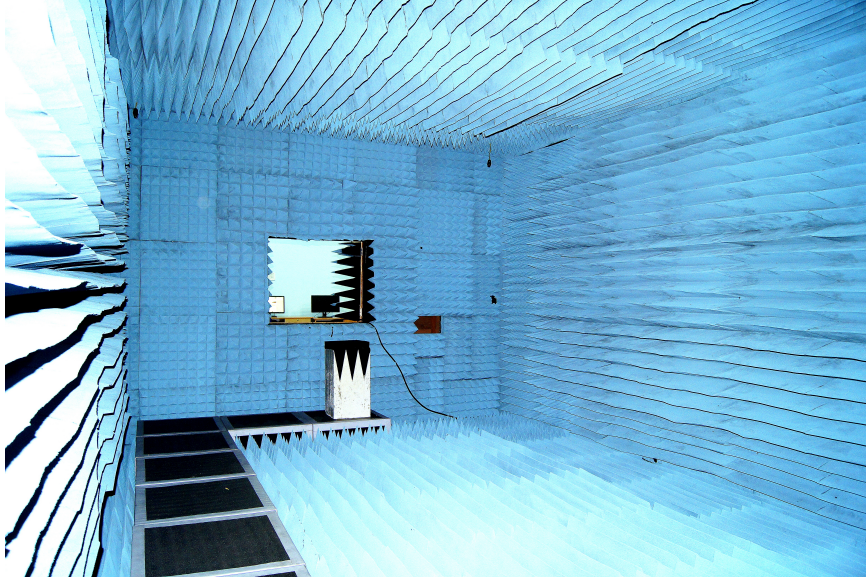


Figure 2.3: Photograph of Anechoic Chamber at Dept. of Electronics, CUSAT

2.3.3.4 Measurement of Return loss

The return loss characteristics of the antenna is measured using one of the available ports of the Network Analyzer. Prior to the measurement, the port selected, say port 1, is calibrated using standard open, short and matched load references. Proper phased delay is introduced in order to ensure the plane of reference for all the measurements in the desired frequency band resides at the zero level, there by taking care of any chances of cable length variation. The Antenna Under Test (AUT) is then connected to the calibrated port of Network Analyzer. The measured return loss S_{11} provides both magnitude and phase response. This data is then exported into ASCII format and saved in a personal computer connected to the Network Analyzer using Standard Commands for Programmable Instruments (SCPI). This is assisted by a proprietary software

2. Literature Review & Methodology

CREMASOFT. The resonant frequency is then determined from S_{11} . The point with maximum dip in the curve gives the resonant frequency of AUT. The return loss is the number in dB that the reflected signal is below the incident signal. As the $VSWR=2$ corresponds to the reflection coefficient,

$$\rho = \frac{VSWR - 1}{VSWR + 1} = \frac{1}{3} \quad (2.2)$$

then

$$20 \log \frac{1}{3} \cong 10dB \quad (2.3)$$

Thus 2:1 VSWR bandwidths are determined by observing the range of frequencies δf_r about the resonant frequency, for which the return loss curves show a -10 dB value. The percentage bandwidth is then calculated as $\frac{\delta f_r}{f_r}$. The input impedance of the microstrip antenna at the resonant frequencies are determined directly from the Smith Chart display in the network analyzer.

2.3.3.5 Measurement of radiation pattern

The radiation pattern measurement setup consists of a network analyzer, a standard horn antenna, a turn table assembly and a software to coordinate all the process. The turn table assembly with AUT is kept inside the anechoic chamber, in the quiet zone. The turn table is attached with a platform to hold the Antenna Under Test (AUT). The AUT is placed at the center of the platform. The standard horn antenna is kept stationary at the same height as that of the AUT on the other side of the chamber. Both the antennas are connected to the Network Analyzer through long cable to port1 and port2. The principle E and H patterns of the antenna are taken keeping the AUT in receiving mode. The turn table is rotated in fixed angles controlled by the software, to obtain the radiation pattern in the selected plane in 2π radian. The antenna positioner will rotate to the step angle and then stop to take the reading for the whole selected frequency band. These readings are then saved in the computer, which is connected to the Network Analyzer through Standard Commands for Programmable Instruments (SCPI). This process is repeated for co and cross polarization of the antennas, and the recorded data can be utilized for different analysis like half power beam

width, cross polar isolation, directivity etc.

2.3.3.6 EMSCAN RFXpert

The EMSCAN RFXpert is a bench-top scanner which provides accurate & repeatable measurements of near-field and predicted far-field antenna patterns in real-time, without the need of an anechoic chamber. Also, it avoids the setup and other delays, like ongoing maintenance and calibrations, associated with far-field measurements in an anechoic chamber. In RFXpert, single frequency scans can be executed, catalogued and visualized within seconds, not an hour. And, an antenna can be completely characterized across its operating range in less than a minute. RFXpert let you quickly measure the performance of an antenna design with far-field pattern data and radiated power levels. You can also gain immediate insight into the root causes of performance challenges by analysing the near-field results.

The RFXpert scanner is connected to a workstation via a USB and comes with a client software which helps you to analyse, compare & archive the scanned results. The scanner has an array of 384 electrically switched probes and there is no mechanical movement or other extra hardware required for its operation. So, the scans will be quick and repeatable. Another advantage of having no motion is that the coupling between the AUT and the probe array is exactly the same throughout the measurement process. These array of probes (small loops) measures the magnetic field (H-Field), including the probe coupling effects, at the very near-field region (Reactive region) of the AUT and projects this data to the far-field using the planar aperture distribution to angular spectrum transformation or plane wave spectrum (PWS) transformation. A second custom algorithm then adjusts the far-field projection to eliminate the predictable coupling effects of the measurement array. The RFXpert can provide meaningful projections that correlate closely to the measured far-field results.

This RFXpert can provide complete near-field and far-field characterization between 700 MHz and 6 GHz, with near-field only data as low as 300 MHz. This can scan an antenna/microwave component having a maximum radiator size of $16 \times 10\text{cm}^2$. It can also integrate with a Network Analyzer to measure

2. Literature Review & Methodology

S-parameters, gain & efficiency, or a base-station emulator to check the cell-phone antennas. Thus, having immediate access to far-field data saves time and cost, by reducing time spend in chamber, and the unique near-field data provide insight into the root cause of problems.

2.3.3.7 Gain Measurement

Antenna gain is one of the key parameter in any antenna specifications. The gain of an antenna is defined as the ratio of intensity of an antenna in that direction to the intensity by an isotropic antenna. Gain is expressed in dBi, where "i" indicates the gain in comparison with isotropic antenna. An isotropic antenna is a hypothetical concept, where an antenna radiates with equal intensity in all directions without any loss.

There are different methods for measuring the gain of an antenna. According to IEEE Standard Test Procedures For Antennas, ANSI/IEEE Std 149-1979, Gain comparison or Gain transfer methods is the most commonly employed antenna power-gain measurement. The gain of the antenna under test is measured using the gain transfer method, utilizing a reference antenna of known gain. The experimental setup for the measurement of gain is same as that used for radiation pattern measurement. A standard antenna with known gain operating in the same frequency band as the test antenna is used as the reference antenna. S21 measurements are then carried out to determine the reference power with the wide band horn as transmitter and the reference antenna as receiver. A Thru response calibration is performed for the frequency band of interest and saved in a new cal set. This is taken as the reference gain response (0 dB). The reference antenna is then replaced with the test antenna, retaining the earlier bore sight alignment. S21 is then measured with the new calibration on and power received in dB, recorded. The gain Gt of the test antenna is calculated from the stored data based $G_t(\text{dB}) = G_s(\text{dB}) \pm Pr(\text{dB})$.

2.3.3.8 Efficiency

The efficiency is measured using Wheeler Cap Method. This is done by making two different impedance measurements. The antenna impedance with and

2. Literature Review & Methodology

without metallic cap are measured. Without cap, total resistance is the sum of loss resistance and the radiation resistance, where as with cap, total resistance is only due to loss. The radiation efficiency is calculated after the measurement using the following equation.

$$Efficiency, \eta = \frac{R_{nocap} - R_{cap}}{R_{nocap}} \quad (2.4)$$

Where R_{cap} and R_{nocap} are the measured resistance of the antenna with and without the metal cap, respectively and can be easily obtained from the S_{11} data in Smith Chart format.

2.3.4 High Frequency Simulation Softwares

Infantile investigation and then the optimization of antenna is done using the commercially available high frequency simulation software Ansoft HFSS.

HFSS (High frequency Structure Simulator) is a 3D electromagnetic field simulator based on Finite Element Method for modeling arbitrary volumetric structures . It integrates simulation, modeling, visualization and automation in an easy to learn environment. With adaptive meshing and brilliant graphics the HFSS gives an unparalleled performance and complete insight to the actual radiation phenomenon in the antenna. With HFSS one can extract the parameters such as S, Y, Z, visualize 3D electromagnetic fields (near- and far-field), and optimize design performance. An important and useful feature of this simulation engine is the availability of different kinds of port schemes. It provides lumped port, wave port, incident wave scheme etc. The parametric set up available with HFSS is highly suitable for Antenna engineer to optimize the desired dimensions. The first step in simulating a system in HFSS is to define the geometry of the system by giving the material properties and boundaries for 3D or 2D elements available in HFSS window. The suitable port excitation scheme is then given. A radiation boundary filled with air is then defined surrounding the structure to be simulated. Now, the simulation engine can be invoked by giving the proper frequency of operations and the number of frequency points. Finally the simulation results such as scattering parameters, current distributions and far field radiation

2. Literature Review & Methodology

pattern can be displayed. The vector as well as scalar representation of E, H, and J values of the device under simulation gives a good insight into the antenna under analysis.

HFSS First solves for the electric field using the equation

$$\Delta \times \left(\frac{1}{\mu_r} \Delta \times E \right) - k_0^2 \epsilon_r E = 0 \quad (2.5)$$

HFSS then calculates the magnetic field using

$$H = \frac{j}{\omega \mu} \Delta \times E \quad (2.6)$$

With these values computed, the other quantities are derived using corresponding constitutive relations. The procedure used in HFSS for the calculation of Electric field is as follows.

- First the structure is divided into small areas. this process is called meshing. In general the structure will be divided into small tetrahedral elements. HFSS uses two types of meshing, the Classic meshing and Tau meshing.
- After the completion of meshing, testing functions, W_n are defined on each tetrahedral elements.
- The field equation (2.5) is then multiplied by the defined testing function and integrate over the volume.

$$\int_v \left(W_n \cdot \Delta \times \left(\frac{1}{\mu_r} \Delta \times E \right) - k_0^2 \epsilon_r E \right) dV = 0 \quad (2.7)$$

this will produce an equation for each test function resulting in thousands of such equations. These equations are then manipulated using Green's theorem and divergence theorem to yield

$$\int_V \left((\Delta \times W_n) \frac{1}{\mu_r} \Delta \times E - k_0^2 \epsilon_r E \right) dV = \int_S (boundary\ terms) dS \quad (2.8)$$

$$E = \sum_m^N x_n W_n \quad (2.9)$$

2. Literature Review & Methodology

$$\sum x_m \int_V \left((\Delta \times W_n) \cdot \left(\frac{1}{\mu_r} \Delta \times W_m \right) - k_0^2 \epsilon_r E \right) dV = \int_S (\text{boundary terms}) dS \quad (2.10)$$

Equation (2.10) has the form

$$\sum x_n A_{n,x} = b_n \quad (2.11)$$

which can be written in matrix form as

$$Ax = b \quad (2.12)$$

Here x is the only unknown term whereas A is an $N \times N$ matrix including the boundary condition terms, b contains port excitations, voltage and current sources and incident waves. Once x is found then the electric field E can be easily calculated and with the calculated E value the magnetic field H can also be calculated. For better accuracy of the system, the whole process is made to be an iterative process by changing the mesh at each iteration depending on the criticality of the area to yield a better solution. This process is known as adaptive iterative solution process. The general flow of HFSS process is shown in Figure 2.4

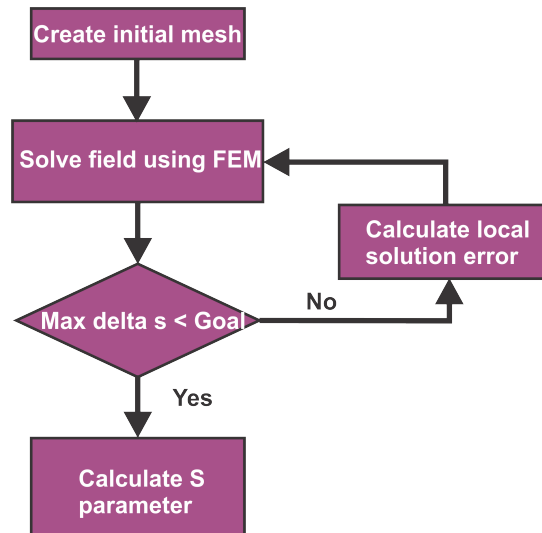


Figure 2.4: Flow diagram of HFSS solution process

2.3.4.1 Steps in HFSS simulation

The HFSS process flow has 6 basic steps

- Create model/geometry
- Assign boundary
- Assign excitation
- Set up solution
- Solve
- Post process the result

The model or geometry creation is the first step in the simulation process. This can be done inside the 3D modeller provided in the HFSS. The 3D modeller gives flexibility to parametrise all the dimensions of the physical structure which makes the optimization process easier. The geometry can be imported from different CAD formats also.

Next step is one of the important step where all the boundaries are defined. HFSS has different types of boundaries. Here we can define the various boundaries like electric, magnetic, impedance, radiation etc. depending on the purpose.

Once the boundaries are defined, then its time to define the excitations. There are different types of excitations available in HFSS. The selection of the desired excitation is critical as this will directly impact the accuracy of the solution.

The next step is to set up a solution where the frequency range, solution frequency, solution methodology, desired convergence criteria and minimum and maximum number of passes are specified. Once the solution set up is ready, then its the time to run the solution process. In the post processing, the SYZ parameters, radiation, near field, gain and efficiency, parameter extraction etc are conducted. Figure 2.5 depicts the general steps in the HFSS simulation.

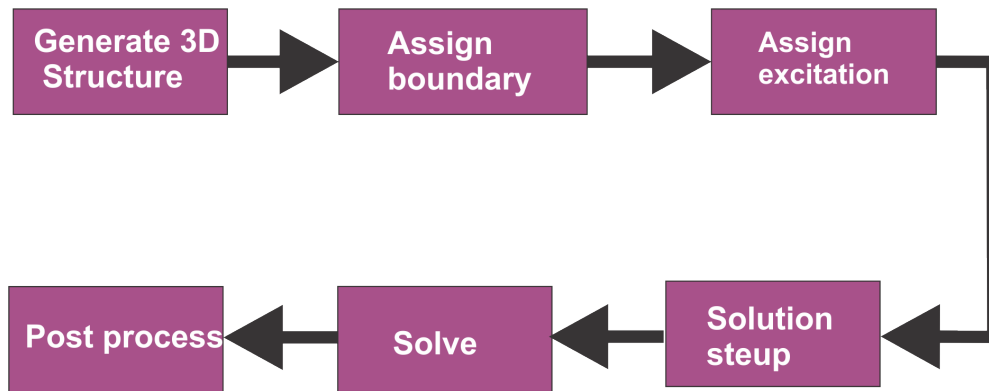


Figure 2.5: Flow diagram of HFSS process steps

2.3.5 Finite Difference Time Domain (FDTD)

Maxwell's equations are the holy book for any person indulged in the field of electromagnetics. His twenty equations, which were later comprehended into four equations by Oliver Heaviside, in the form which we see today, encapsulate the whole world of electromagnetism. It was K. S Yee who envisaged the vivid possibility of utilizing these equations numerically to model the visualisation of electromagnetic wave propagation in real time [68]. This led to the introduction of FDTD analysis in 1966, which was later refined by Taflove in 1970's [4].

This method permits the modelling of electromagnetic wave interactions with a level of detail as high as that of the Method of Moments. Unlike MoM, however, the FDTD does not lead to a system of linear equations defined over the entire problem space. Updating each field component requires knowledge of only the immediately adjacent field components calculated one-half time step earlier. Therefore, overall computer storage and running time requirements for FDTD are linearly proportional to N , the number of field unknowns in the finite volume of space being modelled. The FDTD method has thus emerged as a viable alternative to the conventional Frequency Domain methods because of its dimensionally reduced computational burdens and ability to directly simulate the dynamics of wave propagation [119]. The rapid growth of FDTD in Computational Electromagnetics is presented in the survey paper by Shlager and Schneider [73]. Although FDTD and TLM are time domain methods there are some fun-

2. Literature Review & Methodology

damental differences that make them complement each other than compete each other. TLM is a physical model based on Huygens principle using interconnected transmission lines, but the FDTD is an approximate mathematical model directly based on Maxwells equations. In the two dimensional TLM, the magnetic and electric field components are located at the same position with respect to space and time, whereas in the corresponding two-dimensional FDTD cell, the magnetic field components are shifted by half an interval in space and time with respect to the electric field components. Due to this displacement between electric and magnetic field components in Yees FDTD, [135] modified the FDTD and the new formulation is exactly equivalent to the symmetric condensed node model used in the TLM method. This implies that the TLM algorithm can be formulated in FDTD form and vice versa. However, both algorithms retain their unique advantages. FDTD has a simpler algorithm where constitutive parameters are directly introduced, while the TLM has certain advantages in the modeling of boundaries and the partitioning of the solution region. Furthermore, the FDTD requires less than one-half of the CPU time spent by the equivalent TLM program under identical conditions. A detailed description of FDTD, the method used for the numerical analysis in the present investigation is presented in the following sections.

2.3.5.1 Numerical investigations: Finite Difference Time Domain

Finite difference Time Domain method proposed by Yee in 1966 is extensively used in many areas of science and technology. FDTD, a technique that discretizes the problem domain in both time and space. This method gives time and frequency domain information of the electromagnetic problem of interest. FDTD provides a direct solution of time dependant Maxwells equation for electric and magnetic field intensities in a finite, piecewise homogenous media. Due to the lack of analytical preprocessing and modeling, FDTD is a potential tool for planar antenna problems. Following striking characters of FDTD catches the attention of any antenna designer to include FDTD algorithm for modeling and simulation analysis of antennas.

2. Literature Review & Methodology

- It is a direct implementation of Maxwells curl equations. Therefore, analytical processing of Maxwells equations is almost negligible.
- It can model complex antenna geometries and feed and other structures in the model
- It can model any type of materials of importance to electromagnetic technology, including conductors, dielectrics, dispersive and non linear medium.
- Impulsive excitations in Time Domain gives a broadband response in frequency domain in a single FDTD run through concurrently run Fourier transform.
- The complex near field information is an intrinsic part of FDTD model and the near to far field transformation offers the calculation of far field radiation pattern in single FDTD run
- FDTD is accurate: It is good model of the physical world. The ready availability of time domain and frequency domain data provides a deep physical insight to the problem in different perspectives. Visualization of fields in time provides a clear insight to the actual physics behind the antenna radiation.

2.3.5.2 Fundamental concepts of FDTD

Analysis of antenna problem using FDTD starts with dividing the structure into various regions based on the material properties. The unbounded region, if any, is then bounded by terminating it with absorbing medium which makes the medium free from any reflection. The discretization process of the whole structure is done in the form of cuboid volume $\Delta x \Delta y \Delta z$ called Yee cells, where Δx , Δy and Δz are the dimensions of cuboid in X, Y and Z directions. The Yee cell is the basic building block of the entire structure in which the Electric fields and Magnetic field are interleaved as shown in Figure 2.6. The time domain is also discretised with interval Δt . The excitation of the structure is done with an electromagnetic pulse, which propagates through the structure. The propagation of the pulse is then used for the behavioral analysis of the antenna structure. The

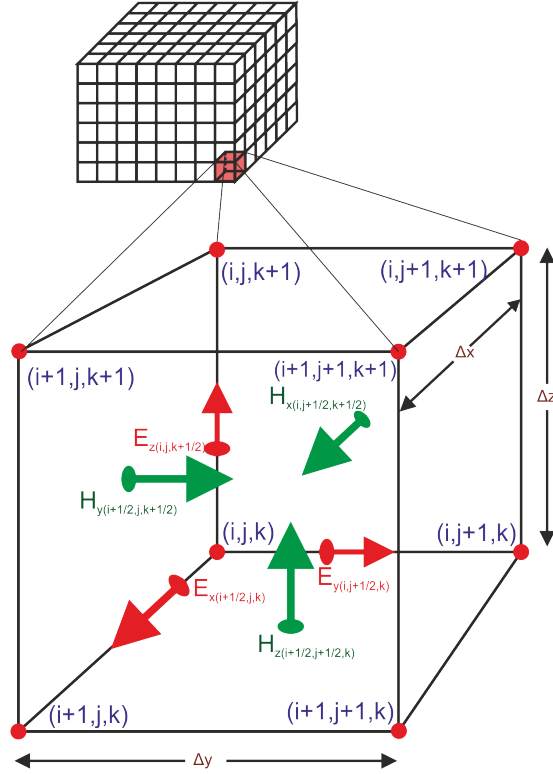


Figure 2.6: Yee Cell illustration

stabilized time-domain waveform is numerically processed to determine the time-domain and frequency domain characteristics of the structures. Convergence, stability, accuracy and consistency are some of the issues to be addressed while implementing FDTD method.

2.4 Conclusion

In the literature, a wide variety of small antennas are presented, starting from 1953, whose definition evolved over time. Different turning points that have happened in the development of those antennas have moulded the present day small antennas, which are competing with other sectors of electronics industry towards miniaturisation. SIR, a void area where not much exploration has happened in terms of antenna development has been chosen for this thesis along with an inductor loading technique for the development of small antennas.

2. Literature Review & Methodology

In this chapter a wide verity of methodologies adopted to help in the design, development and analysis of the antennas to achieve a fruitful outcome are outlined. A number of proven methods in the analysis of antennas are elaborated in this chapter. Studies prior to fabrication are conducted using HFSS and the methods for measurement of reflection characteristics, gain, efficiency and radiation pattern are also explained. These methods are employed in the studies conducted in the following chapters.

Chapter 3

Lumped Inductor Loaded CPW Based Electrically Small Antenna (ESA)

3.1 Introduction

Electrically Small Antennas (ESA) have gained much attraction in the past few years. This chapter details the design and development of an Electrically Small Antenna (ESA) operating at 2.4 GHz. This planar antenna is embedded with a surface mounted inductor, which determines the resonant frequency. Following sections shows the evolution, optimization, evaluated characteristics and parametric analysis of the antenna with detailed discussion. To achieve ESA there are various approaches attempted and implemented. In the proposed design, a novel structure with an embedded lumped element is elaborately discussed.

3.2 Evolution

The year 1969 saw a swift change in the field of Microwave Integrated Circuits (MICs) and in the Monolithic MICs (MMICs), by the introduction of one of the coolest candidate by C. P. Wen, a coplanar waveguide (CPW) fabricated on a dielectric substrate. A conventional CPW on a dielectric substrate consists of a

centre strip conductor with a semi infinite ground plane on either side separated by a gap. A conventional CPW is shown in the figure 3.1.

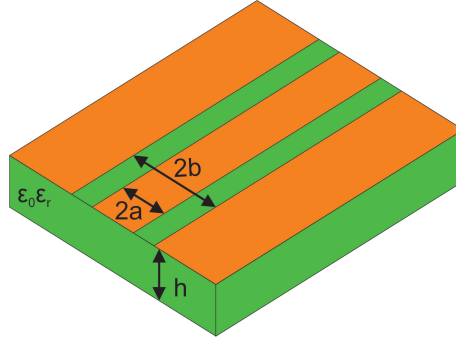


Figure 3.1: Coplanar Waveguide

CPW structure has a lot of advantages. Fabrication of CPW is simple as it can be on a single sided substrate. Since it is a coplanar structure, surface mounting of series and shunt components can be easily done after the fabrication of CPW. It also reduced the wraparound and via holes. The radiation losses is also found to be less compared to the Microstripline. CPW gave unmatched flexibility in scaling its physical dimensions as the characteristics impedance is determined by the ratio a/b . The structural peculiarity, i.e., the ground plane coming between adjacent lines favoured in a great extent to reduce the cross talk effect.

Owing to all these advantages, the CPW found a commendable space in MIC and MMIC applications. Being an integral part of MICs and MMICs, CPW has been used as a feeding mechanism for many microwave antennas. One of the prominent member is the monopole antenna fed by a CPW transmission line. Figure 3.2 shows a conventional CPW fed planar monopole antenna. A lot of variants of this monopole antenna are available in literature. In this work an attempt is made to design an electrically small antenna based on CPW and surface mounted devices. For this purpose a conventional CPW fed monopole is taken initially. The resonant frequency of the antenna is fixed at 2.4 GHz which is commonly used for the LAN application.

The development of proposed antenna is started from a CoPlanar Waveguide

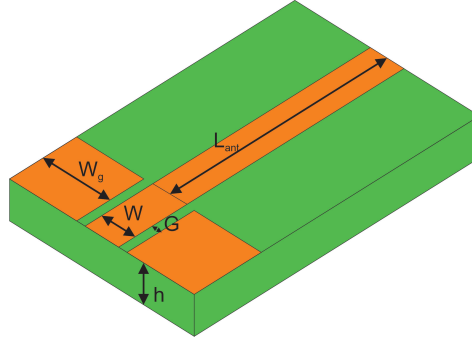
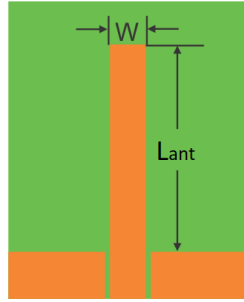


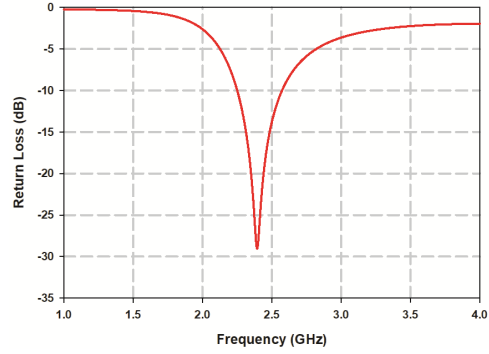
Figure 3.2: CPW fed Monopole Antenna, [$L_{ant} = 31$ mm, W_g , $W = 3$ mm, $G = 0.4$ mm, $h = 1.6$ mm, $\epsilon_r = 4.4$]

(CPW) transmission line. A transmission line structure has two port connectivity with maximum transmission coefficient with negligible radiation to the surroundings. Ideally the ground plane of the CPW is infinite in its width, whereas the practical version has a truncated ground plane. The width of the central conductor is selected based on the relative permittivity ' ϵ_r ' and thickness 'h' of the substrate material, in order to match with the 50Ω characteristics impedance. Figure 3.3(a) shows such a monopole antenna which radiates at 2.4 GHz. The monopole length L of this particular antenna is 31 mm which is 0.5λ and the width is 3 mm. An antenna with a reduced monopole width has been derived from this structure as shown in Figure 3.4(a), in order to see the impact of width reduction in this structure. Here the width of the monopole selected is 1 mm. and the length is 28.9 mm. In both the cases, the width of the ground is kept small as the main intention of the study is to derive a compact antenna. A comparison of the impedance variation of these two antennas reveals that in the first case the reactance is capacitive in nature at resonance whereas in the second antenna with reduced width has increased the inductance. As a first step towards an ESA, the length of the monopole is reduced to 1.6 mm as shown in figure 3.5. This structure is not resonant at 2.4 GHz. It may be resonating at mm wave band. The return loss of this configuration is depicted in Figure 3.6(a) and the antenna is not resonating in the specified frequency band. It is observed from the smith chart that at the 2.4 GHz frequency, the structure is highly capacitive in nature. This structure has a very small size in comparison with the two earlier designs.

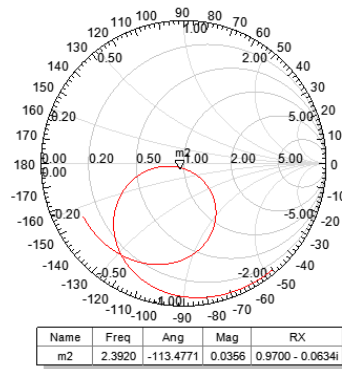
3. Lumped Inductor Loaded ESA



(a) Monopole antenna



(b) Return loss of the antenna



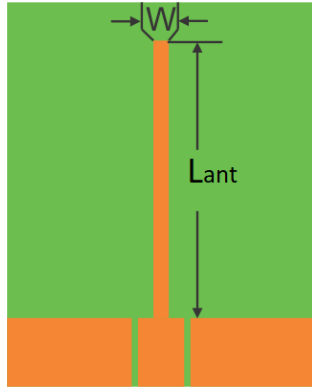
(c) Smith Chart of the Monopole antenna

Figure 3.3: CPW Fed planar Monopole antenna Designed for 2.4 GHz. [$L_{ant} = 31$ mm, $W = 3$ mm, $G = 0.4$ mm, $h = 1.6$ mm, $\epsilon_r = 4.4$]

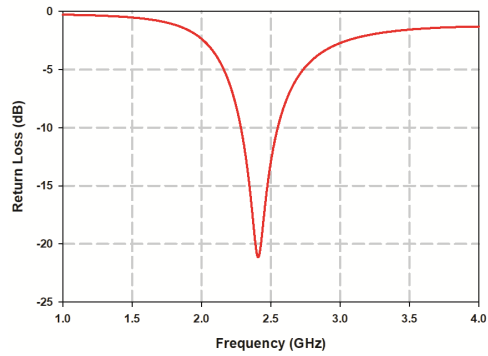
Now the objective of the present work is to make this small structure resonate at 2.4 GHz. In order to make this structure resonate at 2.4 GHz the capacitive nature has to be compensated at 2.4 GHz. The length of the monopole is selected as 1.6 mm to get a continuity in the evolution process of ESA.

A new antenna is derived from the above mentioned monopole antenna which has a much reduced size. In the proposed antenna, instead of the lengthy centre conductor, an equivalent structure is used to achieve the same resonant condition. The equivalent structure consists of a surface mounted inductor and a small metal strip. This introduction of the chip inductor makes the total reactance of the

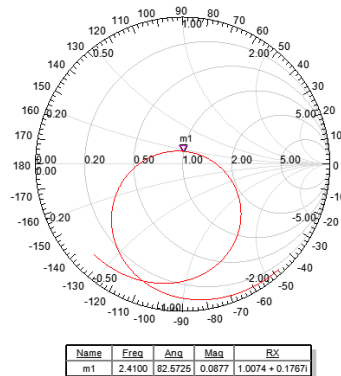
3. Lumped Inductor Loaded ESA



(a) Monopole antenna with reduced width



(b) Return loss of the Monopole antenna with reduced width



(c) Smith Chart of the Monopole antenna with reduced width

Figure 3.4: CPW Fed planar Monopole antenna Designed for 2.4 GHz and the input reflection characteristics. [$L_{ant} = 28.9$ mm, $W = 1$ mm, $G = 0.4$ mm, $h = 1.6$ mm, $\epsilon_r = 4.4$]

antenna almost zero by nullifying the capacitive reactance with the inductive reactance, there by providing a supportive impedance condition for resonance in the structure. The reactive part of the antenna at 2.4 GHz, calculated at the place of chip inductor without loading it is 592 Ohm, which is capacitive in nature. For a resonance to occur at this frequency, the capacitive reactance must be compensated. For this purpose, an inductance should be added to the structure to provide the same reactance at the same frequency. The calculated value of the inductance for this reactance is 39.2 nH. The simulated resonance

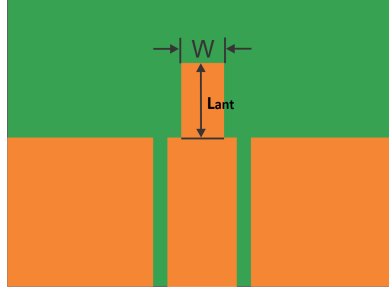


Figure 3.5: Geometry of the antenna with length and width reduction, $L=1.6$ mm, $W = 1$ mm

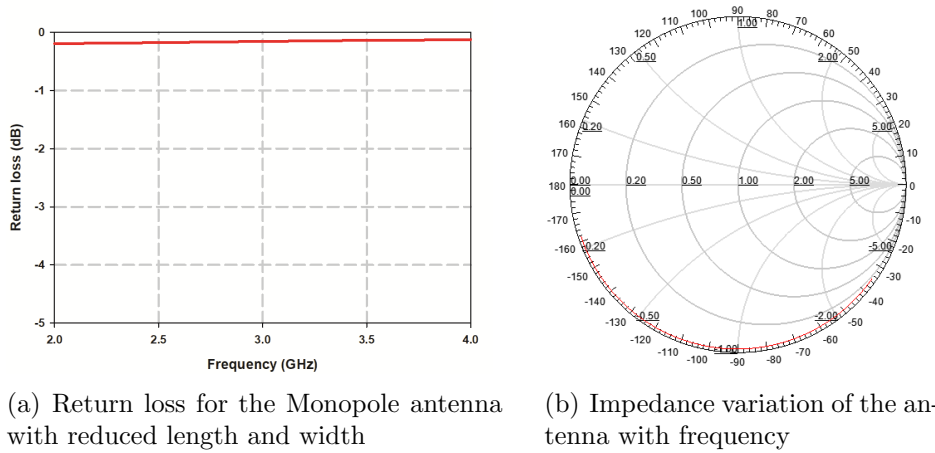


Figure 3.6: Return loss of the CPW Fed planar Monopole with highly truncated length. [$L_{ant} = 1.6$ mm, $W = 1$ mm, $h = 1.6$ mm, $\epsilon_r = 4.4$]

for this inductance value shows a little variation and the resonance happened at 2.35 GHz. The inductance value is tuned for a resonance at 2.4 GHz and is found to be 37.5 nH. The inductor is placed in between the feed line and the monopole, by replacing 0.8 mm of the 1.6 mm monopole starting from the feed line.

3.3 Geometry

The geometry of the proposed antenna is shown in Figure 3.7. The antenna is designed to work at 2.4 GHz on a FR4 substrate of thickness 1.6 mm and relative permittivity of 4.4. The design of the antenna is optimized using Ansys HFSS.

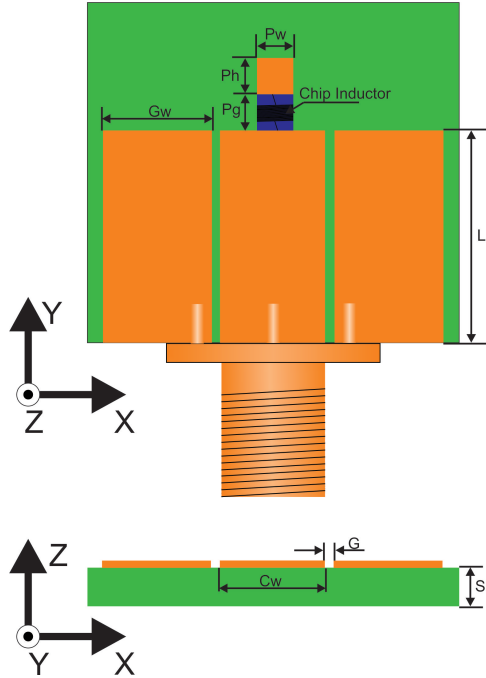


Figure 3.7: Geometry of the proposed antenna

In the present design the width of ground is highly truncated and made equal to that of the central conductor. This truncation is carried out as one of the method to achieve compactness. A 50Ω SMA connector is used for feeding the antenna and the CPW is designed to match with this impedance. Several available chip inductors were experimented to see the implication and out of that a wire wound 0603CS chip inductor with a rated inductance of 23 nH from Coil Craft when connected from the centre conductor to a small metal strip, the antenna resonated at 2.4 GHz.

The geometric specification of the chip inductor as per the data sheet [1] is shown in Figure 3.8. The inductor has an overall width of 1.12 mm and length of 1.8 mm including the plastic case. The coil section has a length of 0.86 mm and the gap provided in the structure for mounting the inductor is 0.8 mm. Figure 3.9 shows the fabricated prototype of the proposed antenna, which is shown in comparison with a coin. A detailed description of the dimensions used in the proposed antenna is given in Table 3.1. The selection of P_g and P_w are

3. Lumped Inductor Loaded ESA

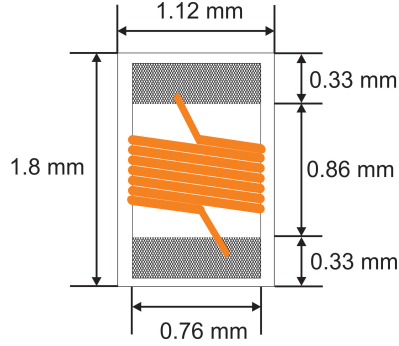


Figure 3.8: Geometry of the Coilcraft 0603CS chip inductor [1]



Figure 3.9: Prototype of the proposed antenna. [$\epsilon_r = 4.4$, $P_h = 0.8$ mm, $P_w = 1$ mm, $G_w = 3$ mm, Coilcraft 0603CS 23 nH Chip Inductor, $S_h = 1.6$ mm]

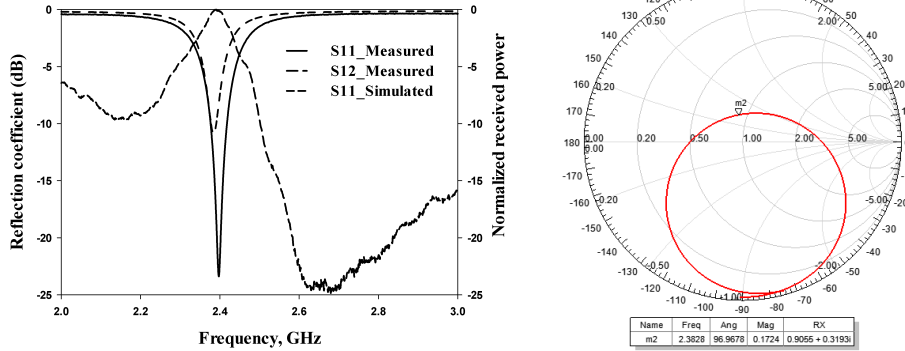
Table 3.1: Physical Dimensions of the Antenna

Parameter	Dimension (mm)	Parameter	Dimension (mm)
G_w	3	L	4
C_w	3	P_g	0.8
S_h	1.6	P_h	0.8
G	0.327	P_w	1

done in such a way that the selected chip inductor should be properly placed in between the feed line and the small metal strip. As shown in Figure 3.8 a gap of 0.8 mm (P_g) and a width of 1 mm (P_w) is adequate enough to mount the chip inductor properly.

3.4 Simulated and measured results

3.4.1 Scattering Parameters



(a) Simulated and Measured Return loss & the normalized transmission coefficient

(b) Smith chart,

Figure 3.10: (a) Return loss and Transmission characteristics of Inductor Loaded ESA. [$L = 0.8$ mm, $W = 1$ mm, Coilcraft 0603CS 23 nH Chip Inductor, $Sh = 1.6$ mm, $\epsilon_r = 4.4$], (b) Impedance Characteristics in Smith chart

Figure 3.10 shows the simulated and measured return loss characteristics of the proposed antenna with a Coilcraft 0603CS chip inductor of 23 nH. The initial simulated resonant frequency of the antenna using a 3D box is 2.385GHz. Experimentally the antenna is resonating at 2.395 GHz. Later inductor is modelled by using RLC boundary condition on a rectangle of size $P_g \times P_w$ mm². The prototype antenna is resonating at 2.395 GHz with a return loss of -23 dB having a 2:1 VSWR bandwidth of 40 MHz from 2.375 GHz to 2.415 GHz which is wide enough to cover a single channel of 2.4 GHz WLAN. Figure 3.10 shows the measured reflection and transmission coefficients of the antenna. The antenna is resonating at 2.395 GHz and the maximum measured received power of the antenna using another identical antenna is also at 2.395 GHz. The gain of the antenna is found to be -6.5 dBi at 2.395 GHz with chip inductor and -20.76 dBi simulated gain without connecting the chip inductor. The negative value of gain implies that the power radiated from the antenna is less than that of an isotropic

3. Lumped Inductor Loaded ESA

antenna. This is due to the decrease in the radiation resistance of the antenna as the size of the antenna decreases. Table 3.2 shows the comparison of some of the reported electrically small antennas. From the comparison, it is evident that, as the ka value of the antenna become smaller, the gain of the antenna is also becoming smaller.

Table 3.2: Comparison of reported ESAs

Antenna	Frequency	Dimension	ka	gain (dBi)
[79]	232.54 MHz	75 mm×75mm×6mm	0.18	-7.1
[78]	2.4 GHz	30 mm×30mm×0.2mm	1	-3.5
[118]	2.4 GHz	25 mm×25mm×0.99mm	0.88	1.7
Proposed Antenna	2.4 GHz	10mm×7mm×1.6mm	0.29	-6.5

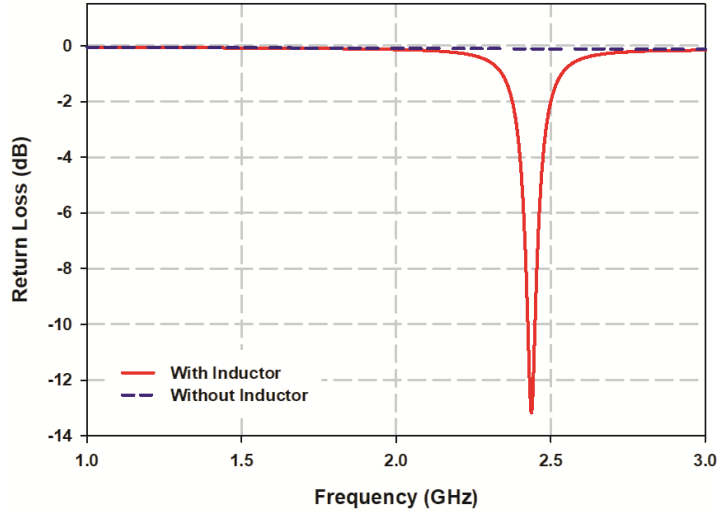


Figure 3.11: Return loss of the antenna with and without inductor. [$\epsilon_r = 4.4$, $P_h = 0.8$ mm, $P_g = 0.8$ mm, $P_w = 1$ mm, $G_w = 3$ mm, Inductor 37.5 nH, $Sh = 1.6$ mm]

The Figure 3.11 shows the return loss characteristics of the structure with and without the chip inductor. The antenna, without the chip inductor is not showing

any resonance in the given frequency range. When the inductor is connected across the small metal strip and the CPW transmission line, the structure shows a resonance. The physical dimension of the antenna is much smaller compared to the operating wave length λ_0 .

3.4.2 The effective inductance

The inductor used for the antenna is 0603CS chip inductor from Coilcraft with a specified inductance value of 23 nH. This 23 nH is the rated value of the chip inductor. The resonance obtained from the prototype using this chip inductor is 2.4 GHz, which was in contradiction with the simulated resonance of the structure, which was above 3 GHz for this 23 nH chip inductor. A closer analysis of the data sheet of this inductor revealed the fact that the rated inductance value of the inductor is measured at 250 MHz [1]. The data sheet also specified two more points on frequency at 900 MHz and 1.7 GHz showing different values of inductance. The data sheet shows that the inductance of the chip inductor is increasing as the frequency increases. In order to find the inductance value of the chip inductor, an interpolation using spline method is conducted in Matlab, using the three available points in the data sheet. Then the obtained curve is curve-fitted using a polynomial function of the form $p1x^2 + p2x + p3$. The interpolated and curve-fitted values are shown in Figure 3.12 and the coefficient of the polynomial functions are given in Table 3.3.

Table 3.3: Coefficients of the curve-fitted polynomial

p1	p2	p3
1.9800e-027	-3.1960e-019	2.3010e-008

The inductance value found using the above curve fitted model at 2.4 GHz is 33.64 nH. This value when initially used in the simulation, the resonance was on the higher side of the measured frequency. The inductance required for the resonance at 2.4 GHz is found to be 37.5 nH from the parametric analysis. This difference could be a numerical error originated because of the unavailability of more number of sample points for interpolation. The whole range of interpolation

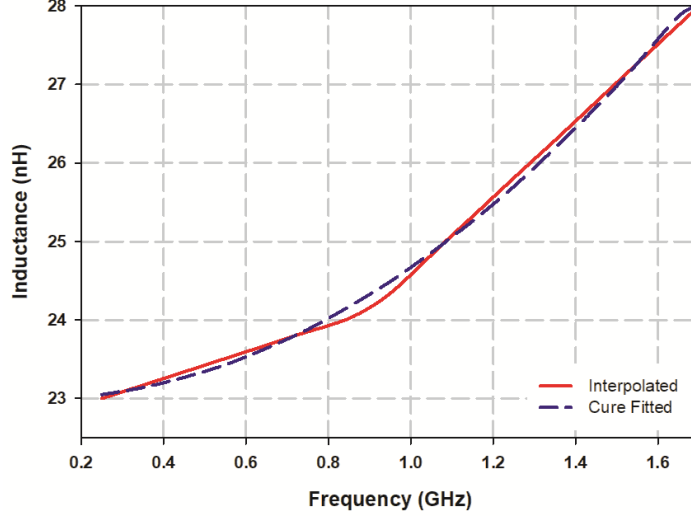


Figure 3.12: Interpolated and curve fitted values of inductance for the data from coilcraft 0603CS chip inductor data sheet

is carried out on three sample points. Further analysis of the antenna is carried out using this optimized value of inductance.

3.4.3 Design

The impedance plot of the proposed antenna structure is shown in the Figure 3.13. The reactance plot shows that initially at lower frequency the structure behaves as capacitive and gradually becoming inductive. At resonance the reactance is almost nil and after that it is inductive. This characteristics is same a that of a series LC resonance. With this assumption, considering the equivalent circuit of the proposed antenna as a series LC resonator, the corresponding capacitance value is calculated using the standard equation for LC resonator (3.1).

$$f = \frac{1}{2\pi\sqrt{L_{chip}C_{eff}}} \quad (3.1)$$

Here, the inductance L_{chip} is the effective inductance value of the chip inductor and the effective capacitance value C_{eff} , thus obtained is 0.113 pF. The effective

3. Lumped Inductor Loaded ESA

inductance and capacitance values are calculated with the help of Ansys HFSS by modelling CPW and metal strip separately and extracting the corresponding parameters. These parameters along with the lumped inductance is used in HFSS Circuits to determine the C_{eff} required to obtain the same resonance. Table 3.4 below shows the simulated resonance of the structure and the calculated resonance using this capacitance value. It also shows the percentage of deviation from the calculated value and the simulated value.

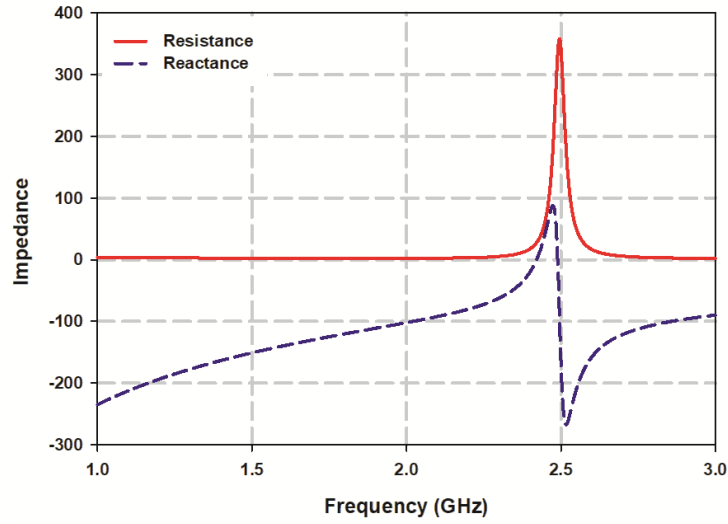


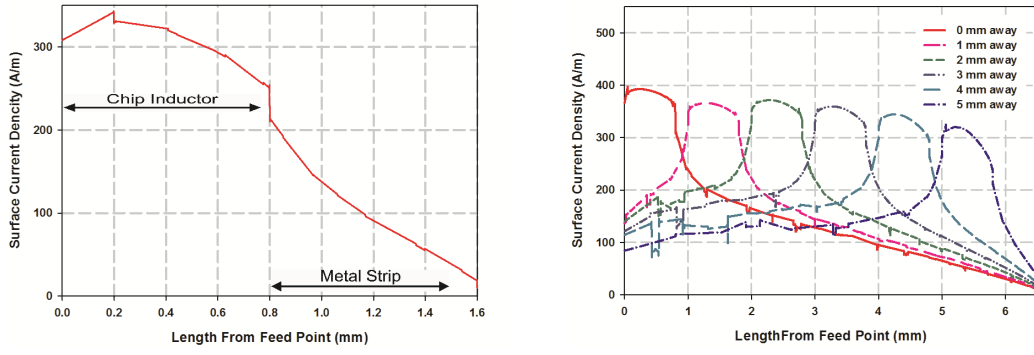
Figure 3.13: Impedance plot of the proposed antenna [$L = 0.8$ mm, $W = 1$ mm, Coilcraft 0603CS 23 nH Chip Inductor, $Sh = 1.6$ mm, $\epsilon_r = 4.4$]

Table 3.4: Simulated and calculated resonance frequency

Inductance (nH)	f Calculated (GHz)	f Simulated (GHz)	% Deviation
37.5	2.444	2.446	+0.0818
34	2.567	2.57	+0.1169
31	2.689	2.694	+0.1859
28	2.829	2.824	-0.17
25	2.994	2.998	+0.133

3.4.4 Surface Current Distribution

The surface current distribution in the antenna structure along the small metal strip and the chip inductor plays a crucial role in the radiation mechanism of the antenna. A detailed analysis is conducted on this in order to characterise the surface current. Figure 3.14(a) shows the surface current distribution in the proposed antenna at 2.4 GHz.



(a) Surface current distribution in the proposed antenna. $Ph = 0.8$ mm

(b) Surface current distribution in the proposed antenna for different chip inductor loading points $Ph = 5.8$ mm

Figure 3.14: Surface current distribution along the small metal strip and the chip inductor, for two different scenarios. [$\epsilon_r = 4.4$, $Ph = 0.8$ mm and 5.8 mm, $Pw = 1$ mm, $Gw = 3$ mm, Inductance = 37 nH]

From the above figure it is noticed that the surface current is maximum around the inductor and it drops drastically after the inductor in the metal strip. To get more clarity to this, a set of analysis is conducted by increasing the length Ph of the metal strip to 5.8 mm and then by changing the loading point of the chip inductor starting from the very end of feeding point to the other end of the metal strip. The loading distance from the feeding point is varied from 1 mm to 5 mm. The surface current obtained is shown in Figure 3.14(b). From the figure it is seen that the surface current always peaks at the inductor loading point, as [47]. It is further noted that as the loading point of the chip inductor is changed starting from the feeding point to the farther end of the small metal strip, the

3. Lumped Inductor Loaded ESA

resonant frequency is shifting towards the higher end of the frequency spectrum. For this analysis, the inductor value is kept constant at 23 nH. The resonance varied from 1.5 GHz to 3.2 GHz as the loading point is varied from 0 mm to 5.8 mm. As the loading point is varied, along with the resonance shift, the impedance matching showed good improvement. There is a sudden increase in the rate at the frequency is shifting when the inductor is loaded at the end point of the metal strip. The smith chart shown in Figure 3.15(b) shows the reactance variation for all the specified combinations. As the inductor loading point is moved away from the feeding point, it is noted that the reactance is becoming more and more capacitive. There will be a gap capacitance between the feeding point and the small metal strip in the structure apart from all other capacitances.

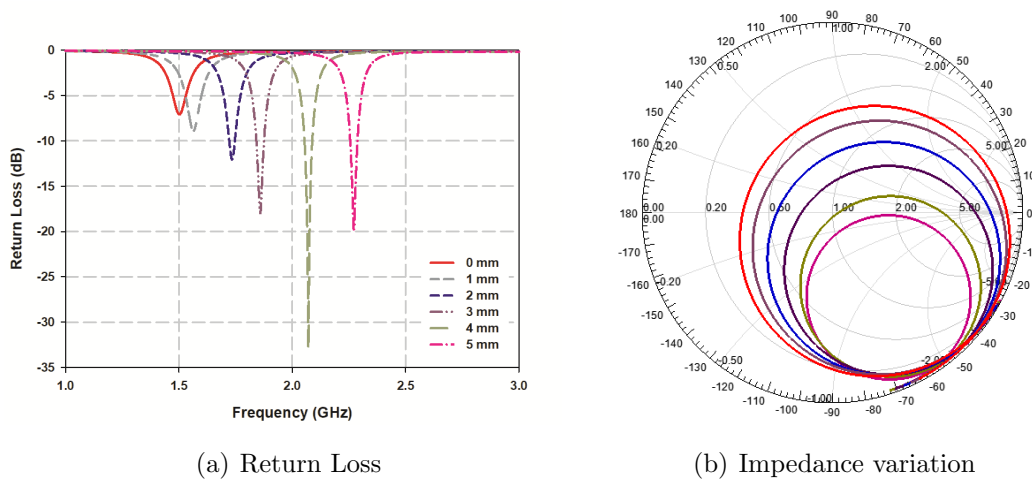


Figure 3.15: Resonance frequency shift for inductor loading at different locations on the small metal strip. [$\epsilon_r = 4.4$, Ph = 5.8 mm, Pw = 1 mm, Gw = 3 mm, Inductance = 37.5 nH]

3.5 Parametric Analysis

Different parametric analysis conducted on the antenna are.

- Effect of transmission line length L
- Effect of ground width Gw

- Effect of length Ph
- Effectt of changing Pw symmetrically
- Effect of asymmetric variation of Pw
- Effect of substrate thickness
- Effect of substrate relative permittivity

3.5.1 Effect of transmission line length L

The effect of CPW length on the antenna resonance is analysed by varying the length L as shown in the Figure 3.16. Here in the simulation the transmission line length is varied from 4 mm to 10 mm to analyse its implication on the resonance of the structure. It is noticed that there are only very negligible effect by L on the antenna resonance.

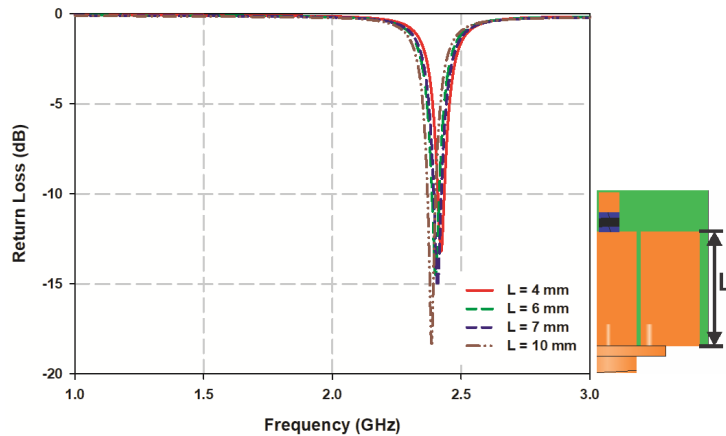


Figure 3.16: Simulated return loss of the antenna w.r.t feed line length. [$\epsilon_r = 4.4$, Pw = 1 mm, Gw = 3 mm, Inductance = 37.5 nH]

Two antennas with varying CPW length L are fabricated and tested, keeping all other parameters unchanged. For prototyping two extreme values are chosen,

i.e. 4 mm and 10 mm. Figure 3.17 shows the measured return loss characteristics. In the measured return loss also the variation in the resonant frequency is negligible. This confirms that the resonant frequency is independent of the length of the feed line.

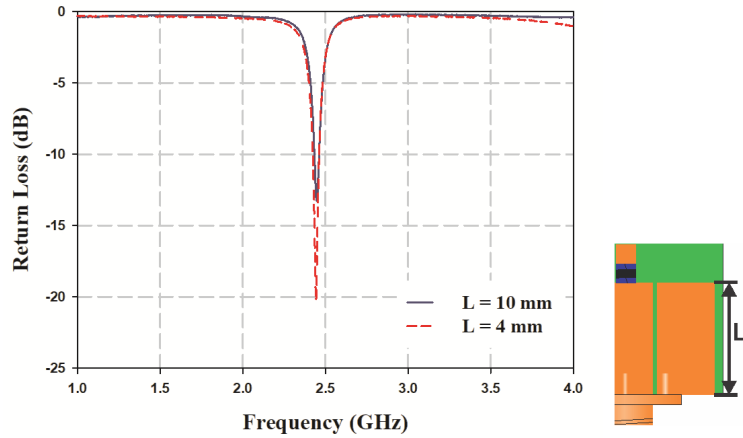


Figure 3.17: Measured return loss of the antenna w.r.t feed line length. [$\epsilon_r = 4.4$, $P_w = 1$ mm, $G_w = 3$ mm, Coilcraft 0603CS 23 nH Chip Inductor]

The shift in resonance for CPW length 4 mm and 10 mm are negligible, however a change in the matching of the resonance is noticed.

3.5.2 Effect of CPW ground width G_w

The analysis on the width G_w of the ground plane of the antenna, keeping all other parameters constant is shown in the figure 3.18(a). The inductance used for the analysis is 37.5 nH. It is evident from the simulation as shown in the figure that, the effect of ground width variation on the resonant frequency of the antenna is negligible. Figure 3.18(b) shows the corresponding impedance variation of the antenna. From this figure it is evident that ground width variation has no much impact on the impedance of the antenna. The width of the ground is increased to 60 mm, but it shows no big impact on the resonance and the impedance of the antenna.

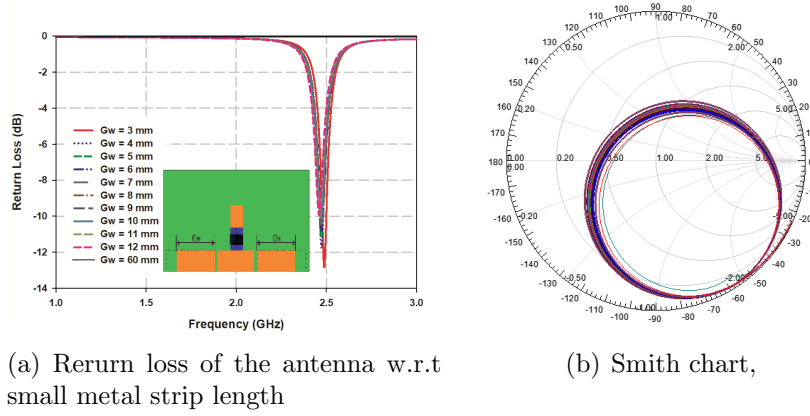


Figure 3.18: a) Simulated return loss of the antenna w.r.t ground width variation. b) Impedance variation [$\epsilon_r = 4.4$, $P_w = 1$ mm, Inductance = 37.5 nH]

3.5.3 Effect of metal strip geometry

3.5.3.1 Effect of length Ph

The length of the small metal strip Ph, where the chip inductor is connected has a significant role to play in deciding the resonant frequency of the antenna. The parametric analysis conducted on Ph by increasing it from 0.8 mm to 3.5 mm shows a significant decrease in the resonance as shown in the Figure 3.19. As the small metal strip length Ph is increased, this will increase the effective length of the antenna which in turn cause an increase in the total inductance and effective capacitance of the antenna to increase. This increase in the inductance and capacitance pushes the resonant frequency of the antenna further down in the frequency spectrum.

3.5.3.2 Effect of changing Pw symmetrically

The width Pw of the small metal strip to which the chip inductor is connected is varied symmetrically w.r.t the centre of the structure in order to analyse its effect on the resonance of the antenna. The expected result is a decrease in the resonant frequency of the antenna. The width is varied from 2 mm to 5 mm. The return loss observed from this observation is shown in the Figure 3.20. As expected the resonant frequency decreased with increase in Pw. Here also,

3. Lumped Inductor Loaded ESA

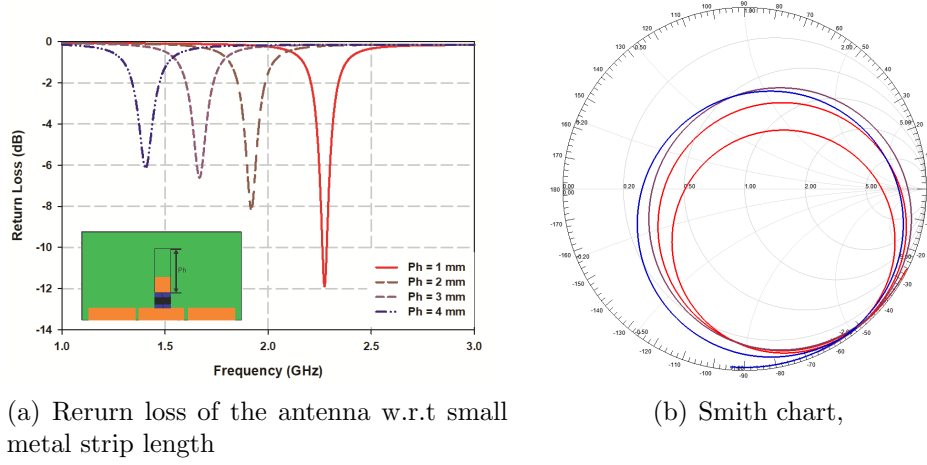


Figure 3.19: Change in the resonance characteristics of the antenna w.r.t change in the small metal strip length. [$\epsilon_r = 4.4$, $P_w = 1$ mm, $G_w = 3$ mm, Inductance = 37.5 nH]

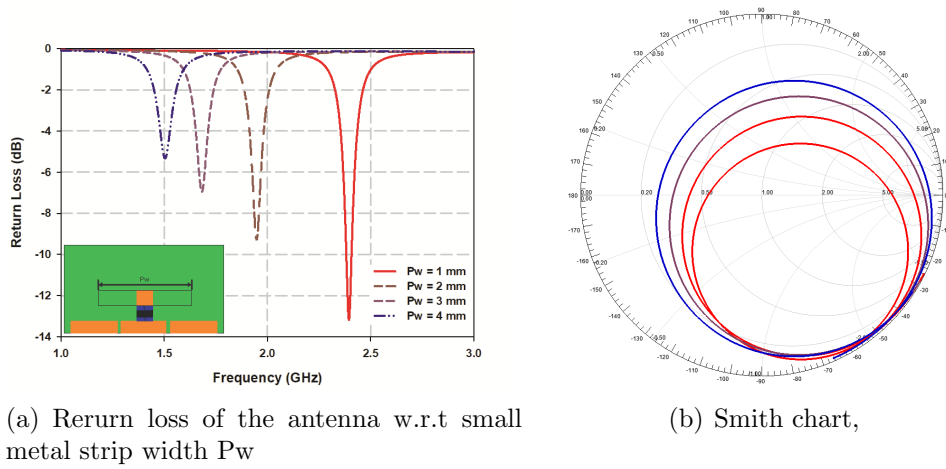


Figure 3.20: Change in the resonance characteristics of the antenna w.r.t change in the small metal strip width $P_w = 2$ mm to 5 mm. [$\epsilon_r = 4.4$, $P_h = 0.8$ mm, $G_w = 3$ mm, Inductance = 37.5 nH]

similar to the case where the metal strip length P_h is varied, change in the width P_w causes an increase in the total inductance and the increase in the coupling between the metal strip and the ground plane increases the effective capacitance of the antenna. This will in turn cause a decrease in the resonant frequency of the antenna

3. Lumped Inductor Loaded ESA

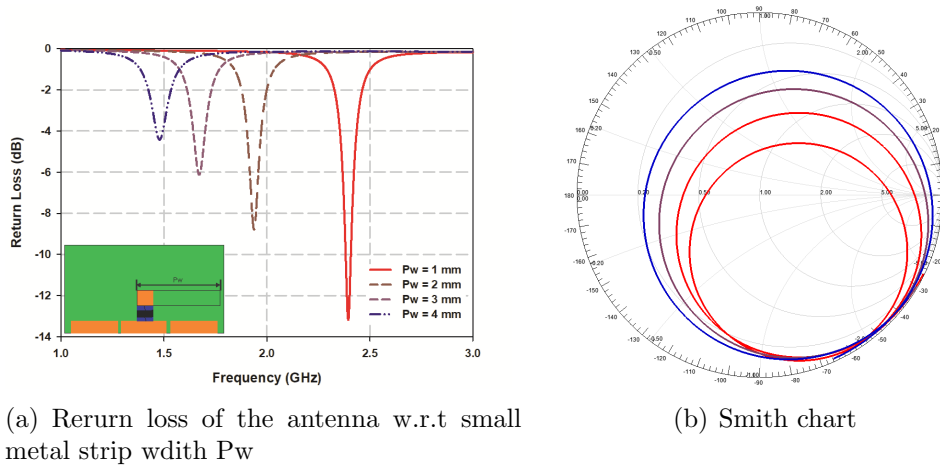


Figure 3.21: Change in the resonance characteristics of the antenna w.r.t asymmetric change in the small metal strip width P_w . [$\epsilon_r = 4.4$, $P_w = 1 \text{ mm} - 4 \text{ mm}$, $ph = 0.8 \text{ mm}$, $G_w = 3 \text{ mm}$, Inductance = 37.5 nH]

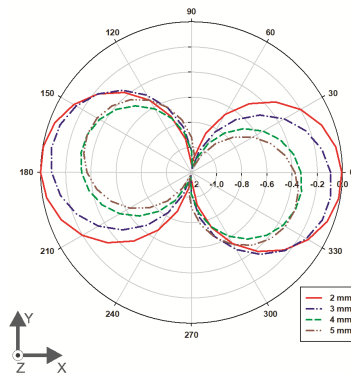


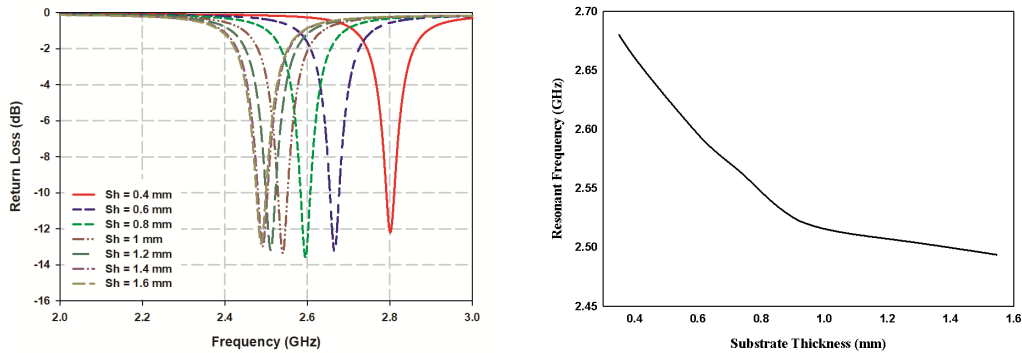
Figure 3.22: Change in the radiation pattern as the width P_w is varied asymmetrically. [$\epsilon_r = 4.4$, $P_w = 2 \text{ mm} - 5 \text{ mm}$, $ph = 0.8 \text{ mm}$, $G_w = 3 \text{ mm}$, Inductance = 37.5 nH]

3.5.3.3 Asymmetric variation of P_w

A parametric analysis is conducted on P_w using its asymmetrical structure. P_w is varied only to one side of the structure. The change in resonance observed in this case is similar to that obtained when P_w is varied symmetrically. Figure 3.21 shows the return loss and the smith chart for the corresponding variation. Even though there is no significant change in the resonance of the antenna, there is a

significant effect on the radiation pattern. Figure 3.22 shows how the radiation pattern of the antenna is varying w.r.t asymmetric variation in P_w . As P_w is varied from 2 mm to 5 mm, the radiation pattern underwent a tilt of nearly 20° . The shift in the radiation pattern is towards the side where the width P_w is varied. This shift is attributed to the asymmetrical distribution of the surface current in the structure and to the coupling between the metal strip and the ground which is dominant in the asymmetrically extended portion of the antenna. Also, there is a reduction in the radiated power of the antenna as the length is increased because of the reduction in the impedance matching, as seen in Figure 3.21(a).

3.5.4 Effect of substrate thickness



(a) Simulated return loss of the antenna w.r.t change in substrate thickness (b) Measured return loss variation of the antenna w.r.t change in substrate thickness

Figure 3.23: Change in the resonance characteristics of the antenna w.r.t change in the substrate thickness Sh . [$\epsilon_r = 4.4$, $Ph = 0.8$ mm, $P_w = 1$ mm - 4 mm, $ph = 0.8$ mm, $G_w = 3$ mm, Chip Inductor = CoilCraft 0603CS 23 nH]

The antenna has been subjected to a parametric variation on the substrate thickness Sh to understand its implications on the resonance. The thickness of the substrate is varied from 0.4 mm to 1.6 mm. This has shown an exponential decrease in the resonant frequency of the antenna as shown in Figure 3.23. The simulated resonance variation is shown in the Figure 3.23(a). A practical study of the substrate thickness is carried out by taking a 1.6 mm commercial FR4

substrate. The thickness of the substrate is changed by milling out the substrate from the bottom side of the antenna. The measured resonant frequency variation with substrate thickness is shown in Figure 3.23(b). This shift in the resonant frequency is due to the increase in the fringing field in the substrate as the thickness is reduced. As the thickness is reduced, the fields are no longer constraints to the substrate. The fields will go through both the substrate and the air. This increase in the fringing of the fields will reduce the effective permittivity of the structure making the antenna to resonate at a higher frequency

3.5.5 Effect of substrate relative permittivity

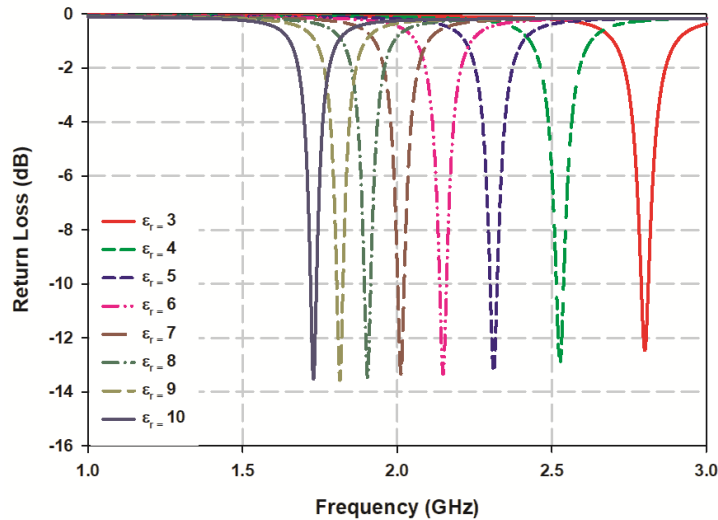


Figure 3.24: Change in the resonance as the relative permittivity is varied. [Ph = 0.8 mm, Pw = 1mm, Gw = 3 mm, Inductance = 37.5 nH]

This analysis is conducted to see how the relative permittivity of the substrate material is effecting the radiation characteristics of the antenna. For this analysis a simulation setup is arranged with a varying permittivity by keeping all other material properties same. The inductance value is kept at 37.5 nH. The simulation result shown in Figure 3.24 shows a decrease in the resonant frequency as the

3. Lumped Inductor Loaded ESA

relative permittivity is increased from 3 to 10.

Considering the equation (3.1), it is seen that the antenna structure could be considered as an LC circuit with an effective capacitance C_{eff} given as 0.113 pF with normal substrate. This includes the capacitance of the CPW, C_{CPW} , gap capacitance and the capacitance due to the small metal strip. Considering C_{eff} as a parallel combination of CPW capacitance C_{CPW} and the other capacitance C_t , the Table 3.5 shows the variation with changes in relative permittivity of the substrate material.

Table 3.5: Capacitance variation w.r.t substrate relative permittivity

ϵ_r	C_{CPW} (pF)	C_t (pF)	C_{eff} (pF)
3	0.6729	0.0986	0.086035
4	0.84289	0.12086	0.1057
5	1.012	0.14439	0.12637
6	1.1827	0.16708	0.1464
7	1.3526	0.19034	0.16686
8	1.5226	0.21231	0.18633
9	1.6925	0.2336	0.20527
10	1.8624	0.25681	0.22569

C_{CPW} is given by [25],[113] as

$$C_{CPW} = C_0 + C_1 \quad (3.2)$$

where

$$C_0 = 4\epsilon_0 \frac{K'(k)}{K(k)} \quad (3.3)$$

and

$$C_1 = 2\epsilon_0(\epsilon_r - 1) \frac{K'(k1)}{K(k1)} \quad (3.4)$$

Now drawing a relation between the relative permittivity ϵ_r and the C_{eff} , it is observed that they follow a linear relation and this could be approximated using a polynomial function. This approximation lead to the equation which gives the

capacitance in pF as.

$$C_{eff} = 0.01997 * \epsilon_r + 0.0263 \quad (3.5)$$

This shows that the change in relative permittivity of ϵ_r of the substrate in turn changes the effective capacitance C_{eff} thereby changing the resonance of the antenna.

3.6 Result and Discussion

3.6.1 Radiation Pattern

The simulated radiation pattern of the antenna shows an omnidirectional radiation pattern as expected from an electrically small antenna. The measured radiation pattern of the antenna is shown in Figure 3.25.

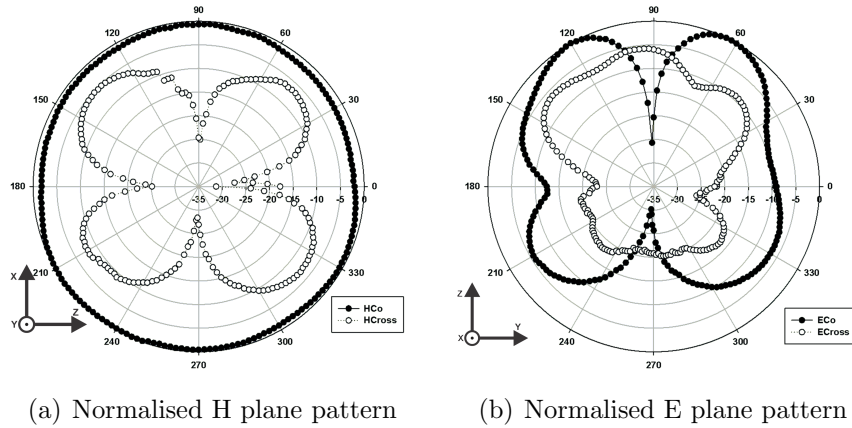


Figure 3.25: Measured radiation pattern of the coplanar antenna at 2.395 GHz. [Ph,Pg = 0.8 mm, Pw = 1 mm, Gw,Cw = 3 mm, G = 0.327 mm, L = 4 mm, Coilcraft 0603CS 23 nH Chip Inductor, $\epsilon_r = 4.4$]

In the E plane, the coplanar component is in the shape of a figure of eight as noticed in the Figure 3.25(b) however, in the H plane as shown in Figure 3.25(a) the coplanar component gives uniform radiation making the antenna to radiate omni directionally.

3. Lumped Inductor Loaded ESA

The 3D radiation pattern of the antenna is measured using EMSCAN RFXpert. Figure 3.26 shows the corresponding measured radiation pattern of this antenna. The measured radiation pattern shows that the antenna radiates omnidirectionally. This is in good agreement with far field data measured inside anechoic chamber as shown in the Figure 3.25.

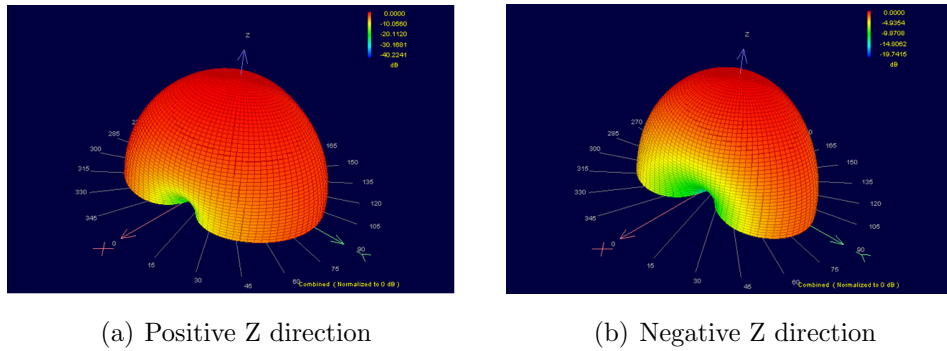


Figure 3.26: Measured 3D radiation pattern of the coplanar antenna at 2.395 GHz using RFXpert. [Ph,Pg = 0.8 mm, Pw = 1 mm, Gw,Cw = 3 mm, G = 0.327 mm, L = 4 mm, Coilcraft 0603CS 23 nH Chip Inductor, $\epsilon_r = 4.4$]

3.6.2 Gain and Efficiency

The gain of an antenna is a very important quantity which defines the ratio of radiation intensity of an antenna relative to an isotropic antenna. The gain of the antenna is measured using gain comparison method, which is the most common method employed in gain measurement [13]. For this purpose, a standard horn antenna with known gain value is used. Owing to the small size of the antenna, the gain of the antenna is expected to be very small. The measured gain of the antenna using this method is -6.5 dBi. Figure 3.27 shows the gain plot of the antenna.

It is observed that the gain of the antenna is improving when the length of the small metal strip is increased. But this will lead to a trade off between the electrical size and the gain of the antenna. An improvement in gain from -6.5 dBi to -1.5 dBi is observed when the metal strip length Ph is increased from 0.8 mm to 6 mm with a corresponding change in the chip inductor value to 11 nH. The

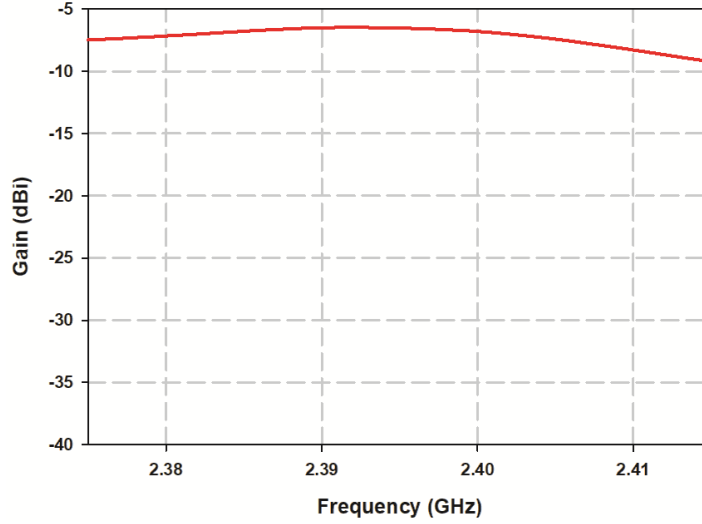


Figure 3.27: Measured gain of the prototype antenna fabricated w.r.t Table 3.1, $\epsilon_r = 4.4$

efficiency of the antenna is measured using the wheeler cap method [129]. The measured efficiency of the antenna is 16%

3.6.3 Design for Different Frequency Bands

For validating the design equations, antenna which operate at different frequency bands are designed using equations (3.1) and (3.5). The resonances obtained with simulation corresponding to those design parameters are in good agreement with the designed values. Three different frequency points, two below and one above 2.4 GHz are carried out. Figure 3.28 shows the return loss characteristics of those designs. Table 3.6 shows the designed parameters and a comparison of the designed values with the simulated one along with the error percentage

3. Lumped Inductor Loaded ESA

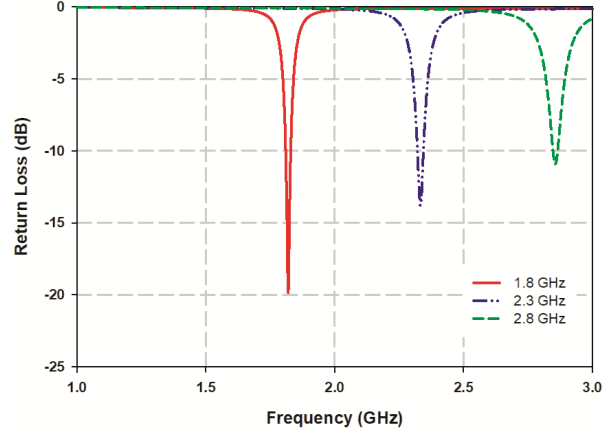


Figure 3.28: Return loss of the antenna designed using equation (3.1) and (3.5) at different frequency bands

Table 3.6: Design parameters for different frequency bands

L_{eff} (nH)	$f_{Calculated}$ (GHz)	$f_{Simulated}$ (GHz)	% Deviation
66.254	1.8	1.82	1.1
40.579	2.3	2.33	1.6
27.38	2.8	2.85	2.7

Another antenna is designed to operate at 2.7 GHz with a corresponding inductance of 30.75 nH. A prototype of this antenna is fabricated and tested. Figure 3.29 shows the comparison of the simulated and fabricated reflection characteristics of the antenna, which are in good agreement. Figure 3.30 shows the measured radiation characteristics of the antenna. In this case also in the E plane the coplanar component is in the shape of figure of eight and in the H plane the coplanar component is radiating uniformly making the antenna radiate omni directionally.

3. Lumped Inductor Loaded ESA

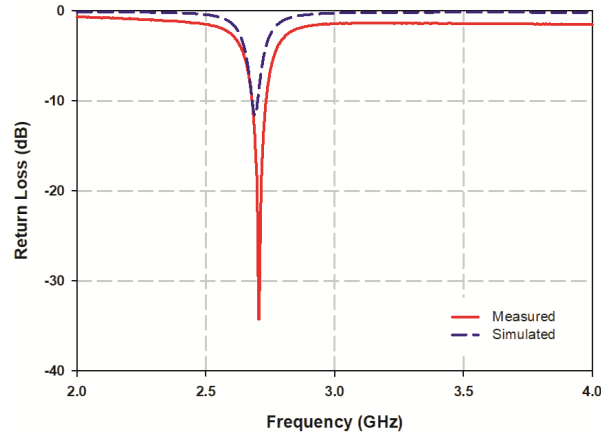


Figure 3.29: Measured and simulated reflection characteristics of the antenna designed at 2.7 GHz [$P_h, P_g = 0.8$ mm, $P_w = 1$ mm, $G_w, C_w = 3$ mm, $G = 0.327$ mm, $L = 4$ mm, Inductance = 30.75 nH, $\epsilon_r = 4.4$]

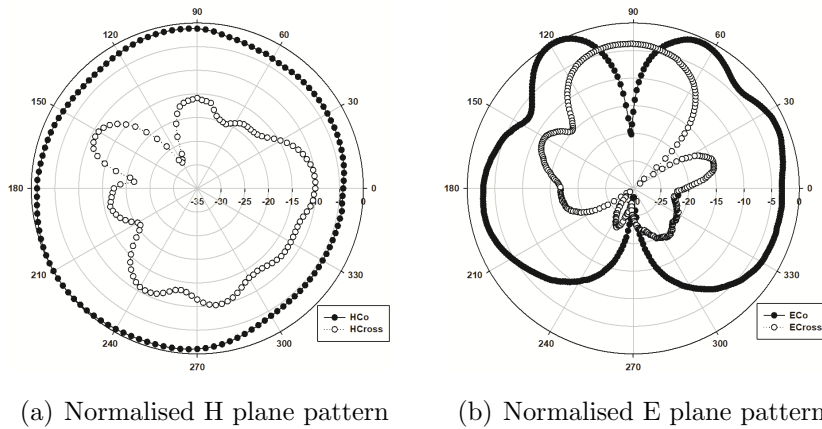


Figure 3.30: Measured radiation pattern of the coplanar antenna designed for 2.7 GHz. [$P_h, P_g = 0.8$ mm, $P_w = 1$ mm, $G_w, C_w = 3$ mm, $G = 0.327$ mm, $L = 4$ mm, Inductance = 30.75 nH, $\epsilon_r = 4.4$]

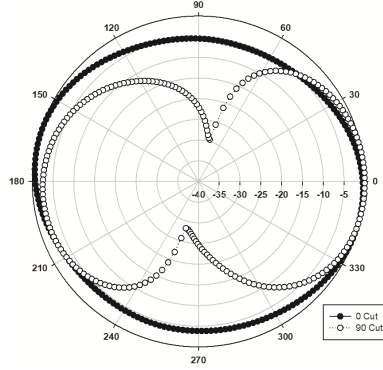


Figure 3.31: Measured radiation pattern of the antenna designed at 2.7 GHz using RFXpert [Ph,Pg = 0.8 mm, Pw = 1 mm, Gw,Cw = 3 mm, G = 0.327 mm, L = 4 mm, Inductance = 30.75 nH, $\epsilon_r = 4.4$]

Figure 3.31 shows the corresponding predicted far field pattern measured using EMSCAN RFXpert. These values are for Phi 0 and Phi 90 degree planes. The measured results are in good agreement with the measured far field pattern of the antenna.

3.6.4 Electrical Size

An antenna whose maximum dimension is very small compared to the wave length of operation comes under the category of small antennas. Under this category, small antennas are further divided into many different classes based on the ka value of the antenna. Here the k indicates the wave number given by,

$$k = \frac{2\pi}{\lambda} \quad (3.6)$$

and a is the radius of the smallest sphere which can enclose the maximum dimension of the antenna [61], [69]. For the proposed antenna the calculated ka value at 2.4 GHz is 0.2924. For a small antenna, there are few constraints on the quality factor (Q) of the antenna. The Q mentioned here is the 3 dB quality factor of the antenna. For a small antenna, the Q of the antenna should be greater than the Q minimum value of the antenna. The Q minimum for a small antenna is

3. Lumped Inductor Loaded ESA

given by, [69]

$$Q_{min} = \frac{1}{ka} + \frac{1}{(ka)^3} \quad (3.7)$$

For the proposed antenna, the Q_{min} calculated using the equation (3.7) is 43.42. The measured 3 dB Q of the antenna is 319.5, which is greater than the Q_{min} .

There is a maximum limit for the achievable gain of an electrically small antenna given by

$$Gain_{max} = (ka)^2 + 2ka \quad (3.8)$$

With the calculated value of ka, the $Gain_{max}$ obtained is -4 dBi. The measured gain of the antenna is -6.5 dBi

With the measured ka, Q and Gain values of the antenna, the proposed antenna is categorized as electrically small antenna (ESA), where the volume is restricted [69]. The electrical size characteristics of the antenna is summarised in the Table 3.7

Table 3.7: ESA Parameters

Parameter	Required	Obtained
ka	<0.5	0.2924
Q	>43.42	319.5
Gain	<-4 dBi	-6.5 dBi

3.7 Conclusions

A novel electrically small antenna based on a coplanar wave guide and a chip inductor has been designed, developed and analysed successfully. The real estate of the antenna has been kept very small, with a very small ka value of 0.2924. For the development of the antenna a 0603CS 23 nH chip inductor from CoilCraft is used. The antenna operates at 2.4 GHz band with necessary bandwidth to cover a single channel of operation for an application. The realised far field radiation pattern of the antenna is omni directional. Owing to the very small size of the antenna, the realized efficiency is small, in the range of 16%. The measures peak gains is -1.6 dBi. The Design equation of the antenna is developed and verified.

Chapter 4

An Electrically Small Frequency Reconfigurable Antenna

4.1 Introduction

This chapter deals with an electrically small reconfigurable antenna operating at 2.4 GHz and 5.4 GHz frequency bands. The chapter explores the working of the antenna in two frequency bands which is based on two different phenomena of the structure. The chapter moves forward by considering the evolution, prototyping, measurements, theory and different parametric analysis of the conceived structure.

4.1.1 Evolution

The whole concept of the proposed reconfigurable antenna started with an attempt to excite a microstrip based Stepped Impedance Resonator (SIR), to make it radiate electromagnetic energy. There are three fundamental types of SIRs available, namely Quarter wave ($\lambda/4$), Half wave ($\lambda/2$) and Full wave (λ) SIRs as shown in Figure 4.1.

4. An Electrically Small Frequency Reconfigurable Antenna

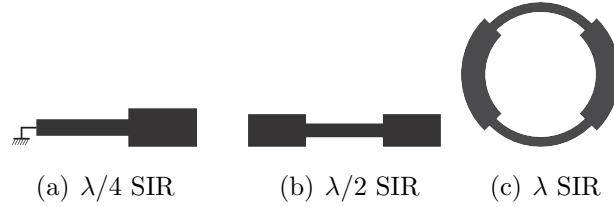


Figure 4.1: Conventional SIRs

The interesting fact about these SIRs is that the fundamental resonant frequency for all these three SIRs are the same, irrespective of the differences in its physical dimension. In SIR the wavelength of the resonant frequency is not directly related to the physical length. It is related through two parameters of the SIR, the impedance ratio k and the electrical length ratio α . By varying these two parameters it is possible to make SIR with different lengths to resonate at same frequency. $\lambda/4$ type SIR has gained notable attention in microwave filter design because of its ability for miniaturisation. The aforesaid peculiarity of these structures sparked the thought of pushing for an Electrically Small Antenna (ESA) using the smallest member of the SIR family, i.e., the $\lambda/4$ type SIR. The frequency of operation of the SIR is preselected as 2.4 GHz. The substrate selected for the initial design of the antenna is the commercially available FR-4 material, with a relative permittivity (ϵ_r) of 4.4 and thickness 1.6 mm.

The evolution of the antenna started with an attempt to excite a $\lambda/4$ SIR to radiate electromagnetic energy. Initially a direct coaxial feeding as shown in the figure 4.2(a) is employed. The return loss for this feeding is shown in Figure 4.2(b). From the figure it is clear that this feeding is unable to excite the SIR. Next a 50Ω microstripline is employed as a feed line for the antenna. Figure 4.3 shows the evolution process of the antenna. Initially an edge coupling technique was employed as shown in Figure 4.3 (a). But this type of feeding technique was not providing a promising result in terms of the impedance matching. Figure 4.4(a) shows the simulated return loss obtained for this geometry, which is very poor in terms of impedance matching. The corresponding smith chart of the antenna shown in Figure 4.4(b) shows that the reactance is highly capacitive at this resonance.

4. An Electrically Small Frequency Reconfigurable Antenna

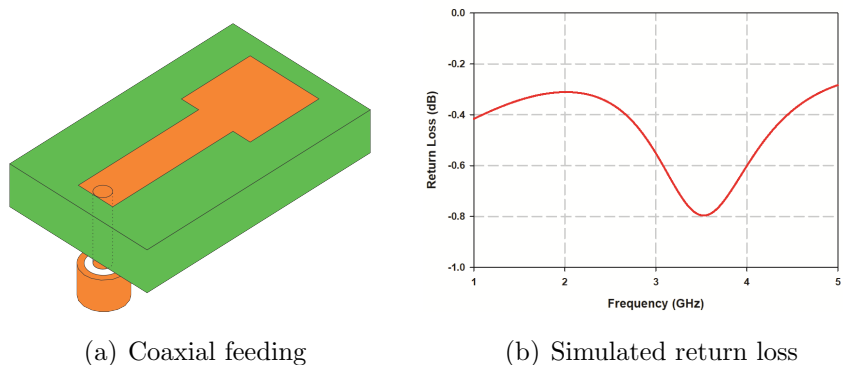


Figure 4.2: a) Coaxial excitation of a $\lambda/4$ SIR, b) simulated return loss of the antenna ($\epsilon_r = 4.4$, $h = 1.6$ mm, $l_1 = 9$ mm, $l_2 = 3.5$ mm, $k = 0.7$, $\alpha = 0.285$)

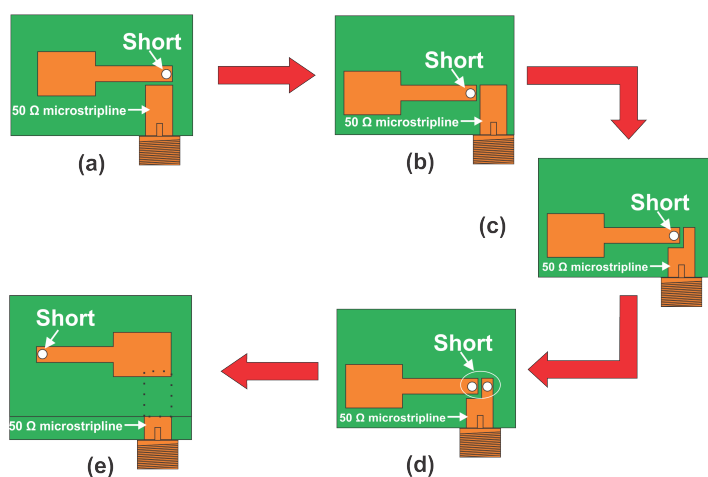


Figure 4.3: Evolution of the excitation of the proposed antenna

To improve the impedance matching of the antenna the orthogonal edge of the feed line is used for exciting the SIR as shown in Figure 4.3 (b). The Corresponding return loss characteristics of the antenna is shown in Figure 4.5(a), where the impedance matching seems to deteriorate again. This is evident from the smith chart that the impedance became more capacitive with this modification as shown in Figure 4.5(b). This triggered the thought of using a hybrid of the first two feeding methods, as shown in Figure 4.3 (c), which gave a better

4. An Electrically Small Frequency Reconfigurable Antenna

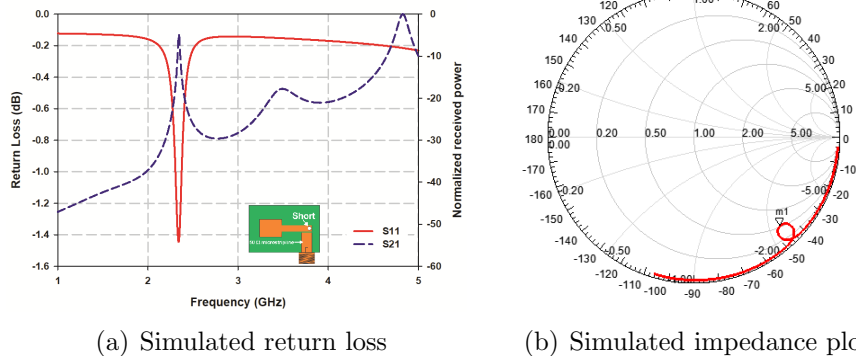


Figure 4.4: Simulated resonant properties of the antenna w.r.t Figure 4.3 (a) ($\epsilon_r = 4.4$, $h = 1.6$ mm, $l_1 = 9$ mm, $l_2 = 3.5$ mm, feed line width = 3 mm, $k = 0.7$, $\alpha = 0.285$)

result than that of the model 4.3 (b), but same as that of model 4.3 (a). The corresponding return loss characteristics and the impedance matching plot are shown in Figure 4.6(a) and 4.6(b), respectively.

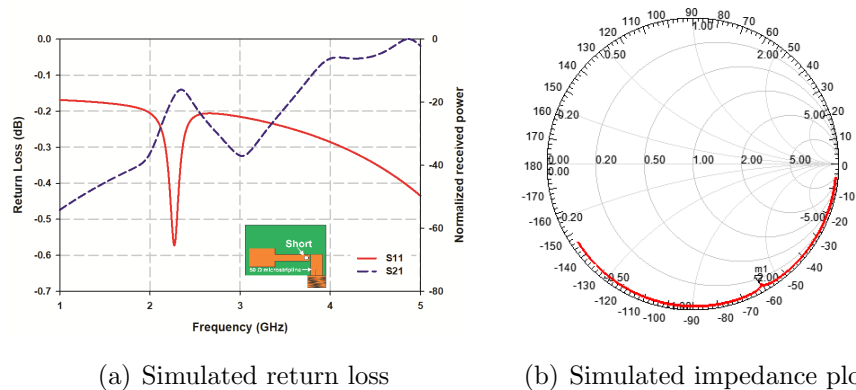


Figure 4.5: Simulated resonant properties of the antenna w.r.t Figure 4.3 (b) ($\epsilon_r = 4.4$, $h = 1.6$ mm, $l_1 = 9$ mm, $l_2 = 3.5$ mm, feed line width = 3 mm, $k = 0.7$, $\alpha = 0.285$)

4. An Electrically Small Frequency Reconfigurable Antenna

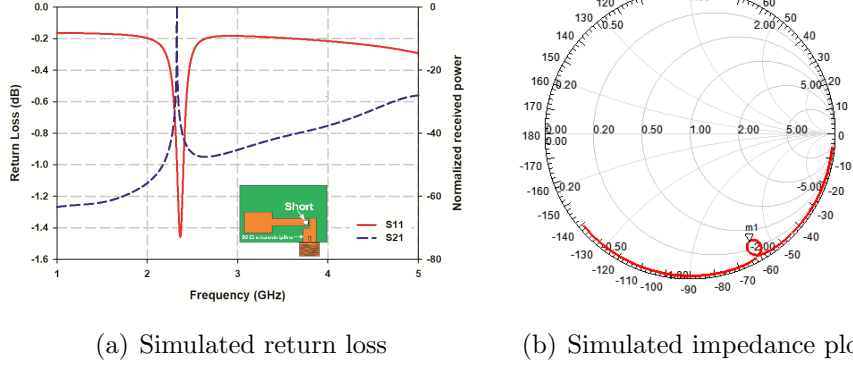


Figure 4.6: Simulated resonant properties of the antenna w.r.t Figure 4.3 (c) ($\epsilon_r = 4.4$, $h = 1.6$ mm, $l_1 = 9$ mm, $l_2 = 3.5$ mm, feed line width = 3 mm, $k = 0.7$, $\alpha = 0.285$)

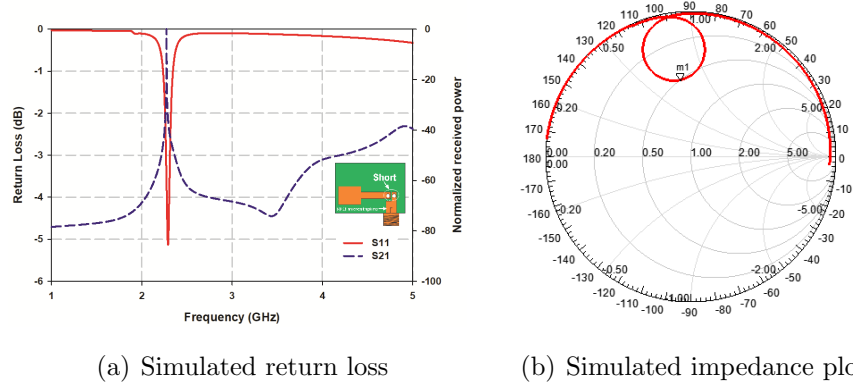


Figure 4.7: Simulated resonant properties of the antenna w.r.t Figure 4.3 (d) ($\epsilon_r = 4.4$, $h = 1.6$ mm, $l_1 = 9$ mm, $l_2 = 3.5$ mm, feed line width = 3 mm, $k = 0.7$, $\alpha = 0.285$)

The impedance plot in the smith chart for all the aforesaid models reveals that the reactance part of the impedance is highly capacitive. To mitigate this capacitive reactance, a shorting pin from the feed line to the ground is applied to the model as shown in Figure 4.3 (d). The corresponding return loss characteristics depicted in Figure 4.7(a) shows a considerable improvement in the impedance matching in comparison with the earlier three models. Here the corresponding impedance plot as in Figure 4.7(b) shows that the reactance has become inductive.

4. An Electrically Small Frequency Reconfigurable Antenna

Even though there was a considerable improvement in the impedance matching, it was not up to the mark in consideration with the 2:1 VSWR.

Finally, a proximity coupled feeding technique as shown in Figure 4.3 (d) is experimented resulting in a promising impedance matching compared to all other type of feeding techniques experimented earlier. To implement this feeding technique, few changes have been incorporated in the SIR geometry. Here the structure has been split into two layers. First layer consists of two microstriplines which forms the SIR structure without the ground plane at bottom side. The second layer consists of ground plane and the feed line. Both are designed using the same FR4 substrate material of thickness 1.6 mm. Here the ground plane of the bottom layer serves the ground to both the SIR and the feed line. To implement $\lambda_g/4$ type SIR, a short is connected from the top layer to the ground in the bottom layer. Figure 4.8(a) and 4.8(b) shows the return loss characteristics and the impedance variation for the proposed proximity coupled feeding technique for the antenna. It is observed that this feeding is providing an improved impedance matching for the antenna compared to all other feeding methods and therefore this feeding method is chosen for the rest of the analysis of this antenna.

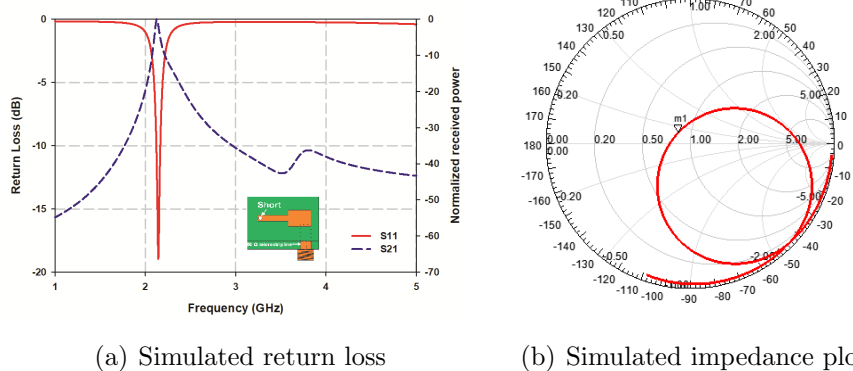


Figure 4.8: Simulated resonant properties of the antenna w.r.t Figure 4.3 (e) ($\epsilon_r = 4.4$, $h = 3.2$ mm, $l_1 = 9$ mm, $l_2 = 3.5$ mm, feed line width = 3 mm, $k = 0.7$, $\alpha = 0.285$)

4.2 Design

4.2.1 SIR Design

The radiating element of the proposed antenna is designed using a quarter wave SIR, as shown in Figure 4.9. The resonant frequency selected for the design is 2.4 GHz. For an SIR, the resonance is not determined by the physical length of the element as in the case of a uniform impedance resonator, rather it is determined by two important factors of the SIR. The impedance ratio k and the length ratio α . The impedance ratio k is defined as in (4.1)

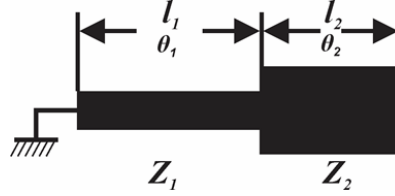


Figure 4.9: Geometry of Quarter wave SIR used in the design (Top View)

$$k = \frac{Z_2}{Z_1} \quad (4.1)$$

where Z_1 and Z_2 are the impedances of the transmission line section l_1 and l_2 , respectively.

The α is the ratio between the electrical length θ_2 to the total electrical length $\theta_1 + \theta_2$

$$\alpha = \frac{\theta_2}{\theta_1 + \theta_2} \quad (4.2)$$

where the electrical length θ is

$$\theta = \frac{2\pi}{\lambda} l \quad (4.3)$$

where λ is the free space wavelength and with a substrate λ will become the guided wavelength λ_g . Based on these parameters the condition for resonance of SIR is given by [75] as

$$k = \tan(\theta_1) * \tan(\theta_2) \quad \text{for odd mode} \quad (4.4)$$

4. An Electrically Small Frequency Reconfigurable Antenna

$$k = -\cot(\theta_1) * \cot(\theta_2) \quad \text{for even mode} \quad (4.5)$$

In the case of a quarter wave SIR, the only possible mode is the odd mode of operation, leading to the selection of equation (4.4) for the design of the antenna. In the design procedure, while considering the length of the strip, the shorting stub length is also included in order to correct the error intruding in the design. The solution is obtained numerically with the help of computer program in matlab. For the proposed design, two transmission lines of width 1.6 mm and 3.6 mm are randomly chosen and the corresponding impedance ratio from the widths is 0.7. This value is used for the calculation of the corresponding lengths of the microstrip lines l_1 & l_2 . The physical length l_1 & l_2 are calculated by subtracting the length ΔL due to fringing field from the effective length. These length l_1 & l_2 are considered as S1 & S2 in the antenna geometry.

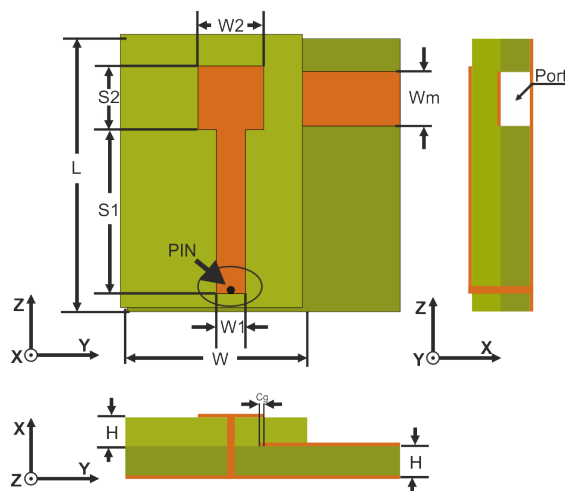


Figure 4.10: Geometry of the proximity coupled antenna

4. An Electrically Small Frequency Reconfigurable Antenna

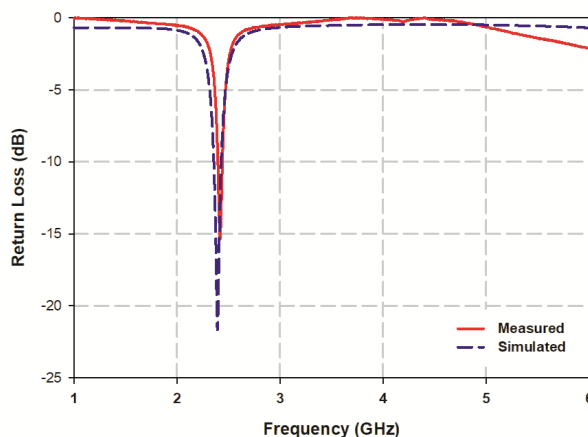


Figure 4.11: Measured and simulated return loss of the antenna at 2.4 GHz. [$L = 15$ mm, $S1 = 9$ mm, $S2 = 3.5$ mm, $W = 10$ mm, $W1 = 1.6$ mm, $W2 = 3.6$ mm, $Wm = 3$ mm, $Cg = 0.6$ mm, $H = 1.6$ mm, $\epsilon_r = 4.4$]

Figure 4.11 shows the simulated and measured return loss of the antenna in the 2.4 GHz band. The dimensions of the antenna are provided in Figure 4.10. In the simulation, the proposed antenna is resonating at 2.412 GHz whereas from the measured return loss, the antenna is resonating at 2.41 GHz. The slight mismatch in the resonance is due to fabrication tolerances. A good matching for the antenna is achieved through the implementation of proximity feeding technique. It is observed that both simulated and measured results are in good agreement.

The simulated return loss of the antenna for different resonant frequencies designed using the equation (4.4) is shown in Figure 4.12. Here the design is carried out on a FR4 substrate with a total thickness of 3.2 mm. The width of the two microstrip transmission lines considered for the design are 1.6 mm and 3.6 mm. The impedance ratio k is 0.7 and the electrical length ratio considered is 0.285. Table 4.1 shows the comparison of the designed resonant frequency to the simulated value. Here in the table, l_1 and l_2 are the physical length corresponding to the microstriplines in the SIR. The table shows the designed resonant frequency as f_d and the simulated resonant frequency as f_s . Both the values are in close congruence as observed from the percentage deviation value of

4. An Electrically Small Frequency Reconfigurable Antenna

the resonance. The percentage deviation is calculated as

$$\%Deviaiotn = \frac{|(f_d - f_s)|}{f_d} \quad (4.6)$$

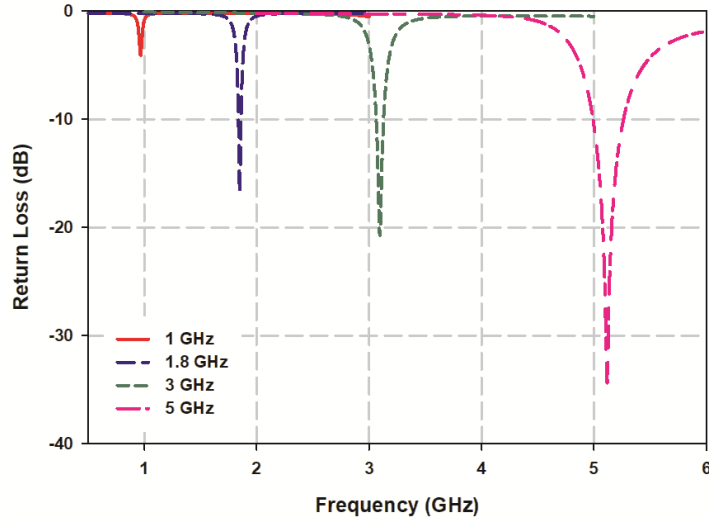


Figure 4.12: Simulated return loss of the antenna designed using (4.4) for different frequencies. [W1 = 1.6 mm, W2 = 3.6 mm, Wm = 3 mm, Cg = 0.6 mm, H = 1.6 mm, $\epsilon_r = 4.4$]

Table 4.1: Designed and simulated resonance w.r.t equation (4.4)

Sl No	f_d (GHz)	l_1 (mm)	l_2 (mm)	f_s (GHz)	% deviation
1	1	25	10.6	0.9712	2.88
2	1.8	11.85	4.93	1.85	2.7
3	3	2.4	5.9	3.1	3.3
4	5	2	1.4	5.12	2.4

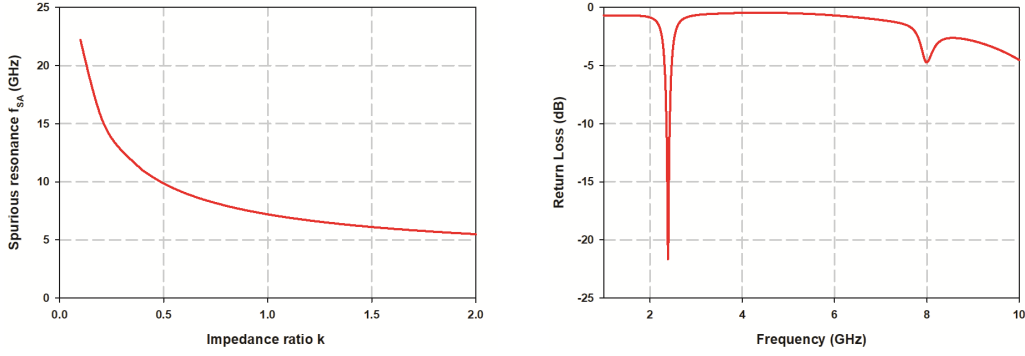
When we consider the spurious frequencies of SIR, the spurious resonances

4. An Electrically Small Frequency Reconfigurable Antenna

for $\lambda_g/4$ SIR is given by

$$\frac{f_{SA}}{f_0} = \frac{\pi}{\tan^{-1}(\sqrt{k})} - 1 \quad (4.7)$$

where f_{SA} is the spurious resonance frequency and f_0 is the fundamental resonance frequency and k is the impedance ratio. Figure 4.13(a) shows the variation of spurious resonance with respect to impedance ratio k . Using this formula, the spurious resonance obtained for the proposed antenna is 8.3 GHz. Figure 4.13(b) shows the simulated spurious resonance for the proposed SIR antenna.



(a) Calculated spurious frequency variation w.r.t equation (4.7)

(b) Simulated first spurious frequency for the proposed design

Figure 4.13: Spurious frequency variation and the simulated spurious frequency for the proposed SIR with $k = 0.71$

For validating the design with respect to electrical length ratio α , three different values for α are considered for obtaining a resonance at 2.4 GHz for the $\lambda_g/4$ SIR and the design is carried out keeping all other parameters constant. The selected value of α and the corresponding values of l_1 and l_2 are given in Table 4.2. Figure 4.14 shows the corresponding simulated resonance obtained for these designs. From the simulated resonance values as shown in the table, the deviation from the designed resonance is considerably small staying within 3% of the design frequency. This shows that the antenna is resonating at the frequency at which the SIR is resonating, affirming the SIR mode of operation in the antenna.

4. An Electrically Small Frequency Reconfigurable Antenna

Table 4.2: Dimensions and resonance of the SIR for different α values

α	l_1 (mm)	l_2 (mm)	f (GHz)
0.2	10	2	2.45
0.3	8.3	3.5	2.42
0.5	5	6.6	2.404

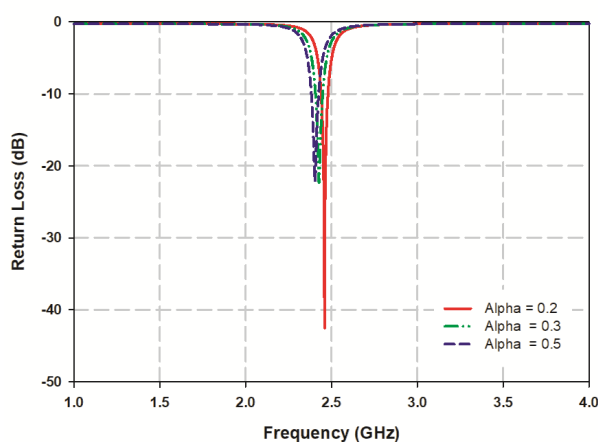


Figure 4.14: Simulated return loss of the antenna designed at 2.4 GHz for different α values [$H = 1.6$ mm, $\epsilon_r = 4.4$]

Figure 4.15 shows the simulated and measured reflection characteristics of the antenna designed for another set of impedance ratio and length ratio. This is carried out to validate that, even with a different set of design parameters for SIR which in turn gives a different dimension for the geometry for a particular frequency, the antenna should also resonate at the same frequency. The impedance ratio k is 0.65 and the length ratio α is 0.6. The simulated and measured data are in good agreement. The slight difference is due to the fabrication tolerances. Figure 4.16 shows the variation in the spurious frequency for different α values. It can be noticed that the spurious frequency become closer to the theoretical value of 8.3 GHz as the α approaches 0.5, since the equation (4.7) is derived for the case $\alpha = 0.5$, [75].

4. An Electrically Small Frequency Reconfigurable Antenna

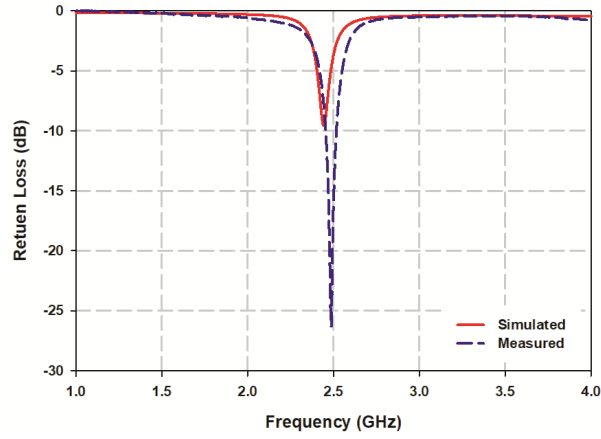


Figure 4.15: Simulated and measured return loss of the antenna designed at 2.4 GHz for $\alpha = 0.6$ and $k = 0.65$ [$H = 1.6$ mm, $\epsilon_r = 4.4$, $l_1 = 4.45$ mm, $l_2 = 6.6$, $W1 = 1.2$ mm, $W2 = 3.6$ mm]

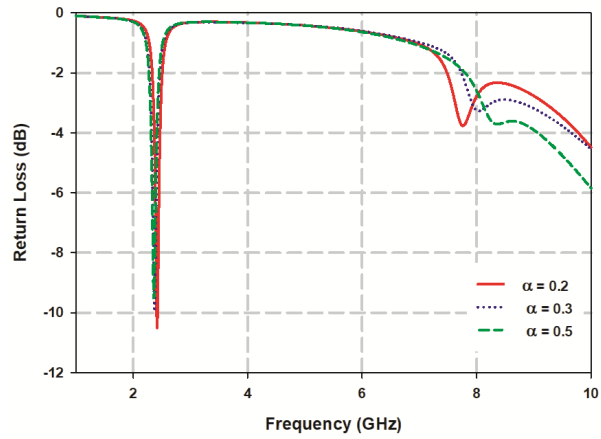


Figure 4.16: Simulated fundamental and first spurious frequency for different α , [$H = 1.6$ mm, $\epsilon_r = 4.4$, $W1 = 1.6$ mm, $W2 = 3.6$ mm, $k = 0.7$]

From all the above experiments, it is concluded that the mode excited in the structure with the short is a SIR mode of operation. The experiments shows that

4. An Electrically Small Frequency Reconfigurable Antenna

the resonant frequency and the physical dimension can be controlled through the SIR parameters k and α

4.2.2 New mode of operation

It was serendipitous that when the short in the SIR is removed from the antenna, another resonance is emerged at 5.4 GHz. This new resonance was not showing much relation to the resonances obtained from any of the SIR modes. The expected resonance frequency from the SIR for the second mode is at 8.3 GHz with the selected k and α values. Moreover, the variation of this resonance is not much sensitive to the variations in k value, whereas the SIR modes are highly sensitive to k . The simulated and measured return loss characteristics of the antenna in the higher 5.4 GHz band is shown in the Figure 4.17. The simulated and measured data are in good agreement. The antenna resonates at 5.45 GHz.

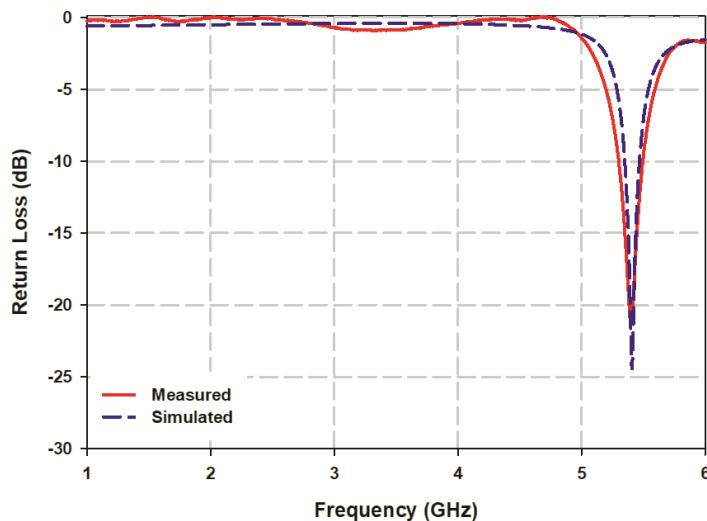


Figure 4.17: Measured and simulated return loss of the antenna at the higher 5.45 GHz. [L = 15 mm, S1 = 9 mm, S2 = 3.5 mm, W = 10 mm, W1 = 1.6 mm, W2 = 3.6 mm, Wm = 3 mm, Cg = 0.6 mm, H = 1.6 mm, $\epsilon_r = 4.4$]

4. An Electrically Small Frequency Reconfigurable Antenna

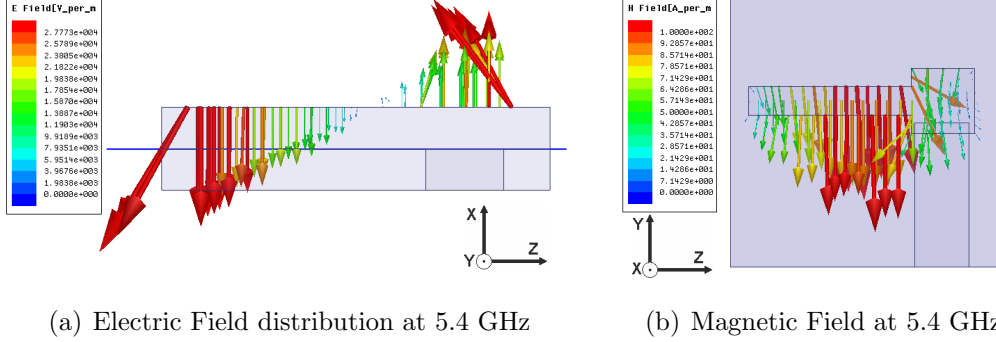


Figure 4.18: Simulated Electric and Magnetic Field in the structure for the open circuited mode [Spatially Orthogonal]. [$L = 15$ mm, $S1 = 9$ mm, $S2 = 3.5$ mm, $W = 10$ mm, $W1 = 1.6$ mm, $W2 = 3.6$ mm, $Wm = 3$ mm, $Cg = 0.6$ mm, $H = 1.6$ mm, $\epsilon_r = 4.4$]

In order to understand the working principle behind the newly generated resonance, the electric and magnetic fields of the structure at this particular resonance are analysed. The electric and magnetic field distribution in the antenna structure for the open circuited mode is given in Figure 4.18. The electric field distribution, shown in Figure 4.18(a) is along the X-direction whereas, the magnetic field distribution, shown in Figure 4.18(b) is along Y-direction of the antenna. Figure 4.19 shows the 2D plot of the magnitude of electric and magnetic field distribution in the antenna along the length L . The electric field as in Figure 4.19(a) is maximum at the two open ends and magnetic field, as in Figure 4.19(b), is minimum at these ends. The peak of magnetic field and minimum of electric field is observed at a point offset to the centre towards the wider strip, near the discontinuity. This offset is due to the surface current distribution in the structure, which dominates at the discontinuity. The surface current distribution in the structure is shown in the Figure 4.20. The distribution of the surface current is asymmetric with the maximum intensity near the discontinuity, i.e. near the step junction. In the whole structure a $\lambda_g/2$ distribution at 5.4 GHz is observed only along the two microstripline.

4. An Electrically Small Frequency Reconfigurable Antenna

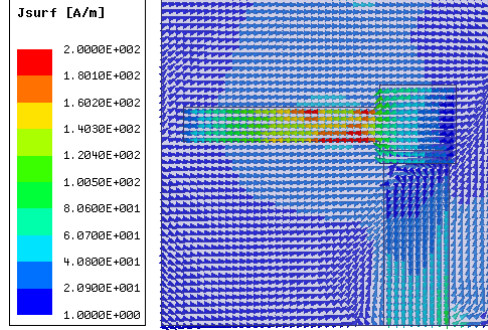


Figure 4.20: The surface current distribution in the open circuited fabry-perot mode of the antenna at 5.4 GHz. [$L = 15$ mm, $S1 = 9$ mm, $S2 = 3.5$ mm, $W = 10$ mm, $W1 = 1.6$ mm, $W2 = 3.6$ mm, $Wm = 3$ mm, $Cg = 0.6$ mm, $H = 1.6$ mm, $\epsilon_r = 4.4$]

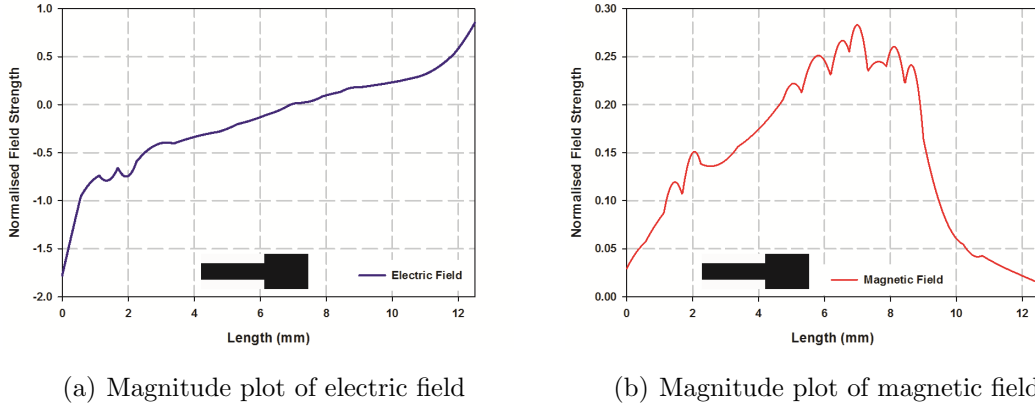


Figure 4.19: Normalised Magnitude of Simulated Electric and Magnetic Field in the structure. [$L = 15$ mm, $S1 = 9$ mm, $S2 = 3.5$ mm, $W = 10$ mm, $W1 = 1.6$ mm, $W2 = 3.6$ mm, $Wm = 3$ mm, $Cg = 0.6$ mm, $H = 1.6$ mm, $\epsilon_r = 4.4$]

It is observed that the electric and magnetic fields in the antenna are orthogonal spatially and are with a phase difference temporally. The spatial orthogonality is shown in Figure 4.18. The analysis in time shows that these fields are not orthogonal in time. The peak temporal component of the electric and magnetic fields are not exactly at a time difference of $\tau/4$, where τ is the total time period at resonance. When expressed in radian, the peaks occurs at a phase difference of

4. An Electrically Small Frequency Reconfigurable Antenna

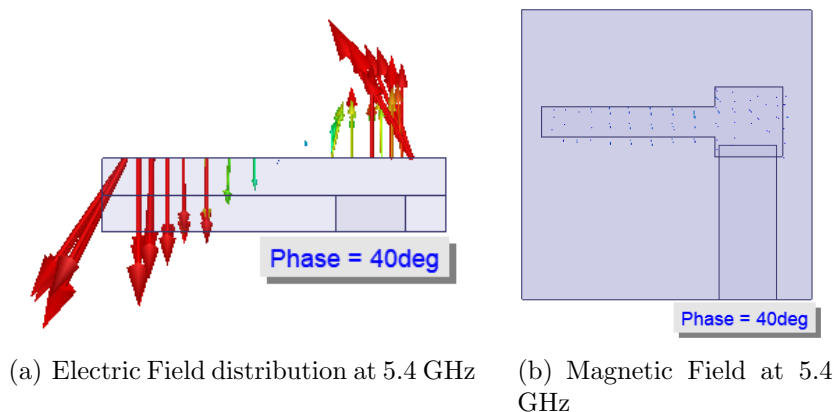


Figure 4.21: Simulated field plot of temporal orthogonality of electric and magnetic fields. [$L = 15$ mm, $S1 = 9$ mm, $S2 = 3.5$ mm, $W = 10$ mm, $W1 = 1.6$ mm, $W2 = 3.6$ mm, $Wm = 3$ mm, $Cg = 0.6$ mm, $H = 1.6$ mm, $\epsilon_r = 4.4$]

40° . At this phase the electric field shows a maximum whereas the time magnetic field is minimum. Figure 4.21 shows both the fields simulated at a particular time instant.

A detailed analysis of the field distribution in the structure echoes the electric and magnetic field distributions observed in a slit cut metallic slab loaded with dielectric [3]. A metallic slab with a slit in it acts as a fabry-perot resonator [3], where the field distributions are a dual of normal etalone fabry-perot resonator with the peak of magnetic field at the centre and electric field at end points. The field distribution of normal etalone fabry-perot resonator and a slit cut metallic slab loaded with dielectric are shown in Figure 4.22 [3]. A comparison of these two figures confirms the point that the mode excited in the antenna structure at higher frequency is same as that of a fabry-perot with slit cut metallic slab loaded with dielectric.

4. An Electrically Small Frequency Reconfigurable Antenna

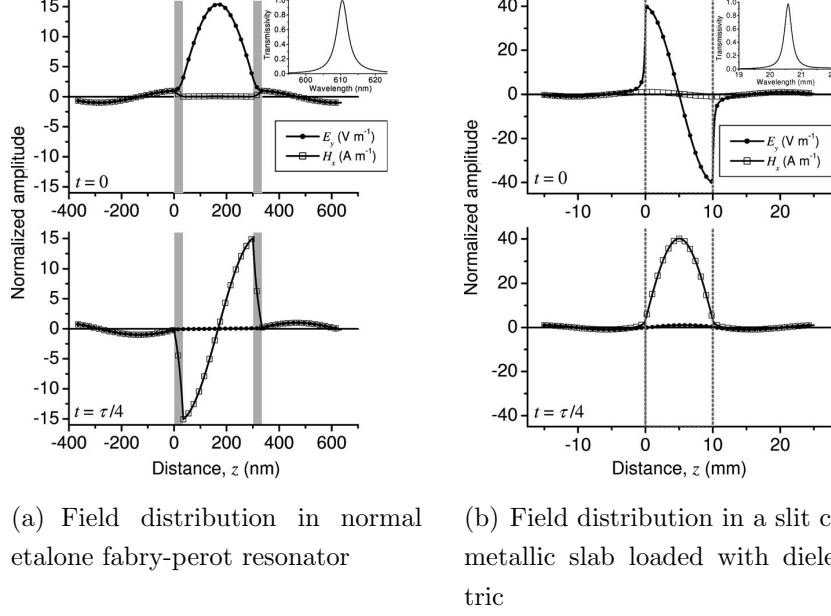


Figure 4.22: Electric and Magnetic field distribution in different fabry-perot resonators. Courtesy: [3]

A closer observation of the fields that we obtained in the open circuited mode of the antenna, it could be easily stated that the resonance mode excited in the open circuited structure is a Fabry-Perot mode. In a Fabry-Perot mode, the electric and magnetic fields are out of phase by 90° both in space and time. Figure 4.22 shows that in a Fabry-Perot resonator the electric and magnetic fields are having a time shift of $\tau/4$. When we look at the field quantities of the proposed open circuited antenna, the electric and magnetic fields are out of phase spatially and temporally. This shows that the mode excited in the antenna in the open circuited configuration is Fabry-Perot mode. The radiation from this structure is caused by the fringing electric and magnetic fields present in the structure.

4.2.3 Fabry-Perot mode

The designed quarter wave SIR is converted in to a Fabry-Perot very easily This is achieved by removing the shorting stub connected to the ground from SIR. In the proposed structure, the standing wave confined between the upper SIR and the lower ground conducting plane causes the electromagnetic mode resonance

4. An Electrically Small Frequency Reconfigurable Antenna

[123] [110]. The resonant frequency is related to the structural parameters as in equation (4.8) [3]

$$f = \frac{Nc}{2L_{eff}\sqrt{\epsilon_{reff}\mu_r}} \quad (4.8)$$

where f is the frequency in vacuum, N indicates the mode excited, L_{eff} is the effective length of the strip, c is the velocity of light, ϵ_r and μ_r are the relative permittivity and permeability of the dielectric material. In the proposed antenna, the substrate chosen is non magnetic and μ_r is taken as 1. The L_{eff} and ϵ_{reff} are given by

$$L_{eff} = L + \Delta L_1 + \Delta L_2 \quad (4.9)$$

$$\epsilon_{reff} = \frac{\epsilon_{reff1} + \epsilon_{reff2}}{2} \quad (4.10)$$

Where L is the total length of SIR, i.e.,

$$L = l_1 + l_2 \quad (4.11)$$

and ϵ_{reff1} and ϵ_{reff2} are the corresponding modified effective permittivity of the transmission line l_1 and l_2 .

$$\epsilon_{reff1or2} = \epsilon_{reffmstrip} + (1 - k) \quad (4.12)$$

where k is the impedance ratio $\frac{Z_2}{Z_1}$ and $\epsilon_{reffmstrip}$ is the effective permittivity corresponding to microstriplines l_1 and l_2 . Here the calculation of ΔL is derived by modifying the design equation of microstrip patch antenna. The ΔL is given by

$$\Delta L = 0.512h \left(\frac{(\epsilon_{effmstrip} + 0.3) \left(\frac{W}{h} + 0.264\right)}{(\epsilon_{effmstrip} - 0.258) \left(\frac{W}{h} + 0.8\right)} \right) \quad (4.13)$$

where h is the combined thickness of both substrates, $\epsilon_{effmstrip}$ is the effective relative permittivity and W is the width of the corresponding microstrip line in the antenna structure. In this equation the scaling factor is adjusted to 0.512 from 0.412 in order to improve the accuracy of the design.

4. An Electrically Small Frequency Reconfigurable Antenna

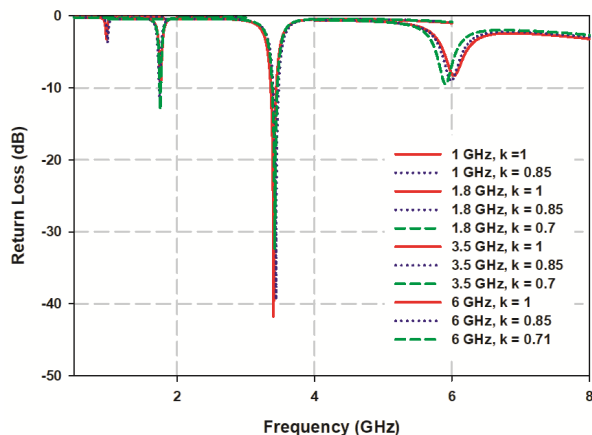


Figure 4.23: Return loss of Antenna designed using equation (4.8) for different frequency bands, w.r.t Table 4.3[$\epsilon_r = 4.4$, $h = 3.2$ mm]

4.2.4 Design for different bands in Fabry-Perot mode

The equation that has been proposed should be capable enough to extend its validity to different range of frequency operations at varying design ambience. This robustness should be verified by designing for different frequency bands. On a first hand the design procedure is extended over a range of frequency starting from 1 GHz to 6 GHz on an FR4 substrate. The frequency points selected are 1 GHz, 1.8 GHz, 3.5 GHz and 6 GHz. While validating the equation with reference to different frequency bands, the validation of the equation for different impedance ratio are also carried out at these points. The validation with k is important as this antenna is proposed in conjunction with a SIR structure. Figure 4.23 shows the simulated return loss characteristics of the antenna designed at different frequency bands.

4. An Electrically Small Frequency Reconfigurable Antenna

Table 4.3: Design for different frequency bands using the equation (4.8)

Designed f (GHz)	k	L (mm)	Simulated f (GHz)	Δf	%deviation
1	1	81.2	0.978	0.022	2.2
1	0.85	80.14	0.9895	0.0105	1.05
1.8	1	43.84	1.7613	0.0387	2.15
1.8	0.85	43.2	1.7537	0.0463	2.57
1.8	0.7	42.8	1.755	0.045	2.47
3.5	1	21	3.405	0.095	2.7
3.5	0.85	20.8	3.44	0.06	1.7
3.5	0.7	20.7	3.4225	0.077	2.2
6	1	11	6.03	0.03	0.5
6	0.85	10.9	5.995	0.005	0.083
6	0.71	11.05	5.902	0.098	1.6

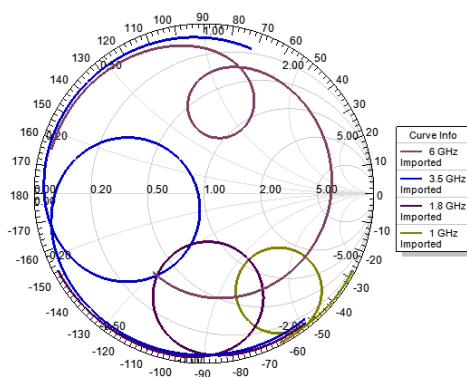


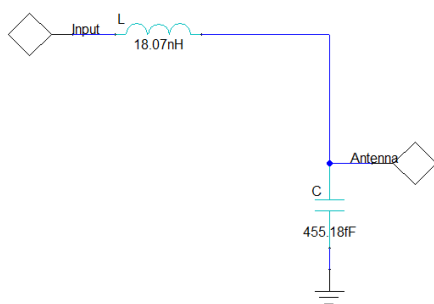
Figure 4.24: Impedance variation of Antenna designed using equation (4.8) for different frequency bands, [$\epsilon_r = 4.4$, $h = 3.2$ mm]

Table 4.3 shows a comparison between the designed frequency and the simulated frequency along with percentage of error. It is observed from the return loss characteristics that the impedance matching of the antenna is varying with respect to frequency. At the lower and higher ends of the frequency, the impedance matching is poor. Figure 4.24 shows the impedance plot at the selected bands for the case where $k = 1$. From this plot it is seen that at lower frequency the reactance is highly capacitive and as the frequency increases it is becoming more and more inductive. In the 3.5 GHz range, both the capacitive and inductive com-

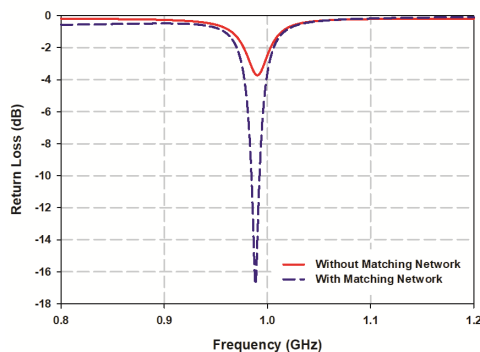
4. An Electrically Small Frequency Reconfigurable Antenna

ponents are almost equal and compensates each other. This provides a better impedance matching in this frequency range. As the frequency increases further, the impedance becoming more inductive and thus deteriorating the impedance matching again.

The impedance matching issue could be compensated by providing a proper impedance matching network to the antenna. For example here at the 1 GHz resonance where the matching is poor, a matching network is used. Figure 4.25(b) shows a comparison of the return loss obtained for 1 GHz design with and without matching network.



(a) LC matching network



(b) Simulated Impedance matching enhancement using LC matching network at 1 GHz.

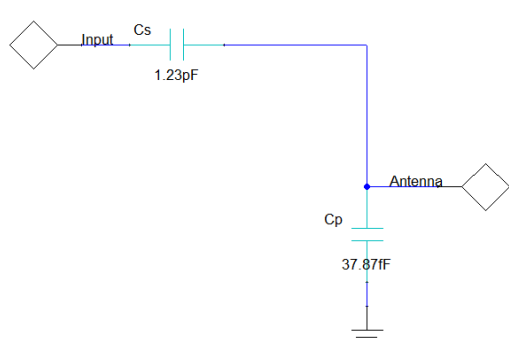
Figure 4.25: LC matching network and return loss characteristics of the antenna at 1 GHz. [$\epsilon_r = 4.4$, $h=3.2$ mm, $S1 = 76.65$ mm, $S2 = 3.5$ mm, $W1 = 2.6$ mm, $W2 = 3.6$ mm]

Without matching network the impedance matching is very poor. From the impedance plot in the smith chart for the corresponding case as shown in Figure 4.24, it is clear that the reactance at this point is highly capacitive. In order to compensate this an inductive element has to be used. An LC network circuit is designed to compensate the capacitive reactance with the help of HFSS circuit designer. After adding matching network, the impedance matching has been improved tremendously. Figure 4.25(a) shows the impedance matching network employed.

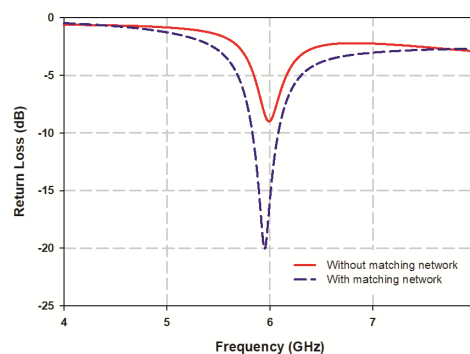
When we look at the other end of the frequency band where the matching

4. An Electrically Small Frequency Reconfigurable Antenna

is very poor, the impedance plot in the smith chart tells that the reactance is highly inductive. For a better impedance matching, this should be compensated with a capacitive network. The Figure 4.26 shows the impedance matching applied to the antenna. Figure 4.26(b) shows the improvement in return loss and Figure 4.26(a) shows the capacitive network used for the matching.



(a) Capacitance matching network



(b) Simulated Impedance matching enhancement using capacitance network at 6 GHz.

Figure 4.26: Effect of capacitive matching network on return loss characteristics of the antenna at 6 GHz. [$\epsilon_r = 4.4$, $h=3.2$ mm, $S1 = 7.55$ mm, $S2 = 3.5$ mm, $W1 = 2.6$ mm, $W2 = 3.6$ mm]]

4.3 Reconfigurability of the antenna

The reconfigurable antennas are class of antennas mainly used in applications which cover different wireless services operating on different frequency bands. They usually employ single antenna configuration which can dynamically vary and adapt to the situation requirements. This ability helps in an economic real estate management of the system.

In general, there are four major configuration properties for a reconfigurable antenna. They can exhibit reconfiguration in frequency, radiation pattern, polarization or a combination of any of these properties. To achieve these reconfiguration properties, there are different techniques available, which are divided in to four major categories as electrical, optical, mechanical and material change [62].

4. An Electrically Small Frequency Reconfigurable Antenna

In the proposed antenna the frequency reconfiguration is employed by using electrical reconfiguration technique. Electrical reconfiguration techniques are based on the use of switches to make and break antenna parts as well as to redistribute the surface current [62]. Frequency reconfiguration has become important for many modern communication systems. Therefore, there has been a notable advancement in adaptable antenna technology. Among them utilizing the same antenna aperture for different frequencies will provide the most compact solution [62].

Frequency reconfigurability can be introduced to the proposed antenna if the shorting stub is replaced with a PIN diode. This will provide two modes of operation, the open circuited and short circuited modes. In the short circuited mode the antenna works as a quarter wave SIR resonating at the 2.4 GHz band, whereas in the case of open circuited mode, the antenna works as a Fabry-Perot resonating at the 5.4 GHz band.

4.4 Optimised Geometry

The optimized geometry of the proposed antenna is shown in Figure 4.27. The structure is fabricated on a FR-4 substrate of thickness 1.6 mm. Proximity coupled feeding technique is adopted for exciting the SIR structure. In the case of the proposed antenna, the ground plane is made common to both microstripline and the SIR. For realising the quarter wave SIR, the shorting stub is drilled through SIR and microstripline substrate to the ground. The centre conductor of the microstripline is made 3 mm wide to match with the 50 Ω coaxial connector. Together with the proximity feeding, the thickness of the SIR structure is 3.2 mm. The SIR consists of two transmission lines S1 and S2 with corresponding widths W1 and W2 over a ground plane separated by a dielectric substrate of thickness 2H. The optimization of these dimensions are carried out based on the standard design equation of SIR. The antenna has a total dimension of $L \times W \times 2H$. The centre conductor of microstripline is protruding under the wider strip of SIR with an overlap of Cg. A 50 Ω SMA connector is used for feeding the centre conductor at the end. The physical dimensions of the proposed antenna is given in Table 4.4

4. An Electrically Small Frequency Reconfigurable Antenna

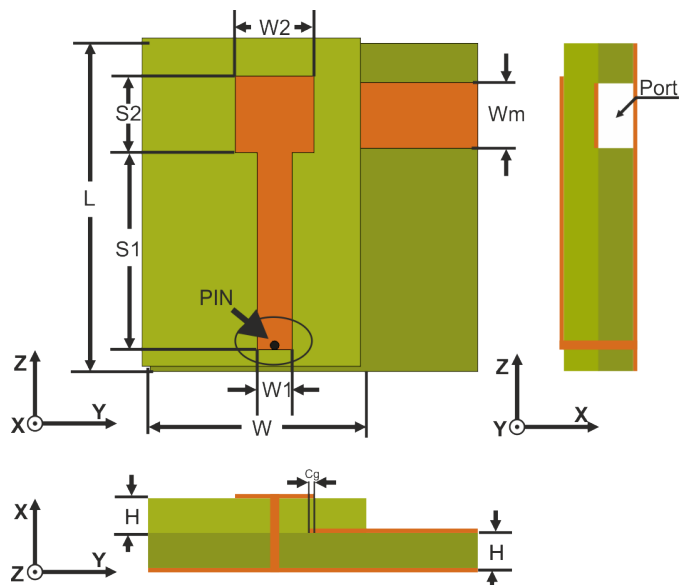


Figure 4.27: Geometry of the proposed antenna, $\epsilon_r = 4.4$

Table 4.4: Physical Dimensions of the Proposed Antenna

Parameter	Dimension (mm)
L	15
S1	9
S2	3.5
W	10
W1	1.6
W2	3.6
W_m	3
C_g	0.6
H	1.6

Figure 4.28 shows the geometry of the two proposed configuration. Figure 4.28(a) shows the short circuited mode where the structure works as a SIR whereas, Figure 4.28(b) shows the open circuited mode where the structure is operating in fabry-perot mode. A prototype for both the configuration has been fabricated and employed in various measurements of the antenna. Figure 4.28 shows the fabricated antennas. Figure 4.29(a) shows the short circuited configuration of the antenna where fundamental SIR mode is getting activated. Fig-

4. An Electrically Small Frequency Reconfigurable Antenna

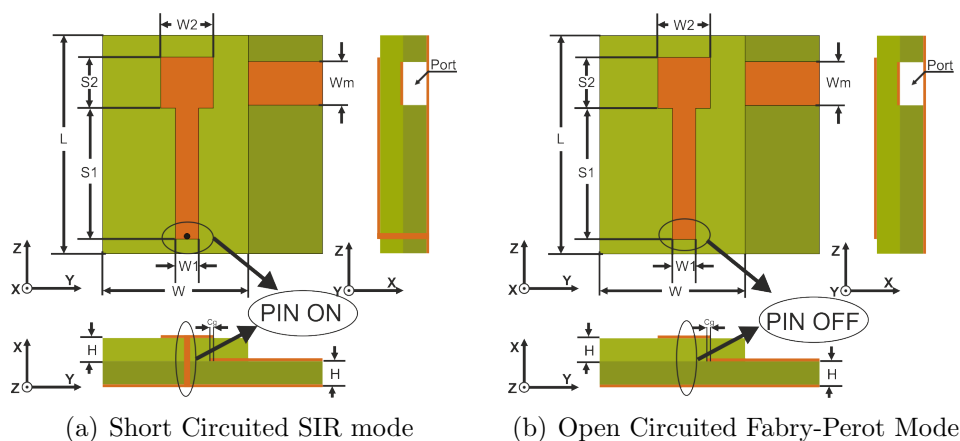
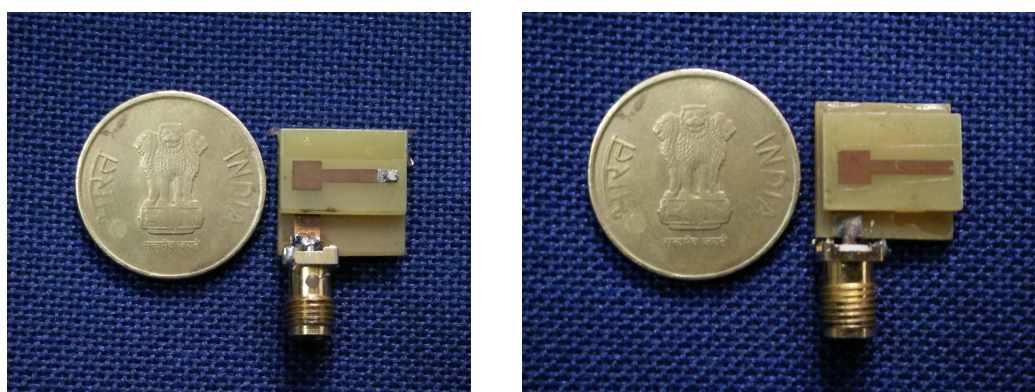


Figure 4.28: Implementation of frequency reconfigurability in the antenna using PIN diode [$L = 15$ mm, $S1 = 9$ mm, $S2 = 3.5$ mm, $W = 10$ mm, $W1 = 1.6$ mm, $W2 = 3.6$ mm, $Wm = 3$ mm, $Cg = 0.6$ mm, $H = 1.6$ mm, $\epsilon_r = 4.4$]



(a) Short Circuited SIR mode Prototype (b) Open Circuited Fabry-Perot Mode Prototype

Figure 4.29: Prototype of open and short circuited SIR antenna [$L = 15$ mm, $S1 = 9$ mm, $S2 = 3.5$ mm, $W = 10$ mm, $W1 = 1.6$ mm, $W2 = 3.6$ mm, $Wm = 3$ mm, $Cg = 0.6$ mm, $H = 1.6$ mm, $\epsilon_r = 4.4$, $k = 0.7$, $\alpha = 0.285$]

Figure 4.29(b) is the prototype of open circuited fabry-perot mode antenna which resonates at the higher frequency band. The optimized design parameter of the antenna is shown in the Table 4.4. All the measurements of the antenna are carried out using Rohde & Schwarz ZVB 20 Network Analyzer and the far field measurements are conducted inside an anechoic chamber with the aid of the turn table, controller and the software mechanism.

4. An Electrically Small Frequency Reconfigurable Antenna

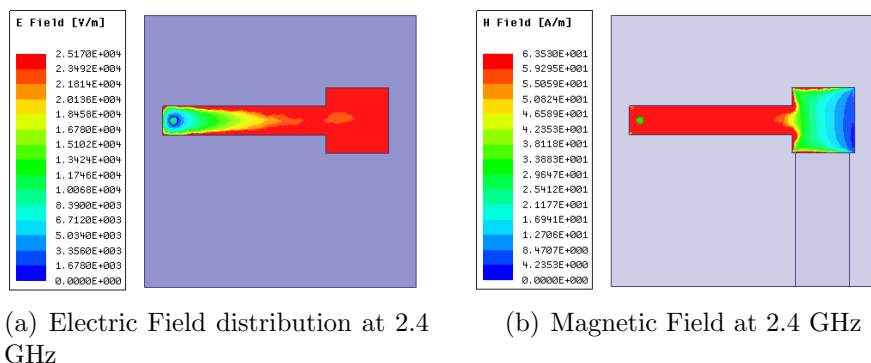


Figure 4.30: Simulated Electric and Magnetic Field in the structure for the short circuited mode. [$L = 15$ mm, $S1 = 9$ mm, $S2 = 3.5$ mm, $W = 10$ mm, $W1 = 1.6$ mm, $W2 = 3.6$ mm, $Wm = 3$ mm, $Cg = 0.6$ mm, $H = 1.6$ mm, $\epsilon_r = 4.4$, $k = 0.7$, $\alpha = 0.285$]

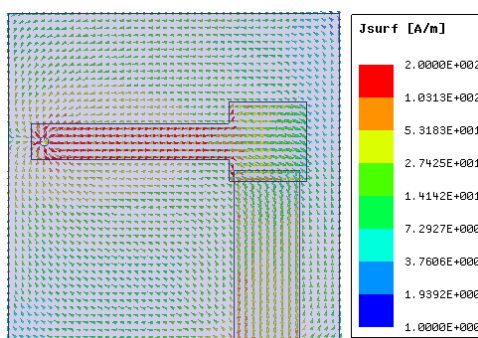


Figure 4.31: The surface current distribution in the short circuited SIR mode of the antenna at 2.4 GHz. [$L = 15$ mm, $S1 = 9$ mm, $S2 = 3.5$ mm, $W = 10$ mm, $W1 = 1.6$ mm, $W2 = 3.6$ mm, $Wm = 3$ mm, $Cg = 0.6$ mm, $H = 1.6$ mm, $\epsilon_r = 4.4$, $k = 0.7$, $\alpha = 0.285$]

4.5 Field Analysis in the SIR Mode

The electric and magnetic field distribution in the structure at 2.4 GHz for the SIR mode of operation is shown in Figure 4.30. The field distribution is that of a $\lambda_g/4$ SIR, with an electric peak at open end and magnetic peak at shorted end. A comparison on the electric and magnetic field strength shows that the electric field in the structure is dominantly higher than the magnetic field strength.

Figure 4.31 shows the surface current distribution in the structure at the SIR

4. An Electrically Small Frequency Reconfigurable Antenna

mode of operation, i.e. at 2.4 GHz. It is observed from the figure that the maximum intensity of current is found around the shorted area at 2.4 GHz. In comparison with the surface current distribution in the ground and the feed line, at 2.4 GHz the maximum surface current distribution is on the two microstriplines forming the SIR

4.6 Parametric Analysis

Different parametric analysis are conducted on the antenna as listed below.

- Ground width variation
- Narrow microstripline width variation
- Stacking height variation
- Feeding position variation
- Effect of K on Fabry-Perot mode
- Effect of Width Variation
- Parametric analysis of substrate permittivity

4.6.1 Ground Width Variation

An analysis on the effect of variation in the antenna radiation property with change in the length L of the ground plane has been carried out. The length is varied asymmetrically from 15 mm to 20 mm as shown in Figure 4.32. The extension of the ground plane shows its implication on the radiation pattern of the lower resonance. Figure 4.33 shows the change in the radiation pattern of the lower resonance with ground plane extension. In the lower resonance the beam shift is possible from a θ variation from 35° to 70° with a corresponding variation in ground plane length from 15 mm to 20 mm.

4. An Electrically Small Frequency Reconfigurable Antenna

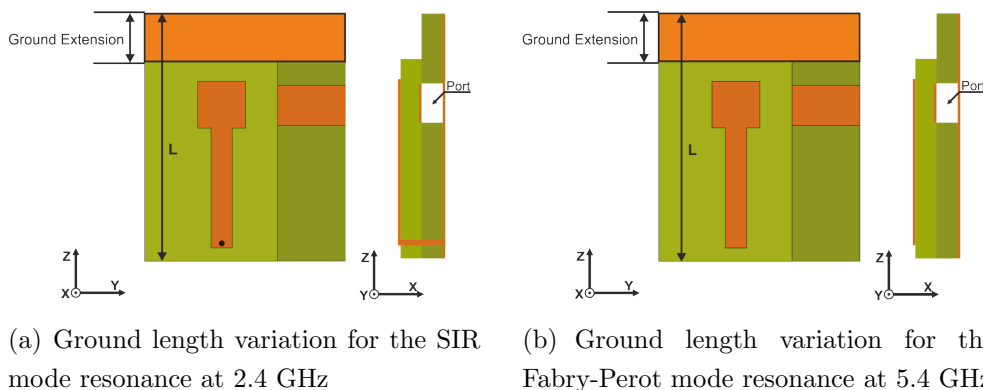


Figure 4.32: Extension of ground plane length for both the SIR mode and fabry-perot mode resonance. The length L is varied from 15 mm to 20 mm. [$S1 = 9$ mm, $S2 = 3.5$ mm, $W = 10$ mm, $W1 = 1.6$ mm, $W2 = 3.6$ mm, $Wm = 3$ mm, $Cg = 0.6$ mm, $H = 1.6$ mm, $\epsilon_r = 4.4$]

As the main objective of the analysis is to achieve an electrically small antenna, we are considering the size reduction as the main objective while optimizing the antenna geometry. For the optimized design, the simulated value of the tilt angle observed is 70° . In the Figure 4.33(c) it shows the total simulated radiation pattern of the antenna. Here the red line represents the radiation pattern for the optimized design. In this case front-to-back ratio of the antenna remains unaltered as the ground plane width is varied from 15 mm to 20 mm, instead it is effecting the direction of the beam. This influence of the ground width on the beam direction is a direct result of the continuous current path existing in between the ground and the upper microstrip lines. When the ground width is extended, the extended current path is influencing the fields resulting in a tilt in the radiation pattern of the antenna.

4. An Electrically Small Frequency Reconfigurable Antenna

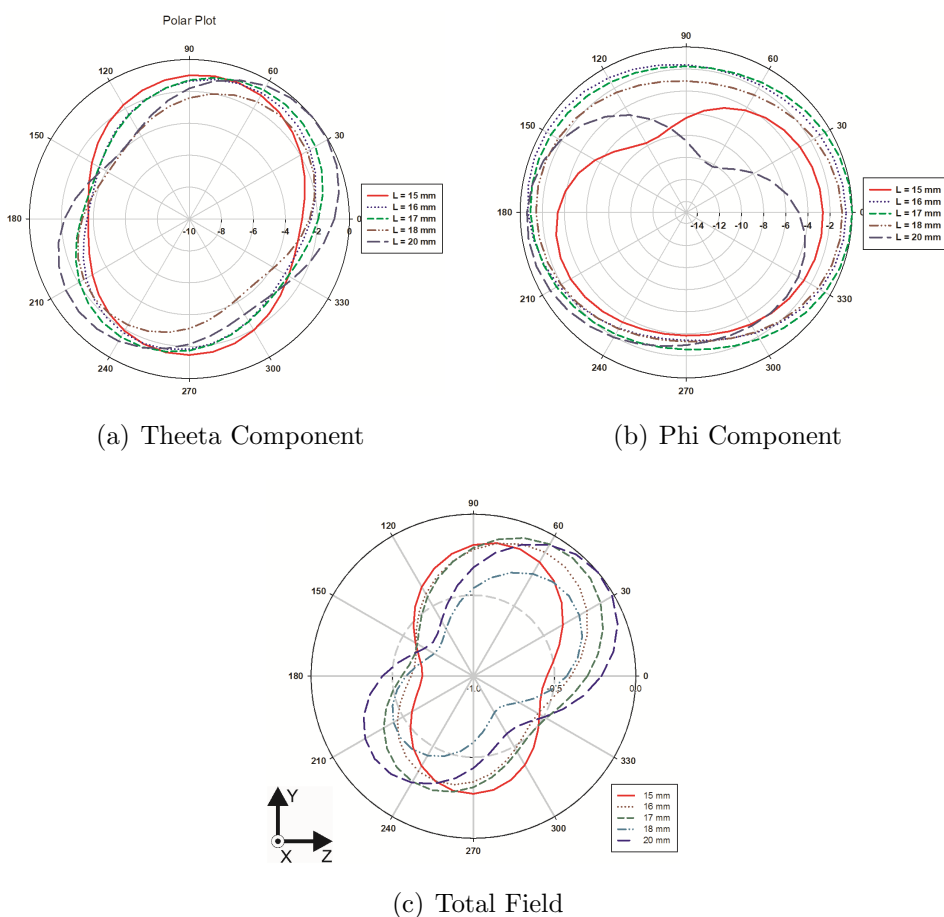


Figure 4.33: Simulated radiation pattern of the antenna in the lower 2.4 GHz. [L = 15 - 20 mm, S1 = 9 mm, S2 = 3.5 mm, W = 10 mm, W1 = 1.6 mm, W2 = 3.6 mm, Wm = 3 mm, Cg = 0.6 mm, H = 1.6 mm, $\epsilon_r = 4.4$]

Figure 4.34 shows the fringing electric field distribution for 15 mm and 20 mm ground plane width. When both the fields are compared, on the right hand side, i.e., at the open ended point, it is observed from Figure 4.34(b) that for 20 mm ground plane width all the field are returning to the microstrip line from the ground where as in Figure 4.34(a) most of the fields are fringing out to air. Here with an increase in the ground plane width of the antenna, the complete pattern of the fringing electric field has been changed. This asymmetry in the fringing electric field is responsible for the tilt in the radiation pattern.

4. An Electrically Small Frequency Reconfigurable Antenna

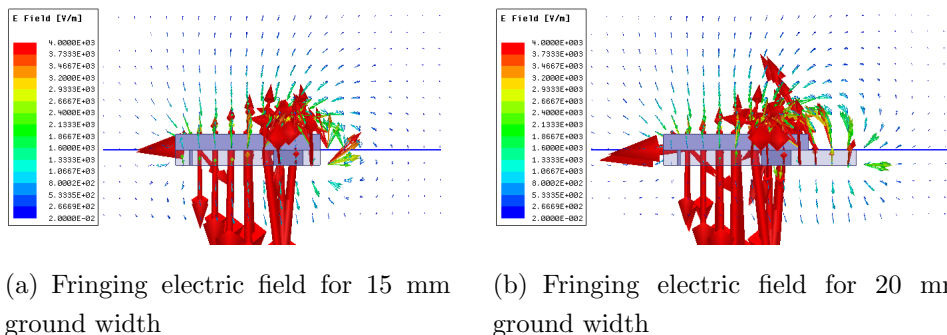


Figure 4.34: Fringing electric field variation with respect to change in ground plane width. [S1 = 9 mm, S2 = 3.5 mm, W = 10 mm, W1 = 1.6 mm, W2 = 3.6 mm, Wm = 3 mm, Cg = 0.6 mm, H = 1.6 mm, $\epsilon_r = 4.4$]

Figure 4.35 shows the variation in the radiation pattern of the proposed antenna in the higher resonance in the fabry-perot mode of operation. Here the change in the ground length of the antenna is not much influencing the radiation pattern. The only noticeable change is in the reduction of the back lobes of the radiation. Table 4.5 shows how the front-to-back ratio of the antenna is changing with respect to change in the ground plane width. As the width of the ground plane is increased, the fringing field towards the bottom side of the antenna reduces further. This causes the reduction in radiation in that direction resulting in smaller back lobes.

Table 4.5: Front to back ratio w.r.t ground width variation

Ground plane width L (mm)	Front To Back Ratio (dB)
15	7.6586
16	8.5756
17	10.7163
18	12.9741
20	16.326

4. An Electrically Small Frequency Reconfigurable Antenna

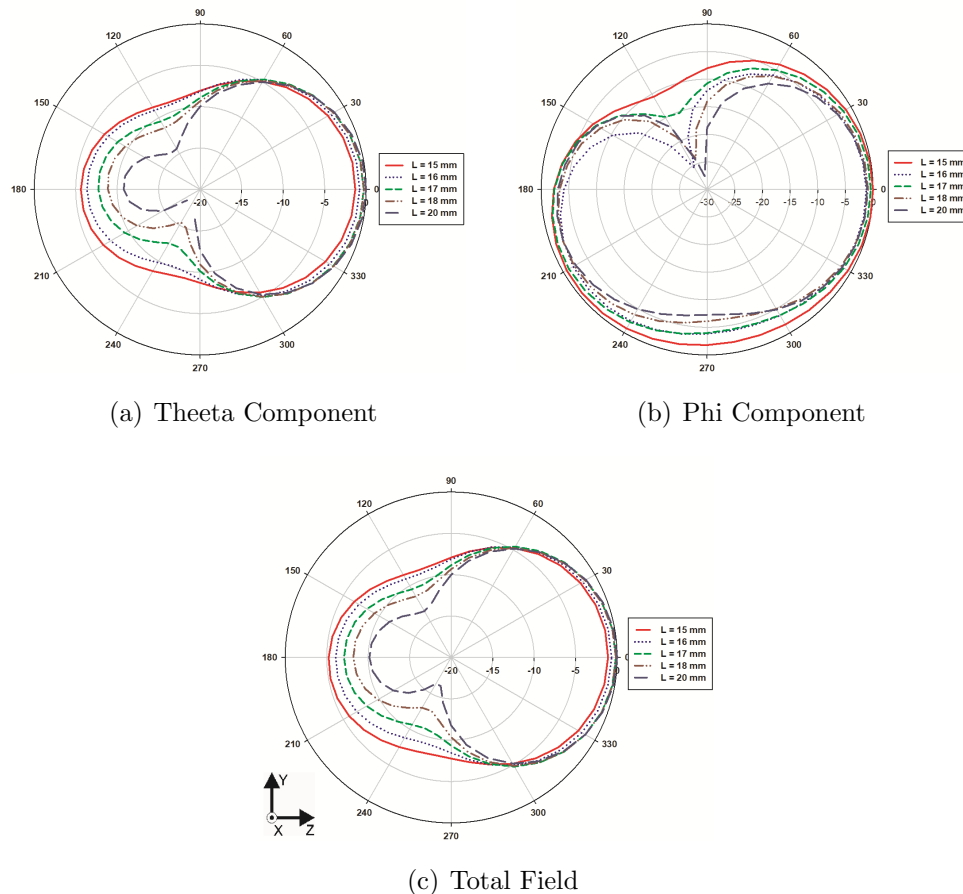


Figure 4.35: Simulated radiation pattern of the antenna in the higher 5.4 GHz. [L = 15 - 20 mm, S1 = 9 mm, S2 = 3.5 mm, W = 10 mm, W1 = 1.6 mm, W2 = 3.6 mm, Wm = 3 mm, Cg = 0.6 mm, H = 1.6 mm, $\epsilon_r = 4.4$]

The fringing electric field of the antenna in the Fabry-Perot mode is shown in Figure 4.36. Here also two cases are considered, width with 15 mm and 20 mm. A closer look at both Figure 4.36(a) and 4.36(b) shows that there is no much change in the fringing field due to increasing in the ground plane width of the antenna.

The simulation is carried out using thin metal strips with metal interconnect placed between each strip to make electrical short where ever required for extending the ground plane. By replacing this metal shorts with electrical switches, an electronic beam steering could be achieved in the lower resonance of the antenna.

4. An Electrically Small Frequency Reconfigurable Antenna

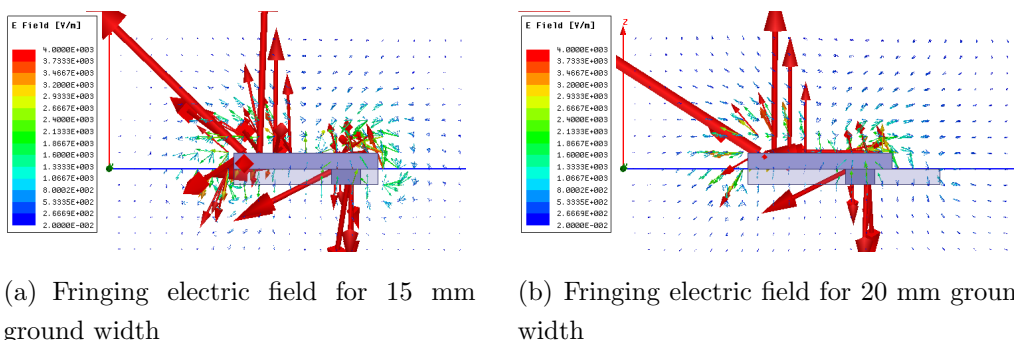


Figure 4.36: Fringing electric field variation with respect to change in ground plane width. [S1 = 9 mm, S2 = 3.5 mm, W = 10 mm, W1 = 1.6 mm, W2 = 3.6 mm, Wm = 3 mm, Cg = 0.6 mm, H = 1.6 mm, $\epsilon_r = 4.4$]

A similar study has been conducted with a very large symmetrical ground plane for both higher and lower frequency bands. This has shown that for SIR mode, the radiation of the antenna has completely shifted to bore sight giving a more directional radiation pattern than with smaller ground plane. The corresponding radiation pattern of the antenna is shown in Figure 4.37. For higher frequency band as the size of the ground plane is increased, a small dip is observed at the bore sight as shown in Figure 4.38.

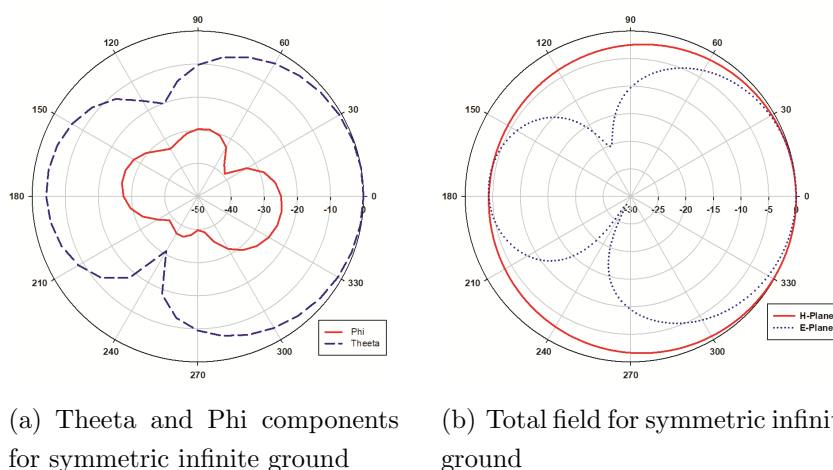
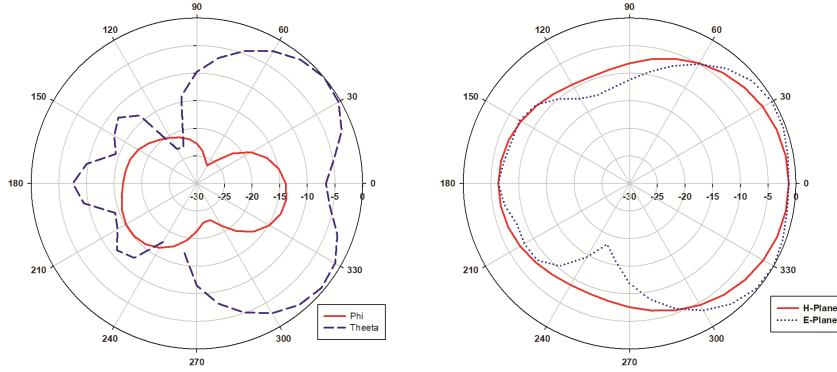


Figure 4.37: Radiation pattern at 2.4 GHz for infinite ground plane. [S1 = 9 mm, S2 = 3.5 mm, W = 10 mm, W1 = 1.6 mm, W2 = 3.6 mm, Wm = 3 mm, Cg = 0.6 mm, H = 1.6 mm, $\epsilon_r = 4.4$]

4. An Electrically Small Frequency Reconfigurable Antenna



(a) Theeta and Phi components for symmetric infinite ground (b) Total field for symmetric infinite ground

Figure 4.38: Radiation pattern at 5.4 GHz for infinite ground plane. [S1 = 9 mm, S2 = 3.5 mm, W = 10 mm, W1 = 1.6 mm, W2 = 3.6 mm, Wm = 3 mm, Cg = 0.6 mm, H = 1.6 mm, $\epsilon_r = 4.4$]

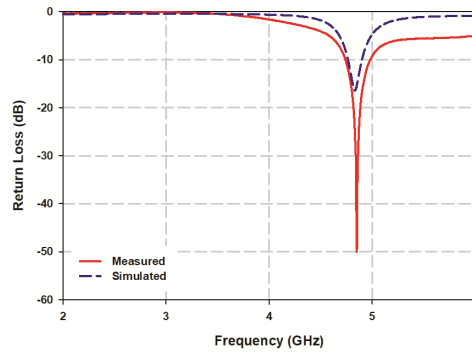


Figure 4.39: Reflection characteristics of the antenna with symmetric large ground plane [S1 = 8 mm, S2 = 6 mm, W = 12 mm, W1 = 2 mm, W2 = 4 mm, Wm = 3 mm, Cg = 0.6 mm, H = 1.6 mm, $\epsilon_r = 4.4$]

4. An Electrically Small Frequency Reconfigurable Antenna

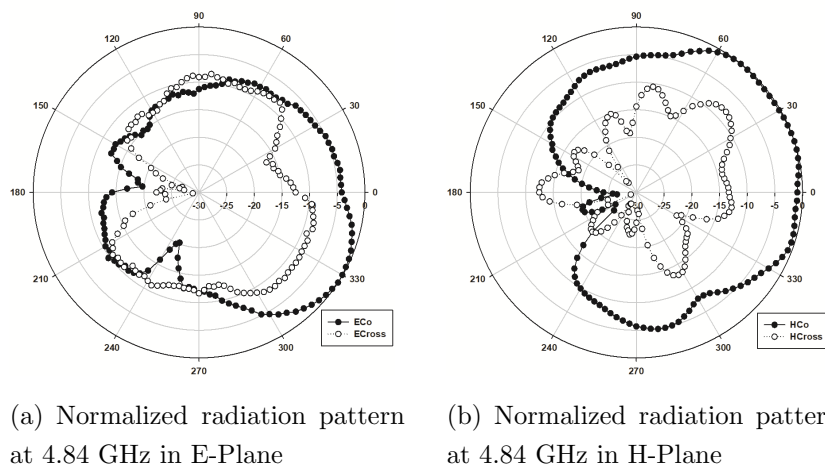


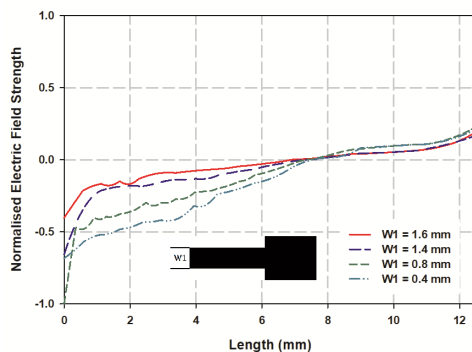
Figure 4.40: Radiation pattern at 4.84 GHz for infinite ground plane. [S1 = 8 mm, S2 = 6 mm, W = 12 mm, W1 = 2 mm, W2 = 4 mm, Wm = 3 mm, Cg = 0.6 mm, H = 1.6 mm, $\epsilon_r = 4.4$]

An antenna is designed to operate at 4.84 GHz in Fabry-Perot mode with a symmetric wide ground plane of size 25 mm \times 43 mm to practically represent the infinite ground plane. A different frequency is selected for the design, to verify that the observed property validates for other frequency also. A prototype of the antenna is fabricated and tested. Figure 4.39 shows the simulated and measured reflection characteristics of the antenna. The antenna has a measured bandwidth of 240 MHz. Figure 4.40 shows the measured radiation pattern of the antenna.

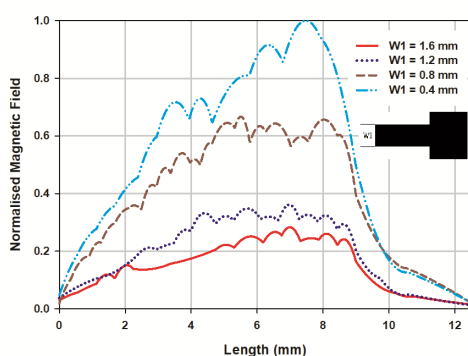
4.6.2 High Impedance Microstripline Width Variation

The width W1 of the narrow microstrip line S1 is varied from 0.4 mm to 1.6 mm for the analysis of the electric and magnetic field distribution in the structure for the fabry-perot mode of operation. As the width of the structure is reduced to 0.4 mm from 1.6 mm, the electric and magnetic field strength are increased inside the structure. Figure 4.41 shows the electric and magnetic filed distribution in the structure. It is observed that the reduction in the width of the high impedance microstripline is causing reduction in the total power radiated from the antenna. For a reduction of 1.2 mm in width, the gain has reduced by 88%.

4. An Electrically Small Frequency Reconfigurable Antenna



(a) Electric field variation with change in W_1



(b) Magnetic field variation with change in W_1

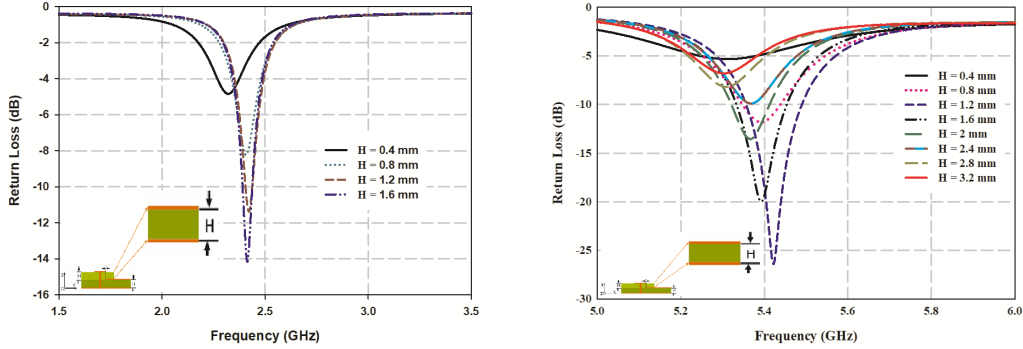
Figure 4.41: The variation of the electric and magnetic field of the fabry-perot mode when the width W_1 of the small microstrip line S_1 is varied from 0.4 mm to 1.6 mm [$L = 15$ mm, $S_1 = 9$ mm, $S_2 = 3.5$ mm, $W = 10$ mm, $W_2 = 3.6$ mm, $W_m = 3$ mm, $C_g = 0.6$ mm, $H = 1.6$ mm, $\epsilon_r = 4.4$]

4.6.3 Stacking height variation

The stacking height H of the superstrate layer is varied from 0.4 mm to 1.6 mm and the corresponding change in the resonance of the SIR and fabry-perot mode of operation of the antenna are observed. In the SIR mode, the changes in the resonance is not effected much as shown in Figure 4.42(a), whereas in the fabry-perot mode the stacking height has a clear implication in its resonance. The resonant frequency initially increased with the increase in stacking height H

4. An Electrically Small Frequency Reconfigurable Antenna

until it reaches 1.2 mm. After that the antenna shows a decline in its resonant frequency as shown in Figure 4.42(b).



(a) Variation in the SIR resonance w.r.t change in stacking height (b) Variation in the Fabry-Perot resonance w.r.t change in stacking height

Figure 4.42: Variation in the SIR and Fabry-Perot resonance w.r.t. change in stacking height from 0.4 mm to 1.6 mm. [$L = 15$ mm, $S1 = 9$ mm, $S2 = 3.5$ mm, $W = 10$ mm, $W1 = 1.6$ mm, $W2 = 3.6$ mm, $Wm = 3$ mm, $Cg = 0.6$ mm, $\epsilon_r = 4.4$]

Since both electric and magnetic fields are existing in the structure, an increase in stacking height will shift the electric resonance to magnetic resonance. This shift causes the reduction in resonant frequency. This variation in the resonance of the fabry-perot mode of the antenna is similar to the variation shown by [110], [123].

4.6.4 Feeding Position Variation

This study is mainly conducted to figure out how the fabry-perot mode observed in this antenna could be excited. For this purpose, the dielectric substrate considered is FR4 material with a relative permittivity of 4.4. The metal strip considered is of 3 mm wide and 12 mm long. Figure 4.43(a) shows the geometrical orientation of the antenna. For brevity of analysis, the step junction is omitted and a UIR is considered for experimental purpose. The feeding position is varied from one of the open end till the middle of UIR. If SIR is considered for this study,

4. An Electrically Small Frequency Reconfigurable Antenna

to keep the feed line overlap constant with the SIR, the microstripline length should be changed as it moves toward the narrow metal strip of the SIR. However a simulated return loss characteristics is shown for the SIR. Figure 4.43(b) shows the return loss obtained from this parametric study using UIR. As the feeding point moves towards the centre of the UIR, the resonance vanishes. When fed at the open end of the antenna, it gives a resonance with a good matching above 2:1 VSWR limit. This clearly shows that the proposed fabry-perot mode will get excited only when fed at the edges of the UIR. Also the resonant frequency shows a slight decrease when the feeding point is shifted to the centre of the UIR. Figure 4.44 shows the same variation carried out over an SIR. Figure 4.45 shows the corresponding measured reflection characteristics of the antenna for feed position change using UIR.

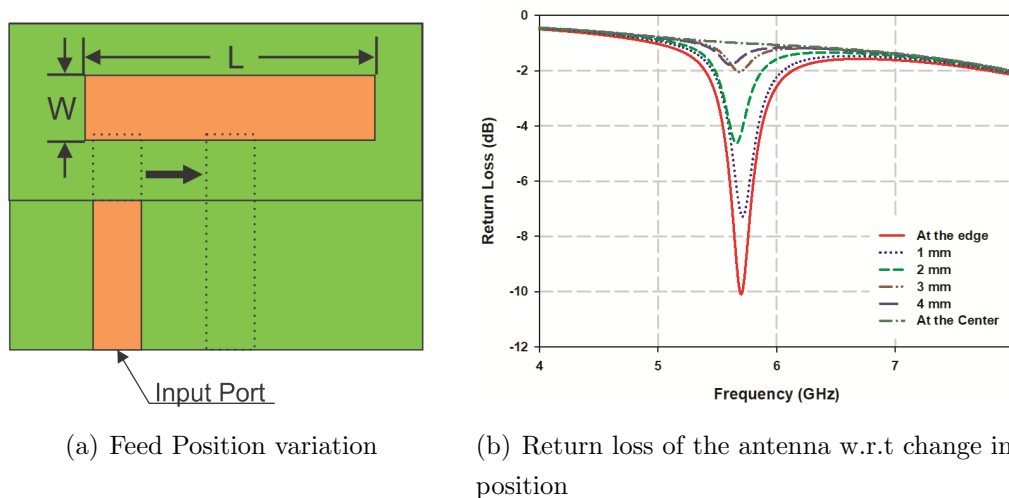


Figure 4.43: Variation in the Fabry-Perot resonance w.r.t. change in the feeding position, $\epsilon_r = 4.4$, $L = 12$ mm, $H = 1.6$ mm, $W = 3$ mm

4. An Electrically Small Frequency Reconfigurable Antenna

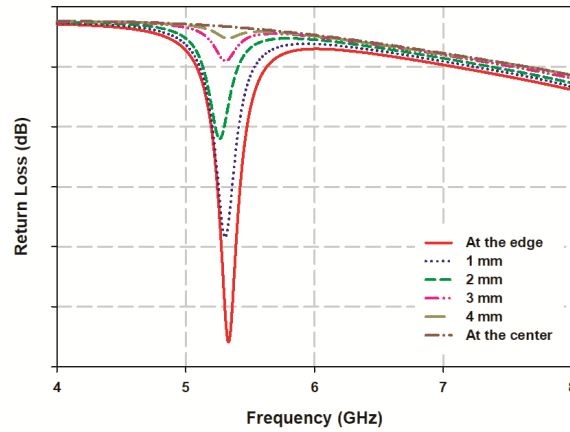


Figure 4.44: Simulated variation in the Fabry-Perot resonance w.r.t. change in the feeding position using SIR, $\epsilon_r = 4.4$, $S1 = 9$ mm, $S2 = 3.5$ mm, $H = 1.6$ mm, $W1 = 1.6$ mm, $W2 = 3.6$ mm

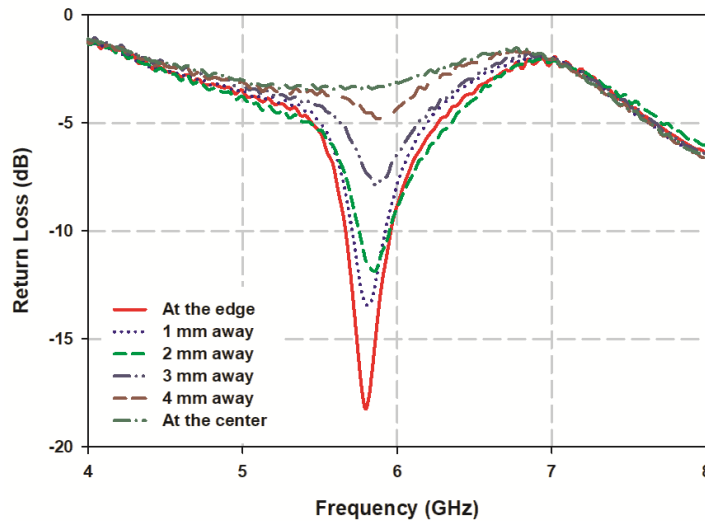
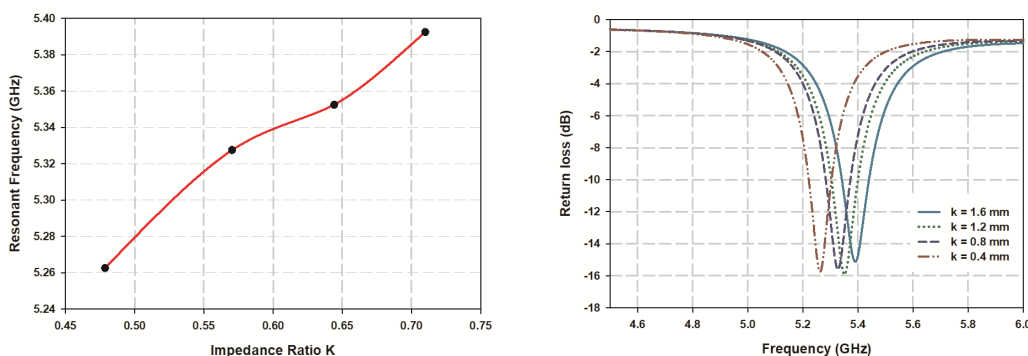


Figure 4.45: Measured variation in the Fabry-Perot resonance w.r.t. change in the feeding position, $\epsilon_r = 4.4$, $L = 12$ mm, $H = 1.6$ mm, $W = 3$ mm, $f = 5.795$ GHz, 5.795 GHz, 5.83 GHz, 5.86 GHz, 5.86 GHz

4.6.5 Effect of k on fabry-perot mode

The impedance ratio k will vary as the width of the microstrip line used is varied. The effect of this variation on the fabry-perot mode is analysed by varying the k value. In order to carry out this analysis, the width of the wider microstrip line is kept at 3.6 mm and the width of the narrow microstrip line is varied. The k value is varied from 0.47 to 0.7 and the change in the resonance is observed. The simulation shows that the resonating frequency shows a slight shift from 5.26 GHz to 5.4 GHz. The variation in k did not effect the matching of the resonance. Figure 4.46 shows the variation in the resonant frequency with respect to k . Here when the k is varied, this in turn changes the average width W of the structure. This change in the average width will change the ΔL and this will in turn changes the L_{eff} of the structure. This change in the L_{eff} causes the change in the resonant frequency.



(a) Resonance shift w.r.t k

(b) Return loss of the antenna w.r.t change in k

Figure 4.46: Variation in the Fabry-Perot resonance w.r.t. change in impedance ratio k . [$L = 15$ mm, $S1 = 9$ mm, $S2 = 3.5$ mm, $W = 10$ mm, $W_m = 3$ mm, $C_g = 0.6$ mm, $H = 1.6$ mm, $\epsilon_r = 4.4$]

4.6.6 Effect of Width Variation

In order to get a clear insight to the working of the antenna structure in its fabry-perot mode, analysis on the effect of the width variation to the resonance

4. An Electrically Small Frequency Reconfigurable Antenna

of the antenna is conducted. For the brevity of analysis, instead of an SIR, a UIR is considered. The UIR has less dependant parameters than a SIR. This reduces the complexity in the analysis of the antenna. The width W of the UIR as shown in Figure 4.47(a) is varied from 1 mm to 7 mm and the resonance variation of the antenna for a particular length L is analysed. Figure 4.47(b) shows the impact of width variation on the resonant frequency of the antenna. Here the length L is kept constant at 12 mm. The results are compared against the values obtained using the equation (4.8) as shown in Table 4.6. Table 4.6 also shows the percentage deviation from the calculated value and the simulated resonance. Here as W is varied, this in turn result in a change in the ΔL which in effect change the effective length L_{eff} . This change in L_{eff} is causing the shift in the resonant frequency as W is varied. As the width is increased, the change in effective length become less sensitive and thus less change in the resonant frequency. Three intermediate widths, 3 mm, 5 mm and 7 mm have been considered for fabrication and the corresponding change in the reflection characteristics are shown in Figure 4.48.

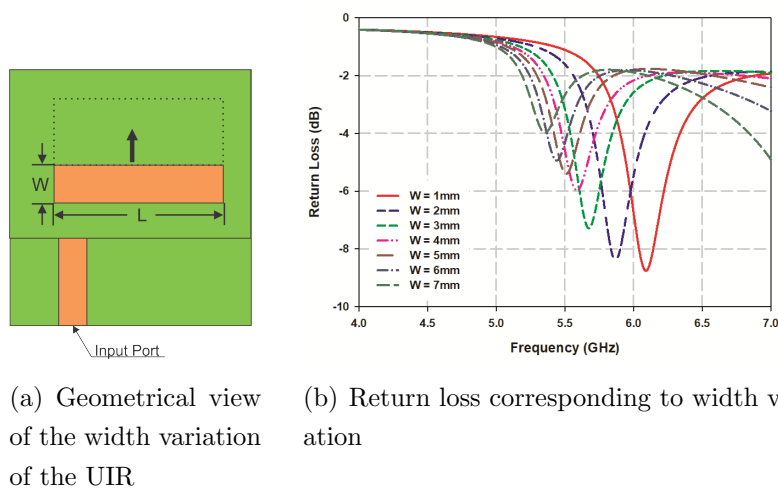


Figure 4.47: The effect of width W on the resonance of the antenna, $L = 12$ mm, $\epsilon_r = 4.4$, $H = 1.6$ mm

4. An Electrically Small Frequency Reconfigurable Antenna

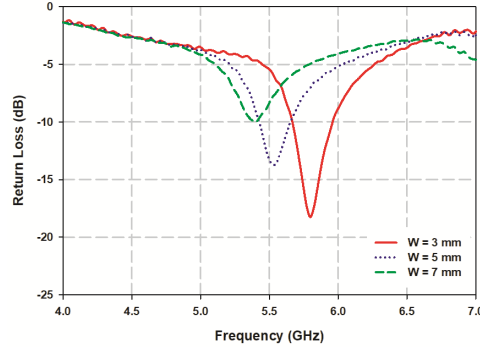


Figure 4.48: The measured effect of width (W) change on the resonance of the antenna, [$L = 12$ mm, $\epsilon_r = 4.4$, $H = 1.6$ mm]

Table 4.6: Design Vs Simulated result w.r.t equation (4.8)

W (mm)	f_{design} (GHz)	$f_{simulation}$ (GHz)	%deviation
1	6.2	6.092	1.74
2	5.9	5.87	0.508
3	5.78	5.672	1.86
4	5.66	5.588	1.27
5	5.555	5.504	0.918
6	5.464	5.438	0.475
7	5.3817	5.354	0.5018

The above result shows that the percentage deviation from the designed value is less and it once gain validates the design equation (4.8).

4.6.7 Parametric analysis of substrate permittivity

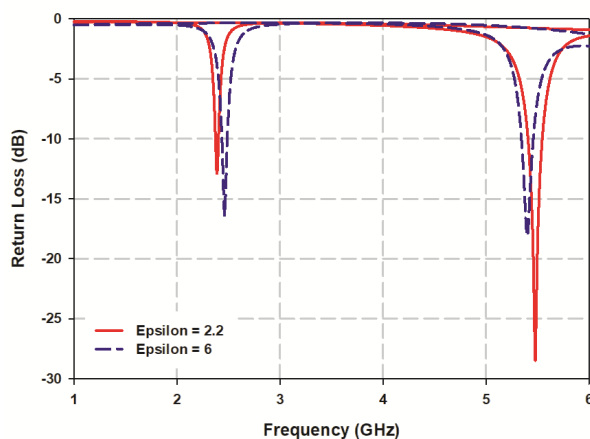


Figure 4.49: Antenna designed to work at 2.4 and 5.4 GHz on two different material with relative permittivity 2.2 and 6

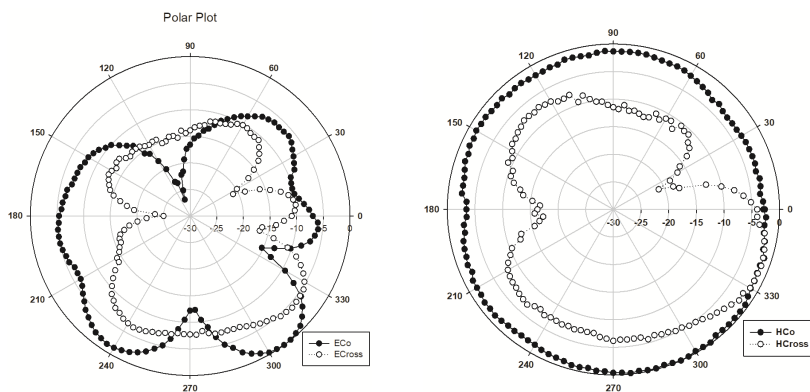
The proposed antenna design should possess the flexibility to go through changes in substrate materials. As with any practical antenna design, as situation demands, the antenna should be able to get designed and fabricated on different materials with different permittivity values. In order to validate this, the antenna has been designed using materials with different permittivity other than 4.4. Figure 4.49 shows the return loss characteristics of the antenna designed for material with ϵ_r 2.2 and 6 for resonating at a lower frequency of 2.4 GHz and higher frequency of 5.4 GHz. This shows that with the derived design method, the antenna could be realised on different materials.

4.7 Radiation Pattern

The expected radiation pattern of the antenna in both the bands are directional. In the lower 2.4 GHz band, the fabricated prototype of the antenna has a ground length of 15 mm resulting in a tilted radiation pattern. The measured radiation pattern is shown in Figure 4.50. Here a similar orientation of the radiation

4. An Electrically Small Frequency Reconfigurable Antenna

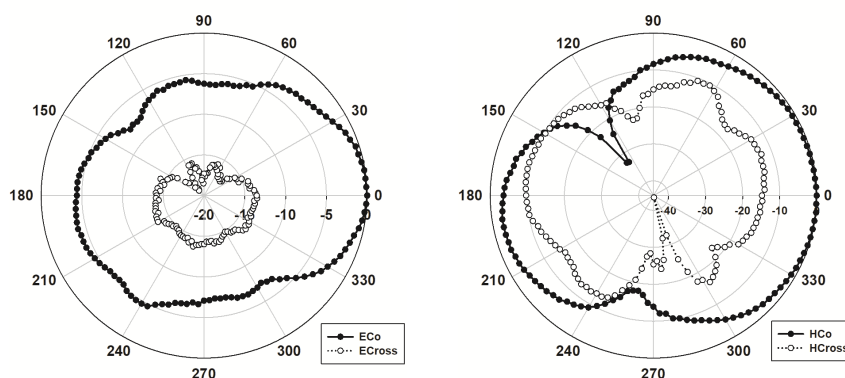
pattern can be observed in the E plane.



(a) Normalized Radiation pattern at 2.4 GHz in E-Plane

(b) Normalized Radiation pattern at 2.4 GHz in H-Plane

Figure 4.50: Normalized Radiation pattern at 2.4 GHz. [$L = 15$ mm, $S1 = 9$ mm, $S2 = 3.5$ mm, $W = 10$ mm, $W1 = 1.6$ mm, $W2 = 3.6$ mm, $Wm = 3$ mm, $Cg = 0.6$ mm, $H = 1.6$ mm, $\epsilon_r = 4.4$]



(a) Normalized Radiation pattern at 5.4 GHz in E-Plane

(b) Normalized Radiation pattern at 5.4 GHz in H-Plane

Figure 4.51: Normalized Radiation pattern at 5.4 GHz. [$L = 15$ mm, $S1 = 9$ mm, $S2 = 3.5$ mm, $W = 10$ mm, $W1 = 1.6$ mm, $W2 = 3.6$ mm, $Wm = 3$ mm, $Cg = 0.6$ mm, $H = 1.6$ mm, $\epsilon_r = 4.4$]

On the other hand the radiation pattern of the higher resonance mode, i.e. the fabry-perot mode is expecting a radiation pattern directed towards the broad

4. An Electrically Small Frequency Reconfigurable Antenna

side. Figure 4.51 shows the measured radiation pattern in the higher resonance frequency at 5.4 GHz. In the measured radiation pattern also it replicate the directionality in the broad side in both the planes

4.8 Gain And Efficiency

The measured gain of the antenna using gain comparison method is shown in Figure 4.52. The antenna shows negative gain in the lower resonance with a peak gain of -1.3 dBi as shown in Figure 4.52(a). The maximum possible gain of the antenna calculated for the proposed size at 2.42 GHz using the equation (4.14) is 0.49 dBi. The peak gain obtained for the antenna in the higher band is 3.459 dBi as shown in Figure 4.52(b) at 5.45 GHz. The gain plot shows a uniform pattern in the 2:1 VSWR band.

$$Gain_{max} = (ka)^2 + 2ka \quad (4.14)$$

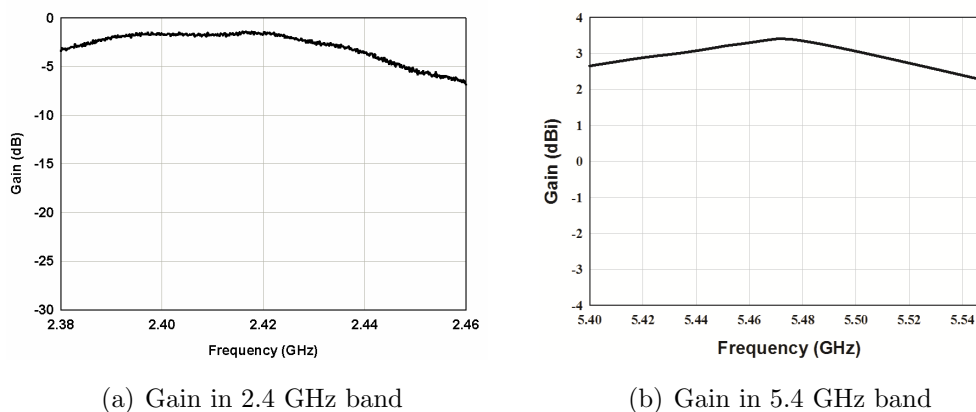


Figure 4.52: Measured gain of the antenna using gain comparison method for both the bands. [L = 15 mm, S1 = 9 mm, S2 = 3.5 mm, W = 10 mm, W1 = 1.6 mm, W2 = 3.6 mm, Wm = 3 mm, Cg = 0.6 mm, H = 1.6 mm, $\epsilon_r = 4.4$]

The radiation efficiency of the antenna is measured using wheeler cap method [129]. In the lower frequency band the antenna resonates at 2.4 GHz with a 2:1 VSWR bandwidth of 44 MHz. The measured radiation efficiency of the antenna

4. An Electrically Small Frequency Reconfigurable Antenna

is 23% in this band . In the 5.4 GHz band the antenna resonates at 5.45 GHz with a 2:1 VSWR bandwidth of 140 MHz. The measured radiation efficiency of the antenna in this band is 77%.

4.9 Electrical Size

The electrical size of an antenna is a very important factor in the discussion of any small antenna. The classification of small antennas are done depending on the electrical size. The factor ka is used for deciding the classification. Here k is the phase constant at the resonant frequency and a is the radius of the smallest sphere which can circumscribe the antenna. For an antenna to be electrically small the ka factor should be less than 0.5. There is a minimum value of Q that an electrically small antenna should maintain is given in equation (4.15). The maximum achievable gain of an ESA is given by (4.16)

$$Q_{min} = \frac{1}{ka} + \frac{1}{(ka)^3} \quad (4.15)$$

$$Gain_{max} = (ka)^2 + 2ka \quad (4.16)$$

Table 4.7 shows these parameters calculated for the proposed antenna against the required parameter values for a same sized antenna.

Table 4.7: ESA Parameters

Parameter	Required	Obtained
ka	<0.5	0.4565
Q	>12.7042	1010
Gain	<0.49 dBi	-1.3 dBi

4.10 Conclusions

A frequency reconfigurable antenna based on SIR and Fabry-perot mode of operation has been successfully designed, developed and analysed. A design equation for the fabry-perot mode antenna has been derived and validated. Various

4. An Electrically Small Frequency Reconfigurable Antenna

parametric analysis has been conducted on the antenna in order to get a good insight to the functioning of the structure. A prototype of the antenna designed for a FR4 substrate has been fabricated and used for various radiation characterisation of the antenna. The fabricated antenna fit well inside the criterion of an electrically small antenna (ESA), which has been confirmed with its various characteristics values. The proposed antenna has the limitation that the design could not be extended to any random selection of frequencies, as the dimension of the SIR selected is the same used for the fabry-perot also. This demands for a careful selection of frequencies for the design.

4. An Electrically Small Frequency Reconfigurable Antenna

Chapter 5

SIR Loaded Modified Dipole Antenna

5.1 Introduction

This chapter voyages through the design, development and analysis of a Stepped Impedance Resonator (SIR) loaded dipole antenna. The chapter starts with the evolution of the antenna, and shows how a planar dipole antenna can be loaded with an SIR effectively, to introduce a new resonance within the limited real estate of the antenna. This novel antenna operates in two different frequency bands with omnidirectional radiation patterns. Chapter deals with various parametric studies of the antenna.

5.2 Evolution of the Antenna

The design procedure of the antenna is started with the selection of the required frequency band of operation. Two bands selected are 5-6 GHz and 2.4 GHz band, used for ISM applications. The 5-6 GHz band has two ISM applications bands located at 5.2 GHz and 5.8 GHz.

A conventional planar dipole antenna is selected for achieving a resonance at the higher band. The planar design consisted of two 2 mm wide metal strips, each having a length of 10 mm, fed at the center using an Sub Miniature Version A (SMA) connector, on a FR4 substrate, as shown in Figure. 5.1(a). The width of the dipole is selected at 2 mm in order to make a compact design. The dipole is designed and optimized using Ansys HFSS.

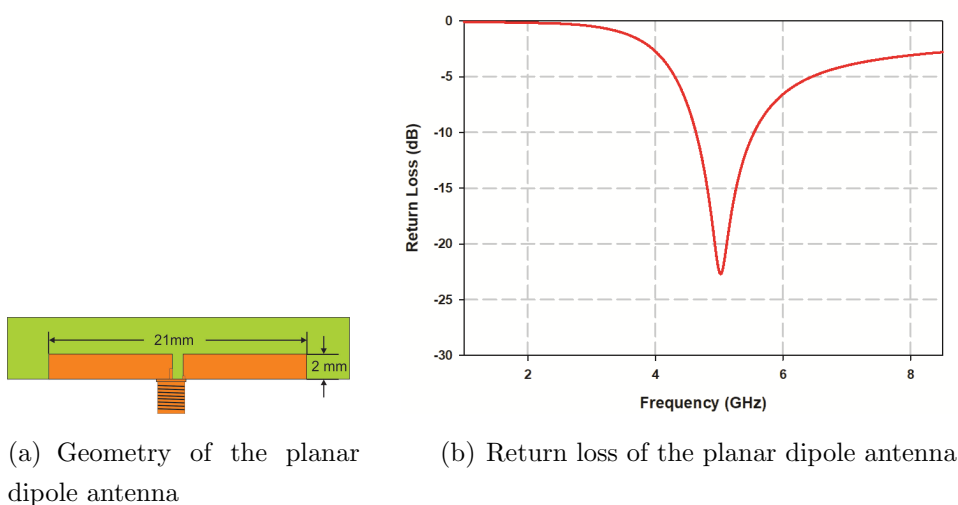


Figure 5.1: Reflection behaviour of the dipole antenna resonating at 5 GHz band. [Width = 2 mm, Length = 10 mm, Substrate thickness = 1.6 mm, $\epsilon_r = 4.4$]

The simulated return loss of the dipole structure is shown in Figure 5.1(b). From the figure it is evident that the antenna provides a 2:1 VSWR bandwidth of 1.07 GHz and good impedance matching characteristics. The center frequency of the resonance is at 5 GHz. To introduce another resonance in the antenna at a lower frequency, the dipole antenna is top loaded with a Uniform Impedance Resonator (UIR) as shown in Figure 5.2(a). This top loading with a parasitic

5. SIR Loaded Modified Dipole Antenna

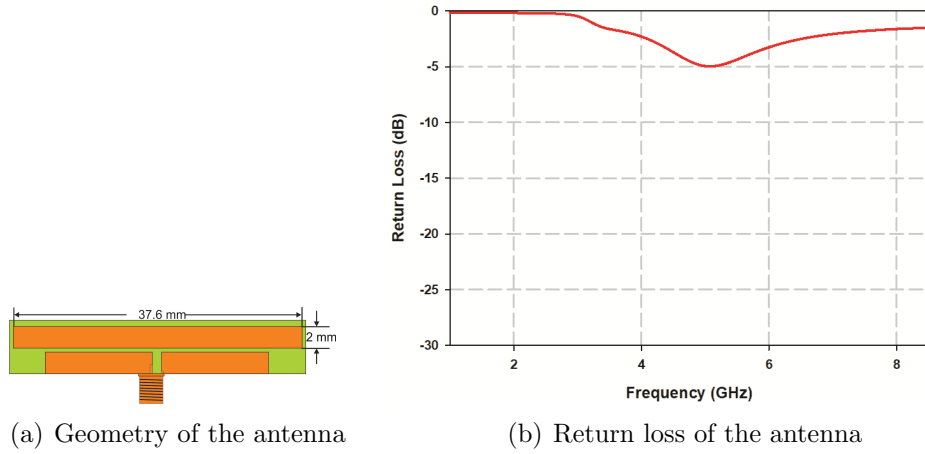


Figure 5.2: Return loss variation of dipole antenna top loaded with UIR resonating at 5-6 GHz band. [Dipole width = 2 mm, Dipole length = 10 mm, Parasitics element width = 2 mm, Parasitics element length = 37.6 mm, Substrate thickness = 1.6 mm, $\epsilon_r = 4.4$]

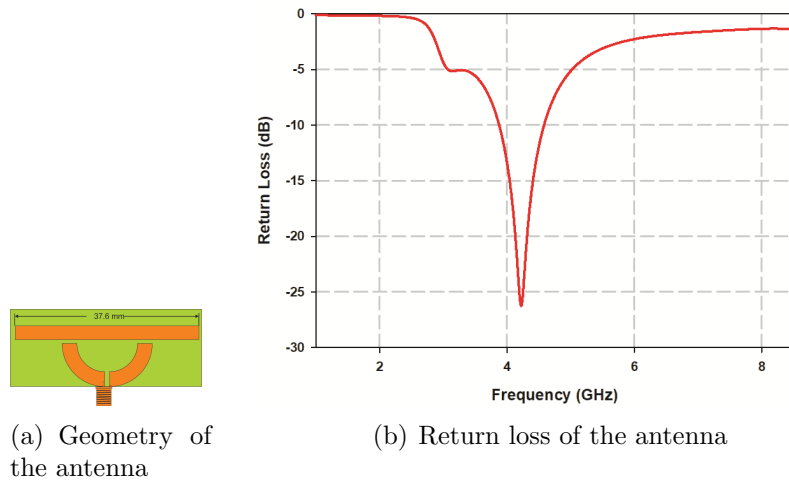


Figure 5.3: Return loss of the bent dipole antenna top loaded with UIR resonating at 5-6 GHz band. [Width = 2 mm, Length = 10 mm, Parasitics element width = 2 mm, Parasitics element length = 37.6 mm, Substrate thickness = 1.6 mm, $\epsilon_r = 4.4$]

UIR has affected the impedance matching of the dipole antenna. The top loading of UIR introduced an inductive shift in the input impedance of the antenna

5. SIR Loaded Modified Dipole Antenna

causing deterioration in the return loss characteristics as shown in Figure 5.2(b). The tight coupling between the dipole and UIR has caused this and it is reduced by increasing the coupling gap between the UIR and dipole without affecting the excitation energy to the parasite. This is achieved by introducing a bent in the dipole antenna as shown in Figure 5.3(a).

This modification in dipole has helped in improving the impedance matching of the antenna with a shift in resonant frequency to 4.2 GHz as shown in Figure 5.3(b). A closer analysis of the reflection characteristics on smith chart shows that this modification to the antenna has brought the impedance of the antenna, which was highly inductive earlier has become less inductive at resonance due to UIR loading. It is further noticed that if the bent dipole is top loaded with a UIR a new resonance is introduced at a lower frequency with a poor impedance matching.

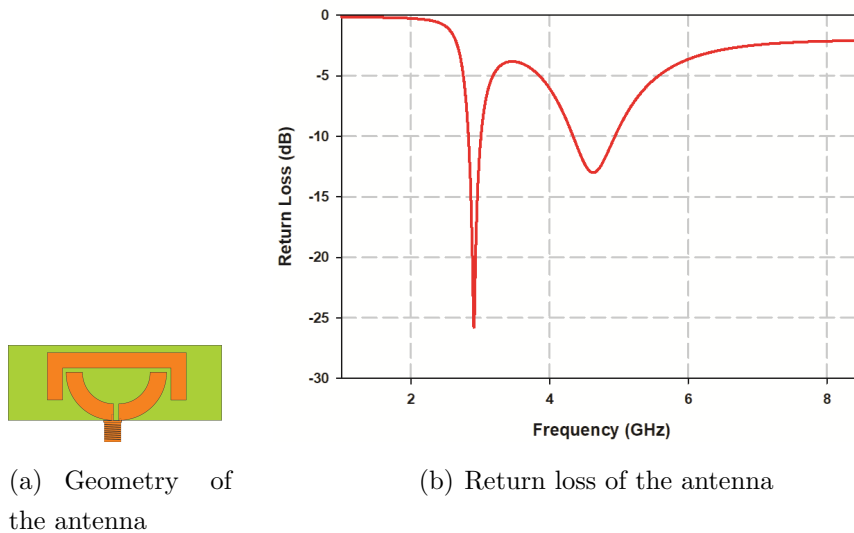


Figure 5.4: Return loss of the bent dipole antenna top loaded with folded UIR resonating at 5-6 GHz and 2.54 GHz band. [Width = 2 mm, Length = 10 mm, $\epsilon_r = 4.4$]

Now by some method, if the impedance matching can be improved for the newly introduced resonance, then the antenna can function as a dual band an-

5. SIR Loaded Modified Dipole Antenna

tenna. For achieving an improved impedance matching, a 90° folding is introduced in the UIR. This new structure is shown in Figure 5.4(a).

This has improved the impedance of the lower resonance to a reasonable level. The lower resonance obtained is at 2.9 GHz and at the same time the dipole resonance has shifted to 4.6 GHz without losing the impedance matching, with a reactance slightly on the capacitive side. In the lower resonance the reactance is slightly inductive. The return loss characteristics is shown in Figure 5.4(b). To make the antenna resonate at the desired application band, without increasing the size further, the UIR is replaced with a SIR structure, as in figure 5.5(a).

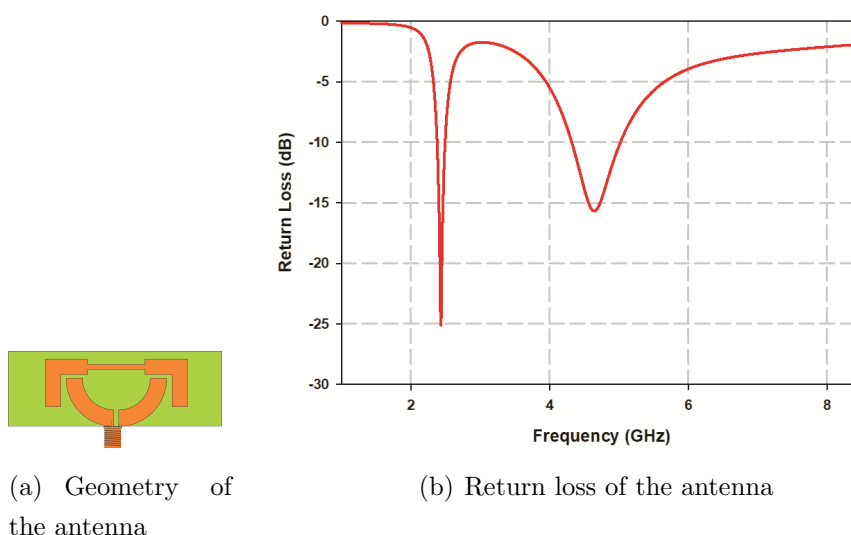


Figure 5.5: Return loss of the bent dipole antenna top loaded with UIR resonating at 5-6 GHz band. [Width = 2 mm, Length = 10 mm, $\epsilon_r = 4.4$]

This is achieved by keeping the total length of the parasitic element intact. This modification has further reduced the lower resonant frequency to 2.4 GHz. The Figure 5.5(b) shows the return loss characteristics of this SIR loaded bent planar dipole antenna.

The selection of SIR for the parasitic element is owing to its many advantages over UIR. A SIR gives more design freedom than UIR. There are two very important parameters of SIR, the impedance ratio k and the electrical length ratio α . By properly selecting these two parameters, a structure which can either have a

5. SIR Loaded Modified Dipole Antenna

total length less than or greater than UIR can still resonate at the same frequency as that of the UIR. At the same time it is possible to bring a non integer relation between the fundamental and harmonic frequencies of the SIR. All these properties prompted for the selection of SIR as a parasitic element. The frequency selected for the design of the SIR is 2.4 GHz. The SIR proposed for this antenna is a modified version of the conventional microstripline based SIR. The design and development of this SIR is explained in details in the coming sections.

5.3 Geometry

The antenna structure thus obtained through the above explained evolution process is further optimized with the help of simulation software. The geometry of the initially proposed antenna is shown in Figure 5.6. The antenna occupies an overall area of 25 mm x 9 mm on a substrate of relative permittivity (ϵ_r) 4.3, loss tangent ($\tan \delta$) 0.02 and thickness 1.6 mm. A planar dipole of length 10 mm is initially designed with an optimized width of 2 mm, and then modified by bending it with an inner radius of 7 mm. The arc length of the bent dipole is made same as that of the length of planar dipole. This dipole resonates at 5 GHz, where the length of the dipole is equal to $\lambda_g/2$, where, λ_g is the guided wavelength of the structure at the resonant frequency. A folded $\lambda_g/2$ stepped impedance resonator (SIR), with lengths L_1 , L_2 & L_3 , widths W_1 & W_2 , is utilized as a parasitic element to the dipole. The total length of the SIR is selected as $\lambda_g/2$ at 2.4 GHz. The optimized physical dimensions of the antenna are given in Table 5.1.

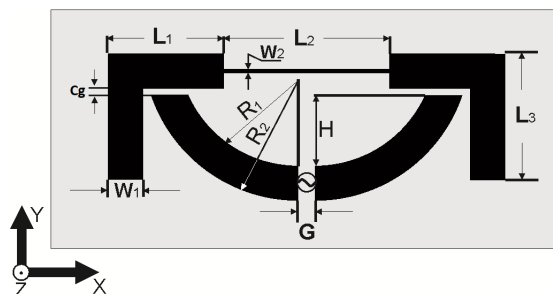


Figure 5.6: Basic geometry of the antenna

Table 5.1: Physical Dimensions of the Antenna

Parameter	Dimension (mm)
L1	9.62
L2	6.7
L3	7.7
W1	2
W2	0.2
R1	7
R2	9
Cg	0.4
G	1
H	4.1

5.4 Analysis of the effect of the radiation characteristics on top loading

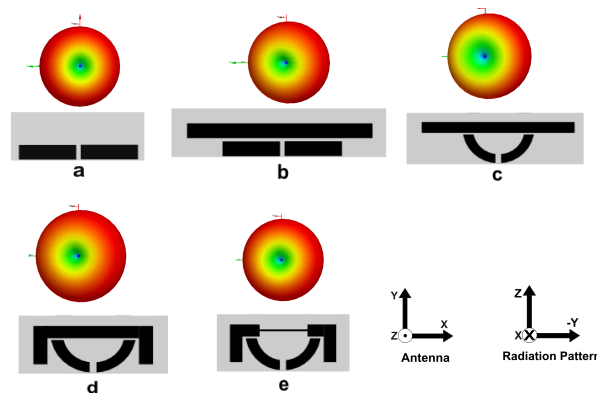


Figure 5.7: Simulated Radiation Pattern for different antenna configurations

Figure 5.7 illustrates the simulated radiation characteristics in the Y-Z plane of the antenna, corresponding to all the aforesaid evolution scenarios. A detailed analysis shows that the planar dipole is resonating at 5 GHz, as seen in Figure 5.1(b), with a corresponding omnidirectional radiation pattern shown in Figure

5. SIR Loaded Modified Dipole Antenna

5.7(a). Even though the introduction of a parasitic UIR, as shown in Figure 5.2(b) worsened the reflection characteristics of the planar dipole, there is a possibility for a new resonance in the lower end of the frequency.

In the present antenna, the parasitic element is placed very close to the driven element and here the parasitic element is exciting a new resonant mode instead of acting as a reflector to the dipole. This newly excited resonant mode is enhanced for obtaining a resonance at the lower 2.4 GHz in the proposed antenna. The simulated peak gain for the dipole resonance, in this case is 2.9 dBi, with a slight directional radiation pattern as shown in Figure 5.7(b). The unmatched lower resonance deteriorates when the UIR is moved away from the dipole. The bending of the dipole and the employment of the two ends of the dipole for coupling to the parasitic element, has improved the reflection characteristics of the dipole, with a downward shift in the resonance as shown in Figure 5.3(b). This shift in the resonance is due to the increase in the effective length of the dipole through the capacitively coupled UIR. Figure 5.8 shows the simulated surface current distribution at resonance. The surface current at this frequency is distributed both in the UIR and the bent dipole, there by increasing the effective length.

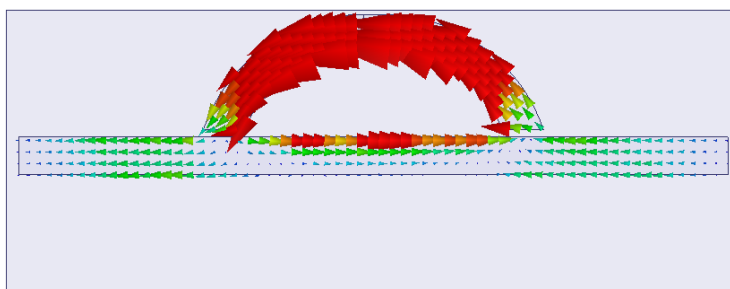


Figure 5.8: Surface current distribution at 4.2 GHz in the antenna with bent dipole and UIR top loading [UIR length = 37.6 mm, UIR width = 2 mm, dipole width = 2 mm, $\epsilon = 4.4$, substrate thickness = 1.6 mm]

A peak gain of 3 dBi, resulting in a directional pattern towards the Y direction, is achieved in the dipole radiation pattern as shown in Figure 5.7(c), with slightly improved return loss in the lower resonance. As seen in the Figure 5.4(b), by folding the UIR with an angle of 90° , the shift in the dipole resonance has

5. SIR Loaded Modified Dipole Antenna

reduced because of the cancellation of the current at the two ends of the UIR at higher band, which in turn reduces the effective length of the dipole, whereas the reflection characteristics of the lower resonance has enhanced considerably. The peak gain of the dipole antenna remained the same, whereas the radiation pattern has become nearly omnidirectional, as seen in Figure 5.7(d). With folded UIR having a total length of 34.42mm, the lower resonance is at 2.9 GHz. Further reduction in the lower resonance to 2.4 GHz is achieved by replacing the UIR with an SIR of the same length. The radiation pattern is nearly omnidirectional in this case, as seen in Figure 5.7(e). The polarization of the dipole is kept intact in all these modifications.

The radiation performance of the antenna is analyzed with and without placing the SIR as parasitic element. Figure 5.9 shows the reflection coefficient of the antenna with the above said configurations. Without SIR the antenna is resonating at 5 GHz, whereas the addition of SIR introduces a new resonance at 2.4 GHz. The inclusion of SIR to the structure caused a small shift in the higher resonance towards the lower frequency side, as seen in the Figure 5.9. This shift is attributed to the capacitive coupling between the SIR and the dipole, which extends the surface current of the dipole to the SIR structure, which in turn reduces the resonant frequency of dipole.

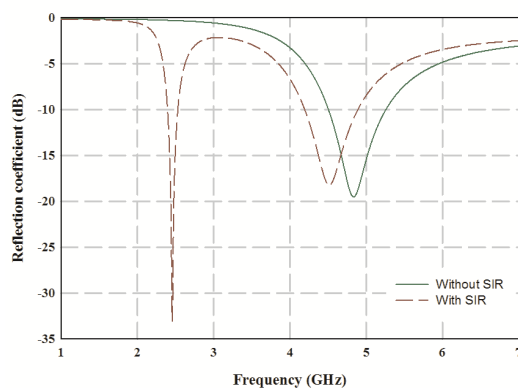


Figure 5.9: Simulated reflection characteristics of the structure with and without SIR [$k = 0.45$, $\alpha = 0.73$, $\epsilon_r = 4.4$, $h = 1.6$ mm]

5. SIR Loaded Modified Dipole Antenna

Figure 5.10 shows two different cases of the antenna. In the figure, the return loss characteristics shown by continuous line represents the response of a modified dipole with an UIR as the parasitic element. The dashed line graph shows the response when the UIR is replaced with a SIR of the same total length. Even though the total length of the UIR and the SIR are the same, by replacing UIR with SIR, the lower resonance has shown a considerable reduction in its resonance. This is because in a SIR the resonance is not determined by the length of the resonator, rather by the electrical length ratio and impedance ratio; which will be explained in the coming section. One important point to be noted from the return loss characteristics, in the Figure 5.10 is that the incorporation of SIR has made little effect on the higher resonance of the antenna. This shows that the resonances of the antenna can be independently controlled with some conditions applied; which will be explained in the following sections.

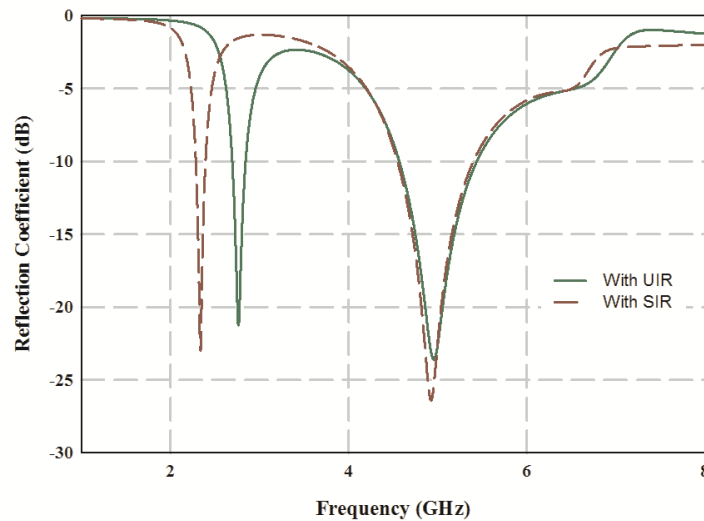


Figure 5.10: Simulated Reflection Coefficient for UIR and SIR top loading [UIR length = 37.6 mm, UIR width = 2 mm, $k = 0.45$, $\alpha = 0.73$, $\epsilon_r = 4.4$, $h = 1.6$ mm]

A prototype of the proposed antenna is fabricated using photo lithography technique and fed using a SMA connector at the centre, as depicted in the Fig-

5. SIR Loaded Modified Dipole Antenna

ure 5.11. This prototype antenna is tested inside an anechoic chamber. The measured and simulated return loss characteristics of the antenna is depicted in the Figure 5.12. The antenna has a measured 2:1 VSWR bandwidth of 90 MHz in the lower band, ranging from 2.38-2.47 GHz and 2.5 GHz in the higher band, ranging from 4.75-7.3 GHz.

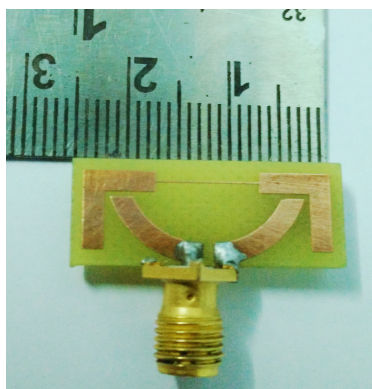


Figure 5.11: Fabricated prototype of planar antenna as per Table 5.1, $\epsilon_r = 4.4$, substrate thickness = 1.6 mm

A closer look at the antenna's reflection and radiation characteristics reveals that there are discrepancies in the measured and simulated data. The return loss characteristics of the higher frequency band shown in the Figure 5.12, shows a variation in the measured data in comparison to the simulation. In the measured return loss, the higher resonance has a wider bandwidth than the expected one. Moreover, the resonance shows higher vulnerability to the nearby objects close to the feeding cable, implying a less stable system. This is an outcome of the unbalanced/inefficient transformation between a balanced transmission line and an unbalanced transmission line, which resulted in a return current to flow through the outer surface of the coaxial cable, which is connected to the ground. While paving a path for this return current, spurious resonances are occurred in the antenna structure, causing a distorted radiation characteristics. The measured radiation pattern for this planar antenna is shown in Figure 5.13. The effect of spurious frequencies can be seen from the distortions present in the radiation pattern at the higher frequency bands as depicted in Figure 5.13(b). The obtained

5. SIR Loaded Modified Dipole Antenna

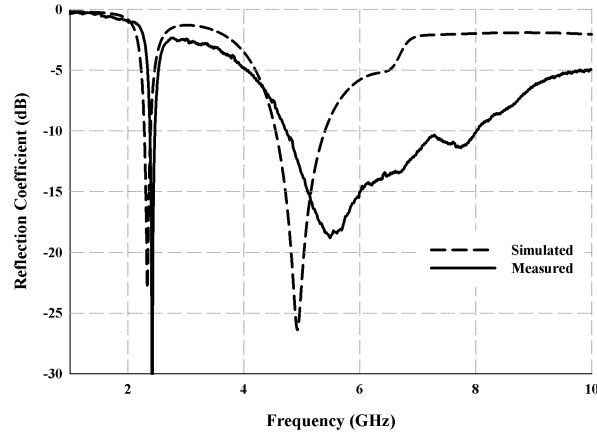


Figure 5.12: Measured and Simulated Reflection Coefficient of the coplanar antenna fabricated according to the dimensions given in Table 5.1, $\epsilon_r = 4.4$, substrate thickness = 1.6 mm

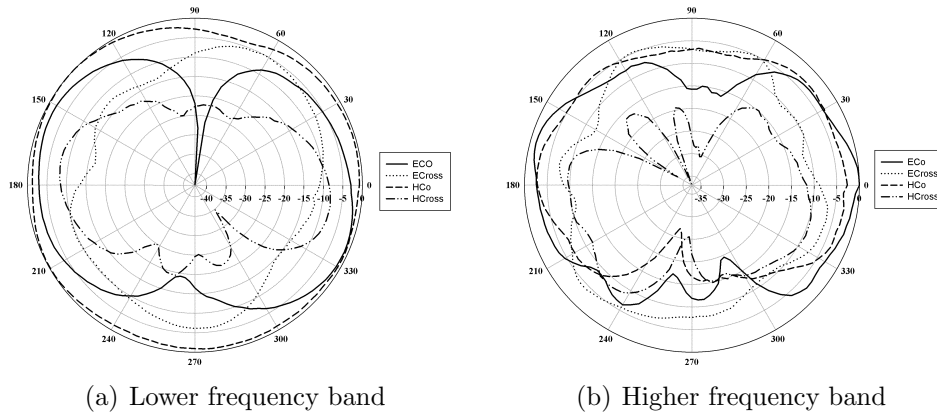


Figure 5.13: Measured radiation pattern of the coplanar antenna fabricated according to the dimensions given in Table 5.1, $\epsilon_r = 4.4$, substrate thickness = 1.6 mm

pattern is not agreeing with the expected omni-directional radiation pattern of the antenna. This distortion in the radiation characteristics of the antenna will impact the purpose of the antenna and therefore this distortion should be mitigated. The following session elaborate on the mitigation process.

5.5 Optimised Geometry

The return current present in the coplanar model of the antenna is a disadvantage, while the antenna is considering for any practical application. In order to implement the antenna in any practical system, the return current in the structure has to be eliminated by some means. To curb the return current, the coplanar dipole structure is modified into a double sided dipole structure as illustrated in the Figure 5.14(a). The direct SMA feeding mechanism to the dipole employed in the coplanar antenna is abolished, instead, the feeding for the modified antenna is done through a microstrip line with highly truncated ground plane. Now the interconnection is in between the SMA connector and the microstrip line. Since both the transmission lines are unbalanced lines, the antenna requires no external balancing act to support the seamless propagation of EM waves. The SMA connector used has a standard 50Ω characteristics impedance, whereas the 2 mm wide dipole or microstrip line has a higher characteristics impedance value. This demands for an impedance transformation in between the two transmission lines. For this purpose, an impedance transformer is designed and implemented at the feeding point of the antenna. The 50Ω transmission line with a length L_5 connecting directly to the SMA connector having a width W_3 of 3 mm is employed. This is then connected to the 2 mm wide transmission line with a length of L_4 forming an impedance transformer. This impedance transformer is connected to one arm of the modified dipole. A mirror copy of the dipole arm is created on the other side of the substrate material and is flipped along the Y axis to create the other arm of the antenna. These two arms together forms the modified dipole antenna. The optimised length for the impedance transformer is $L_5 = 7$ mm and $L_4 = 4$ mm. Table 5.2 shows the details of the dimensional changes came into the structure because of the aforesaid modifications. A prototype for this antenna is also fabricated and tested. All the measurements are conducted using PNA E8362B Network Analyzer inside an anechoic chamber. Figure 5.15 shows the fabricated prototype of the antenna.

Figure 5.14(b) shows the measured and simulated reflection coefficient of the optimized double sided dipole antenna. In contrast to the result obtained for the coplanar version of the antenna, the measured and simulated results are in

5. SIR Loaded Modified Dipole Antenna

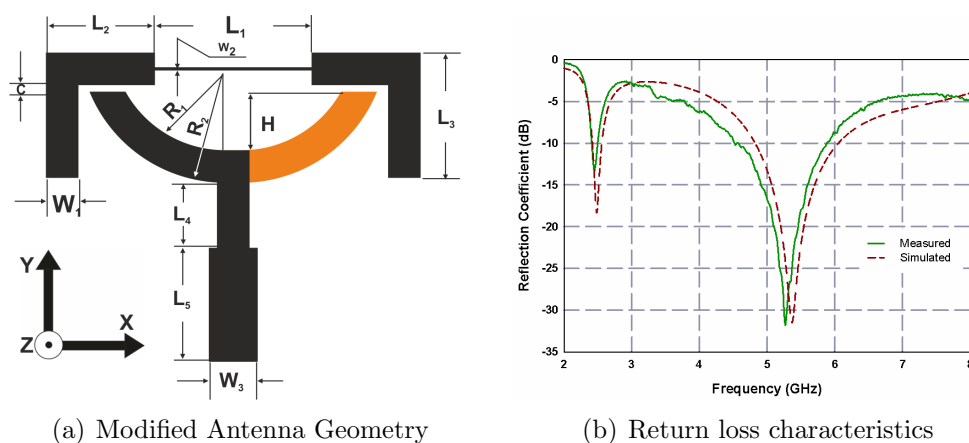


Figure 5.14: Modified antenna and return loss characteristics [$L1 = 9.62$ mm, $L2 = 6.7$ mm, $L3 = 7.7$, $L4 = 4$ mm, $L5 = 7$ mm, $W1 = 2$ mm, $W2 = 0.2$ mm, $W3 = 3$ mm, $R1 = 7$ mm, $R2 = 9$ mm, $C = 0.4$ mm, $H = 4.1$ mm, $\epsilon_r = 4.4$, Substrate thickness = 1.6 mm, $k = 0.45$, $\alpha = 0.73$]

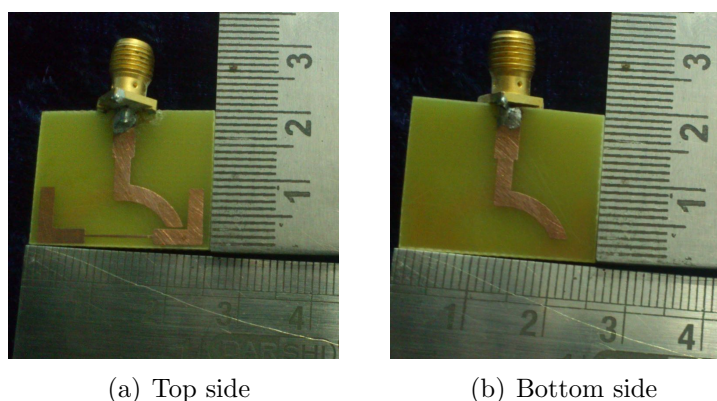


Figure 5.15: Fabricated prototype of the modified antenna [$L1 = 9.62$ mm, $L2 = 6.7$ mm, $L3 = 7.7$, $L4 = 4$ mm, $L5 = 7$ mm, $W1 = 2$ mm, $W2 = 0.2$ mm, $W3 = 3$ mm, $R1 = 7$ mm, $R2 = 9$ mm, $C = 0.4$ mm, $H = 4.1$ mm, $\epsilon_r = 4.4$, Substrate thickness = 1.6 mm, $k = 0.45$, $\alpha = 0.73$]

good agreement. A marginal increment in the higher resonance compared to the coplanar antenna is due to the reduction in the electrical length of the dipole caused from the cancellation of surface current components at the overlapping area. The slight variation in the measured and simulated data are due to the fabrication tolerances.

Table 5.2: Dimensions of the Modified Feed

Parameter	Dimension	Parameter	Dimension
L1	9.62	Cg	0.4
L2	6.7	G	1
L3	7.7	H	4.1
W1	2	L4	4 mm
W2	0.2	L5	7 mm
R1	7	W3	3 mm
R2	9		

5.6 Analysis of the parasitic element

The most important thing in the design of this proposed antenna is the successful modification of the dipole and UIR for achieving the necessary impedance matching without sacrificing the application bandwidth and compactness. SIR is introduced instead of an UIR to achieve compactness in the structure.

The most common and typical transmission line resonator used in the microwave field is the microstripline half wavelength resonator with two open circuited ends. Figure 5.16(a) shows the physical structure of a microstripline resonator. The strip conductor is of uniform width with length equivalent to half wavelength in the dielectric substrate with an uniform impedance, Z_0 . This resonator is termed as Uniform Impedance Resonator (UIR). An UIR has harmonic resonances which are the integer multiples of fundamental resonance. Moreover, it has got limited design parameters.

This limitation is overcome by introducing a lumped capacitance at the two open ends of the UIR. Figure 5.16(b) shows this variant of UIR, with capacitor loaded UIR. Considering the electrical length of the UIR, as indicated in the figure, it has a characteristics impedance Z_1 and electrical length of $2\theta_1$. The loading capacitance is given by [75],

$$C = \frac{Y_1 \tan(\theta_2)}{\omega_0} \quad (5.1)$$

5. SIR Loaded Modified Dipole Antenna

where,

$$Y_1 = \frac{1}{Z_1}, \quad \theta_2 = \frac{\pi}{4} - \theta_1 \quad (5.2)$$

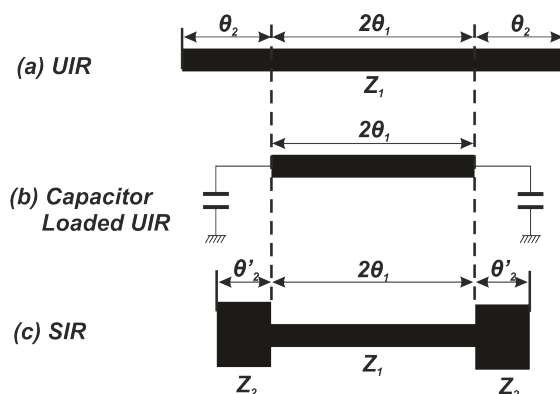


Figure 5.16: The evolution SIR from UIR

The two structures are made equivalent by taking the capacitance corresponding to θ_2 . This has the advantage of reducing the physical length of the resonator. Since the harmonics of the structure is dependent on the electrical length $2\theta_1$. This will make possible the spurious resonance suppression. The lumped capacitor loaded UIR has the disadvantage that at higher microwave frequencies, i.e. frequency above 1 GHz, the circuit losses in the lumped capacitor increases which demands for the requirement of frequency adjustment.

The lumped capacitor can be replaced by an equivalent transmission line as shown in figure 5.16(c). at $Y_2 \tan(\theta'_2) = Y_1 \theta_2$ i.e., at the basic resonance condition, all three resonators will resonate at the same frequency.

Stepped impedance resonators are available in three fundamental configurations viz. the $\lambda/4$, $\lambda/2$ and λ type SIR. Figure 5.18 shows the three different configuration of SIR. The one selected for the design of this particular antenna is the $\lambda/2$ type SIR. The governing equations for all the three SIR are the same. Figure 5.18 shows the conventional microstrip line type $\lambda/2$ SIR.

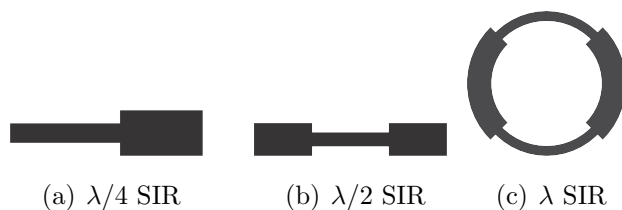


Figure 5.17: Conventional SIRs

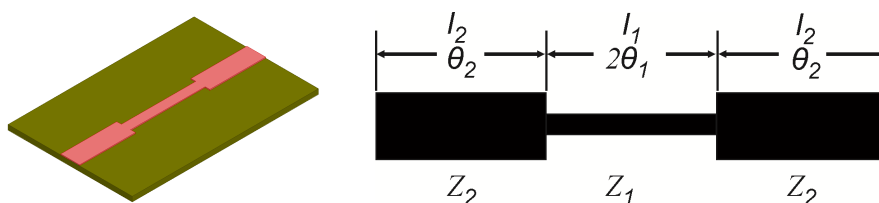


Figure 5.18: $\lambda/2$ SIR

5.6.1 Resonant Condition

Resonance is a phenomena where a body oscillates when it is subjected to an external driving force. These oscillations occurs at a particular frequency called natural frequency or resonant frequency of the structure. There are many factors which determines the resonant frequency of a particular structure. In the case of an UIR, it is the physical length which is directly related to the resonant frequency.

The resonant frequency determining factors of a SIR are the impedance ratio (k) and the electrical length ratio (α). Z_1 and Z_2 are the characteristics impedances of the narrow and broad microstrip lines, respectively and θ_1 and θ_2 are the electrical lengths of the lines corresponding to l_1 and l_2 . The impedance ratio k and electrical length ratios α of SIR are given by, [75]

$$k = \frac{Z_2}{Z_1} \quad (5.3)$$

$$\alpha = \frac{\theta_2}{(\theta_1 + \theta_2)} \quad (5.4)$$

5. SIR Loaded Modified Dipole Antenna

The fundamental condition for the resonance to occur in any resonant structure is that, at resonance the impedance should be purely resistive. The total impedance/admittance of the composite $\lambda/4$ SIR is given as [75],

$$Y_i = jY_2 \frac{2(k \tan(\theta_1) + \tan(\theta_2))2(k - \tan(\theta_1) \tan(\theta_2))}{k(1 - \tan^2(\theta_1))(1 - \tan^2(\theta_2)) - 2(1 + k^2) \tan(\theta_1) \tan(\theta_2)} \quad (5.5)$$

At resonance

$$Y_i = 0 \quad (5.6)$$

Application of (5.6) in (5.5) gives the resonant condition for the odd mode of operation as

$$k \cot(\theta_2) = \tan(\theta_1) \quad (5.7)$$

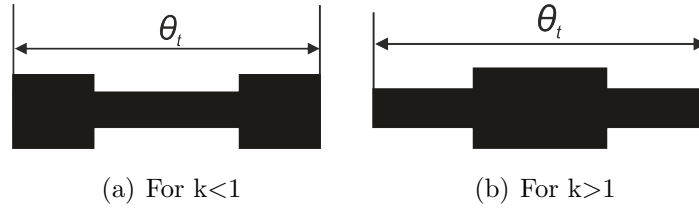


Figure 5.19: Different types of SIR based on Impedance Ratio

The impedance ratio k is a very important parameter in the design of SIR. Depending on the range of values of k , there are two types of SIRs, for $k < 1$ and for $k > 1$. Figure 5.19(a) & 5.19(b) shows the basic structure of microstrip version of SIR for $k < 1$ and $k > 1$, respectively. For $k < 1$ the total electrical length θ_t of the SIR is less than that of the UIR whereas, for $k > 1$ the electrical length θ_t is greater than that of UIR. θ_t will be larger than the physical length of the SIR because of the fringing fields at the open ends, which adds an effective length ΔL to the physical length. As the objective of the design of the proposed antenna is to make the parasitic element smaller than UIR, the impedance ratio opted for the design is $k < 1$, i.e., the $\lambda/2$ SIR shown in Figure 5.19(a).

5. SIR Loaded Modified Dipole Antenna

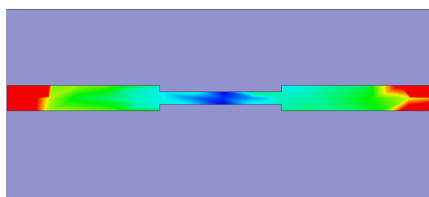


Figure 5.20: Electric field distribution in the SIR at fundamental mode

The fundamental resonance of SIR is represented by odd mode equation (5.18). The electric field/ voltage distribution in the odd mode resonance has a null at the center of the SIR and two peaks at the end points out of phase by 180° . Figure 5.20 shows the electric field distribution in the SIR at resonance.

For the design of this antenna, the SIR considered is a newly derived coplanar version of the microstrip line SIR. Two different CPS, one is symmetric and the other one asymmetric are combined to form a coplanar SIR. The evolution of the SIR is shown in Figure 5.21.

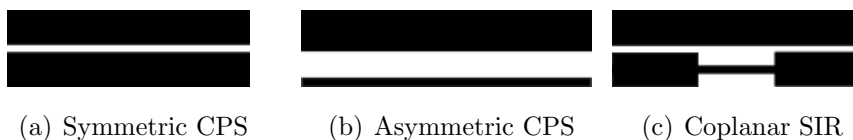


Figure 5.21: Evolution of coplanar SIR

The SIR employed in this antenna is a variant of the microstrip line based SIR. Here the SIR is implemented using coplanar transmission lines, by modeling it as a composite coplanar stripline (CCPS). Two CPS transmission lines with different characteristics impedances are combined to form a composite CPS. In the optimized design, one transmission line is symmetric and the other one is asymmetric.

When two transmission lines are combined together, then the resonant condition for that particular structure does not have a direct relation to the physical length of the structure as in the case of a UIR. The resonant condition for this CCPS structure is derived based on the very basic condition for a resonance to occur in any electrical circuit, i.e. at resonance the total impedance of the structure should be purely resistive. The characteristics impedance of CPS lines are

5. SIR Loaded Modified Dipole Antenna

calculated as in [113].

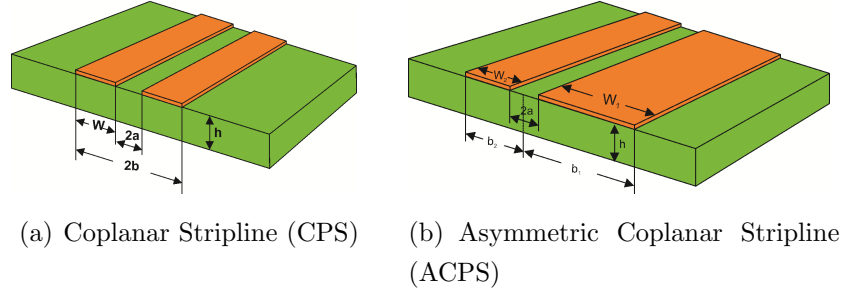


Figure 5.22: CPS and ACPS line Design

Figure 5.22(a) shows a CPS line. The characteristics impedance of CPS line is given as [113],

$$Z_0^{CPS} = \frac{120\pi}{\sqrt{\epsilon_{eff}^{CPS}}} \frac{K(k')}{K(k)} \quad (5.8)$$

where K is the complete elliptical function of first kind

$$\frac{K(k')}{K(k)} = \begin{cases} \frac{\pi}{\ln[2(1+\sqrt{k'})]} & ; \text{for } 0 \leq k \leq 1/\sqrt{2} \\ \frac{\ln[2(1+\sqrt{k})]/(1-\sqrt{k})}{\pi} & ; \text{for } 1/\sqrt{2} \leq k \leq 1 \end{cases} \quad (5.9)$$

where

$$k = \sqrt{1 - \left(\frac{a}{b}\right)^2} \quad (5.10)$$

$$k' = \sqrt{1 - k^2}$$

$$\epsilon_{eff}^{CPS} = 1 + \frac{\epsilon_{rs} - 1}{2} \frac{K(k)K(k_i')}{K(k')K(k_i)} \quad (5.11)$$

where,

$$k_i = \sqrt{1 - \frac{\sinh^2\left(\frac{\pi a}{2h_i}\right)}{\sinh^2\left(\frac{\pi b}{2h_i}\right)}} \quad (5.12)$$

$$k_i' = \sqrt{1 - k_i^2}$$

For an asymmetric coplanar strip line shown in Figure 5.22(b), the characteristics

5. SIR Loaded Modified Dipole Antenna

impedances are calculated by,

$$Z_0^{ACPS} = \frac{60\pi}{\sqrt{\epsilon_{eff}^{ACPS}}} \frac{K(k)}{K(k')} \quad (5.13)$$

where K is the complete elliptical function of first kind

$$k = \sqrt{\frac{2a(b_1 + b_2)}{(a + b_1)(a + b_2)}} \quad (5.14)$$

$$k' = \sqrt{1 - k^2}$$

$$\epsilon_{eff}^{ACPS} = 1 + \frac{\epsilon_{rs} - 1}{2} \frac{K(k)K(k_2')}{K(k')K(k_2)} \quad (5.15)$$

$$k_2 = \sqrt{\frac{(\exp(2\pi(b_1 + a)/h) - \exp(2\pi(b_1 - a)/h))(\exp(2\pi(b_1 + b_2)/h) - 1)}{(\exp(2\pi(b_1 + b_2)/h) - \exp(2\pi(b_1 - a)/h))(\exp(2\pi(b_1 + a)/h) - 1)}} \quad (5.16)$$

$$k_2' = \sqrt{1 - k_2^2} \quad (5.17)$$

Using equation 5.3 and 5.4 the characteristics impedance of the CPS and ACPS lines are found out and the k ratio for the CCPS SIR is calculated.

The k and α values of the new coplanar SIR are calculated using the impedance and θ value obtained for the CPS lines. The resonance condition for an SIR based on the impedance and electrical lengths are,

$$k = \tan(\theta_1) * \tan(\theta_2) \quad ;\text{for odd mode} \quad (5.18)$$

$$k = -\cot(\theta_1) * \cot(\theta_2) \quad ;\text{for even mode} \quad (5.19)$$

For a $\lambda/2$ SIR, considering the total electrical length of the structure as $\theta_t = 2(\theta_1 + \theta_2)$, the resonance condition for the SIR can be rewritten as

$$k \cot(0.5\alpha\theta_t) = \tan((1 - \alpha)0.5\theta_t) \quad (5.20)$$

5. SIR Loaded Modified Dipole Antenna

Table 5.3: Physical Dimensions of the Antenna for $k = 0.45644$, $\alpha = 0.7306$

Analytical		Simulated		Frequency (GHz)
$l_1(mm)$	$l_2(mm)$	$l_1(mm)$	$l_2(mm)$	
15.08	18.79	14.14	17.62	1.5
12.571	15.66	11.31	14.098	1.8
10.29	12.8	9.62	12.4	2.2
8.7	10.84	8.08	10.07	2.6

For this particular design, the k and α values selected are 0.45644 and 0.7306, respectively. This k and α are selected based on the optimization done for the antenna, using Ansys HFSS. For the fundamental mode, the range of θ_t is $0 < \theta_t < \pi$. By numerically evaluating the equation 5.20, for a particular value of k and α , the electrical lengths θ_1 & θ_2 of the SIR are calculated. From these electrical lengths the corresponding physical lengths l_1 & l_2 for a particular frequency is calculated. Table 5.3 shows the calculated and simulated dimensions of the SIR using equations 5.3 and 5.20 for different frequencies for the above mentioned k and α value. The slight variation in the analytical data as compared to the simulated one is because of the fringing field in the substrate. For evaluating the resonance of the designed CPS SIR, the structure is analyzed in 3D simulation software using plane wave excitation method. Figure 5.23 shows the plane wave excitation response of the structure for different design values as mentioned in Table 5.3. A change in the electric field can be seen at the resonant frequency of SIR. The physical dimension of the SIR is selected as per the dimensions used in the simulations and, for the fabrication of the antenna, the values selected for l_1 & l_2 are 9.62 mm and 12.4 mm, respectively. The validation of the SIR design using the equations derived from the CPS and ACPS lines are carried out using HFSS simulation. For obtaining the resonance of the structure, back scattering analysis is carried out using plane wave excitation technique in HFSS. For the excitation, a plane wave polarized along \mathbf{X} axis is employed in the simulation. A change in the electric field of the back scattered signal is observed at the point of resonance of the structure. Figure 5.23 shows the scattered electric field of the structure.

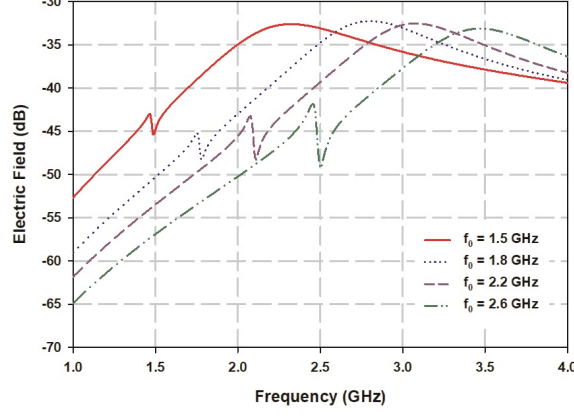


Figure 5.23: The Electric field at different frequencies with plane wave excitation of different coplanar SIR configurations as mentioned in Table 5.3

5.6.2 Design Equation for Parasitic Element

In the case of the proposed antenna, the SIR does not take an exact structure as discussed so far. In the antenna the modified dipole serves a twofold purpose. While it acts as a dipole antenna at 5 GHz band, in the lower frequencies the dipole acts as a ground plane for the SIR. Because of this structural deviation in the ground plane of the SIR, the resonance of the SIR is shifted upward from the designed resonance of the SIR. This shift is found to be a constant percentage of the designed resonance for all the frequencies, while keeping all other parameters constant. When the structure metalization of the SIR ground changes, this makes the effective permittivity at the resonance shift from the value obtained for CPS and ACPS configuration. This is the reason for the resonance shift in the structure. This shift in the effective permittivity is taken care by modifying the equation for the effective permittivity of the structure by

$$\epsilon_{eff}^{CPS} = 0.916 * \left(1 + \frac{\epsilon_{rs} - 1}{2} \frac{K(k)K(k'_i)}{K(k')K(k_i)} \right) \quad (5.21)$$

$$\epsilon_{eff}^{ACPS} = 0.916 \left(1 + \frac{\epsilon_{rs} - 1}{2} \frac{K(k)K(k'_2)}{K(k')K(k_2)} \right) \quad (5.22)$$

5. SIR Loaded Modified Dipole Antenna

where k value in the equation (5.21) and (5.22) for the elliptical function $K(k)$ are different, and are given by the equation (5.10) and (5.14), respectively. This concept of effective permittivity improves the SIR design to fit the resonance frequency of the antenna close to the desired frequency. With this newly derived design equation, the parasitic element has been designed on different dielectric substrates with permittivity varying from 2.1 to 9.2. The SIR design is also carried for different α values. Figure 5.24(a) and 5.24(b) shows the simulated return loss characteristics of the lower resonance for different substrate materials and for different α values, respectively. Table 5.4 shows the corresponding SIR dimensions designed for 2.4 GHz with different permittivity values and α values. This shows that the derived equation is capable enough to mitigate the deviation in the SIR and can be effectively used for the design of the lower resonance of the antenna, irrespective of the substrate.

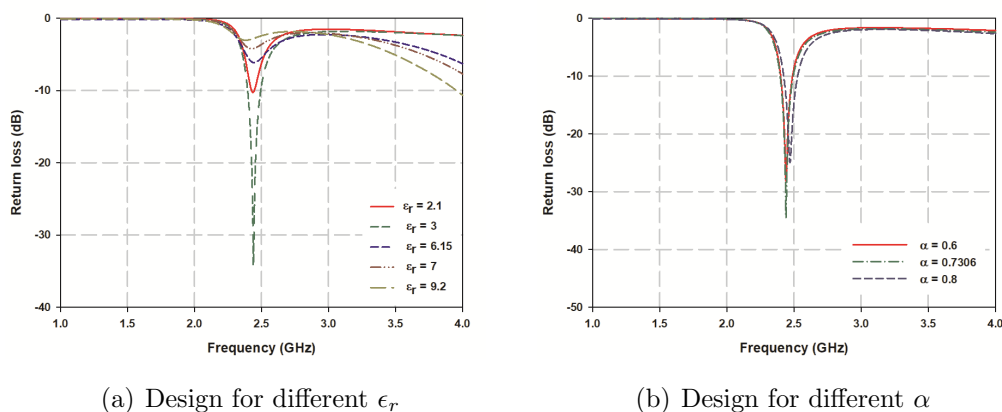


Figure 5.24: Simulated Return loss for the lower band of antenna designed with the derived design equation for SIR corresponding to the dimension mentioned in Table 5.4 $\epsilon_r = 4.4$, $h = 1.6$

5. SIR Loaded Modified Dipole Antenna

Table 5.4: Physical Dimensions of the SIR in the Antenna

Different Substrate				Different α			
ϵ_r	$L_1(mm)$	$L_2(mm)$	$L_3(mm)$	α	$L_1(mm)$	$L_2(mm)$	$L_3(mm)$
2.1	12.29	5.365	12.395	0.6	15.79	3.615	9.495
3	11.12	5.95	10.36	0.7306	11.12	5.95	10.36
6.15	8.66	7.18	5.62	0.8	8.57	7.225	11
7	8.24	7.39	4.65				
9.2	7.377	7.82	3.07				

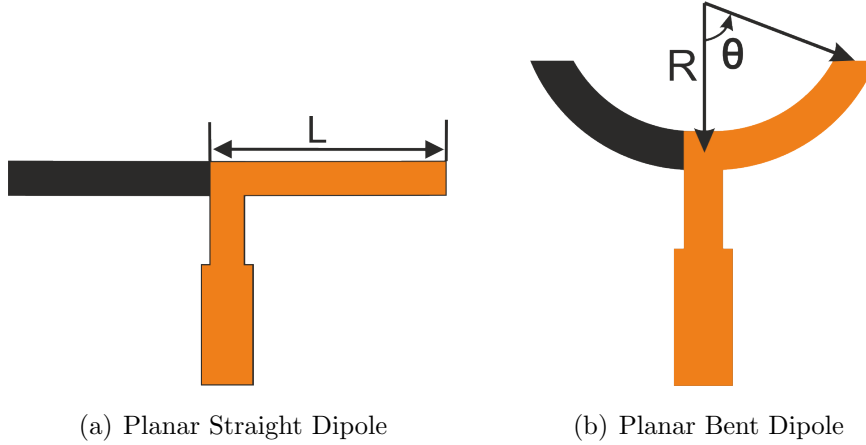


Figure 5.25: Transformation from straight dipole to a bent dipole

5.6.3 Design Equation for Bent Dipole

The bent dipole presented here is a modified form of a straight planar dipole. The transformation is carried out by relating the straight dipole length to the arc length of the bent dipole. While designing an equivalent bent dipole from a straight planar dipole antenna, two major parameters taken into consideration are the arc radius and the arc angle θ , as depicted in Fig. 5.25. Out of vivid combinations available between these two parameters, an optimized range, where the design errors are minimum is selected. Through out the design process, the width of the dipole is kept a constant at 2 mm. The radius R of the arc is given by

$$R = \frac{L}{\theta} \quad (5.23)$$

5. SIR Loaded Modified Dipole Antenna

where θ is in radian. Table 5.5 shows the radius calculated for different values of θ , keeping L constant at 12 mm. The 12 mm length straight planar dipole resonates at 5.014 GHz.

Table 5.5: Physical Dimensions of the Antenna

$\theta(\text{radian})$	$R(\text{mm})$	$f(\text{GHz})$
$\pi/6$	22.9183	5.266
$\pi/4$	15.2789	5.176
$\pi/3$	11.4592	5.248
$4\pi/9$	8.5944	5.338
$\pi/2$	7.6394	5.365

From the table it is perceived that at the lower range of θ , the deviation from the indented resonance is not predominant. beyond $\pi/3$ radian the deviation increases. This is due to the domination of the vertical component, i.e. x component of the surface current along the open ends of the dipole as the angle approaches $\pi/2$. In order to get rid of this error, the span of the angle θ is limited to a maximum of 65 degrees. A comparative study of a normal dipole designed for different resonant frequencies to that of corresponding bent dipole using (5.23) is shown in Table 5.6. The table shows there are differences in the expected and observed values of resonances. This difference is mitigated by adding a correction factor to the equation (5.23) as;

$$R = \frac{1.0518L}{\theta} \quad (5.24)$$

Here the dipole length L is given as

$$L = \left(\frac{\lambda}{4\sqrt{\epsilon_{\text{reff}}}} + 2 \right) P \quad (5.25)$$

$$\epsilon_{\text{reff}} = \frac{\epsilon_r + 1}{2} \quad (5.26)$$

$$P = 1.1085 \quad (5.27)$$

5. SIR Loaded Modified Dipole Antenna

The peak deviation from the desired resonant frequency without the correction factor was 6.7%, as seen from the table. After applying the correction factor, the peak deviation observed is only 1.8%. This keep the desired resonance and the observed resonance in good agreement.

Table 5.6: Planar bent dipole for different frequencies (f_d : designed frequency, f_s : simulated Frequency, f_c :Corrected frequency) corresponding straight planar dipole

$L(mm)$	$R(mm)$	$f_d(GHz)$	$f_s(GHz)$	%deviation	$f_c(GHz)$	%deviation
10	9.5	5.959	6.364	6.7	6.004	0.75
12	11.4	5.014	5.248	4.6	4.987	-0.53
14	13.3	4.393	4.555	3.6	4.348	-1
16	15.2	3.808	4.015	5.4	3.817	0.2
18	17.1	3.385	3.565	5.3	3.322	-1.8

5.7 Analysis of Electric Field, Surface Current and Polarization of the Antenna

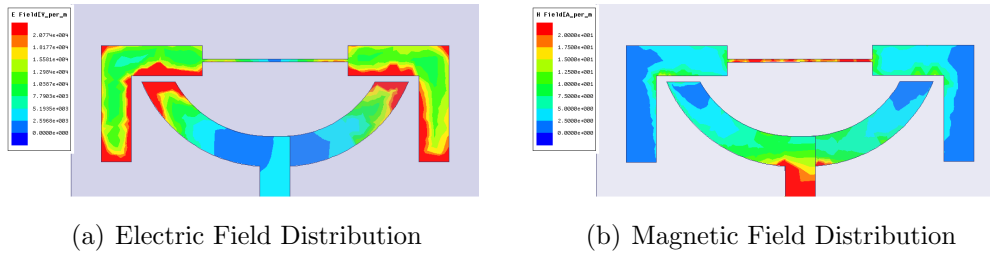


Figure 5.26: Field Distribution on the antenna at 2.4 GHz [L1 = 9.62 mm, L2 = 6.7 mm, L3 = 7.7, L4 = 4 mm, L5 = 7 mm, W1 = 2 mm, W2 = 0.2 mm, W3 = 3 mm, R1 = 7 mm, R2 = 9 mm, C = 0.4 mm, H = 4.1 mm, $\epsilon_r = 4.4$, Substrate thickness = 1.6 mm, $k = 0.45$, $\alpha = 0.73$]

In the proposed antenna, the modified dipole is fed through a microstrip transmission line connected via a SMA connector. The SIR used for obtaining the lower 2.4 GHz resonance do not have any direct electrical connection either

5. SIR Loaded Modified Dipole Antenna

with the dipole or with the SMA connector. In order to find the mechanism of excitation of the SIR, the field distribution in the antenna has to be analyzed at the resonant frequency. Figure 5.26 shows the electric and magnetic field distribution in the antenna at 2.4 GHz. The magnetic field strength at this frequency is very feeble in comparison with the electric field strength as shown in Figure 5.26(a) & 5.26(b), whereas, the electric field at the end points of the dipole is at maximum. The ratio of electric field to magnetic field (E/H) is found to be 558.5 at this frequency. Thus, the electric field is getting coupled to the SIR which is used as a parasitic element in the antenna. From the figure the electric field distribution in the SIR at the point which comes closer to the dipole ends are at maximum, whereas the magnetic fields distribution do not have much impact in the coupling process. From this it is concluded that the coupling is electrical in nature rather than magnetic.

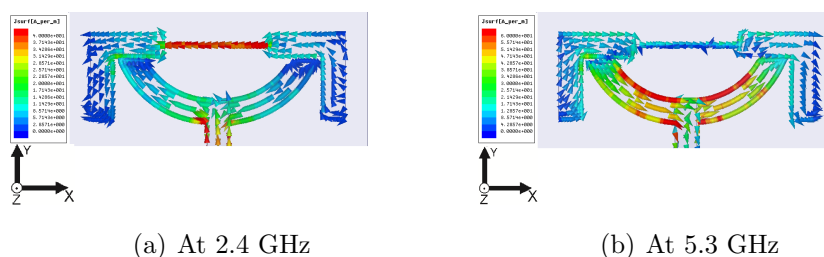


Figure 5.27: Surface Current Distribution at 2.4 GHz and 5.3 GHz [L1 = 9.62 mm, L2 = 6.7 mm, L3 = 7.7, L4 = 4 mm, L5 = 7 mm, W1 = 2 mm, W2 = 0.2 mm, W3 = 3 mm, R1 = 7 mm, R2 = 9 mm, C = 0.4 mm, H = 4.1 mm, $\epsilon_r = 4.4$, Substrate thickness = 1.6 mm, $k = 0.45$, $\alpha = 0.73$]

The surface current distributions of the antenna in both the bands are depicted in Figure 5.27. The surface current distribution shows that there is an half wavelength relation between the current distribution and the resonant frequency. At 2.4 GHz, there is a $\lambda g/2$ distribution of surface current in the SIR whereas the surface current in the dipole do not show such relation. In the higher resonance, the $\lambda g/2$ variation is seen only in the dipole. In the SIR at 2.4 GHz, the current along the Y direction on either side is anti-parallel and will cancel at far field, leaving behind a net current in the X direction. At 5.3 GHz the Y components of

the current on either side of the dipole is anti-parallel and will cancel at far field, leaving behind a net current in the X direction. This results in the polarization of the antenna along X direction, which is experimentally verified.

5.8 Parametric Analysis

The optimised antenna has been fabricated and measured in an anechoic chamber. For obtaining a clear insight to the response of the antenna on different antenna parameters, each and every parameter has to be analysed separately. For this purpose, a variety of parametric studies has been conducted on the antenna, there by concluding on the behaviour of the structure with changes in different design parameters.

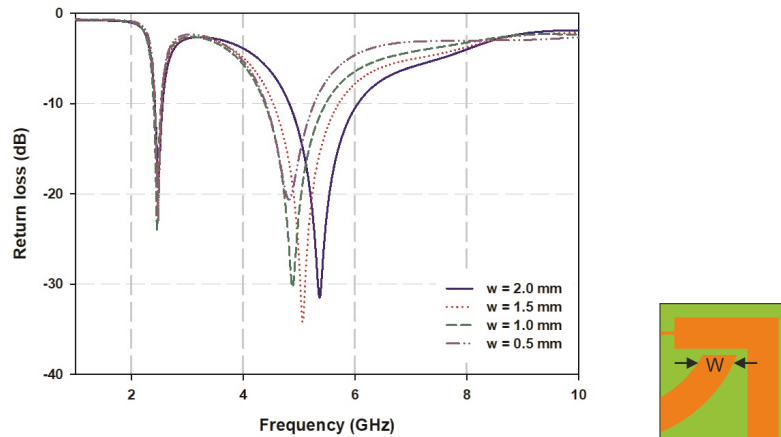


Figure 5.28: Effect of dipole width on return loss of the antenna [L1 = 9.62 mm, L2 = 6.7 mm, L3 = 7.7, L4 = 4 mm, L5 = 7 mm, W1 = 2 mm, W2 = 0.2 mm, W3 = 3 mm, C = 0.4 mm, H = 4.1 mm, $\epsilon_r = 4.4$, Substrate thickness = 1.6 mm, $k = 0.45$, $\alpha = 0.73$]

5.8.1 Parametric Analysis of the dipole width

The width of the modified dipole is varied to understand its implication on the dipole and the SIR resonance. The width is varied from 0.5 mm to 2 mm. Figure 5.28 shows the effect of width variation on the return loss characteristics

5. SIR Loaded Modified Dipole Antenna

of the antenna. The resonant frequency is increasing with increase in the dipole width, whereas the impedance matching is almost intact. In the lower frequency band, the change in the dipole width has made little effect in its resonance. The change in the width of the dipole is changing the net reactive loading of the dipole and as the width is decreased, the net reactance is increasing and become more inductive. This increase in the inductive reactance is decreasing the resonant frequency of the dipole, as shown in the Figure 5.28.

Table 5.7: Resonance variation with dipole width

Dipole Width (mm)	Resonant Frequency (GHz)
0.5	4.8158
1	4.8844
1.5	5.0657
2	5.3695

5.8.2 Parametric Analysis of coupling gap C_g

An analysis on the coupling gap C_g is carried out to find its implication on the resonant frequencies of the antenna. Figure 5.29(b) shows the simulated return loss characteristics of the antenna for different values of C_g in the higher frequency band. Here as C_g is varied from 0.2 mm to 1.4 mm., the resonant frequency showed an upward shift. Here the gap capacitance C_g acts as a capacitive loading to the dipole antenna, whose capacitance varies with respect to the change in the gap between the modified dipole and the modified SIR. As the gap changes, the gap capacitance also changes which in turn changes the capacitive loading of the dipole. This capacitive loading changes the effective length of the modified dipole. In the lower frequency band, the resonant frequency is increasing with the increase in the coupling gap C_g . The variation in the resonant frequency in this band is not predominant as in the case of higher frequency band. Figure 5.29(a) shows the simulated return loss characteristics of the antenna for the lower band.

5. SIR Loaded Modified Dipole Antenna

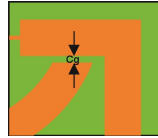
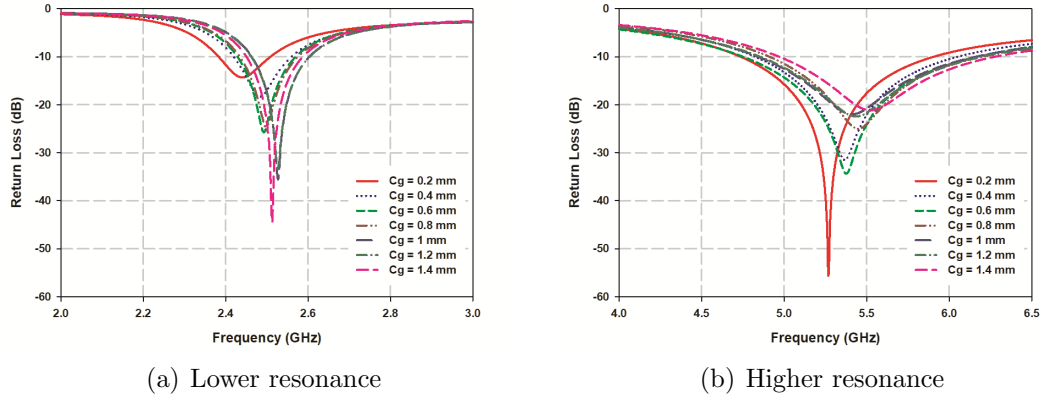


Figure 5.29: Effect of coupling gap on return loss of the antenna (C_g) [$L_1 = 9.62$ mm, $L_2 = 6.7$ mm, $L_3 = 7.7$, $L_4 = 4$ mm, $L_5 = 7$ mm, $W_1 = 2$ mm, $W_2 = 0.2$ mm, $W_3 = 3$ mm, $R_1 = 7$ mm, $R_2 = 9$ mm, $H = 4.1$ mm, $\epsilon_r = 4.4$, Substrate thickness = 1.6 mm, $k = 0.45$, $\alpha = 0.73$]

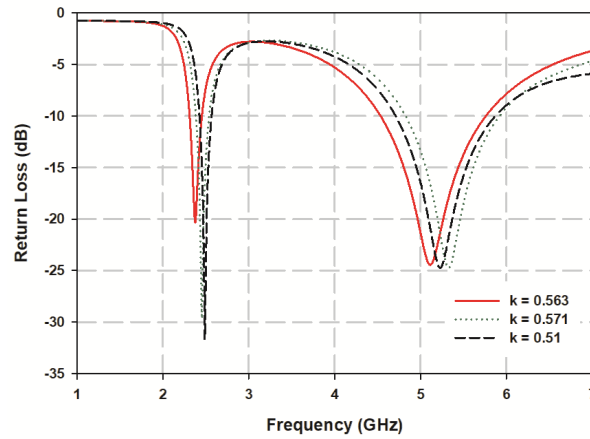


Figure 5.30: Return loss of the antenna with different impedance ratio k with constant α [$L_4 = 4$ mm, $L_5 = 7$ mm, $W_3 = 3$ mm, $R_1 = 7$ mm, $R_2 = 9$ mm, $C = 0.4$ mm, $H = 4.1$ mm, $\epsilon_r = 4.4$, Substrate thickness = 1.6 mm, $\alpha = 0.73$]

5.8.3 Parametric Analysis of impedance ratio k

One of the important parameter in the design of the proposed antenna is the impedance ratio k , of the SIR used in the antenna. The antenna can be made to resonate at the same frequency for different values of k by properly selecting the lengths of the stripline used. Here the antenna has been designed for different values of k on a substrate of thickness 1.6 mm, relative permittivity 4.3 and a $\tan \delta$ of 0.02. The design frequencies for all the k values are kept at 2.4 GHz and 5.4 GHz in the lower and upper frequency bands, respectively. Figure 5.30 shows the corresponding return loss characteristics of the antenna. The SIR dimensions for the corresponding impedance ratio are given in Table 5.8. This shows that antenna could be designed with parasitic element having different lengths to resonate at the desired resonant frequency by properly selecting the SIR parameters. This will provide more flexibility in the design process.

Table 5.8: SIR Dimensions for different k values

k	$L_1(mm)$	$L_2(mm)$	$L_3(mm)$	$W_1(mm)$	$W_2(mm)$
0.51	11.41	6.795	5.015	0.2	4
0.563	11.27	5.865	9.335	0.4	2
0.571	11.9	5.805	9.776	0.6	2

5.8.4 Parametric Analysis of the α ratio

The electrical length ratio α is a very important parameter in the design of SIR. An SIR can be designed with different total length by keeping the impedance ratio k constant and for different values of α , resonating at the same frequency. First SIR is designed for 2.4 GHz for a k value of 0.45644 and α values varying from 0.4 to 0.9. These dimensions thus derived are then used in the design of the antenna. Figure 5.31 shows the return loss characteristics of the proposed antennas with respect to the change in the α .

5. SIR Loaded Modified Dipole Antenna

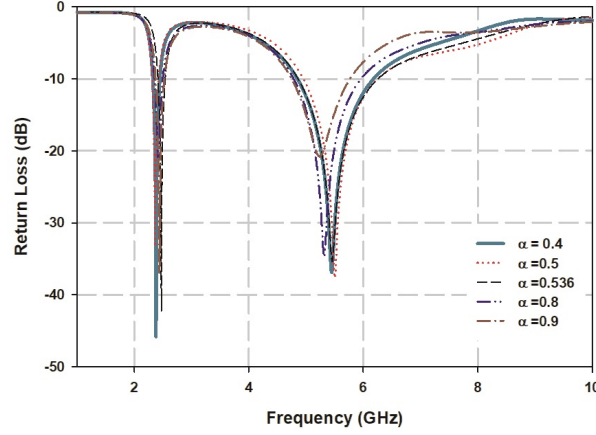


Figure 5.31: Return loss of the antenna designed for different values of α with constant k [$L_3 = 7.7$, $L_4 = 4$ mm, $L_5 = 7$ mm, $W_3 = 3$ mm, $R_1 = 7$ mm, $R_2 = 9$ mm, $C = 0.4$ mm, $H = 4.1$ mm, $\epsilon_r = 4.4$, Substrate thickness = 1.6 mm, $k = 0.45$]

Table 5.9: SIR Dimensions for different α values

α	$L_1(mm)$	$L_2(mm)$	$L_3(mm)$
0.4	21.93	0	6.72
0.5	18.10	2.46	7.85
0.5306	17.1	3.375	7.085
0.8	7.9399	7.53	9
0.9	4.2976	9.3612	10.4188

In the design of SIR, the width of the two strips are kept constant at 0.2 mm and 2 mm., respectively, for keeping the impedance ratio a constant at 0.45644. The placement of the SIR with respect to the modified dipole and the geometry of the dipole are kept intact during the variation analysis. The changes applied to the electrical length ratio α will only effect the physical length of the SIR. Here the lengths of both CPS lines are varied for its corresponding α value. Table 5.9 shows the different values of α opted for design and the corresponding metal strip lengths.

The design of the modified SIR is carried out at of 2.4 GHz. Though the

5. SIR Loaded Modified Dipole Antenna

position of the SIR is kept intact, as the α varies, the coupling gap C_g changes depending on, to which part of the SIR the ends of the dipole are coupling (i.e., whether coupling to wider strip L_2 or to narrow strip L_1). This effect is evident from the graph (figure 5.31) corresponding to the α values 0.8 and 0.9. In the case of 0.8, the overlap is partially on both the CPS lines, whereas in the case of 0.9, the overlap is completely on the narrow strip, which in turn increases the coupling gap C_g . In both these cases the resonant frequency of the dipole shows a downward shift. These results shows that the antenna could be designed to resonate at desired resonant frequency for different electrical length ratios. This one also improves the design flexibility of the antenna.

5.8.5 Parametric Analysis of folded SIR

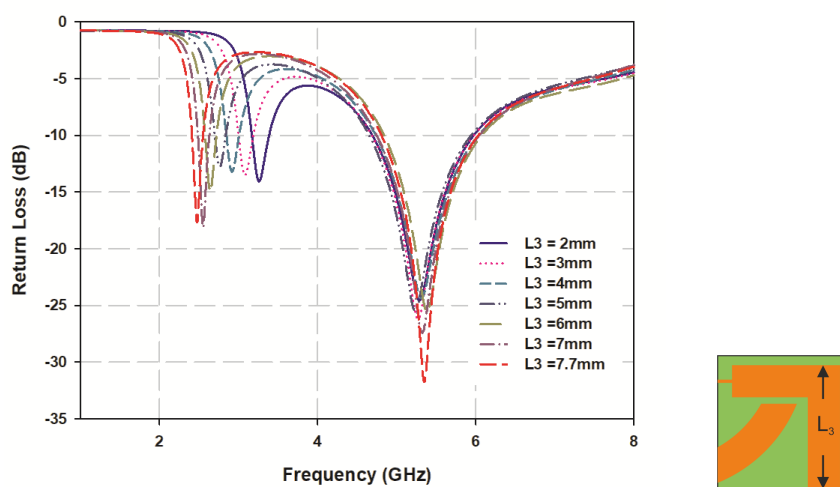


Figure 5.32: Effect of L_3 on return loss of the antenna [$L_1 = 9.62$ mm, $L_2 = 6.7$ mm, $L_4 = 4$ mm, $L_5 = 7$ mm, $W_1 = 2$ mm, $W_2 = 0.2$ mm, $W_3 = 3$ mm, $R_1 = 7$ mm, $R_2 = 9$ mm, $C = 0.4$ mm, $H = 4.1$ mm, $\epsilon_r = 4.4$, Substrate thickness = 1.6 mm, $k = 0.45$]

The length L_3 , which is the folded length of SIR is varied keeping L_1 and L_2 constant. The return loss characteristics of the antenna for this variation is shown in the Figure 5.32. This variation has a predominant effect in the lower frequency.

5. SIR Loaded Modified Dipole Antenna

As the length L_3 is reduced, the resonant frequency is increased. The reduction in L_3 has also reduced the impedance matching of the lower resonance. L_3 hardly affects the higher resonant frequency. Neither it shows a change in its resonance nor in its impedance matching. So it can be concluded that this particular portion of the antenna influences only the lower resonance. The change applied to the length of L_3 makes changes in the electrical length ratio α of the SIR. This change in α effects the resonant frequency of SIR. This shows that the antenna has an advantage of designing and controlling the two bands independently.

5.8.6 Parametric Analysis of the aspect ratio

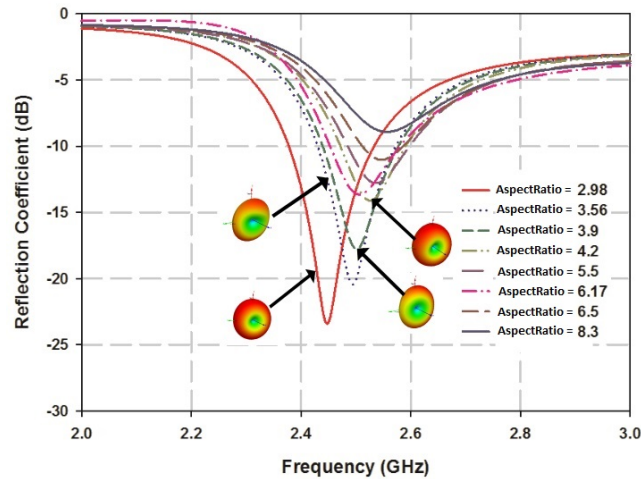


Figure 5.33: Reflection characteristics of the antenna with change in the aspect ratio [$L_4 = 4$ mm, $L_5 = 7$ mm, $W_1 = 2$ mm, $W_2 = 0.2$ mm, $W_3 = 3$ mm, $R_1 = 7$ mm, $R_2 = 9$ mm, $C = 0.4$ mm, $H = 4.1$ mm, $\epsilon_r = 4.4$, Substrate thickness = 1.6 mm, $k = 0.45$]

The aspect ratio of the SIR, i.e., the ratio between the length and breadth of the SIR is varied to see the change in radiation characteristics of the antenna in the lower band. The aspect ratio is defined as $\frac{L_1+2L_2}{L_3}$. At one point the radiation pattern is showing a slight directive nature. For an aspect ratio between 3.9

5. SIR Loaded Modified Dipole Antenna

and 5 the antenna is radiating slightly more toward the Y direction. At this aspect ratio, the bent dipole is acting as a director for the SIR and makes it directive. Figure 5.33 shows the change in radiation pattern with aspect ratio. As the aspect ratio is decreased from 8.3 to 2.98, the impedance matching of the antenna showed a commendable improvement giving the optimum aspect ratio as 2.98.

5.8.7 Parametric Analysis of the substrate thickness

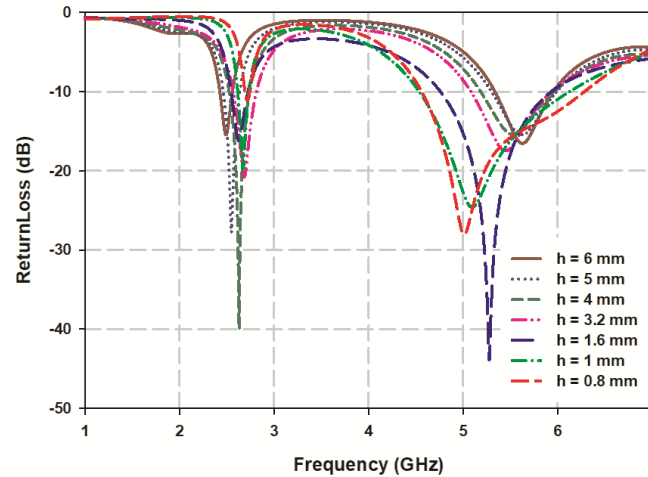


Figure 5.34: Variation of return loss of the antenna with substrate thickness of the antenna [L1 = 9.62 mm, L2 = 6.7 mm, L3 = 7.7, L4 = 4 mm, L5 = 7 mm, W1 = 2 mm, W2 = 0.2 mm, W3 = 3 mm, R1 = 7 mm, R2 = 9 mm, C = 0.4 mm, H = 4.1 mm, $\epsilon_r = 4.4$, $k = 0.45$, $\alpha = 0.73$]

An analysis on the thickness of the substrate material shows a variation in the resonant frequency of both the bands. In the lower frequency band, an increase in the substrate thickness caused a reduction in the resonant frequency, whereas in the higher frequency band the resonant frequency is increasing with the increase in the substrate thickness. As it is a two sided structure, there exists a capacitance between the two arms of the dipole, at the overlapping area. As the thickness is

5. SIR Loaded Modified Dipole Antenna

increased, this capacitance will get reduced and thus dipole resonates at a higher frequency. The thickness of the substrate is varied from 0.8 mm to 3.2 mm for a relative permittivity value of 4.3. For obtaining proper impedance matching, the feed dimensions of the antenna are redesigned for each value of the substrate thickness. Figure 5.34 shows the simulated return loss characteristics for different substrate thickness. From the figure, it is concluded that the increase in the substrate thickness has enhanced the impedance matching of the resonance, till $h = 4$ mm. But it is found that further increase in thickness more than 4 mm has reduced the impedance matching of the resonances imposing a limitation on the thickness of the substrate.

5.8.8 Parametric Analysis of the substrate permittivity

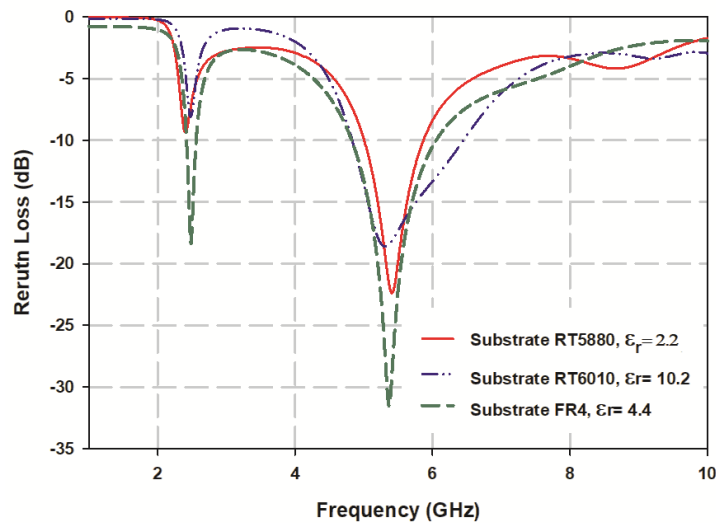


Figure 5.35: Reflection characteristics of the antenna with change in relative permittivity

One of the key parameter in the development of an antenna design is in the robustness in designing the antenna on different substrate materials. Practical applications demands for the use of variety of materials with different permittivity

5. SIR Loaded Modified Dipole Antenna

values to meet the circumstantial requirements. The antenna has been designed to operate in the proposed application bands on different substrate material with a reasonable range of relative permittivity. Figure 5.35 shows the return loss characteristics of the antenna for RT5880 substrate with ϵ_r 2.2, FR4 substrate with ϵ_r 4.4 and RTDuroid 6010 with ϵ_r 10.2 designed to operate in 2.4 GHz and 5-6 GHz bands. For the design of the lower resonance, a planar SIR is designed for a frequency of 2.4 GHz. The coupling gap Cg is kept constant in all the design. From Figure 5.35 it is clear that the designed antenna on three different substrates (ϵ_r 2.2 and 10.2) with considerable difference in relative permittivity, could still resonate at the designed resonant frequencies. This shows the proposed antenna could be realised on different substrates as requirement demands.

5.9 Result and Discussion

In this section, the measured radiation characteristics of the optimized antenna viz. radiation pattern, gain, efficiency & electrical size are discussed.

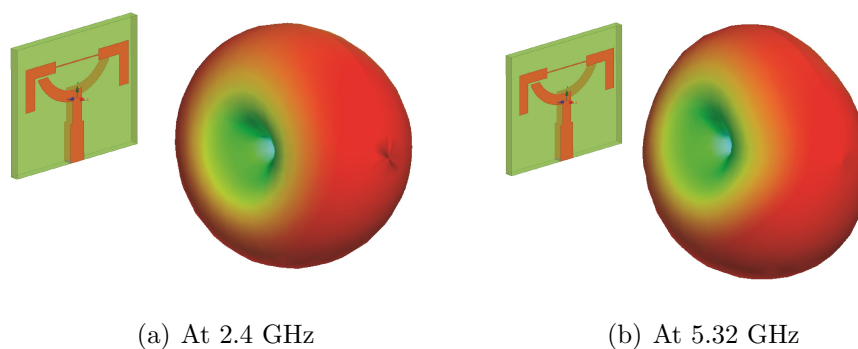


Figure 5.36: Simulated radiation pattern of the antenna [L1 = 9.62 mm, L2 = 6.7 mm, L3 = 7.7, L4 = 4 mm, L5 = 7 mm, W1 = 2 mm, W2 = 0.2 mm, W3 = 3 mm, R1 = 7 mm, R2 = 9 mm, C = 0.4 mm, H = 4.1 mm, ϵ_r = 4.4, Substrate thickness = 1.6 mm, k = 0.45, α = 0.73]

5.9.1 Radiation Pattern

At 2.4 GHz band, as the antenna size is very small compared to the free space wavelength, the radiation pattern is expected to be omnidirectional [69]. A peep into the surface current distribution on the antenna at 2.4 GHz as given in Figure 5.27(a) shows that the anti parallel components along the Y direction will cancel at far field. This will make the antenna to radiate with an omnidirectional pattern, with X polarization. Figure 5.36(a) shows the simulated 3D radiation pattern in the 2.4 GHz band. The surface current distribution on the antenna at higher frequency band is shown in Figure 5.27(b). Here the current can be resolved in to X and Y components. The resolved X components are in the same direction whereas the Y components are anti parallel with equal magnitude. This anti parallel components will get canceled at far field, leaving behind only the X component. Figure 5.36(b) shows the simulated 3D radiation pattern in the higher band.

Measured radiation pattern of the antenna in both bands are nearly omnidirectional. Figure 5.37 shows the radiation pattern of the antenna at 2.4 GHz. The Co-polar component of electric field in the E plane is in the shape of figure-of-eight while the Co-polar component of electric field in the H plane is a circle. Figure 5.38 shows the measured radiation pattern at at 5.2 GHz. Here also the electric field in the E plane is in the shape of figure of eight and a circle in H plane. The E-plane Half Power Beam Width (HPBW) is 80° in the lower band and 68° in the higher band.

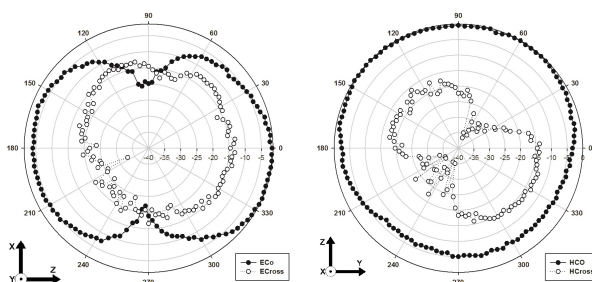


Figure 5.37: Measured radiation pattern at 2.48 GHz

5. SIR Loaded Modified Dipole Antenna

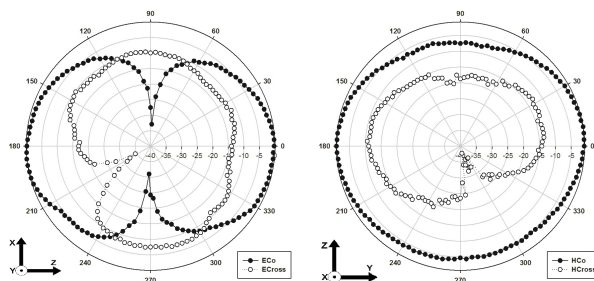


Figure 5.38: Measured radiation pattern at 5.32 GHz

5.9.2 Gain of the antenna

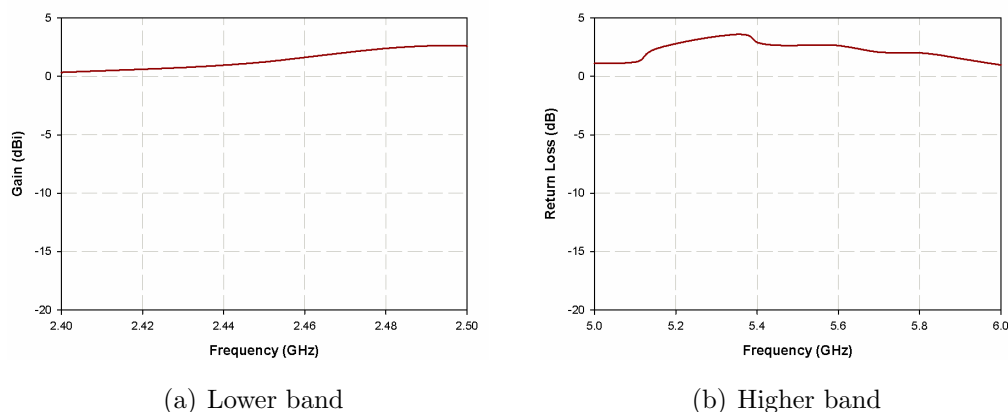


Figure 5.39: Measured Gain of the antenna [L1 = 9.62 mm, L2 = 6.7 mm, L3 = 7.7, L4 = 4 mm, L5 = 7 mm, W1 = 2 mm, W2 = 0.2 mm, W3 = 3 mm, R1 = 7 mm, R2 = 9 mm, C = 0.4 mm, H = 4.1 mm, $\epsilon_r = 4.4$, Substrate thickness = 1.6 mm, $k = 0.45$, $\alpha = 0.73$]

Gain is one of the important specification of any antenna. It is defined as the ratio of intensity of an antenna relative to the isotropic antenna. There are different methods for the measurement of the gain of an antenna. Out of all, Gain comparison or Gain transfer method is the most common method employed in gain measurement, as per IEEE standard test procedure for antennas, ANSI/IEEE std 149-1979. The gain measurement of the antenna is carried out

5. SIR Loaded Modified Dipole Antenna

using the gain comparison method [13]. In this method, the antenna gain is measured in comparison with the gain of a standard antenna whose gain is known. A wide band horn antenna is used for this purpose. The measured gain of the antenna in the lower frequency band is given in Figure 5.39(a). In the 2.4 GHz band, the gain obtained is nearly uniform with an average value of 1.4 dBi and peak gain of 2.6 dBi at 2.48 GHz.

In the higher resonant band also the gain obtained is nearly uniform in nature. The measured gain of the antenna is depicted in Figure 5.39(b). In this band the average gain obtained is 2.2 dBi and the peak measured gain is 3.6 dBi at 5.35 GHz.

5.9.3 Efficiency of the antenna

One of the important figure of merit of an antenna is the radiation efficiency. Radiation efficiency shows how good an antenna in radiating the input power received by it. The input power received by a well matched antenna can be either radiated away into the free space or can be dissipated in the antenna structure itself because of the losses in the material. Wheeler has proposed a method to measure the radiation efficiency of an antenna, which is known as wheeler cap method [129]. This method is employed in the measurement of radiation efficiency. In this process, the input resistance of the Antenna Under Test (AUT) is taken in the free space first and then the same is measured by placing the antenna inside a metal sphere whose radius is $\lambda/6$. This will result in two resistances, the first R_r+R_l and the second R_l alone, where R_r is the radiation resistance and R_l is the loss resistance of the antenna. From these measured values, the radiation efficiency is calculated by,

$$\frac{R_r}{R_r + R_l} \quad (5.28)$$

The efficiency expressed in (5.28) is obtained from the measured values using the equation (5.29)

$$Efficiency, \eta = \frac{R_{nocal} - R_{cal}}{R_{nocal}} \quad (5.29)$$

5. SIR Loaded Modified Dipole Antenna

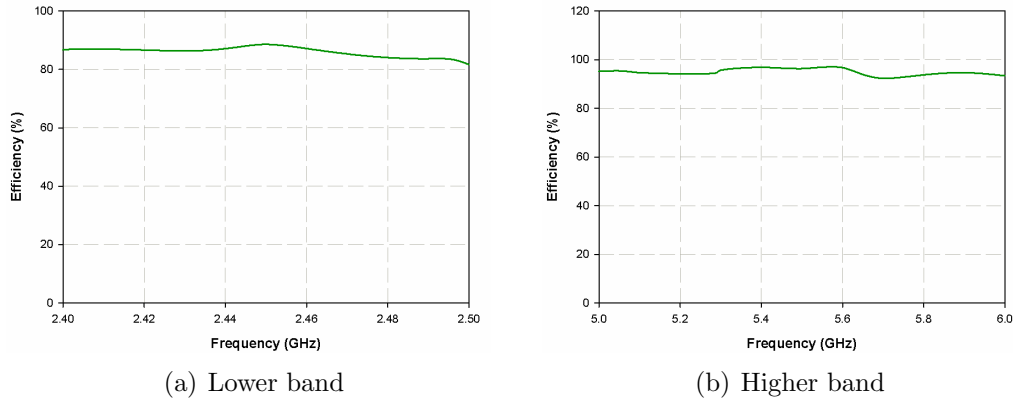


Figure 5.40: Measured radiation efficiency of the antenna

Figure 5.40(a) shows the measured radiation efficiency in the lower frequency band. The peak efficiency achieved in this band is 88.6%

The measured radiation efficiency in the higher resonance band of the antenna is shown in the Figure 5.40(b). The achieved peak efficiency in this band is 96.87%.

5.9.4 Bandwidth measurement

The proposed antenna provides sufficient bandwidth in both higher and lower frequency bands. As per IEEE 802.11 standard, the bandwidth required at 2.4 GHz band is 85 MHz. The frequency range of this band is from 2.4 GHz to 2.485 GHz. The measured 2:1 VSWR bandwidth achieved by the proposed antenna is 95 MHz from 2.405 GHz to 2.5 GHz. In the higher frequency band the antenna shows a 2:1 VSWR bandwidth of 1.38 GHz from 4.52 GHz to 5.9 GHz. This bandwidth is sufficient to cover the 5.2 GHz, 5.4 GHz and 5.8 GHz application bands.

5.10 Electrical Size

An antenna whose maximum dimension is very small compared to the wave length of operation comes under the category of small antennas. Under this category, small antennas are further divided into many different classes based on the ka value of the antenna. Here the k indicates the wave number given by,

$$k = \frac{2\pi}{\lambda} \quad (5.30)$$

and a is the radius of the smallest sphere which can enclose the maximum dimension of the antenna [61], [69]. For the proposed antenna the calculated ka value at 2.4 GHz is 0.8042. For a small antenna, there are few constraints on the quality factor (Q) of the antenna. The Q mentioned here is the 3 dB quality factor of the antenna. For a small antenna, the Q of the antenna should be greater than the Q minimum value of the antenna. The Q minimum for a small antenna is given by, [69]

$$Q_{min} = \frac{1}{ka} + \frac{1}{(ka)^3} \quad (5.31)$$

For the proposed antenna, the Q_{min} calculated using the equation (5.31) is 3.165. The measured 3 dB Q of the antenna is 439, which is greater than the Q_{min} .

With the measured ka and Q values of the antenna, the proposed antenna is categorized as physically small antenna, where the volume is restricted within $30cm^3$. The measured volume of the proposed antenna is $0.8cm^3$ [69].

5.11 Conclusions

A novel dual band antenna based on a modified dipole and parasitic SIR has been designed, developed and analysed successfully. The real estate of the antenna has been managed well without much compromise on the radiation characteristics of the antenna, with a ka value of 0.8042. The antenna operates in 2.4 GHz band and in the 5-6 GHz band which covers the 5.2 GHz, 5.4 GHz and 5.8 GHz application bands with necessary bandwidth to cover each application band. The realised far field radiation pattern of the antenna is omni directional in both the bands. A good efficiency is obtained which are 88.6% and 96.87%

5. SIR Loaded Modified Dipole Antenna

in the lower and upper band, respectively. The measured peak gains are 2.6 dBi and 3.6 dBi in lower and upper bands, respectively. Design equations for the folded SIR and the bent dipole is derived and analysed. The SIR is implemented to realize any lower frequency in the dual band antenna which could be designed using the derived equation, whereas the modified dipole is used for the design of the higher band.

Chapter 6

Conclusions ...

6.1 Summary

In this thesis three different small antennas have designed, analysed, fabricated and tested. The main objectives of the work presented are to design and develop novel antennas which are very small. Two out of these antennas are electrically small antennas (ESA) and one is a physically small antenna (PSA). The antennas designed are operating in the ISM bands. The first proposed antenna is a single band antenna, second one is a frequency reconfigurable antenna whereas the third one is a dual band antenna. Lumped element loading is employed in the first antenna to achieve miniaturisation, whereas Stepped Impedance Resonator (SIRs) are successfully excited and implemented in the second and third antenna as a radiating element to achieve miniaturisation. This study reveals the potential of using design robustness of SIR in the design and development of antennas, especially in small antennas. Two variations of the SIR are implemented in two antennas resulting in different aspects of performance. Following section discuss each chapter in detail.

6.1.1 Lumped Inductor Loaded CPW Based ESA

The chapter 3 deals with a lumped inductor loaded CPW based electrically small antenna. This antenna is derived from a CPW based planar monopole antenna by replacing the monopole with a lumped inductor loaded radiating

element. By replacing the lengthier monopole with a small metal strip connected to the feed line through a lumped wire wound inductor. Loading of this inductor compensated for the high capacitive reactance at 2.4 GHz due to the length reduction of monopole. The proposed antenna radiated similar to a dipole with figure-of-eight E-Plane pattern and producing a constant radiation in the H-Plane. With this change the size of the antenna is reduced to a great extent. At 2.4 GHz the total size of the proposed antenna is $0.09\lambda_0 \times 0.09\lambda_0$. As with any ESA, this miniaturisation was in expense of gain and efficiency of the antenna. The measured gain of the antenna is -6.5 dBi and the efficiency is 16%. The ka factor for this antenna is 0.2924. The 3 dB quality factor for the antenna is 319.5 and the 2:1 VSWR bandwidth is 40 MHz. A 23 nH chip inductor measured at 250 MHz which on interpolation to 2.4 GHz and up on small corrections giving an effective inductance of 37.5 nH is used in the antenna to achieve the resonance at 2.4 GHz. This antenna met the size, quality factor and gain criteria for an ESA. Based on the data derived from the parametric studies conducted on the antenna, a design equation has been derived and validated at different frequencies.

6.1.2 An Electrically Small Frequency Reconfigurable Antenna

The fourth chapter deals with a novel idea for reducing the size of an antenna. Stepped impedance resonators (SIR) were in use in microwave filters for a quite long time. They have immense potential in terms of design robustness. This has been widely utilized in filter design but rarely found a place in the antenna design. In this chapter a successful attempt is made to convert an SIR to a radiating element. There are three fundamental SIRs, $\lambda/4$, $\lambda/2$ and λ . As the primary motive of the thesis was miniaturization, the smallest member of the SIR family i.e., $\lambda/4$ SIR was chosen for the antenna design. The next hurdle to cross was the excitation of the SIR. Different methods of excitation were experimented and cornered on proximity coupled feeding technique which gave a promising impedance matching. An SIR is designed at 2.4 GHz and successfully implemented. Though serendipitous, during the development of this antenna, when the short in the SIR

was removed a new resonance was observed at a higher frequency. The analysis on this resonance showed the newly generated resonance is a Fabry-Perot mode. This resonance is at 5.4 GHz. This possibility of switching between two different modes in the antenna by making and breaking short circuit without any dimensional change provoked the thought for going for a reconfigurable antenna where a PIN diode could be used for the mode control. In the SIR mode the antenna resonates at 2.41 GHz with a 2:1 VSWR bandwidth of 44 MHz and gain of -1.3 dBi with an efficiency of 23%. In the Fabry-Perot mode the antenna resonates at 5.45 GHz with a 2:1 VSWR bandwidth of 140 MHz and gain of 3.459 dBi with an efficiency of 77%. The antenna has a ka value of 0.4565 and a 3dB quality factor of 1010 at 2.4 GHz. This antenna also met the size, quality factor and gain criteria for an ESA. Conclusions from the parametric studies carried out on the antenna has mathematically formulated into design equations for both SIR and Fabry-Perot modes and are validated. In comparison to the antenna proposed in chapter 3, this antenna achieved improved gain and radiation efficiency.

6.1.3 SIR Loaded Modified Dipole Antenna

As a continuation to the previous chapter on exciting an SIR for electromagnetic radiation, in this chapter a $\lambda/2$ SIR is considered and a different way of excitation is employed. Here the SIR is used in connection with a modified planar dipole antenna as a parasitic element. The SIR is employed to resonate at 2.4 GHz where as the modified dipole is designed to resonate at 5-6 GHz band functioning as a dual band antenna. As a difference from chapter 4, a novel SIR structure is employed, which is a coplanar form of microstripline based SIR. At 2.4 GHz the antenna radiates with a 2:1 VSWR bandwidth of 95 MHz covering the entire ISM band. The gain achieved at this resonance is 2.6 dBi with an efficiency of 88.6%. At 5G GHz band, the antenna resonates with a 2:1 VSWR bandwidth of 1.38 GHz covering all the ISM bands. The gain achieved is 3.6 dBi with an efficiency of 96.87%. In both the bands the antenna exhibited an omni directional radiation pattern. The ka value for this antenna at 2.4 GHz is 0.8042 making the antenna a physically small one. A comparison with the earlier two antennas shows that this antenna has a better gain, efficiency and band-

width. Design equation for the SIR and the for the modification of the dipole are developed validated.

Table 6.1 shows a comparison in performance between the antennas proposed in this thesis. It is observed that there was improvement in the antenna performance without having much compromise on the total size of the antenna in the lower frequency band. A comparison between the reconfigurable antenna and the dual band antenna shows that in dual band antenna, at lower frequency the modification of SIR made it radiate efficiently than in the case of reconfigurable antenna.

Table 6.1: Comparison of three proposed antenna performance

Antenna	ka	Frequency (GHz)		Gain		Efficiency		Bandwidth	
		Lower	Higher	Lower	Higher	Lower	Higher	Lower	Higher
Inductor loaded	0.2924	2.4		-6.5 dBi		16%		40MHz	
Reconfigurable	0.4565	2.4	5.4	-1.3 dBi	3.459 dBi	23%	77%	44MHz	140MHz
Dual band	0.8042	2.4	5.32	2.6 dBi	3.6 dBi	88.6%	96.87%	95MHz	1.38GHz

6.2 Future possibilities

From the cognition with the work conducted, the SIR reveals a wide possibility to be used in antenna design. Studies may be conducted in a direction that could improve the bandwidth, gain and efficiency of the $\lambda/4$ type SIR as this is the smallest member of the SIR family and it has all the design robustness with the other counterparts. At the same time further electronic beam steering studies could also be conducted on the $\lambda/4$ SIR based antennas. Possibilities of including metamaterial structures in the design of SIR without compromising gain, efficiency and bandwidth while using SIR as a radiating element could be pondered.

Another perspective where more studies could be conducted is in utilising the harmonics of SIR in the antenna design. The biggest advantage of the SIR is that the harmonics can be controlled and could be positioned at different frequency points by varying the impedance ratio k . By making use of this property and by properly enhancing the radiation by harmonics, SIRs could be designed for multiple bands without compromising much on the size of the antenna. The pos-

sibility of including electronic reconfigurability in the harmonics selection could also be experimented.

The inductor loaded antenna could be made in the form of array which could enhance the gain and bandwidth. The use of nearby inductance value in the array could help to merge the resonances to increase the bandwidth.



Appendix A

A Compact ACS Fed ESA

A.1 Introduction

This section goes through the design and development of an electrically small antenna which is fed through an Asymmetric Coplanar Stripline (ACS). This antenna is inspired from the fundamentals of Composite Right Left Handed (CRLH) transmission line theory. The antenna resonates at 2.4 GHz band. The antenna has an overall dimension of only $0.082\lambda_0 \times 0.1322\lambda_0$. The uniplanar design, simple feeding and compactness make it easy to be integrated in circuit boards

A.2 Evolution of the Antenna

The motivation for the development of this antenna came from a Composite Right Left Handed (CRLH) based antenna by [131]. This is a bisected antenna with an Asymmetric Coplanar Stripline (ACS) feed, which is derived from a symmetrical structure with a Coplanar Stripline (CPS) feed by [26]. The bisection is implemented to improve the bandwidth and efficiency of the antenna. The proposed antenna is derived from this antenna by replacing the unit cell with a series LC structure and employing ACS feed, there by achieving more compactness to the structure resulting in a 47.47% reduction in total area. A meanderline shorted to the ground plane is providing the required inductance to the antenna. This meanderline is capacitively coupled to the feed line. The dimensions of the meanderline and the coupling gap between the feed line and the meanderline plays important role in the working of the proposed antenna. The capacitance C at the coupling gap and the inductance L of the meanderline together acts as a series LC resonator governed by

$$f = \frac{1}{2\pi\sqrt{LC}} \quad (\text{A.1})$$

A.3 Antenna Design and Geometry

The geometry of the proposed antenna is as shown in Figure A.1. The antenna is printed on a substrate with relative permittivity 4.4, loss tangent ($\tan(\delta)$) of 0.02 and thickness 1.6 mm. The antenna consists of a meandered line, whose one end is capacitively coupled to the Asymmetric Coplanar Stripline (ACS) feed and the other end is shorted to the ground. The antenna occupies a total area of $0.082\lambda_0 \times 0.1322\lambda_0$ (16.1 mm x 10.5 mm)

The proposed antenna is fed by an asymmetric coplanar strip line. A traditional coplanar strip line has two conductors with same width. Since one line is substantially wider than the other line, the asymmetric coplanar strip line can be treated as a coplanar strip line with infinitely wide ground plane (CPSWG). The antenna geometry at the optimum design is as given in Table A.1

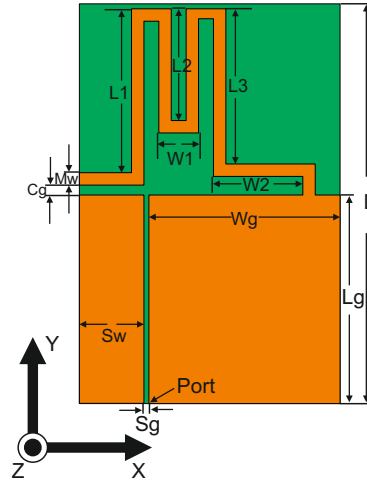


Figure A.1: Geometry of the proposed antenna. $\epsilon_r = 4.4$, $h = 1.6$ mm

Table A.1: Physical Dimensions of the Antenna

Parameter	Dimension (mm)	Parameter	Dimension (mm)
L	16.1	W	10.5
Lg	7.4	Wg	7.7
Sw	2.6	L1	7.6
L2	4.5	L3	6.25
W1	1.6	W2	3.6
Mw	0.5	Cg	0.4
Sg	0.2		

A.4 Reflection characteristics

Figure A.2 shows the simulated and measured reflection characteristics of the proposed antenna. The antenna is designed to resonate at 2.4 GHz by making appropriate changes in the meander line and in the coupling gap between the feed

line and the meander line. The measured reflection characteristics shows that the antenna is resonating 2.48 GHz. The electric field distribution of the antenna at resonance is shown in Figure A.3 with a maximum field at the gap Cg

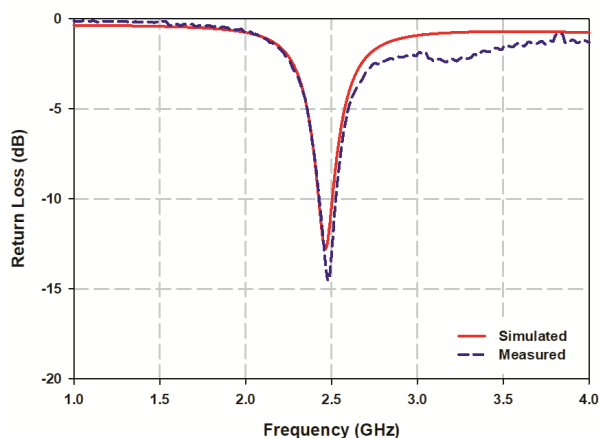


Figure A.2: Simulated and measured reflection characteristics of the antenna fabricated according to Table A.1. [$\epsilon_r = 4.4$, $h = 1.6$ mm]

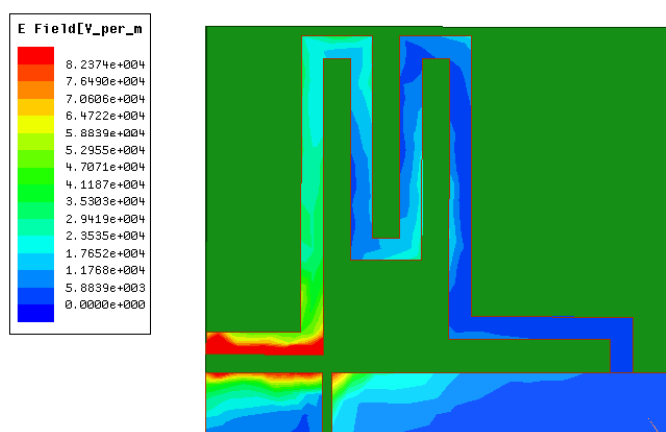


Figure A.3: Simulated electric field for the antenna at 2.48 GHz designed according to Table A.1. [$\epsilon_r = 4.4$, $h = 1.6$ mm]

A.5 Parametric Analysis

Different parametric analysis are conducted on the antenna as listed below.

- Meander line width variation
- Meander line to feed line coupling gap variation
- Meander line length L1 variation
- Substrate thickness variation

A.5.1 Meander line width variation

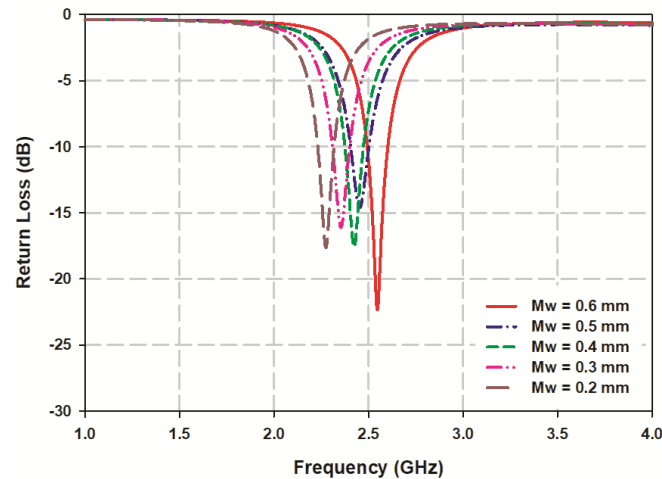


Figure A.4: Effect of variation in the width of the meander line [$L = 16.1$ mm, $L_g = 7.4$ mm, $L_1 = 7.6$ mm, $L_2 = 4.5$ mm, $L_3 = 6.25$ mm, $W = 10.5$ mm, $W_g = 7.7$ mm, $W_1 = 1.6$ mm, $W_2 = 3.6$ mm, $S_w = 2.6$ mm, $S_g = 0.2$ mm, $C_g = 0.4$ mm, $\epsilon_r = 4.4$, $h = 1.6$ mm]

To understand the impact of change in meander line width on the radiation characteristics of the antenna, the width of the meander line is varied from 0.2

mm to 0.6 mm. The width of the line is varied in such a way that the coupling gap C_g between the meander line and the feed line is kept constant. Figure A.4 shows how the resonance of the antenna is varying with respect to the changes in the width of the meander line. It is observed that the resonant frequency of the antenna is increasing with respect to the increase in the width of the meander line. When the width of the meander line is increased, the inductance is decreased. This decrease in the inductance causes an increase in the resonant frequency of the antenna. Table A.2 shows the simulated inductance of the meander line at 2.4 GHz corresponding to the different widths considered.

Table A.2: Inductance change with meander line width

Width (mm)	Inductance (nH)
0.2	48.894
0.3	40.957
0.4	36.93
0.5	32.795
0.6	29.534

A.5.2 Meander line to feed line coupling gap variation

The gap between the ACS feed line and the meander line is a crucial component in this proposed antenna. This particular gap is the key to the resonance of the antenna. To understand the effect of this gap C_g on the radiation characteristics of the antenna, a parametric analysis is conducted by varying the gap from 0 mm to 0.4 mm. Figure A.5(a) shows the return loss of the antenna for each of the gap and Figure A.5(b) shows the corresponding impedance plot. From the figure it is observed that when there is no gap between the ACS feed line and the meander line, the proposed antenna is not showing any radiation property. The dark green line in the Figure A.5 shows the corresponding return loss and impedance characteristics. Here the return loss is a straight line at 0 dB indicating zero resonance. As the gap C_g is increased from 0 to 0.1 mm, the resonance

appears, clearly indicating the importance of the gap in the antenna. As the gap is increased further from 0.1 mm to 0.4 mm, the resonant frequency starts to increase. This is because the gap introduces a capacitance and as the gap increases the value of the capacitance starts to decrease, which in turn reduces the resonant frequency.

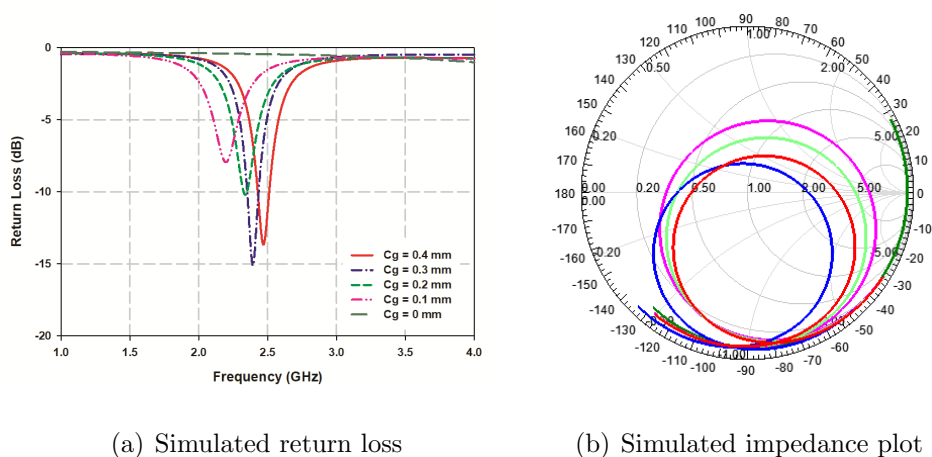


Figure A.5: Effect of variation in the gap between the meander line and the feed line [$L = 16.1$ mm, $L_g = 7.4$ mm, $L_1 = 7.6$ mm, $L_2 = 4.5$ mm, $L_3 = 6.25$ mm, $W = 10.5$ mm, $W_g = 7.7$ mm, $W_1 = 1.6$ mm, $W_2 = 3.6$ mm, $M_w = 0.5$ mm, $Sw = 2.6$ mm, $S_g = 0.2$ mm, $\epsilon_r = 4.4$, $h = 1.6$ mm]

A.5.3 Meander line length L1 variation

Figure A.6 shows the variation in resonant frequency as the length L_1 of the meander line is varied from 7.6 mm to 10.6 mm. Here also as we increase the length L_1 , the total inductance of the meander line will increase and thereby a reduction in the resonant frequency is observed.

A.5.4 Substrate thickness variation

The substrate thickness of the antenna is varied from 0.2 mm to 3.2 mm to see its implication on the resonance of the antenna. It is observed that the

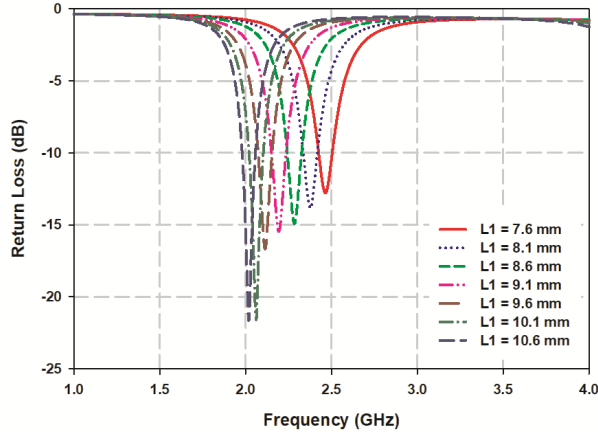


Figure A.6: Effect of variation in the length L_1 of the meander line [$L = 16.1$ mm, $L_g = 7.4$ mm, $L_2 = 4.5$ mm, $L_3 = 6.25$ mm, $W = 10.5$ mm, $W_g = 7.7$ mm, $W_1 = 1.6$ mm, $W_2 = 3.6$ mm, $M_w = 0.5$ mm, $S_w = 2.6$ mm, $S_g = 0.2$ mm, $C_g = 0.4$ mm, $\epsilon_r = 4.4$, $h = 1.6$ mm]

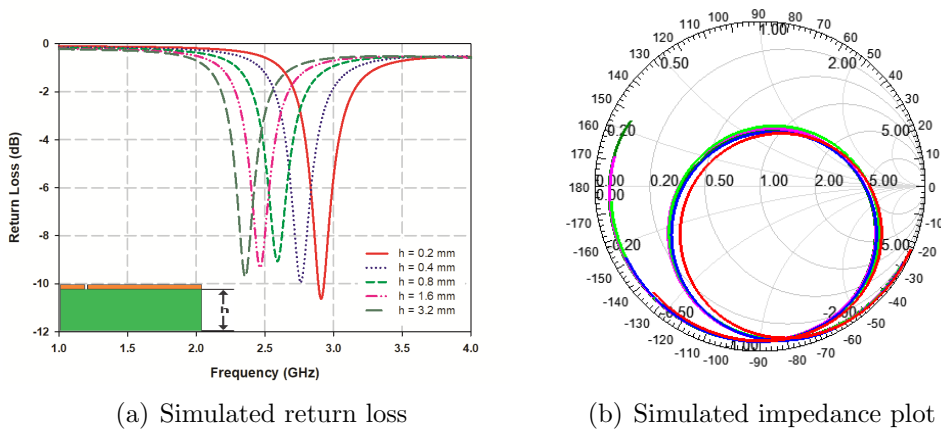


Figure A.7: Effect of variation in the substrate thickness h of the antenna [$L = 16.1$ mm, $L_g = 7.4$ mm, $L_1 = 7.6$ mm, $L_2 = 4.5$ mm, $L_3 = 6.25$ mm, $W = 10.5$ mm, $W_g = 7.7$ mm, $W_1 = 1.6$ mm, $W_2 = 3.6$ mm, $M_w = 0.5$ mm, $S_w = 2.6$ mm, $S_g = 0.2$ mm, $C_g = 0.4$ mm, $\epsilon_r = 4.4$]

resonant frequency of the antenna is decreasing as the thickness of the substrate is increased. This is shown in Figure A.7(a). The corresponding change in the impedance of the antenna is shown in Figure A.7(b). As the thickness of the

substrate is increased, the fringing of the field is getting reduced and this high density of the electric field will cause an increase in the gap capacitance which in turn reduces the resonance of the antenna. It is observed that beyond a particular limit, the variation in the resonant frequency with respect to change in substrate thickness is negligible, as most of the field are confined in the substrate at this point.

A.6 Radiation Pattern

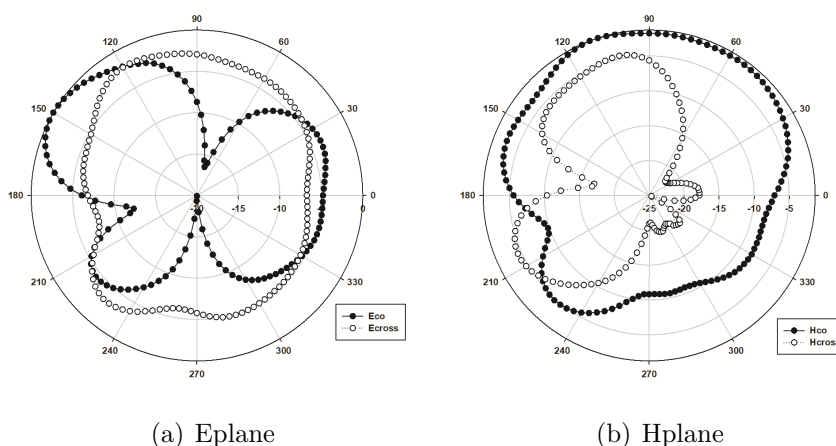


Figure A.8: Radiation pattern of the prototype antenna [$L = 16.1$ mm, $L_g = 7.4$ mm, $L_1 = 7.6$ mm, $L_2 = 4.5$ mm, $L_3 = 6.25$ mm, $W = 10.5$ mm, $W_g = 7.7$ mm, $W_1 = 1.6$ mm, $W_2 = 3.6$ mm, $M_w = 0.5$ mm, $S_w = 2.6$ mm, $S_g = 0.2$ mm, $C_g = 0.4$ mm, $\epsilon_r = 4.4$, $h = 1.6$ mm]

Figure A.8 shows the measured radiation pattern of the prototype antenna. In the E-plane the coplanar component is nearly in the shape of figure-of-eight and in the H-plane the coplanar component is radiating nearly constantly.

A.7 Gain

Figure A.9 shows the measured gain plot of the antenna in the 2.4 GHz band using gain transfer method. The antenna is showing nearly constant gain in the 2:1 VSWR bandwidth. The variation in the measured gain is less than 3 dB. The peak gain of the antenna is -0.23 dBi at 2.48 GHz.

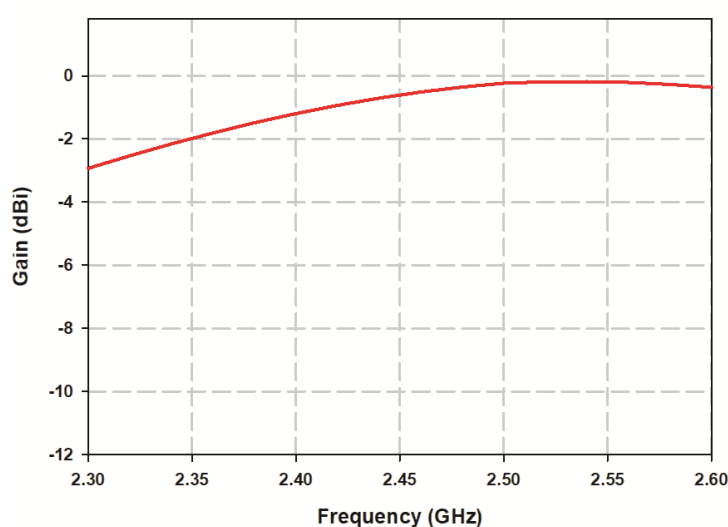


Figure A.9: Measured gain of the prototype antenna [$L = 16.1$ mm, $L_g = 7.4$ mm, $L_1 = 7.6$ mm, $L_2 = 4.5$ mm, $L_3 = 6.25$ mm, $W = 10.5$ mm, $W_g = 7.7$ mm, $W_1 = 1.6$ mm, $W_2 = 3.6$ mm, $M_w = 0.5$ mm, $S_w = 2.6$ mm, $S_g = 0.2$ mm, $C_g = 0.4$ mm, $\epsilon_r = 4.4$, $h = 1.6$ mm]

A.8 Electrical size

The free space wave number ‘ k ’ and the radius ‘ a ’ of the smallest circle circumscribing the largest dimension of the antenna together classifies an antenna on its electrical size. To classify an antenna to the electrically small category, the

primary condition that should be satisfied, taking k and a in to account is

$$ka < 0.5 \tag{A.2}$$

and the second most important criteria is on the 3dB quality factor. This quality factor measured for an electrically small antenna should be greater than the Q_{min} calculated for that particular antenna, where Q_{min} is

$$Q_{min} = \frac{1}{ka} + \frac{1}{(ka)^3} \tag{A.3}$$

For the proposed antenna, k is 0.519 rad/sec at resonant frequency and a is 9.61 mm. The corresponding ‘ ka ’ value is 0.499, which is at the boundary of the aforesaid criteria for electrically small antenna (ESA). The calculate Q_{min} of the antenna is 10.052 and the corresponding measured Q is 33.513, which is satisfying the second criteria for an ESA. The third criteria is on the maximum possible gain of the antenna given by

$$Gain_{max} = (ka)^2 + 2ka \tag{A.4}$$

Table A.3 summarises the electrical size characteristics of the proposed antenna.

Table A.3: ESA Parameters

Parameter	Required	Obtained
ka	<0.5	0.499
Q	>10.052	33.513
Gain	<0.958 dBi	-0.23 dBi

A.9 Conclusion

A compact asymmetric coplanar strip line fed electrically small antenna for wireless local area network is proposed. The antenna resonates at 2.4GHz with a bandwidth of 95MHz. The measured peak gain of the antenna is -0.23 dBi in spite of its small size. The antenna has a measured radiation efficiency of 81% at 2.48 GHz.

References

- [1] Chip Inductors-0603CS Series (1608). Data Sheet from CoilCraft. xvii, 57, 58, 61
- [2] J.B.; Holden A.J.; Robbins D.J.; Stewart W.J. Pendry. Magnetism from conductors and enhanced nonlinear phenomena. *IEEE transaction on Microwave Theory and Techniques*, 47:20752084, 1999. 28
- [3] Mathew J Lockyear Alastair P Hibbins and J Roy Sambles. The resonant electromagnetic fields of an array of metallic slits acting as a fabry-perot cavities. *Journal of Applied Physics*, 99, 2006. xxi, 97, 98, 99
- [4] Allen Taflov. *Numerical issues regarding finite-difference timedomain modelling of Microwave structures*. Tatsuo Itoh and Bijan Houshmand, IEEE Press, 1992. 46
- [5] Edward E. Altshuler. Electrically small self-resonant wire antennas optimized using a genetic algorithm. *IEEE transaction on Antennas and Propagation*, 50:297300, 2002. 27
- [6] J B Anderson. Antennas for vhf/uhf personal radio: A theoretical and experimental study of characteristics and performance. *IEEE Transactions on Vehicular Technology*, 26:349–357, 1977. 24
- [7] Hans G. Schantz Andrew J. Compston, James D. Fluhler. A fundamental limit on antenna gain for electrically small antennas. *IEEE Sarnoff Symposium*, pages 1–5, 2008. 29

REFERENCES

- [8] Hans G. Schantz Andrew J. Compston, James D. Fluhler. A fundamental limit on antenna gain for electrically small antennas. *Sarnoff Symposium*, pages 1–5, 2008. 29
- [9] Hiroyuki Arai. Antenna clearance, an index factor for electrical size of small antennas. *Proceedings of iWAT*, pages 91–94, 2008. 29
- [10] Richard W. Ziolkowski Aycan Erentok. Metamaterial-inspired efficient electrically small antennas. *IEEE TRANSACTIONS ON ANTENNAS AND PROPAGATION*, 56:691–707, 2008. 30
- [11] A Bahr. On the use of active coupling networks with electrically small receiving antennas. *IEEE transaction on antennas and propagation*, 25: 841–845, 1977. 23
- [12] C. A. Balanis. *Modern Antenna Handbook*. New York: Wiley-IEEE Press, 2008. 13
- [13] Constantine A. Balanis. *Antenna Theory, Analysis and Design*. Wiley Interscience, 2005. 75, 169
- [14] Richard J. Ingleby Benito sanz Izquierdo, John C. Batchelor and Mohammed I. Sobhy. Single and double layer planar multi band pifas. *IEEE Transactions on Antennas and Propagation*, 54:416–422, 2006. 12
- [15] Steven R. Best. A low q electrically small magnetic (te mode) dipole. *IEEE ANTENNAS AND WIRELESS PROPAGATION LETTERS*, 8:572–575, 2009. 30
- [16] Altan M. Ferendeci Bo Zhao, Ruirong Shi. Zeroth-order resonator antennas using composite right/left-handed microstrip transmission lines. *IEEE National Aerospace and Electronics Conference*, pages 154–158, 2008. 30
- [17] R Bohley P. DeVore. The electrically small magnetically loaded multiturn loop antenna. *IEEE transaction on antennas and propagation*, 25:496505, 1977. 22

REFERENCES

- [18] K. BONDYOPADHYAY. Sir j. c. bose's diode detector received marconi's first transatlantic wireless signal of december 1901 (the italian navy coherer scandal revisited). *PROCEEDINGS OF THE IEEE*, 86:259–285, 1998. 3
- [19] S. K. Buchmeyer. An electrically small cassegrain antenna with optically shaped reflectors. *IEEE transaction on antennas and propagation*, 25:436–451, 1977. 23
- [20] C.M. Butler. Formulation of integral equations for an electrically small aperture in a conducting screen. *Antennas and Propagation Society International Symposium*, 12:101–104, 1974. 23
- [21] E. V. Byron. A new flush mounted antenna element for phased array applications. *A new flush mounted antenna element for phased array applications*, page 187192, 1970. 8
- [22] C. Caloz and T. Itoh. *Electromagnetic Metamaterials: Transmission Line Theory and Microwave Applications*. New York: Wiley-IEEE Press, 2005. 12
- [23] C. Caloz and A. Rennings. Crlh travelling wave and resonant metamaterial antennas. *IEEE Antennas Propag. Mag*, 50:25–39, 2008. 13
- [24] Rajeev Bansal John P. Casey. Analysis and optimization of an electrically small receiving antenna. *IEEE transaction on antennas and propagation*, 33:197204, 1991. 25
- [25] Erli Chen and Stephen Y. Chou. Characteristics of coplanar transmission lines on multilayer substrate: Modeling and experiments. *IEEE Transactions on Microwave Theory and Techniques*, 45:939–944, 1997. 73
- [26] Hsueh-Jyh Li Shih-Yuan Chen Chien-Pai Lai, Shih-Chia Chiu. Zeroth-order resonator antennas using inductor-loaded and capacitor-loaded cpws. *IEEE TRANSACTIONS ON ANTENNAS AND PROPAGATION*, 59:3448–3453, 2011. 180
- [27] R. Liu T. J. Cui and D. R. Smith. *Metamaterials: Theory, Design and Applications*. New York: Springer, 2010. 12

REFERENCES

- [28] D. C. Vier S. C. Nemat-Nasser D. R. Smith, W. J. Padilla and S. Schultz. Composite medium with simultaneously negative permeability and permittivity. *Phys. Rev. Lett*, 84:4184–4187, 2000. 12
- [29] Hala A. Elsadek Dalia Mohammed Nashaat and Hani Ghali. Single feed compact quad band pifa antenna for wireless communication applications. *IEEE Transactions on Antennas and Propagat*, 53:2631–2635, 2005. 12
- [30] M A Astrahan P. S. DeBicki. Input impedance of electrically small insulated antennas for microwave hyperthermia. *IEEE transaction on Electromagnetic Compatibility*, 41:357360, 1993. 25
- [31] G.A. Deschamps. Microstrip microwave antennas. *3rd USAF symposium on Antennas*, 1953. 4, 8
- [32] D.R.; Banks D.J.; Kinman D.M.; Martin A.M.; Dinger R.J.; Forse R.; Cook G. Bowling. A three-element, superdirective array of electrically small, hightemperature superconducting half-loops at 500-mhz. *Antennas and Propagation Society International Symposium*, 3:18461849, 1993. 25
- [33] J.L. Jimnez E. Ugarte-Muoz J. Herraiz-Martnez L.E. Garcia-Muoz D.Segovia-Vargas, V. Gonzalez-Posadas. Negative impedance converters (nics) in the design of small and multifrequency antennas. *EuCAP 2011*, pages 2724–2728, 2011. 30
- [34] G. V. Elftheriades and K. G. Balmain. *Negative Refraction Materials: Fundamental Principles and Applications*. New York: Wiley-IEEE Press, 2005. 12
- [35] N. Engheta and R. W. Ziolkowski. *Electromagnetic Metamaterials: Physics and Engineering Explorations*. New York: Wiley-IEEE Press, 2005. 12
- [36] Aycan Erentok and Richard W. Ziolkowski. Lumped element capacitor based two-dimensional efficient metamaterial-inspired electrically-small antenna. *International Workshop on Antenna Technology: Small and Smart Antennas Metamaterials and Applications*, pages 19–22, 2007. 28

REFERENCES

- [37] Richard W. Ziolkowski Aycan Erentok. Efficient electrically small antenna design using an electric dipole in a multi-layered eng metamaterial shell. *IEEE International Workshop on Antenna Technology Small Antennas and Novel Metamaterials*, pages 400–403, 2006. 28
- [38] P. Baccarelli F. Frezza S. Paulotto and D. R. Jakson. Full wave model dispersion analysis and broadside optimization for a class of microstrip crlh leaky-wave antennas. *IEEE Trans. Microw. Theory Tech*, 56:28262837, 2008. 13
- [39] Chih-Yi Fang. A planar chip antenna for 2.4/5.2ghz ism band applications. *IEEE Antennas and Propagation Society International Symposium*, 1B:455–458, 2005. 32
- [40] R.C. Fenwick. A new class of electrically small antennas. *IEEE transaction on antennas and propagation*, 13:379383, 1965. 22
- [41] Kyohei Fujimoto and Hisashi Morishita. *Modern Small Antennas*. New York: Cambridge University Press, 2013. 14, 15, 16, 17
- [42] Shabnam Ghadarghadr and Hossein Mosallaei. Characterization of metamaterial-based electrically small antennas. *Antennas and Propagation Society International Symposium*, pages 5415 – 5418, 2007. 28
- [43] D. Nashaat; H. A. Elsadek; H. Ghali. Dual-band reduced size pifa antenna with u-slot for bluetooth and wlan applications. *IEEE Conference Publications, APS*, 2:962–965, 2003. 32
- [44] D. Nashaat; H. A. Elsadek; H. Ghali. Small chip antenna for 2.4/5.8-ghz dual ism-band applications. *IEEE Antennas and Wireless Propagation Letters*, 2:313–315, 2003. 32
- [45] Stefano Selleri Giuseppe Pelosi and Barbara Valotti. Antennae). *IEEE Antennas And Propagation Magazine*, 42:61–63, 2000. 3
- [46] Craig A. Grimes. Efficient radiation from an electrically small antenna: Control of higher order modes. *Aerospace Application Conference*, 4:147160, 1996. 26

REFERENCES

- [47] R C Hansen. Efficiency and matching tradeoffs for inductively loaded short antennas. *IEEE Transactions on Communications*, 4:430–435, 1975. 64
- [48] J.S.McLean H.D.Foltz. Limits on the radiation q of electrically small antennas restricted to oblong bounding regions. *Antennas and Propagation Society International Symposium*, 4:27022705, 1999. 27
- [49] G. R. Kadambi; S. Yarasi; J. L. Sullivan; T. Hebron. Miniaturized dualism band internal antennas. *IEEE Conference Publications, APS*, 2:26–29, 2003. 32
- [50] H. Hertz. On the finite velocity of propagation of electromagnetic action. *Sitzungsber. D. Berl. Akad. D. Wiss*, 34, 1888. 3
- [51] D. A Hill. M Kanda. A three-loop method for determining the radiation characteristics of an electrically small source. *IEEE transaction on Electromagnetic Compatibility*, 34:1–3, 1992. 25
- [52] Alex Pidwerbetsky Howard R. Stuart. Electrically small antenna elements using negative permittivity resonators. *IEEE TRANSACTIONS ON ANTENNAS AND PROPAGATION*, 54:1644–1653, 2006. 28
- [53] J.Q. Howell. Microstrip antennas. *Dig. International Symposium on Antennas Propagation Society*, page 177180, 1972. 8
- [54] Jennifer T. Bernhard Jacob J. Adams. Tuning method for a new electrically small antenna with low q . *IEEE ANTENNAS AND WIRELESS PROPAGATION LETTERS*, 8:303–306, 2009. 30
- [55] J. R. James. Electrically short monopole antennas with dielectric or ferrite coatings. *Proc IEEE*, 25:793803, 1978. 23
- [56] J Y Jan. Low-profile dual-frequency circular microstrip antenna for dualism bands. *ELECTRONICS LETTERS*, 37:999–1000, 2001. 31
- [57] Karl G. Jansky. Directional studies of atmospheric waves at high frequencies. *Proceedings of the I.R.E*, 20:1920–1932, 1932. 3

REFERENCES

- [58] Karl G. Jansky. Electrical disturbances of extraterrestrial origin. *PROC. I.R.E.*, 21:1387–1398, 1933. 3
- [59] Karl G. Jansky. A note on the source of interstellar interference. *PROC. I.R.E.*, 23:1158–1163, 1935. 3
- [60] Karl G. Jansky. Minimum noise levels obtained on short-wave radio receiving stations. *PROC. I.R.E.*, 25:1517–1530, 1937. 3
- [61] Kyohei Fujimoto John L. Volakis, Chi-Chih Chen. *Small Antennas, Miniaturization Technique & Applications*. Mc Graw Hill, 2010. 79, 171
- [62] Silvio E Barbib Joseph Costantine and Christo G Christodoulou. Reconfigurable antennas: Design and applications. *Poceedings of the IEEE*, 103: 424–437, 2015. 103, 104
- [63] G. P. Karakoussis; A. I. Kostaridis; C. G. Biniaris; D. I. Kaklamani. A dual-band inverted-f antenna printed on a pc card for the ism and unni bands. *IEEE Conference Publications*, 1:88–92, 2003. 32
- [64] Shantanu K. Padhi Nemaï C. Karmakar. Study of electrically small printed chakra (wheel) antenna. *IET*, 37:269271, 2001. 27
- [65] Cook G. G. Kingsley S. P. Woods R C. Khamas S. Significance of matching networks in enhanced performance of small antennas when supercooled. *Electronics Letters*, 26:654655, 1990. 24
- [66] C. D. Sarris T. Kokkinos and G. V. Elftheriades. Periodic fdtd analysis of leakywave structures and applications to the analysis of negative refractive index leaky-wave antennas. *IEEE Trans. Microw. Theory Tech*, 54: 16191630, 2006. 13
- [67] JOHN D. Kraus. Antennas since hertz and marconi. *IEEE TRANSACTIONS ON ANTENNAS AND PROPAGATION*, 33:131–137, 1985. 3
- [68] K.S.Yee. Numerical solution of initial boundary value problems involving maxwells equations in isotropic media. *IEEE Trans. Antennas Propagat*, 14:302–307, 1996. 46

REFERENCES

- [69] Hisashi Morishita Kyohei Fujimoto. *Modern Small Antennas*. Cambridge University Press, 2013. 79, 80, 167, 171
- [70] P. M. Mendes L. A. Rocha. Electrically small mems antenna for wireless biomedical microsystems. *Proceedings of the 38th European Microwave Conference*, pages 262–265, 2008. 29
- [71] M. Tzortzakakis; R. J. Langley. A practical high gain dual-band antenna for ism systems. *5th International Conference on Antenna Theory and Techniques*, pages 319–322, 2005. 32
- [72] I-Fong Chen; Chia-Mei Peng; Sheng-Chieh Liang. Single layer printed monopole antenna for dual ism-band operation. *IEEE Transactions on Antennas and Propagation*, 53:1270–1273, 2005. 32
- [73] Kurt L.Shlager and John B.Schneider. A selective survey of the finitedifference time-domain literature. *IEEE Antennas Propagat. Mag*, 37:39–57, 1995. 46
- [74] Fournier M. Leo Hong. Signal to noise performance of cryogenic electrically small receiving antenna. *IEEE transaction on antennas and propagation*, 20:509–511, 1972. 23
- [75] S. Yamashita M. Makimoto. *Microwave Resonators and Filters for Wireless Communication, Theory, Design and Application*. Springer, 2000. 87, 92, 143, 145, 146
- [76] D. Ma and W. X. Zhang. A dual-band dual-polarized antenna for body area network. *Proceedings of the Fourth European Conference on Antennas and Propagation*, pages 1–5, 2010. 32
- [77] Morooka T. Maeda T. Radiation efficiency measurement method for electrically small antennas using radio wave scatterers. *Antennas and Propagation Society International Symposium*, 1:324–327, 1988. 24
- [78] Makoto Higaki Makoto Sano, Keiju Yamada. Design of an electrically small antenna using a broadside-coupled split ring resonator. *IEEE International*

REFERENCES

- Symposium on Antennas and Propagation and USN-URSI National Radio Science Meeting*, pages 537–538, 2017. 60
- [79] Majid Manteghi. Electrically small naturally circularly polarised antenna. *IET Microwaves, Antennas and Propagation*, 12:641–646, 2018. 60
- [80] Markku Kivikoski Mari Komulainen, Pekka Salonen. Dual frequency microstrip patch antenna for wlan/bluetooth and hiperlan applications. *IEEE Radio and Wireless Conference*, pages 207–209, 2001. 31
- [81] F. Martin R. Marques and M. Sorolla. *Materials with Negative Parameters: Theory, Design and Microwave Applications*. New York: Wiley-IEEE Press, 2008. 12
- [82] Shane Merritt John S. Minor Christian A. Zorman Maximilian C. Scardelletti1, George E. Ponchak. Electrically small folded slot antenna utilizing capacitive loaded slot lines. *IEEE Radio and Wireless Symposium*, pages 731–734, 2008. 29
- [83] J. C. Maxwell. A dynamical theory of the electromagnetic field. *Phil. Trans*, 166:459–512, 1865. 2
- [84] E McCann. Electrically small d. f. antenna. *I R E Internation Convention Record*, pages 64–73, 1958. 22
- [85] A McCorkle J. Scarzello J. Syeles A. Krall. The omni microstrip antenna: A new small antenna. *IEEE transaction on antennas and propagation*, 27: 850–853, 1979. 24
- [86] J. S. McLean. The application of the method of moments to the analysis of electrically-small compound antennas. *IEEE International Symposium on Electromagnetic Compatibility*, page 199124, 1995. 26
- [87] J. S. McLean. A re-examination of the fundamental limits on the radiation Q of electrically small antennas. *IEEE transaction on Antennas and Propagation*, 44:672676, 1996. 26

REFERENCES

- [88] Jessie Yao Chin Ruopeng Liu Tie Jun Cui Meng Li, Xian Qi Lin. A novel miniaturized printed planar antenna using split-ring resonator. *IEEE ANTENNAS AND WIRELESS PROPAGATION LETTERS*, 7:629–631, 2008. 29
- [89] Michal Vyhnalik Milan Svanda Milan Polivka, Alois Holub. Impedance properties and radiation efficiency of electrically small double and triple split-ring antennas for uhf rfid applications. *IEEE ANTENNAS AND WIRELESS PROPAGATION LETTERS*, 12:221–224, 2013. 31
- [90] L.P.; Lancaster. M.J.; Maclean T.S.M.; Alford N.McN. Ivrisimtzis. On the design and performance of electrically small printed thick film $\text{YBa}_2\text{Cu}_3\text{O}_{7-x}$ antennas. *IEEE transaction on Applied Superconductivity*, 4:33–44, 1994. 25
- [91] Majid Manteghi Mohsen Salehi. Transient characteristics of small antennas. *IEEE TRANSACTIONS ON ANTENNAS AND PROPAGATION*, 62:2418–2429, 2014. 31
- [92] Amuda Yusuf Abdul Rahman Tharek Abdul Rahman Muhammad Zairil Muhammad Nor Evizal Mursyidul Idzam Sabran, S. K. A. Rahim. A dual-band diamond-shaped antenna for rfid application. *IEEE ANTENNAS AND WIRELESS PROPAGATION LETTERS*, 10:979–982, 2011. 33
- [93] Pi-Wei Chen Nalbandian V. Choon Sae Lee. Electrically small microstrip antennas. *Antennas and Propagation Society Internation Symposium*, 2:778781, 2000. 27
- [94] Daniel J. Miley Jerry D. Neal. Broad banding of electrically small hf antenna for frequency agile applications by use of pin diode switched matching networks. *Military communication conference*, 2:544–548, 1983. 24
- [95] Zainal Arifin Ahmad Mohd Zaid Abdullah Ubaid Ullah Mohd Fadzil Ain Nor Muzlifah Mahyuddin, Mohamadariff Othman and Arjuna Marzuki. Antenna in ltcc technologies: A review and the current state of the art. *IEEE Antennas Propag. Mag*, 57:241260, 2015. 14

REFERENCES

- [96] Arthur D. Yaghjian Oleksiy S. Kim, Olav Breinbjerg. Electrically small magnetic dipole antennas with quality factors approaching the chu lower bound. *IEEE TRANSACTIONS ON ANTENNAS AND PROPAGATION*, 58:1898–1906, 2010. 30
- [97] D. Otto. Singular integral equation solution for electrically small short cylindrical antenna. *IEEE transaction on antennas and propagation*, 19: 532533, 1971. 23
- [98] P. L. Overfelt. Electric lines of force of an electrically small dipole-loop antenna array. *IEEE transaction on Antennas and Propagation*, 46:451456, 1998. 27
- [99] J. I. Moon; D. U. Sim; S. O. Park. Compact pifa for 2.4/5 ghz dual ism-band applications. *Electronics Letters*, 40:844–846, 2004. 32
- [100] Jerzy Guterman; Yahya Rahmat-Samii; Antonio A. Moreira; Custodio Peixeiro. Quasi-omnidirectional back-to-back e-shaped patch antenna for dual-band 2.4/5.2ghz laptop integrated wireless interface. *2006 First European Conference on Antennas and Propagation*, pages 1–5, 2006. 32
- [101] D. H. Werner J. S. Petko. Theoretical formulation for an electrically small microstrip patch antenna loaded with negative index materials. *Antennas and Propagation Society Internation Symposium*, 3B:343346, 2005. 28
- [102] J. T. Reese R. Bolljahn. Electrically small antennas and the low-frequency aircraft antenna problem. *I R E Transactions - Antennas And Propagation*, 1:46–54, 1953. 22
- [103] R.E.Munson. Single slot cavity antennas. *US Patent no-3713162*, 1973. 8
- [104] D.C. Rispin L. Chang. A method for computing the input conductance of an electrically small antenna. *IEEE transaction on antennas and propagation*, 28:404–406, 1980. 24
- [105] Logan J. C Rockway J. W. Simspson T.L. Equivalent circuits for electrically small antennas using ls-decomposition with the method of moments. *IEEE transaction on antennas and propagation*, 37:16321635, 1989. 24

REFERENCES

- [106] R.; Hao Ling Hosung Choo; Rogers. Design of electrically small wire antennas using genetic algorithm taking into consideration of bandwidth and efficiency. *Antennas and Propagation Society International Symposium*, 1: 330–333, 2002. 27
- [107] R.; Hao Ling Hosung Choo; Rogers. Design of planar, electrically small antennas with inductively coupled feed using a genetic algorithm. *Antennas and Propagation Society International Symposium*, 1:300–303, 2003. 27
- [108] R.; Hao Ling Hosung Choo; Rogers. Design of electrically small wire antennas using a pareto genetic algorithm. *IEEE transaction on Antennas and Propagation*, 53:10381046, 2005. 27
- [109] W. L. Weeks V. H. Rumsey. Electrically small ferrite loaded loop antennas. *I R E Transactions - Antennas And Propagation*, 4:165–170, 1956. 22
- [110] V P Sarin. Tailoring the spectral response of a dogbone soublet metamaterial. *Microwave and optical technology letters*, 58, 2016. 99, 117
- [111] Pei Cheng Ooi; Krishnasamy T. Selvan. A dual-band cpw-fed printed square loop antenna for wireless applications. *International Conference on Electromagnetics in Advanced Applications (ICEAA)*, pages 79–82, 2010. 32
- [112] Hossein Mosallaei Shabnam Ghadarghadr, Akram Ahmadi. Negative permeability-based electrically small antennas. *IEEE ANTENNAS AND WIRELESS PROPAGATION LETTERS*, 7:13–17, 2008. 28
- [113] Rainee N. Simons. *Coplanar waveguide circuits, components and systems*. A JOHN WILEY and SONS, 2001. 73, 148
- [114] G.G.; Khamas. S.K. Cook. Control of radar cross sections of electrically small high temperature superconducting antenna elements using a magnetic field. *IEEE transaction on Antennas and Propagation*, 42:888–890, 1994. 26
- [115] Glenn S. Smith. Radiation efficiency of electrically small multiturn loop antennas used in upper atmosphere propagation experiment. *Antennas and Propagation Society International Symposium*, 9:113–141, 1971. 22

REFERENCES

- [116] Glenn S. Smith. Radiation efficiency of electrically small multiturn loop antennas used in upper atmosphere propagation experiment. *IEEE transaction on antennas and propagation*, 20:656657, 1972. 22
- [117] Glenn S. Smith. On the electrically small bare loop antenna in a dissipative medium. *IEEE transaction on antennas and propagation*, 24:533–537, 1976. 23
- [118] Asim Egemen Yilmaz Sultan Can, Kamil Yavuz Kapusuz. An efficient metamaterial-inspired, electrically small antenna for ism band applications. *European Conference on Antennas and Propagation (EUCAP)*, pages 1122–1125, 2017. 60
- [119] Allen Taflove and Morris E. Brodwin. Numerical solution of steady state electromagnetic scattering problems using the time-dependent maxwells equations. *IEEE Trans. Microwave Theory Tech*, 23:623–630, 1975. 46
- [120] D Thiele G. A. Shreve. An electrically small antenna, the multiturn loop. *Antennas and Propagation Society International Symposium*, 8:113–141, 1970. 22
- [121] Rajeev Bansal DavidA. Tonn. Practical considerations for increasing radiated power from an electrically small antenna by application of a double negative metamaterial. *Antennas and Propagation Society International Symposium*, 2A:602–605, 2005. 28
- [122] E. Turner. A regenerative broadband electrically small folded dipole antenna. *Military communication conference*, 10:348351, 1972. 23
- [123] G Donzelli A Vallecchi. Metamaterial made of paired planar conductors: Particle resonances, phenomena and properties. *Metamaterials*, 3:10–27, 2009. 99, 117
- [124] V. G. VESELAGO. The electrodynamic of substances with simultaneously negative values of eps and mu. *SOVIET PHYSICS USPEKHI*, 10:509–514, 1968. 12

REFERENCES

- [125] V. G. Veselago. The electrodynamics of substances with sumultaneously negative values of epsilon and mu. *Soviet Physics USPEKHI*, 10:509514, 1968. 28
- [126] Thomas J. Minardo Thomas J. Warnagiris. Performance of a meandered line as an electrically small transmitting antenna. *IEEE transaction on Antennas and Propagation*, 46:17971801, 1998. 26
- [127] R. E. Webster. A single control tuning circuit for electrically small antennas. *I R E Transactions - Antennas And Propagation*, 3:1215, 1955. 22
- [128] Harold A. Wheeler. The radiansphere around a small antenna. *Proceedings of IRE*, 53:13251331, 1959. 16
- [129] Harold A. Wheeler. The radiansphere around a small antenna. *PROCEEDINGS OF T'HE IRE*, 47:1325–1331, 1959. 76, 125, 169
- [130] Shyh-Tirng Fang; Shih-Huang Yeh; Kin-Lu Wong. Planar inverted-f antennas for gsm/dcs mobile phones and dual ism-band applications. *IEEE Antennas and Propagation Society International Symposium*, 4:524 – 527, 2002. 31
- [131] Kehn M N M Yang S Y. A bisected miniaturized zor antenna with increased bandwidth and efficiency. *IEEE Antenna Wireless Propagation Letters*, 12: 159–162, 2013. 180
- [132] Kuei-Chien Chen Yih-Chien Chen, Shi-Li Yao. Dual band hybrid cpw fed planar monopole/dielectric resonator antenna. *Proceedings of the 2009 IEEE 9th Malaysia International Conference on Communications*, pages 37–40, 2009. 32
- [133] Kin-Lu Wong Yun-Wen Chi. Compact multiband folded loop chip antenna for small-size mobile phone. *IEEE TRANSACTIONS ON ANTENNAS AND PROPAGATION*, 56:3797–3803, 2008. 29
- [134] Kin-Lu Wong Yun-Wen Chi. Optimal design of a broadband matching network for an electrically small antenna. *International Symposium on Antennas, Propagation and EM Theory*, pages 847–850, 2008. 29

REFERENCES

- [135] M. Ney Z. Chen and W.J.R. Hofer. A new finite-difference time-domain formulation and its equivalence with the tlm symmetrical condensed node. *IEEE Trans. Micro. Theo. Tech*, 39:21602169, 1992. 47
- [136] W. M. Dorsey; A. I. Zaghoul. Dual-polarized dual-band antenna element for ism bands. *IEEE Conference Publications,APS*, pages 1–4, 2009. 32
- [137] Allison D. Kipple Richard W. Ziolkowski. Application of double negative materials to increase the power radiated by electrically small antennas. *IEEE transaction on Antennas and Propagation*, 51:26262640, 2003. 28
- [138] Richard W. Ziolkowski. Applications of metamaterials to realize efficient electrically small antennas. *IEEE International Workshop on Antenna Technology: Small Antennas and Novel Metamaterials*, 51:7–10, 2005. 28

REFERENCES

Resume of the Author



U Deepak

Senior Research Fellow
Department of Electronics
Cochin University of Science and Technology
Kerala, India
Mobile: +91 9747594592
E-mail : deepak.palath@gmail.com

Summary

- **7 years** of research experience in Microwave communication, Antennas, RFID, Electromagnetics and Dielectric measurements
- **Publications-36; International journals-16; Conferences-20**
- Proficiency in **Design and Development of small antennas**
- Proficiency in **Microwave material characterization**
- Proficiency in **performing Finite Difference Time Domain analysis**

Honours, Awards & Achievements

- Qualified **National Eligibility Test (NET)** for lectureship by University Grants Commission (UGC) Government of India
- Qualified **Graduate Aptitude Test for Engineers (GATE)**
- **University Second Rank Holder** in M Sc. Applied Electronics from National Institute of Technology, Tiruchirappalli, Tamilnadu
- Qualified **DAT 2010** of Cochin University of Science and Technology
- Received **Best Paper Award** at Recent Advancements in Electronic Communication and Allied Areas Conference, Kerala, India.

Areas of Interest

Electrically small antennas, Zeroth Order Antennas, RFID, Ultra WideBand (UWB) antennas, Multiple-Input Multiple Output (MIMO) antennas, FDTD, Filters, Reconfigurable antennas, RF Circuits, Implantable and Wearable antennas, Biological effects of Microwaves, Microwave medical diagnostic devices, Microwave Sensors, Microwave material characterization etc.

Technical Skills

- Experienced in using various Vector Network Analyzers like HP 8510C, Agilent PNA E8362B & R&S ZVB20. Measured the S parameters and far field characteristics like gain, radiation efficiency and radiation pattern of antennas using these Network Analyzers. Have a good hands on experience with Anritsu Spectrum Analyzer and radiation characterization inside Anechoic chamber.
- Experienced in microwave material characterisation measurements
- Experienced in the measurement of microwave absorption studies and cavity perturbation method
- Experienced in Antenna and RF/Microwave circuit design tools like Ansys HFSS, CST MWS, Agilent ADS, EMPro etc. and in integrating ADS with EMPro. Attended different workshops on ADS, EMPro, HFSS and CST
- Gained six years of experience in using FEM based high frequency simulation software HFSS from Ansys for the analysis and design of many single band, multi band and wide band antennas. The optimization of antennas have been carried out using the parametric analysis of HFSS. HFSS has been extensively used for the scattering and far field analysis of antennas. Scattering analysis is conducted in HFSS while designing the stepped impedance resonator and RFIDs, and Eigenmode analysis is extensively used for the characterisation of the unit cells of periodic structures while finding the dispersion diagram. It is also used for the design and analysis of a dielectric based biomedical sensor. Well experienced in using different types of excitations in HFSS.
- Experienced in FDTD analysis
- Involved in the designing of various ultra compact wide band uniplanar antennas for multiband applications highly suitable for compact mobile phones
- Involved in the designing of biomedical sensor for the measurement of blood sugar based on dielectric resonator.
- Hands-on experience in antenna prototyping using photolithography and CNC tool.
- Experienced in programming with languages like, C, C++, Python, Matlab etc

Scholarly work and services

- Active member in IEEE Antenna Propagation Society.
- Member, Organizing Committee, Antennas and Propagation Symposium (APSYM), 2010
- Member, Organizing Committee, International Symposium on Ocean Electronics (SYMPOL) 2011

- Member, Organizing Committee, Antennas and Propagation Symposium (APSYM), 2012
- Member, Organizing Committee, International Symposium on Ocean Electronics (SYMPOL) 2013
- Member, Organizing Committee, Antennas and Propagation Symposium (APSYM), 2014
- Member, Organizing Committee, International Symposium on Ocean Electronics (SYMPOL) 2015
- Actively engaged in organizing various events and workshops
- Attended National and International Conferences and presented research papers

Work experience including research projects

- 2002-2003: **Home Automation through PSTN:** Successfully developed a 8085 micro processor based home automation system with password authentication
- 2002-2003: **Heart beat monitoring through PSTN:** Successfully developed a 8051 micro controller based system for the automated monitoring of patients heart beat
- 2004-2005: **Plug and Play Master Slave Control System:** Developed a plug and play master slave control system for control system automation
- 2005-2008: **Worked as a programmer analyst with Cognizant Technology Solutions:** This gave a good exposure in the data warehousing, dealing with ETL tools like Informatica and Abinitio and reporting tool like SAS. During this period, I got introduced into python, which was used for automating the data flow process. In the RDBMS side oracle was used. This two plus years were so helpful in improving the leadership qualities, since I got chance to lead few modules of the project
- 2008-2010: **Worked as Teacher:** From 2008 to 2010 I work as a teacher for training B.Tech students who is preparing for Graduate Aptitude Test for Engineers (GATE). This is the time that I found teaching is the best way to learn things with better understanding. Here I was able to figure out the limits of my knowledge, which eventually ended up in selecting PhD.

2010-Current: **Pursuing PhD**, at Centre for Research in Electromagnetics and Antennas (CREMA), Cochin University of Science and Technology, India - working on the design, development and analysis of small antennas. Small antennas have found good space in the rapidly growing technology of wireless communication, because of the demand to cope with the compactness achieved in the semiconductor industry. The compactness of antenna is crucial in achieving the overall compactness of wireless communication systems. Such antennas should have small size, at the same time, keeping the radiation performance unhindered. The Ph.D. work is nearing completion. Meanwhile I am also involved in the design and development of MIMO antenna systems and Chip less RFID tags, which are booming technologies of the current era.

Education

- 2010–ongoing **Pursuing PhD**, *From Department of Electronics, Cochin University of Science and Technology, Kerala, India, .*
Specialized in Compact Antennas
- 2003–2005 **Master of Science(M.Sc)**, *From National Institute of Technology, Tiruchirappalli, Tamil Nadu, India, .*
Specialized in Applied Electronics
- 2000–2003 **Bachelor of Science (B.Sc)**, *From Calicut University, Kerala, India, .*
Specialized in Electronics
- 1998–2000 **Higher Secondary: THSSLC**, *Kerala Board of Higher Secondary Education, Technical Higher Secondary School, Vazhakkad, Malappuram, Kerala, India, .*
- 1997-1998 **Tenth: THSLC**, *Kerala Board of Secondary Education, Technical Higher Secondary School, Vazhakkad, Malappuram, Kerala, India, .*

Personal Vitae

Date Of Birth 05.05.1983
Gender Male
Blood Group O positive
Marital Status Married
Nationality Indian
Address Vadakkan parambath
Palath (P.O.)
Kakkodi (Via)
Kozhikode-673611, Kerala
India.
Mob:(91) (9747594592)

References

Address **Prof. (Dr.) P. Mohanan, Senior Member, IEEE**

Professor

Department of Electronics

Cochin University of Science and Technology

Kochi-22, India.

Email: drmohan@gmail.com

Ph. 91-9447325765, Fax : 91-484-2575800

Address **Prof. (Dr). C.K Aanandan, Senior Member, IEEE**

Professor

Department of Electronics

Cochin University of Science and Technology

Kochi-22, India.

Email: aanandan@gmail.com

Ph. 91-9447667267, Fax : 91-484-2575800

Address **Prof. (Dr.) K. Vasudevan, Senior Member, IEEE**

Emeritus Professor

Department of Electronics

Cochin University of Science and Technology

Kochi-22, India.

Email: vasudevankdr@gmail.com

Ph. 91-9447357328, Fax : 91-484-2575800

List of Publications

International Journals

- 1 Laila.D, Sujith.R, Shameena V.A, **Deepak U.**, Nijas.C.M and P.Mohanan "CPW fed antenna for mobile handset with metal wire mesh", International Journal of Computer Applications. pp. 25-28 (2011).
- 2 R. Sujith, Graham, Ben, **U., Deepak**, G., Jaijith V., Mohanan, P., Timmons, Nick, Morrisson, Jim "Compact CPW Fed Slot Dipole Antennas with Different Excitation Techniques" International Journal on Communications Antenna & Propagation, vol. 2 , no. 3 , pp. 194 , June 2012

- 3 Nijas C M, Dinesh R, **Deepak U.**, Abdul Rasheed, Mridula S, K. Vasudevan and P. Mohanan , "Chipless RFID Tag using Multiple Microstrip Open Stub Resonators" IEEE Transactions on Antennas and Propagation, vol. 60, no. 9, pp. 4429-4432, Sept. 2012
- 4 R. Dinesh, V. K. T. Vinod, **U. Deepak**, P. V. Vinesh, P. Mohanan "CPW-fed zeroth-order Resonator Antenna Using Shorted CRLH Transmission Line" Microwave and Optical Technology Letters, vol. 55, no.12, pp. 2844-2847, Dec. 2013.
- 5 **U. Deepak**, P. Mohanan, C. M. Nijas, and T. K. Roshna, "Compact CPW fed electrically small antenna for WLAN application," Electron. Lett., vol. 50, no. 2, pp. 62-64, Jan. 2014.
- 6 T. K. Roshna, **U. Deepak**, V. R. Sajitha, K. Vasudevan, P. Mohanan, "Modified Bowtie Antenna for Zeroth Order Resonance", Pier C, Vol. 48, pp 45-52, 2014.
- 7 Nijas C M, **Deepak U.**, Vinesh P V, Sujith R, Mridula S , K. Vasudevan and P. Mohanan , "Low Cost Multiple Bit Encoded Chipless RFID Tag Using Stepped Impedance Resonator" IEEE Transactions on Antennas and Propagation, Vol. 62, no. 9, pp 4762-4770, Sept. 2014.
- 8 Roshna T. K., **Deepak U.**, Nijas C. M., Sajitha V. R., Mohanan P., "A high gain Compact Coplanar Stripline fed Antenna for Wireless Application", Microwave and Optical Technology Letters , Vol. 56, No. 8, August 2014.
- 9 **U. Deepak**, T. K. Roshna, C. M. Nijas, K. Vasudevan, and P. Mohanan, "A Dual Band SIR Coupled Dipole Antenna for 2.4/5.2/5.8 GHz Applications", IEEE Transactions on Antennas and Propagation, Vol. 63, no. 4, pp- 1514-1520, April 2015
- 10 T. K. Roshna, **U. Deepak**, V. R. Sajitha, K. Vasudevan, and P. Mohanan, "A Compact UWB MIMO Antenna with Reflector to Enhance Isolation", IEEE Transactions on Antennas and Propagation, Vol. 63, no. 4, pp- 1873-1877, April 2015.
- 11 T. K. Roshna, **U. Deepak**, V. R. Sajitha, and P. Mohanan, "A coplanar stripline fed compact UWB antenna," Electronics Letters, Vol. 50, no. 17, pp 1181-1182, Aug. 2014.
- 12 Mathew, S., Anitha, R., **Deepak U.**, Aanandan, C.K., Mohanan, P., Vasudevan, K. "A Compact Tri-Band Dual Polarized Corner Truncated Sectoral Patch Antenna", IEEE Transactions on Antennas and Propagation, Vol. 63, no. 12, pp- 5842-5845, September 2015.
- 13 **U. Deepak**, T. K. Roshna, and P. Mohanan, "A Dual Band SIR Coupled Dipole Antenna for 2.4/5.2/5.8 GHz Applications", Elsevier Procedia Computer Science, Vol. 46, pp. 1311-1316, 2015.

- 14 T. K. Roshna, **U. Deepak**, and P. Mohanan, "A coplanar stripline fed compact UWB antenna", Elsevier Procedia Computer Science, Vol. 46, pp. 1365-1370, 2015.
- 15 T. K. Roshna, **U. Deepak**, V. R. Saijtha, P. Mohanan.; "An ACS-fed Compact Antenna for UWB Applications", International Journal of Advances in Microwave Technology, Vol. 1, No. 1, May 2016.
- 16 T. K. Roshna, **U. Deepak**, P. Mohanan.; "Compact UWB MIMO antenna for tridirectional pattern diversity characteristics", IET Microwaves, Antennas & Propagation, Vol. 11, No. 14, Nov 2017.

Conference paper

- 1 Laila.D, Sujith.R, Shameena V.A, **Deepak U.**, Nijas.C.M and P.Mohanan, "CPW fed antenna for mobile handset with metal wire mesh", ICVCI-2011, St.Gits,Kottayam, INDIA.
- 2 Sujith.R, Laila.D, Nijas.C.M, **Deepak U.**, R.Dinesh and P.Mohanan, "CPW Feeding techniques to excite slot on an Open Ended coplanar waveguide transmission line" PIERS 2012 Kuala Lumpur, MALAYSIA, March 27 - 30, 2012.
- 3 V. A. Shameena, **U. Deepak**, R. Sujith, D. Laila, R. Dinesh and P. Mohanan,"Band notched ultra wide band slot antenna", PIERS 2012 Kuala Lumpur, MALAYSIA, March 27 - 30, 2012.
- 4 **U. Deepak**, T. K. Roshna, C. M. Nijas, R. Dinesh, and P. Mohanan, "Compact CPW fed ZOR antenna for WLAN application," 2013 IEEE Antennas Propag. Soc. Int. Symp., pp. 984-985, Jul. 2013.
- 5 Dinesh R , Vinod V K T, **Deepak U.**, Anila P V and P Mohanan "Chip Inductor Loaded Microstrip fed antenna for WLAN applications," Indian Antenna week, Aurangabad, Maharashtra, Jun. 3-7, 2013.
- 6 Nijas C. M., Sreekala Suseela, **Deepak U.**, Parveen Wahid and P. Mohanan "Low Cost Chipless Tag with Multi-bit Encoding Technique" 2013 IEEE MTT-S International Microwave and RF Conference (IMaRC), December 14-16, 2013, New Delhi, India.
- 7 Susan Thomas, **U. Deepak**, P.Mohanan, "Compact Asymmetric Coplanar Strip Fed Dual Band Antenna," IETE Conference on RF and Wireless, ICon-RFW 2014, 8-10 May,2014.
- 8 **Deepak U.**, Roshna T. K., Nijas C. M., Mohanan P., "An SIR loaded modified dipole antenna" IEEE XXXIth URSI General Assembly and Scientific Symposium (URSI GASS). 2014.
- 9 Roshna T. K., **Deepak U.**, Sujith R. and Mohanan P., "A high gain Compact Coplanar Stripline fed Antenna for Wireless Application", IEEE XXXIth URSI General Assembly and Scientific Symposium (URSI GASS). 2014.

- 10 **U. Deepak**, T. K. Roshna, C. M. Nijas, K. Vasudevan and P. Mohanan, "A Dual Band SIR Coupled Dipole Antenna for 2.4/5.2/5.8 GHz Applications", International Conference on Information and Communication Technologies (ICICT), Kerala, India, Dec. 2014.
- 11 T.K. Roshna, **U. Deepak**, and P. Mohanan, "A coplanar stripline fed compact UWB antenna", International Conference on Information and Communication Technologies (ICICT), Kerala, India, Dec. 2014.
- 12 **U. Deepak**, Susan Thomas, T. K. Roshna and P Mohanan, "A Compact ACS fed Electrically Small Antenna", Antennas and propagation Symposium (APSYM), Kerala, India. Dec. 2014.
- 13 **U. Deepak**, Susan Thomas, T. K. Roshna and P. Mohanan , "An Electrically Small ACS fed Compact Antenna ", Future of Electromagnetic Communication and Materials, SPECTRUM 2014 Proceedings, Kerala, India
- 14 Roshna T.K., **Deepak U.** and Mohanan P , "A Coplanar Stripline fed High Gain Compact Antenna ", Future of Electromagnetic Communication and Materials, SPECTRUM 2014 Proceedings, Kerala, India
- 15 **U. Deepak**, T. K. Roshna, V. R. Sajitha and P. Mohanan, "A Capacitively Coupled Meanderline Loaded Electrically Small Antenna ", Recent Advancements in Electronic Communication and Allied Areas Conference Proceedings, Kerala, India, 2015
- 16 T. K Roshna, **U. Deepak**, V. R. Sajitha, Sumitha Mathew and P. Mohanan, "A Reflector based UWB MIMO Antenna", Antennas and propagation Symposium (APSYM), Kerala, India. Dec. 2014.
- 17 **U. Deepak**, T.K. Roshna and P. Mohanan, "An SIR excited ESA for 2.4 GHz band", Applied Electromagnetic Conference (AEMC) 2015.
- 18 T. K. Roshna, **U. Deepak**, V. R. Sajitha and P. Mohanan, "A 3 port UWB MIMO antenna with enhanced isolation", Applied Electromagnetic Conference (AEMC) 2015.
- 19 T. K. Roshna, **U. Deepak** and P. Mohanan, "A 4-port mimo antenna for high speed uwb applications", 28th Kerala Science Congress, University of Calicut, Thenhipalam, Malappuram, India, Jan. 2016.
- 20 T. K. Roshna, **U. Deepak** and P. Mohanan, "A Compact Coplanar 4-Port MIMO Antenna For High-Speed UWB Applications", International Conference on Electromagnetics in Advanced Applications and IEEE-APS Topical Conference on Antennas and Propagation in Wireless Communications (ICEAA & IEEE APWC 2016), Cairns, Australia, Sept. 2016.